OUKA
The University of Osaka
Institutional Knowledge Archive

Title	Seismic Evaluation and Retrofit of Seismically Vulnerable Existing RC Flat Plate Structures
Author(s)	Samdani, H M Golam
Citation	大阪大学, 2022, 博士論文
Version Type	VoR
URL	https://doi.org/10.18910/89633
rights	
Note	

The University of Osaka Institutional Knowledge Archive : OUKA

https://ir.library.osaka-u.ac.jp/

The University of Osaka

Doctoral Dissertation

Seismic Evaluation and Retrofit of Seismically Vulnerable Existing RC Flat Plate Structures

H M GOLAM SAMDANI

June 2022

International Program of Maritime and Urban Engineering
Division of Global Architecture
Graduate School of Engineering
Osaka University

Abstract

Reinforced concrete (RC) flat plate structural system is a beamless structure in which the slab load is directly transferred to the column without using a column-capital or drop panel. This structural system is famous worldwide because of its cost-effectiveness, simplicity of construction, low height and weight of the building, and versatility of architectural design provided by the absence of beams in residential and commercial buildings. However, a significant number of reinforced concrete (RC) flat plate structures are at severe risk of punching shear failure around the plate-column connection under lateral loadings in Asian developing countries such as Bangladesh. In addition, Bangladesh is located in an earthquake-prone area and has experienced rapid economic and urbanization growth, resulting in densely populated cities. Therefore, a reliable estimate of the seismic load-carrying capacity and the deformation capability of existing RC flat plate structures is required for seismic strengthening to avoid catastrophic damage from earthquakes. In addition, many flat plate buildings require seismic strengthening against punching. This can be attributed to a number of factors, including design or construction flaws, low-quality materials, failure to comply with new code provisions, and an increase in vertical load. Therefore, some appropriate strengthening techniques should be implemented to minimize the probability of this type of brittle structural failure.

On the other hand, the research is quite limited, and seismic evaluation and retrofit of poorly constructed flat plate structures are not well established in the code for a particular zone in Asian developing countries such as Bangladesh. Thus, this research focuses on a typical existing flat plate structure made of low-strength concrete in Bangladesh, representing one of the most seismically vulnerable flat plate structures in Asian developing countries. The objective of this study is to propose a seismic evaluation and retrofit method for the existing vulnerable RC flat plate structures, based on the experimental findings.

Firstly, as an initial effort, we performed experiments on a series of two half-scaled specimens to evaluate the seismic performance of existing interior flat plate-column joints that were constructed using low-strength concrete. The experimental study on existing RC flat plate-column joints made of low-strength concrete is described in Chapter 2 of this thesis. In the experimental tests, the brick aggregate concrete was used to construct the specimens with low strength, which was typical of Bangladeshi building construction. One specimen (FP-1) was tested and constructed in Japan while the other specimen (FP-2) was constructed and tested in Bangladesh using local materials. Static cyclic vertical displacements with increasing amplitudes were applied to both ends of the plate to represent inter-storey drifts under seismic action, and their behaviors were monitored. Both specimens exhibited poor seismic performance showing brittle punching shear failure near the plate-column joints. Therefore, seismic retrofit is recommended to prevent this type of brittle structural collapse.

In this context, appropriate, reliable, effective, and low-cost retrofitting is challenging for the existing low-performance RC buildings in developing countries. Therefore, this study also emphasizes two strengthening schemes for seismically vulnerable existing flat plate structures. The experimental study on existing flat plate column joints that were strengthened using RC wing walls is briefly described in Chapter 3 of this thesis. The experimental investigation (in Japan) on a series of two half-scaled interior plate-column joints was conducted to explore the effectiveness of the proposed seismic strengthening scheme using post-installed RC wing walls and analyze the punching shear capacity of the joints. Wing walls were installed in two principal directions, i.e., along the loading direction for specimen FP-W1 and orthogonal direction for specimen FP-W2. Both specimens were constructed by simulating low-strength concrete and tested in Japan. Specimen FP-1 which is described in Chapter 2, is utilized as a benchmark specimen for the purpose of making comparisons between cases strengthened and cases not strengthened. Both of the strengthened specimens were able to successfully show higher resistances to punching shear failure. As a result, the test results experimentally verified that installing RC wing walls is a feasible method of upgrading flat plate-column joints, even with low-strength concrete, thereby preventing collapse under seismic action.

Another experimental investigation (in Bangladesh) on a series of three half-scaled interior plate-column joints was conducted to explore the effectiveness of the proposed seismic strengthening using post-installed RC drop panel. Chapter 4 of this thesis describes an experimental study on existing flat plate column joints that were strengthened using RC drop panels. Standard design practices and locally available materials were selected for the test specimens to represent typical RC buildings constructed earlier in Bangladesh. The series of three specimens with identical panel thickness and similar reinforcement details were constructed with RC drop-panel varying in different dimensions. Post-installed bonded anchors were applied to connect the drop panel with the existing structure. All the specimens were constructed and tested in Bangladesh while the specimen FP-2 which describes in chapter 2, served as a standard case for comparing cases with and without strengthening. It was experimentally verified that installing the RC drop panel effectively upgraded flat plate-column joints with low-strength concrete under seismic loading by increasing the effective depth of the plate and/or periphery of the column critical section.

To avoid catastrophic damage from earthquakes, it is essential to identify a reliable estimate of the seismic load-carrying capacity and the deformation capacity of existing reinforced concrete flat plate structures in earthquake-prone areas and to use that information to design of seismic strengthening. Therefore, chapter 5 intends to introduce a simplified evaluation methodology for the seismic capacity of existing flat plate structures commonly used in Bangladesh, based on the Japanese seismic evaluation guideline concepts. Based on the experimental findings in Chapter 2, the evaluation methodology of existing seismically vulnerable flat plate structures was introduced with slight modifications to the

Japanese standard. The evaluation procedure was proposed based on the Japanese seismic evaluation method with simplified modifications in calculating *C*-index and *F*-index by conservative estimation based on the experimental investigations. The interior plate-column connection exhibited very low shear resistance with punching failure; thus, the shear resistance of the interior column was neglected, and the upper bound of ${}_cR_{max}$ was recommended to prevent punching failure. A practical example of how the evaluation procedures could be applied effectively was then used to demonstrate the procedures following that.

The implementation and retrofit strategy were briefly introduced in chapter 6. An effective and appropriate retrofit scheme for the existing building is required to meet the seismic performance requirements in this situation. This can be accomplished by increasing either the strength or ductility of the structure, as appropriate. In this context, appropriate, reliable, effective, and low-cost retrofitting is challenging for the existing low-performance RC buildings in developing countries. Therefore, this study emphasizes two strengthening schemes for the up-gradation of seismically vulnerable flat plate-column connections in existing flat plate structures. Through this study, two retrofitting schemes are introduced, both of which have been proven to be effective and feasible through this study, as explained in Chapters 3 and 4. This chapter provides a synopsis of the retrofit strategy, as well as their theoretical implementation mechanism. Afterward, the retrofit measures were demonstrated with a practical example of how they could be applied effectively.

This thesis proposes two strengthening schemes using wing walls and drop panel, and describes experimental investigations on the behavior of reinforced concrete flat-plate column joints with low-strength concrete. The seismic evaluation workflow for flat plate structures is also proposed in this study. Suggestions are given for the construction of retrofitting method using wing walls and drop panel. Recommendations for future research work are also presented in this paper.

Acknowledgments

First and foremost, I would like to admit the blessings of almighty, merciful, gracious Allah who has enabled me to successfully accomplish this thesis.

I would like to take this opportunity to express my profound gratitude and deep regard to my thesis supervisor Prof. Yasushi Sanada, for his exemplary guidance, quick response, and constant encouragement that motivated me during my study at Osaka University. His insightful recommendations and encouraging supervision were of tremendous assistance to me throughout the entirety of my research work. It's impossible to imagine having a more knowledgeable/better advisor to guide me through my doctoral studies. Moreover, my sincere gratitude to Prof. Motohide Tada and prof. Hisatoshi Kashiwa for reviewing the thesis.

I would like to express my gratitude and give my heartfelt thanks to respected Dr. Susumu Takahashi, Assoc. prof. of Daido University, for his continuous support during the experiment as well as his valuable advice and assistance in reviewing this thesis. I am very appreciative of all that he had done for me during the journey of my Ph.D.

Moreover, my deepest gratitude and thanks to Ass. Prof. Rokhyun Yoon of Osaka University for his great contribution to my study and also for his genuine interest and insightful comments on my work. I would also like to thank all fellow students of Concrete Structure Laboratory for their suggestions, cooperation, and help during the experiments. Throughout the course of my pursuit of Ph.D., Ms. Naomi Sakata has been an incredible support for me, and I would like to take this opportunity to thank her.

My sincere thanks to Prof. Iftekhar Anam (UAP, Bangladesh), Prof. Abdur Rahman Bhuiyan (CUET, Bangladesh), and Mr. Abdul Malek Sikder (HBRI) for their suggestions, motivations, and effort during the experiments in Bangladesh. Also, I would like to thank Dr. Suguru Suzuki (Kochi University of Technology) for his assistance with the experiments in Japan.

I would like to express my appreciation to the Japanese Government (MEXT) for awarding me the scholarship. Furthermore, this research was supported by the JST/JICA SATREPS-TSUIB project “Technical Development to Upgrade Structural Integrity of Build-ings in Densely Populated Urban Areas and Its Strategic Implementation towards Resilient Cities in Bangladesh (TSUIB)” (principal investigators: Prof. Yoshiaki Nakano, U. Tokyo, and Mr. Md. Ashraful Alam, HBRI, Bangladesh). I gratefully acknowledge the support for this research.

Finally, I would like to thank my parents (Md. Taleb Hossain, and Ferdousi Hossain), my sisters (Foujia Sultana, and Salma Sultana), and my wife (Sadia Dastageer) for their spiritual support and encouragement throughout my life. I would like to dedicate this thesis to them.

List of Publications

Peer-Reviewed Papers

1. **Samdani HMG**, Takahashi S, Yoon R, Sanada Y. Strengthening Seismically Vulnerable Reinforced Concrete Flat Plate-column Connections by Installing Wing Walls, *Japan Architectural Review*, Vol. 4, No. 3, pp. 442–454, 2021.06. https://doi.org/10.1002/2475-8876.12232 **[Chapters 2 and 3]**

2. **Samdani HMG**, Takahashi S, Yoon R, Sanada Y. Seismic Evaluation of Existing Flat Plate Structure and Retrofit with Wing Wall and Drop Panel, *Transactions of the Japan Concrete Institute*, Vol. 44, No. 2, pp. 181-186, 2022.07 **[Chapters 5 and 6]**

3. **Samdani HMG**, Takahashi S, Yoon R, Sanada Y. A Theoretical Evaluation Scheme of the Ultimate Flexural Strength of Multi-Storey Column with Wing Walls in RC Flat Plate Structure. *Proceedings of the 12th National Conference on Earthquake Engineering*. Earthquake Engineering Research Institute, paper ID:10350, 2022.07, Salt Lake City, UT **[Chapter 6]**

International Conference Paper:

1. **Samdani HMG**, Sanada Y, Takahashi S, Suzuki S, Yoon R, Anam I. Experimental study on A new strengthening technique of flat plate-column connections using wing walls. *17th World Conference on Earthquake Engineering* 2020, Paper No. 3b-0059, Sendai, Japan. **[Chapters 2 and 3]**

Academic Conference Papers:

1. **Samdani HMG**, Kim S, Takahashi S, Suzuki S, Sanada Y. Experimental Study on Flat Plate-Column Connection Made with Low-Strength Concrete; Part 1: Experimental Program. *AIJ Annual Conference*, pp.445-446, September 2018, Sendai, Japan. **[Chapter 2]**
2. Kim S, **Samdani HMG**, Takahashi S, Suzuki S, Sanada Y. Experimental Study on Flat Plate-Column Connection Made with Low-Strength Concrete; Part 2: **Experimental Results**. *AIJ Annual Conference*, pp.447-448, September 2018, Sendai, Japan. **[Chapter 2]**
3. **Samdani HMG**, Takahashi S, Sanada Y, Suzuki S Yoon R. Experimental Study on a Strengthening Technique by Wing Walls for Flat Plate-Column Connections with Low-Strength Concrete" *Japanese Society of Architecture Kinki Branch Research Report Collection,* Vol.59 (Structures), pp.485-488, June 2019, Meeting Report/Oral presentation. **[Chapters 2 and 3]**

4. Takahashi S, **Samdani HMG**, Sanada Y, Suzuki S, Yoon R. Experimental Study on Flat Plate-Column Connection Made with Low-Strength Concrete; Part 3: Strengthening Proposal with Wing Walls. *AIJ Annual Conference*, September 2019, Kanazawa, Japan. **[Chapter 3]**
5. **Samdani HMG**, Takahashi S, Sanada Y, Suzuki S, Yoon R. Experimental Study on Flat Plate-Column Connection Made with Low-Strength Concrete; Part 4: Effectiveness of the Proposed Strengthening Technique. *AIJ Annual Conference*, September 2019, Kanazawa, Japan. **[Chapter 3]**
6. **Samdani HMG**, Takahashi S, Yoon R, Sanada Y. Experimental Study on Flat Plate-Column Connection Made with Low-Strength Concrete; Part 5: Effect of Drop Panel. *AIJ Annual Conference*, September 2020, Chiba, Japan. **[Chapter 4]**
7. **Samdani HMG**, Takahashi S, Yoon R, Sanada Y. Experimental Study on Flat Plate-Column Connection Made with Low-Strength Concrete; Part 6: Nonlinear Finite Element Analysis. *AIJ Annual Conference*, September 2021, Chiba, Japan.
8. **Samdani HMG**, Takahashi S, Yoon R, Sanada Y. Experimental Study on Flat Plate-Column Connection Made with Low-Strength Concrete; Part 7: Seismic Evaluation. *AIJ Annual Conference*, September 2022, Hokkaido, Japan. **[Chapter 5]**
9. Takahashi S, **Samdani HMG**, Yoon R, Sanada Y. Experimental Study on Flat Plate-Column Connection Made with Low-Strength Concrete; Part 8: Seismic Retrofit. *AIJ Annual Conference*, September 2022, Hokkaido, Japan. **[Chapter 6]**

Table of contents

Abstract ..... **i**

Acknowledgments ..... **v**

List of Publications ..... **vii**

Table of Contents **ix**

List of Figures ..... **xiii**

List of Tables ..... **xvii**

CHAPTER 1

Introduction **1**

1.1 General **1**

1.2 Background **1**

1.2.1 Flat Plate **1**

1.2.2 Punching shear failure **2**

1.2.3 Context of Bangladesh **3**

1.3 Significance **8**

1.4 Literature Review **8**

1.5 Research Objectives **21**

1.6 Outline of the thesis **22**

CHAPTER 2

Experimental Study on an Interior Flat Plate-Column Joint Using Low-strength Concrete **25**

2.1 General **25**

2.2 Target Building of Interests **25**

2.3 Specimen design/details **26**

2.3.1 Specimen FP-1 ..... **27**

2.3.1 Specimen FP-2 ..... **28**

2.4 Material mechanical properties of concrete and steel **29**

2.4.1 Specimen FP-1 ..... **30**

2.4.2 Specimen FP-2 ..... **30**

2.5 Loading and Measurement Methods **32**

2.5.1 Experimental setup of the specimen **32**

2.5.2 Instrumentation measurements **35**

2.6 Experimental results **36**

2.6.1 Specimen FP-1 ..... **36**

2.6.2 Specimen FP-2 ..... **38**

2.7 Strength estimation of the specimens …… **40**
2.8 Experimental discussion …… **44**
2.9 Summary ……... **45**

CHAPTER 3

Experimental Study on Strengthening of the Interior Flat Plate-column Joint using Post-installed RC Wing Walls ……... 47

3.1 General …….. **47**
3.2 Wing Wall …… **47**
3.3 Specimen design/details …… **48**
3.4 Material mechanical properties of concrete and steel …… **49**
3.5 Loading and Measurement Methods ……. **50**
3.5.1 Experimental setup ……... **50**
3.5.2 Instrumentation measurements ……. **52**
3.6 Experimental results …….. **53**
3.6.1 Specimen FP-W1 …….. **53**
3.6.2 Specimen FP-W2 …….. **54**
3.6.3 Strain Distribution of the Slab Reinforcement …….. **56**
3.7 Strength estimation of the specimens …… **57**
3.8 Experimental discussion …… **60**
3.9 Summary ……... **62**

CHAPTER 4

Experimental Study on Strengthening of the Interior Flat Plate-column Joint using Post-installed RC Drop Panels …….. 65

4.1 General …….. **65**
4.2 Specimen design/details …… **65**
4.3 Material mechanical properties of concrete and steel …… **68**
4.4 Loading and Measurement Methods ……. **68**
4.4.1 Experimental setup ……... **68**
4.4.2 Instrumentation measurements ……. **70**
4.5 Experimental results …….. **70**
4.5.1 Specimen FP-D1 …….. **71**
4.5.2 Specimen FP-D2 …….. **72**
4.5.3 Specimen FP-D3 …….. **74**
4.6 Strength estimation of the specimens …… **76**
4.7 Experimental discussion …… **78**

4.8 Summary 79

CHAPTER 5

Seismic Evaluation of Existing Flat Plate Structure 81

5.1 General 81

5.2 Scope 81

5.3 Seismic Evaluation Work-flow 82

5.4 Column Failure Mechanism and Shear Resistance 83

5.5 Calculation of *C*-index 87

5.6 Calculation of *F*-index 88

5.7 Judgment of the evaluation 89

5.8 Example of application 90

5.9 Summary 93

CHAPTER 6

Seismic Retrofit of Flat Plate Structure 95

6.1 General 95

6.2 Scope 96

6.3 Strengthening Strategy 96

6.4 Seismic Retrofit using wing walls 98

6.4.1 Design concept using wing wall 101

6.5 Seismic Retrofit using drop panel 103

6.5.1 Design concept using drop panel 104

6.6 Example of application 106

6.7 Summary 109

CHAPTER 7

Conclusions and Recommendations 111

7.1 General 111

7.2 Summary 111

7.3 Conclusions 114

7.4 Limitations and Recommendations 114

References 117

Appendix A1 Position of strain gauges on reinforcing bars and strain of reinforcing bars of each specimen **121**

Appendix A2 Position of displacement transducers and deflection of slab of each specimen ... **155**

Appendix A3 Detailed procedure of the sample calculation of the example building **169**

List of Figures

Figure 1.2.1	Difference between flat plate and conventional RC structure ……	**2**
Figure 1.2.2	Flat plate structure in Dhaka, Bangladesh ……..	**2**
Figure 1.2.3	Punching shear failure in flat plate structure ……..	**3**
Figure 1.2.4	Potential Source of active faults …….	**4**
Figure 1.2.5	Major earthquakes in and around Bangladesh ……	**5**
Figure 1.2.6	Brick aggregate …….	**6**
Figure 1.2.7	Rana plaza collapse ……	**7**
Figure 1.2.8	Failure of flat plate structure in Bangladesh …….	**7**
Figure 1.4.1	Shear bolt and its installation system …….	**11**
Figure 1.4.2	Specimen details using shear bolt ……..	**11**
Figure 1.4.3	Backbone curve of the moment vs drift ration for all specimens ……	**12**
Figure 1.4.4	Details of the specimen and loading program …….	**13**
Figure 1.4.5	Detail configuration of the shear bolt …….	**13**
Figure 1.4.6	Moment vs drift angle relationship (envelop curves) for all specimens ….	**14**
Figure 1.4.7	Reinforcing of post-installed inclined shear reinforcement using the anchor with nut and washers ……	**14**
Figure 1.4.8	The testing setup and the layout of the post-installed inclined shear reinforcement …….	**15**
Figure 1.4.9	Setup of the experiments and details of the specimen using CFRP stirrups	**16**
Figure 1.4.10	The external CFRP stirrups installation …….	**17**
Figure 1.4.11	The load vs deflection behavior of the specimens using CFRP stirrups ….	**17**
Figure 1.4.12	The configuration of bolt and pattern of the steel plate ……..	**19**
Figure 1.4.13	The layout of the strengthened plate …….	**19**
Figure 1.4.14	The load vs drift relationship of the tested specimens ……	**20**
Figure 2.2.1	Building of interest: Focused flat plate-column joint …….	**26**
Figure 2.2.2	The typical result obtained from the test performed on a cylinder core ….	**26**
Figure 2.3.1	Details of the specimen FP-1 ……..	**27**
Figure 2.3.2	Placement of steel plates ……	**28**
Figure 2.3.3	Installation of studs ……	**28**
Figure 2.3.4	Details of the specimen FP-2 ……..	**29**
Figure 2.5.1	Loading setup of the experimental program ……..	**32**
Figure 2.5.2	Photograph of the loading setup during the experiment …….	**33**
Figure 2.5.3	Position of LVDT and definition of *R* ……	**34**
Figure 2.5.4	Loading history ……..	**34**

Figure 2.5.5 Position of displacement transducers of both specimens …… **35**
Figure 2.6.1 (A) Relationship of the nodal moment versus the drift ratio (Specimen FP), and (B) damage after punching shear failure ……. **37**
Figure 2.6.2 Crack pattern comparison in different cycles for FP-1 …….. **37**
Figure 2.6.3 Comparison of the transitions of the strain distributions under different cycles for specimen FP-1 ……... **38**
Figure 2.6.4 (A) Relationship of the nodal moment versus the drift ratio (Specimen F2), and (B) damage after punching shear failure ……. **39**
Figure 2.6.5 Crack pattern comparison in different cycles for FP-2 …… **39**
Figure 2.6.6 Comparison of the transitions of the strain distributions under different cycles for specimen FP-2 ……... **40**
Figure 2.7.1 Moment diagram for both specimens ……. **41**
Figure 2.7.2 Punching shear mechanism due to bending, shearing, and twisting …….. **42**
Figure 2.8.1 Backbone curve of both specimens …… **44**
Figure 2.8.2 Comparison of the component of the punching shear estimation using AIJ standard ……. **45**
Figure 3.2.1 Seismic retrofit by RC flat plate-column joint by installing post-installed wing walls …….. **48**
Figure 3.3.1 Details of the strengthening specimens using wing walls ……. **49**
Figure 3.5.1 Photographic view of the experimental setup ……. **51**
Figure 3.5.2 Arrangement of LVDTs and the definition of *R* ……. **51**
Figure 3.5.3 Loading history using wing wall …… **52**
Figure 3.5.4 Picture of data acquisition system during testing …….. **52**
Figure 3.5.5 Position of displacement transducers ……. **53**
Figure 3.6.1 (A) Nodal moment versus drift ratio relationship (specimen FP-W1) and (B) damage after punching shear failure …… **54**
Figure 3.6.2 Failure process on the top surface of the plate of specimen FP-W1 …… **54**
Figure 3.6.3 (A) Nodal moment versus drift ratio relationship (specimen FP-W2) and (B) damage after punching shear failure …… **55**
Figure 3.6.4 Failure process on the top surface of the plate of specimen FP-W2 …… **55**
Figure 3.6.5 Comparison of strain distribution transitions under different cycles for specimen FP-W1 ……..... **56**
Figure 3.6.6 Comparison of strain distribution transitions under different cycles for specimen FP-W2 ……..... **57**
Figure 3.7.1 Moment diagram of specimen FP-W1 ……... **58**
Figure 3.7.2 Moment diagram of specimen FP-W2 ……... **58**

Figure 3.7.3 Punching shear mechanism due to bending, shearing, and twisting for specimen FP-W1 …… **59**
Figure 3.7.4 Punching shear mechanism due to bending, shearing, and twisting for specimen FP-W2 …… **59**
Figure 3.7.5 Assumed critical section …… **59**
Figure 3.8.1 Performance comparisons of the strengthened specimens with that of the control specimen …… **61**
Figure 4.2.1 Details of the specimen FP-D1 …….. **66**
Figure 4.2.2 Details of the specimen FP-D2 …….. **67**
Figure 4.2.3 Details of the specimen FP-D3 ……. **67**
Figure 4.4.1 Photographic view of the experimental setup ……. **69**
Figure 4.4.2 Loading history using drop panel ……... **69**
Figure 4.4.3 Overall image through the online platform …… **70**
Figure 4.5.1 (A) Nodal moment versus drift ratio relationship (specimen FP-D1) and (B) damage after punching shear failure …… **71**
Figure 4.5.2 Crack pattern of specimen FP-D1 ……. **72**
Figure 4.5.3 Comparison of strain distribution transitions under different cycles for specimen FP-D1 ……..... **72**
Figure 4.5.4 (A) Nodal moment versus drift ratio relationship (specimen FP-D2) and (B) damage after punching shear failure …… **73**
Figure 4.5.5 Crack pattern of specimen FP-D2 ……. **74**
Figure 4.5.6 Comparison of strain distribution transitions under different cycles for specimen FP-D2 …… **74**
Figure 4.5.7 (A) Nodal moment versus drift ratio relationship (specimen FP-D3) and (B) damage after punching shear failure …… **75**
Figure 4.5.8 Crack pattern of specimen FP-D3 ……. **76**
Figure 4.5.9 Comparison of strain distribution transitions under different cycles for specimen FP-D3 …… **77**
Figure 4.6.1 Moment diagram for specimens using drop panel …….. **77**
Figure 4.6.2 Assumed critical section of punching shear failure using drop panel ……. **77**
Figure 4.7.1 Performance comparison using backbone curve …… **79**
Figure 5.2.1 Conceptual image of the seismic evaluation for a typical floor plan …….. **82**
Figure 5.3.1 Flowchart of the seismic evaluation process ……. **83**
Figure 5.4.1 Failure mechanisms governed from the slab ……. **85**
Figure 5.4.2 Assumed moment diagram …… **86**
Figure 5.4.3 Induced vertical load and moment with assumed critical section …….. **87**

Figure 5.5.1	Experimental flat plate-column joint capacity ……..	**88**
Figure 5.8.1	Typical floor layout with exterior beams ……..	**91**
Figure 5.8.2	Column schedule of the existing structure …….	**92**
Figure 5.8.3	Comparison between seismic demand and capacity ……..	**93**
Figure 6.1.1	Basic concept of seismic up-gradation ……..	**95**
Figure 6.3.1	Proposed flowchart of seismic retrofit ……...	**96**
Figure 6.3.2	An example of flat plate structure to which this section is applied …….	**97**
Figure 6.4.1	Experimental results with the proposed critical section using wing wall	**99**
Figure 6.4.2	Moment diagram image of the column retrofitted by wing walls for Eq. (6.4.1) ……	**100**
Figure 6.4.3	Assumed moment diagram with wing walls ……	**101**
Figure 6.4.4	Flowchart of seismic retrofit of existing RC flat plate-column joint by wing walls …….....	**102**
Figure 6.4.5	Column with wing walls ……	**103**
Figure 6.4.6	The nodal moment at the flexural yielding of slab ……	**103**
Figure 6.5.1	Experimental results on the contribution of drop panel …….	**104**
Figure 6.5.2	Assumed moment diagram with drop panel ……..	**104**
Figure 6.5.3	Flowchart of seismic retrofit of existing RC flat plate-column joint by drop panel……...	**105**
Figure 6.5.4	The nodal moment at the flexural yielding of slab (before retrofit) (Grid Y2)……..	**103**
Figure 6.6.1	The plan of existing columns with an arrangement of post-installed wing walls and drop panels …….	**108**
Figure 6.6.2	Comparisons between the seismic demand and capacity before/after retrofit……	**109**

List of Tables

Table 2.1 Concrete mixture in kg/m^3 (for specimen FP-1) …….. **30**

Table 2.2 Material properties of concrete (for specimen FP-1) …… **30**

Table 2.3 Material properties of steel (for specimen FP-1) …….. **30**

Table 2.4 Material properties of concrete (for specimen FP-2) …… **31**

Table 2.5 Concrete mixture in kg/m^3 (for specimen FP-2) …… **31**

Table 2.6 Material properties of steel (for specimen FP-2) …… **31**

Table 2.7 Calculated ultimate strengths compared to the ultimate strengths obtained from the experimental data ……. **43**

Table 3.1 Concrete mixture in kg/m^3 (using wing wall) ……. **50**

Table 3.2 Material properties of concrete (using wing wall) ……. **50**

Table 3.3 Material properties of steel (using wing wall) …… **50**

Table 3.4 Calculated ultimate strengths compared to the ultimate strengths obtained from the experimental data (using wing wall) ……. **60**

Table 4.1 Concrete mixture in kg/m^3 (using drop panel) …… **68**

Table 4.2 Material properties of concrete (using drop panel) ……. **68**

Table 4.3 Calculated ultimate strengths compared to the ultimate strengths obtained from the experimental data (using drop panel) …… **78**

Table 5.1 Summary of materials …… **91**

Table 5.2 Summary of the seismic evaluation ……. **92**

Table 6.1 Summary of the seismic evaluation using wing walls ……. **108**

CHAPTER 1

Introduction

1.1 General

Nowadays, the flat plate structural system has been one of the most eminent structural systems worldwide, particularly for its architectural view, use of space, ease of formwork and construction, and faster construction time. However, the structural efficiency of this system has been impaired due to its flexibility and low moment resistance to transferring in the plate-column joint. This plate-column joint is more vulnerable when the seismic load is applied during an earthquake along with its gravity load, leading to progressive brittle punching shear failure of the partial/overall structure. Moreover, several low-performance flat plate structures are located in developing countries in earthquake-prone regions like Bangladesh, which leads to the threat of life safety and property damage during seismic action. Therefore, a reliable estimate of the seismic load-carrying capacity and the deformation capacity of existing reinforced concrete (RC) flat plate structures is required for seismic strengthening to avoid catastrophic damage from earthquakes. Thus, this research aims to reduce the potential risk of low seismic performance flat plate structures in developing countries. In this context, this chapter discusses the background, scope/significance, objective of this study, and literature study briefly addressed in the following sections.

1.2 Background

1.2.1 *Flat Plate Structure*

The flat plate is one of the most common structural floor systems for large-span residential and commercial buildings. It is a two-way reinforced concrete frame system that utilizes a slab of uniform thickness with direct load transfer to the column. The structure is either beamless or sometimes consists of beams in the perimeter frame. An illustration of the difference between a flat plate and a conventional RC structure is shown in **Figure 1.2.1**. The use of a flat plate structural system has numerous advantages. It allows architects more freedom in designing spaces, and easier formwork, resulting in a shorter timeline for construction. In addition to facilitating architectural flexibility, it provides low floor-to-floor heights that reduce the total building height, reducing lateral and vertical loads, mechanical and electrical costs that reduce overall building costs. Due to the enormous advantages, this structure is becoming popular nowadays. The structural performance and design of flat plates are well established for vertical loads; however, many aspects of their behavior are uncertain for lateral loads. In Bangladesh,

flat plate structures have beams in the periphery frames, and the interior columns are not connected with beams. The example of a flat plate structure in Bangladesh is shown in **Figure 1.2.2**.

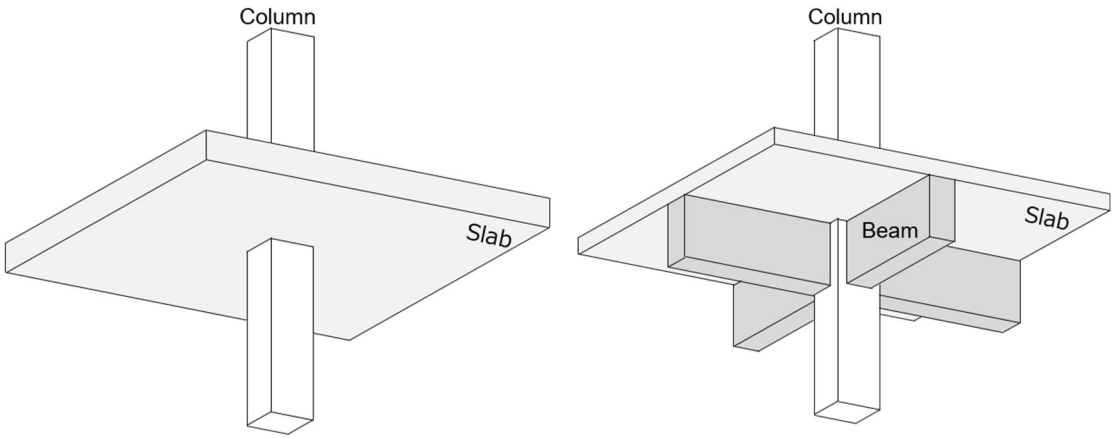

Figure 1.2.1 Difference between flat plate and conventional RC structure



Figure 1.2.2 Flat plate structure in Dhaka, Bangladesh

1.2.2 *Punching shear failure*

This structural system has a lack of resistance to lateral loads on the plate-column joint, resulting in building collapse under past earthquakes. Therefore, it should be well-designed/managed in developed countries with high/moderate seismicity, such as the United States, New Zealand, and Japan. Similarly, many flat plate structures exist in developing countries, even in high/moderate seismic areas, in contrast, where it's become a vital issue to ensure the safety and integrity of flat plate structures because of their insufficient seismic resistance. Consequently, the flat plate structures are most

vulnerable due to their punching phenomena during an earthquake. As a consequence of the 1985 Mexico City earthquake, the 1989 Loma Prieta earthquake, and the 1994 Northridge earthquake, many slab-column connections in flat-plate structures were damaged and failed in punching shear (Widianto et al. 2010). Punching shear failure is a failure pattern caused by extreme stresses on the cross-section of the plate close to the plate-column joint, which are created by transferring lateral and vertical forces and bending moments between the plate and column. This tremendously brittle failure sometimes leads to overall structural failure, as shown in **Figure 1.2.3,** demonstrating progressive collapse due to punching shear failure (Wood 2003). This type of failure is catastrophic because there are no visible signs shown prior to failure. Disasters caused by punching shear failure have taken place on multiple occasions over the course of this past decade. An example of punching shear failure is shown in **Figure 1.2.3**.

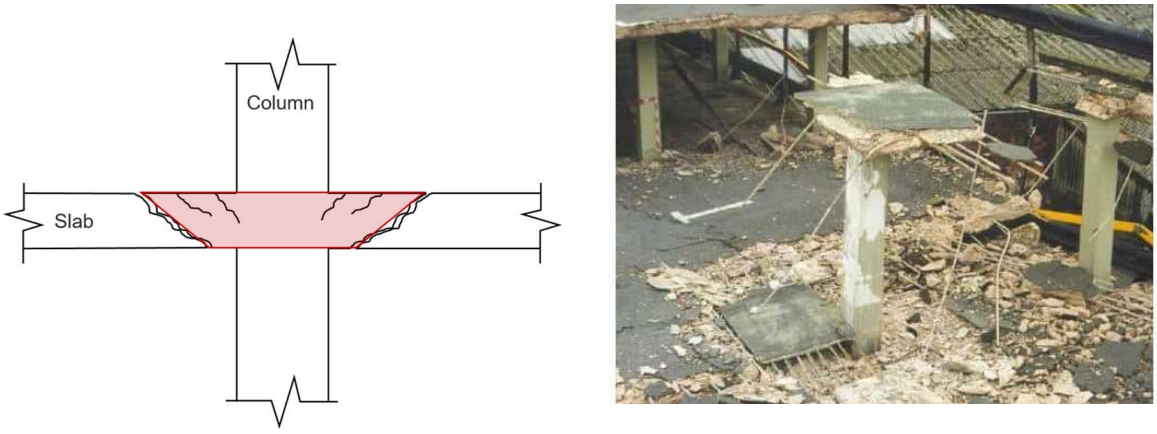

Plate-column connection

Photograph of Punching shear failure (Wood 2003)

Figure 1.2.3 Punching shear failure in flat plate structure

1.2.3 *Context of Bangladesh*

The context of Bangladesh is almost similar to other Asian developing countries such as Nepal, India, Myanmar, Indonesia, etc. However, Bangladesh is primarily focusing on the background of this research.

Seismic vulnerability

There are a significant number of developing countries like Bangladesh that are situated in areas that are at high risk of earthquakes (Steckler et al. 2018; Rahman et al. 2020). Geographically, Bangladesh is one of the most earthquake-prone zones due to its position at the juncture of several active tectonic plate boundaries. Many geologically active fault lines run across the country, as shown in **Figure 1.2.4**. However, a limited number of devastating earthquakes have been reported to occur in Bangladesh over the past 100 years. **Figure 1.2.5** shows a picture of the seismic vulnerability in

Bangladesh with the potential source of significant earthquakes. The history of Bangladesh reveals that earthquakes that occurred in or close to Bangladesh in 1762, 1885, and 1897 caused widespread damage throughout the nation. (Al zaman and Jahan Monira 2017). The recurrence of similar earthquakes from any of these active seismic sources could cause substantial damage to major population centers in Bangladesh (Islam et al. 2016; Alam 2019). Bangladesh is woefully unprepared to deal with the aftermath of a major earthquake of any moderate to a large magnitude. In fact, frequent earthquakes have recently occurred in the surrounding regions (e.g., the Nepal earthquake in 2015 (Hossain et al. 2015) and the Myanmar earthquake in 2016 (Shiddiqi et al. 2018)), which warns Bangladesh to take necessary precautions awareness among general people, engineers, and the government.

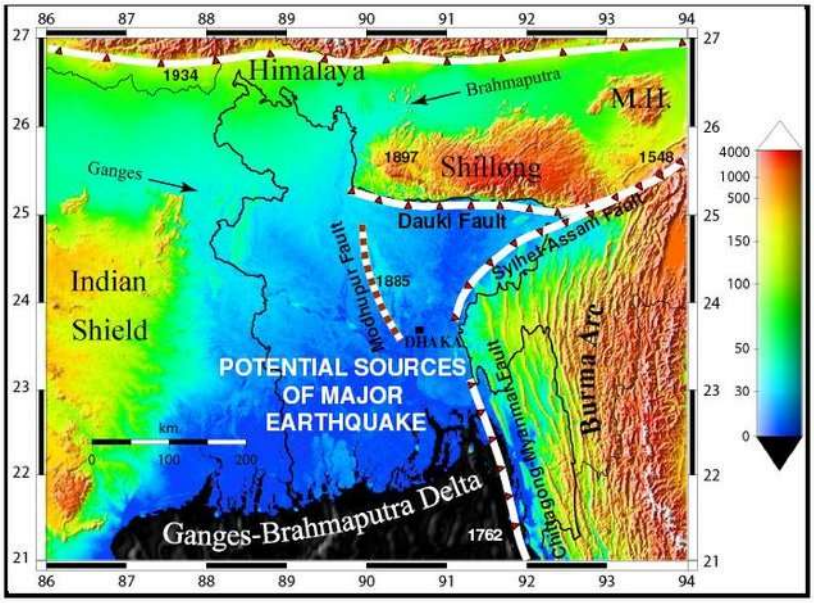

Figure 1.2.4 Potential Source of active faults (Islam et al. 2016)

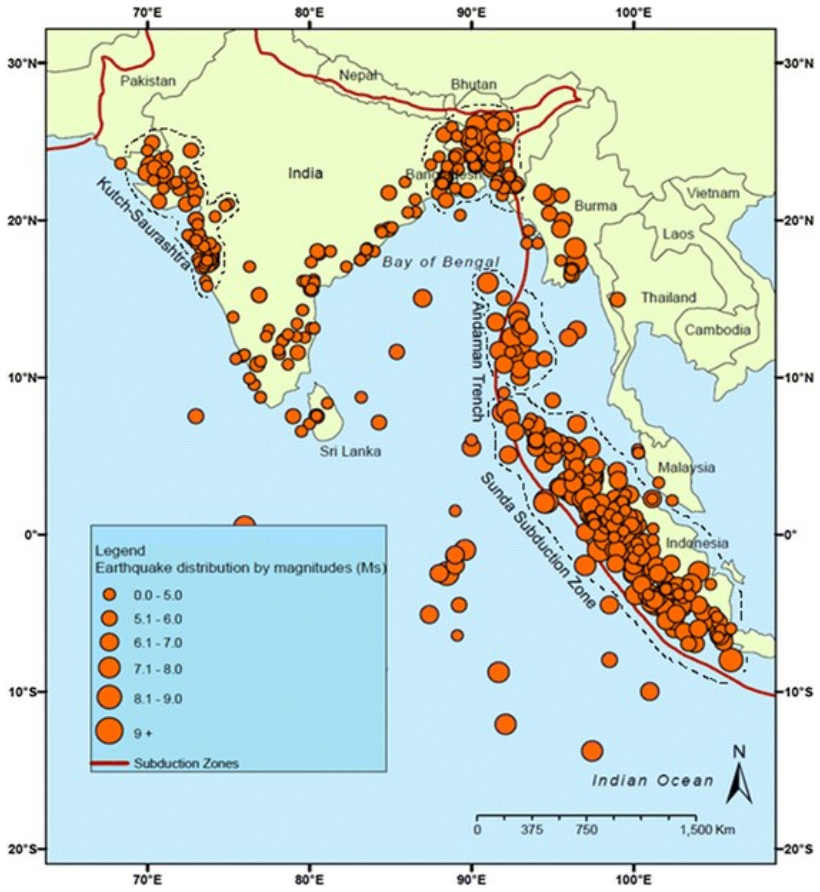

Figure 1.2.5 Major earthquakes in and around Bangladesh (Alam and Dominey-Howes 2016). The distribution of 562 earthquakes between 810BC and 2012, showing four clusters (shown by black dashed lines) of earthquakes: west coast of Sumatra, Andaman and Nicobar Island, Bangladesh and adjoining regions and NW coast of India.

Improper construction management with Low-strength concrete:

Many flat-plate buildings were designed considering the gravity load only in the older part of Dhaka, Chittagong, and Sylhet city in Bangladesh (Public Works Department (PWD) 2015). In addition, according to a recent survey conducted in Bangladesh, many old reinforced concrete (RC) buildings suffer from a variety of deficiencies, including low-strength concrete, a high axial load ratio with small column size, and so on ((JICA) 2015). Because Bangladesh has a limited supply of natural stone aggregates, brick aggregate concrete has been used for the majority of the reinforced concrete buildings that are already in existence in the country. This is due to the abundant availability of brick aggregate concrete, which has led to a reduction in the cost of these structures. Such usage of brick aggregate concrete has led to a large number of buildings being constructed with low-strength concrete (Wardi et al. 2020). **Figure 1.2.6** shows the brick aggregate. Moreover, most of the existing RC flat plate buildings, especially those in the older part of Dhaka city in Bangladesh, were constructed under inappropriate construction management before or even after the inception of the Bangladesh National Building Code

(hereafter, BNBC (HBRI 1993)). The deficiency of construction management is one of the most significant concerns that lead to inappropriate design and lower concrete strength. Change in the building occupancy as residential buildings to commercial and/or industrial buildings is very common in Bangladesh. It also might cause be a structural failure without an earthquake (Ex. Rana Plaza building collapse in Savar), Dhaka, Spectrum garments factory collapse in Dhaka)). An increase in the number of floors without proper design or analysis is also an important issue. The Rana Plaza building that collapsed in 2013 is a terrible example of the demonstration of inappropriate design and poor construction management, as shown in **Figure 1.27**. **Figure 1.2.8** provides an example of flat plate structure failure in Bangladesh, reflecting collapse due to inappropriate design and construction management (The Daily Star 2007). The disaster occurred despite the absence of an earthquake. The damage caused by such structural design errors, as well as the earthquake, should serve as a reminder to Bangladeshi authorities to take the necessary steps to identify and retrofit existing old and unsafe structures. As a result of this, many existing RC buildings in Bangladesh, which typically include a flat plate system, are at risk of damage or collapse during future earthquakes. As a consequence of this, strengthening is currently required in order to reduce the severity of the damage caused by earthquakes. Moreover, numerous poorly constructed flat plate structures already exist, and new structures are continuously developing without proper seismic design in Bangladesh. Therefore, seismic strengthening of the existing building stock is a vital issue to avoid catastrophic damage from future earthquake events.



Figure 1.2.6 Brick aggregate



Figure 1.2.7 Rana plaza collapse (The New York Times (photo courtesy of Abir Abdullah) 2015)



Figure 1.2.8 Failure of flat plate structure in Bangladesh (The daily Star (Photo courtesy of SK Enamul Haq) 2005)

Seismic design and retrofitting provisions in Bangladesh

Bangladesh has not experienced frequent or moderate to large earthquakes frequently, so people don't pay as much attention to the seismic resistance of buildings when they build them. The Bangladeshi National Building Code (BNBC) 2015, which was recently published, contains stringent requirements for seismic detailing in reinforced concrete buildings. But many existing buildings are already constructed with less attention to the code. The Bangladesh National Building Code (BNBC) was first drafted in 1993 and officially adopted by the government in 2006. It adhered to the ACI code (ACI 318-08) until 1993, and then to the BNBC code thereafter for the application of structural design only. Moreover, there was no standard for seismic evaluation of reinforced concrete structures in Bangladesh until 2015. But strict adherence to the code, particularly the seismic provisions, came into practice very recently, as mandated by the CNCRP Manual (Public Works Department (PWD) 2015)

in 2015 based on the JBDPA, (JBDPA 2005). However, this latest manual has not included the seismic evaluation of flat plate structures. Since many flat plate structures still exist in Bangladesh; thus, it is essential to evaluate this large number of building stock. It is assumed that the existing building stock is supposed to have low-seismic performance. Those low-performance buildings should be implemented with an appropriate retrofit plan; otherwise, a large number of building stock should be demolished, which is quite impossible.

1.3 Significance

A large number of existing RC flat plate building stock required seismic evaluation. Therefore, experimental investigations have been conducted for interior flat plate-column joints constructed using low-strength concrete to introduce a seismic evaluation methodology. Failure of flat plate structures can occur through punching shear, which is a mode of failure that is extremely brittle. It is urgent to enhance the punching shear capacity to prevent brittle failure, especially for flat plate structures made of low-strength concrete in developing countries such as Bangladesh. Consequently, Effective and appropriate seismic retrofitting for the existing buildings must be implemented by increasing the strength or ductility when the existing seismic performance does not meet the requirement. Therefore, two retrofitting schemes have been proposed in this study, and their effectiveness was verified. The proposed wing wall installation approach can be adopted as a promising method to upgrade existing RC flat plate structures, even for those made of low-strength concrete. The experimental results show that the strength of flat plate-column connections strengthened with wing walls improves significantly with increasing punching shear strength, while the existing components exhibit deplorable conditions with a concrete strength equivalent to or less than 10 N/mm^2. On the other hand, drop panel retrofit methodology is introduced which was cross verified with low strength concrete using experimental investigations. Drop panel is effective for those buildings which don't need the additional lateral resistance of the existing columns but need the prevent punching shear failure in addition to the increase of the ductility of a structure.

1.4 Literature Review

Seismic evaluation is essential for ensuring the structural integrity and stability of existing flat plate buildings. The building code provision of many countries is provided a brief evaluation procedure for normal moment-resisting structures. Flat plate structure, on the other hand, differs significantly from conventional moment-resisting structures. Therefore, it should be well-designed/managed in developed countries with high/moderate seismicity, such as the United States, New Zealand, and Japan. Because of the frequency with which earthquakes strike in Japan, the country's design guidelines are well-known, dependable, and widely accepted. Many countries, including Bangladesh, are planning to follow the evaluation procedure outlined in the Japanese guidelines, which is expected to be implemented in the

near future ((JICA) 2015) (Public Works Department (PWD) 2015). The flat plate structure, on the other hand, is not included in the scope of application because the flat plate is not commonly found in Japanese construction practices. The identification of punching shear strength for normal strength concrete can be evaluated according to the Japanese standard. Nonetheless, low-strength concrete is commonly available in many Asian developing countries, which is one of the most serious concerns, in addition to the seismic vulnerability of the existing buildings, in this region. Therefore, the identification of punching shear strength estimation for low-strength concrete is necessary for the evaluation of the existing flat plate structure. The interior columns are not connected with beams that are often found in Bangladesh and are likely to fail in brittle punching shear failure prior to the slab flexure due to the absence of beams. However, the plate-column joint is more vulnerable when the seismic load is functioned during an earthquake along with its gravity load, leading to progressive brittle punching shear failure of the partial/overall structure. Therefore, the failure mode of the slab should also be considered as well as the calculation of vertical members to assess the seismic performance of an existing building. However, the research is quite limited to low-strength concrete structures under seismic loading conditions focusing on developing countries.

Punching shear failure is the most serious concern in the flat plate structure. The flat plate structure is going to flexible structure because of the absence of the beams. The column can sustain with the vertical load but under lateral loads, the shear resistance of the column is becoming very low; thus, the punching shear failure can happen near the joint which can lead the partial or overall damage to the structure. Previously many researchers worked with this phenomenon as it made the structure more vulnerable.

Japanese Seismic Evalaution Standard:

This standard is intended to be used in the seismic evaluation and verification of seismic retrofitting of existing low- and medium-rise reinforced concrete buildings that have been seismically retrofitted. This evaluation and verification will take place in existing buildings. In accordance with this standard, three levels of screening procedures have been developed for the seismic evaluation: the first-level screening procedures, the second-level screening procedures, and the third-level screening procedures: screening processes at the first, second, and third levels respectively. It is acceptable to use any level of screening procedures provided that they are appropriate for the purpose of the evaluation and consider the structural characteristics of the structure that is the focus of the evaluation. In the absence of any other instructions to the contrary, the seismic evaluation should be carried out in accordance with the procedures outlined in the provisions and the commentary of this standard. It is also possible to use other methods for seismic evaluation that are based on the concept of this standard and have been proven through experimental data or detailed analyses to be equivalent to the methods of this standard.

Recently, Bangladesh adopted its seismic evaluation Manual, which called as CNCRP Manual (Public Works Department (PWD) 2015) based on the Japanese Standard. In the CNCRP Manual, second-level screening from Japanese standards was recommended based on some research through a joint Japan Bangladesh research project ((JICA) 2015). According to the Japanese seismic evaluation Guidelines, only vertical members are considered to evaluate existing buildings. But flat plate structural type is still out of scope in that CNCRP Manual, which was the limitation of this Manual.

Brief overview of Previous Researches:

The implementation of an effective and appropriate seismic retrofitting for existing buildings is required when the seismic performance of the existing buildings does not meet the required standards. This can be accomplished by increasing the strength or ductility of the structure. In the early stages of the research, shear strengthening was one of the first methods of preventing punching shear failure by increasing the deformability of the structure. The utilization of the shear reinforcement enhanced the punching shear capacity in the vicinity of the plate column joints. The use of drop panel is yet another alternative. By extending the column perimeter closer to the plate column joint, the drop panel is a conventional method that can increase the punching shear capacity. Many alternative methods have already been developed in the literature to improve the performance of existing flat plate structures. Among them, the most well-known retrofit technologies are adding post-installed shear bolts (Adetifa and Polak 2005; Bu and Polak 2009), post-installed shear reinforcement (Ghali et al. 1974; Mokhtar et al. 1985; Ruiz et al. 2010), post-installed punching shear reinforcement (Wörle 2014; Walkner et al. 2021), post-installed steel plate (Ebead and Marzouk 2002; Abbas and Hwee 2014; Elbakry and Allam 2015), CFCRP strip (Binici and Bayrak 2005; Durucan and Anil 2015), FRP strip (Lawler and Polak 2011a; Saleh et al. 2018; Jafarian et al. 2020), etc. Some of the past research studies are summarised the below:

Recently shear bolt retrofit methodology is becoming popular and adopted by many building code regulations such as (ACI 318-08 2008; BNBC 2020). The shear bolts retrofit method has been tested in the past on slab-column joints under static loads (El-Salakawy et al. 2003) and (Adetifa and Polak 2005). In those tests, the slab-column joints strengthened with shear bolts showed a significant increase in punching shear capacity and ductility. On the other hand, (Bu and Polak 2009) presented an experimental investigation on the seismic behavior of RC slab joints under increasing cyclic lateral drift and a constant gravity loading program. Three specimens were retrofitted using shear bolt while the other two were un-retrofitted. Shear bolts were installed externally in three specimens in holes that were drilled through the thickness of the slabs in the vicinity of the columns. The shear bolt and its installation system are shown in **Figure 1.4.1.** These shear bolts were used as transverse shear reinforcement. The details of the specimens are shown in **Figure 1.4.2**. Shear bolts are not used to reinforce the joints SW1 and SW5, but they are used to reinforce the joints SW2, SW3, and SW4 respectively. These shear bolts

are made of steel and have varying numbers of rows. The results of the tests revealed that shear bolts enhance the lateral load-resisting capacity of the slab column joints, as well as the lateral drift capacity at peak and ultimate loads, as well as the ductility of the slab column joints. Additionally, shear bolts transform the brittle failure mode of the slab-column joints into the ductile failure mode and increase the energy dissipation capacity of the structure. The test results and damage of the specimens are briefly showing in **Figure 1.4.3**.

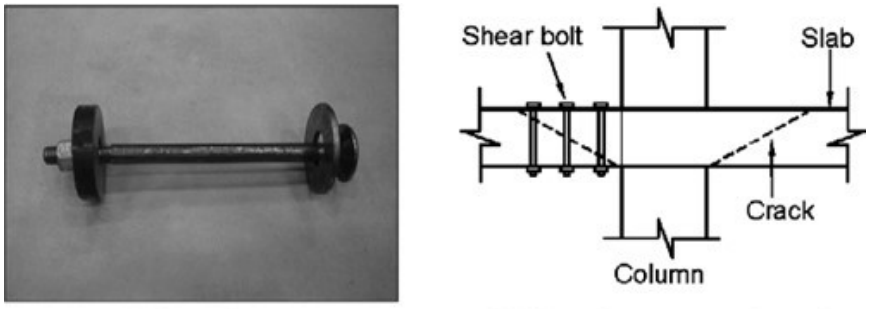

(a) Shear bolt *(b) Shear bolt installed in slab*

Figure 1.4.1 Shear bolt and its installation system (Bu and Polak 2009)

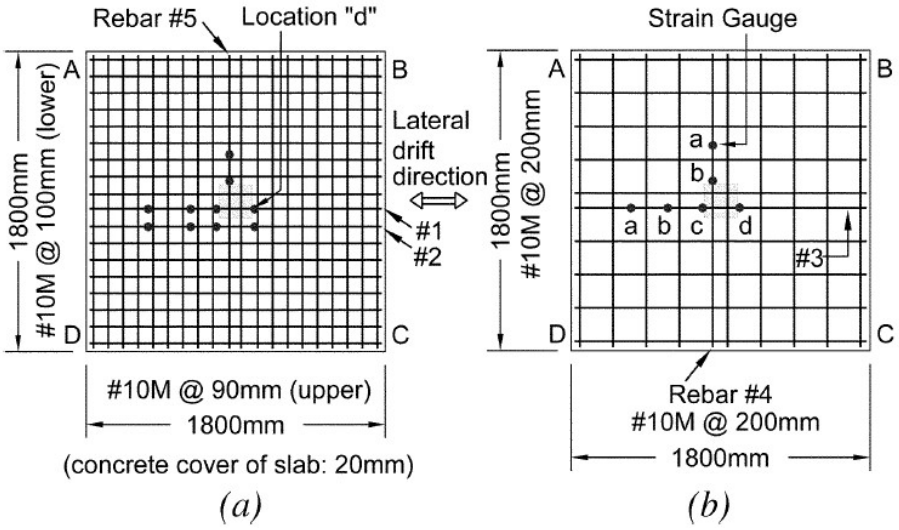

Figure 1.4.2 Specimen details(Bu and Polak 2009)

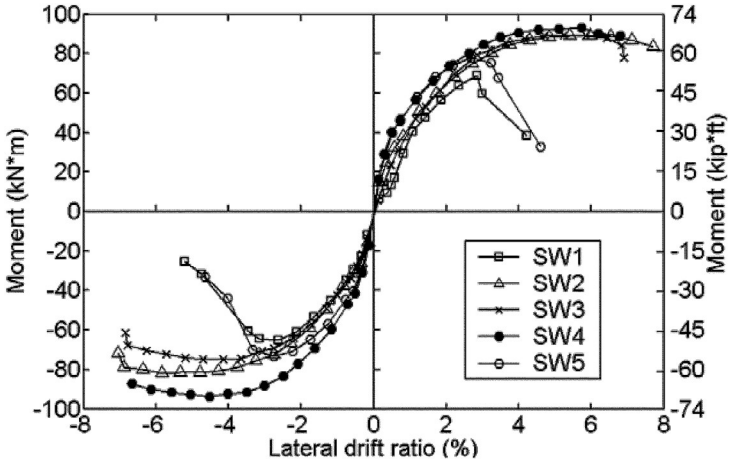

Figure 1.4.3 Backbone curve of the moment vs drift ration for all specimens (Bu and Polak 2009)

(Topuzi et al. 2017) performed an experimental study on the behavior of reinforced concrete slab-column connections that were retrofitted with a new type of shear reinforcement while being subjected to a combination of constant gravity loading and increasing cyclic lateral drift; the study was carried out in a laboratory setting. The testing program used six specimens: five specimens were retrofitted using steel bolts and flexible washers while one was retrofitted to compare with and without retrofitting. Four specimens were arranged that were strengthened with steel bolts and flexible washers had similar strength to the un-strengthened specimen and deformation capacity to the specimen retrofitted with steel bolts only, proving the efficiency of this shear retrofitting technique. The details of the specimen and loading program are shown in **Figure 1.4.4,** and the detailed configuration of the shear bolt is shown in **Figure 1.4.5.** According to the findings, this particular variety of shear reinforcement was able to enhance the lateral load-deformation response of the joints. As a result, the ductility is improved, but the stiffness and strength are not affected in the same proportion, as shown in **Figure 1.4.6.** However, the research was done based on moderate to high strength concrete. On the other hand, it was not improved the lateral resistance of the column, which is also important to strengthen the existing structure with the prevention of punching shear failure.

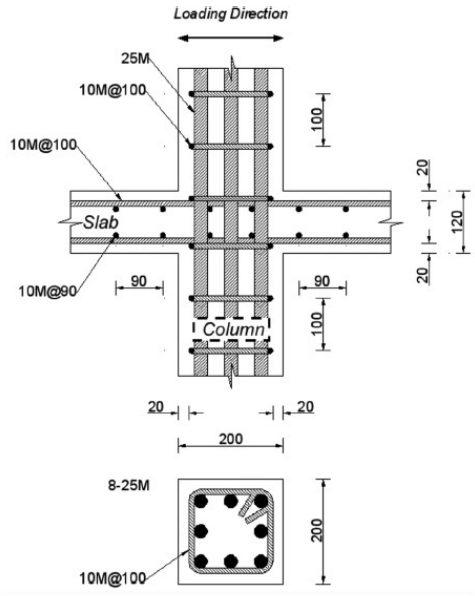

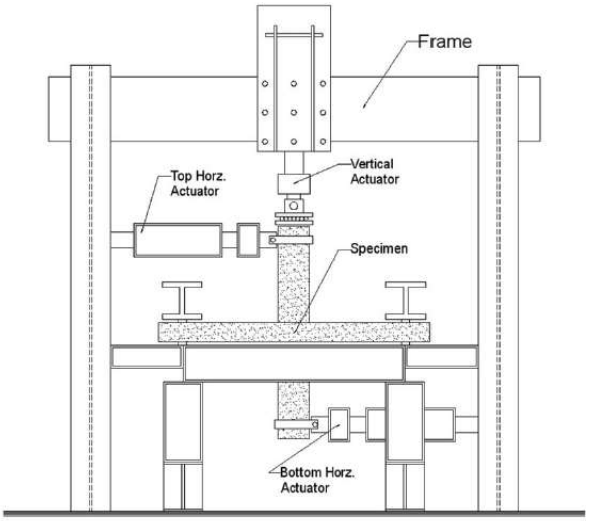

Details of slab and column reinforcement

Testing Loading frame

Figure 1.4.4 Details of the specimen and loading program (Topuzi et al. 2017)

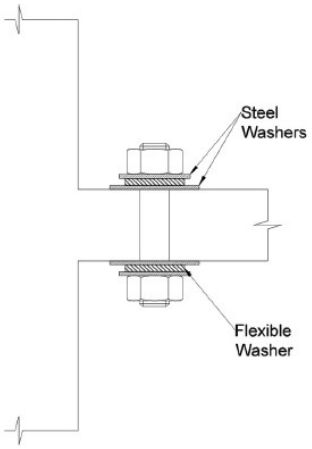

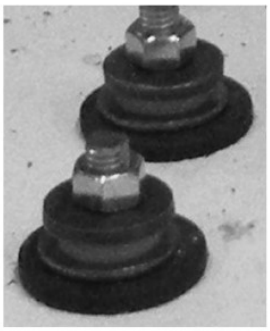

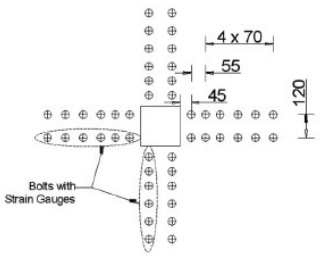

a) Schematic of steel bolt and washers assembly

b) Installed bolts assembly

c) Bolts plan configuration (4x2x6)

Figure 1.4.5 Detail configuration of the shear bolt (Topuzi et al. 2017)

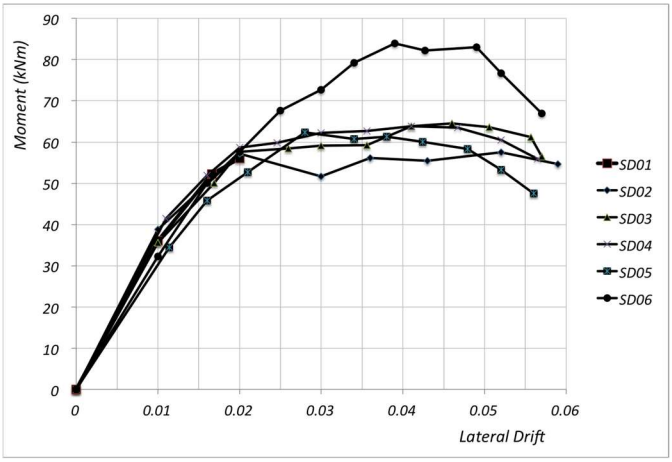

Figure 1.4.6 Moment vs drift angle relationship (envelop curves) for all specimens (Topuzi et al. 2017)

(Ruiz et al. 2010), proposed a new system that was suggested to solve most of the problems that have come up in the past is proposed and described in detail. This system is made up of two parts. The first is inclined shear reinforcement, which is put into existing slabs by drilling holes through the slab's soffit and bonding it with high-performance epoxy adhesive. **Figure 1.4.7** demonstrates the reinforcement of post-installed inclined shear reinforcement using the anchor with nuts and washers. An investigation into the idea of strengthening was carried out on 12 specimens with varying reinforcement ratios and shear strengthening arrangements in order to verify the concept. The testing setup and the layout of the post-installed inclined shear reinforcement are shown in **Figure 1.4.8**. Experimental data showed that the strength and deformation capacity of shear-reinforced slabs can be significantly improved when compared to those used without it. Finally, the critical shear-crack theory (CSCT) is used to design the reinforcement, which is discussed.

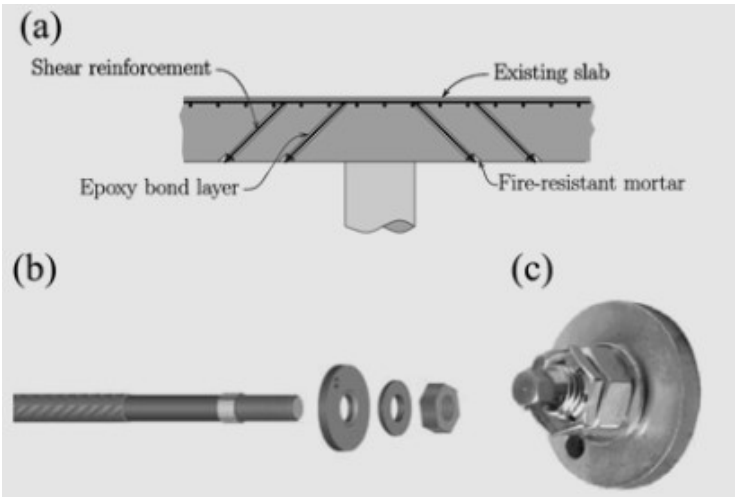

Figure 1.4.7 Reinforcing of post-installed inclined shear reinforcement using the anchor with nut and washers (Ruiz et al. 2010)

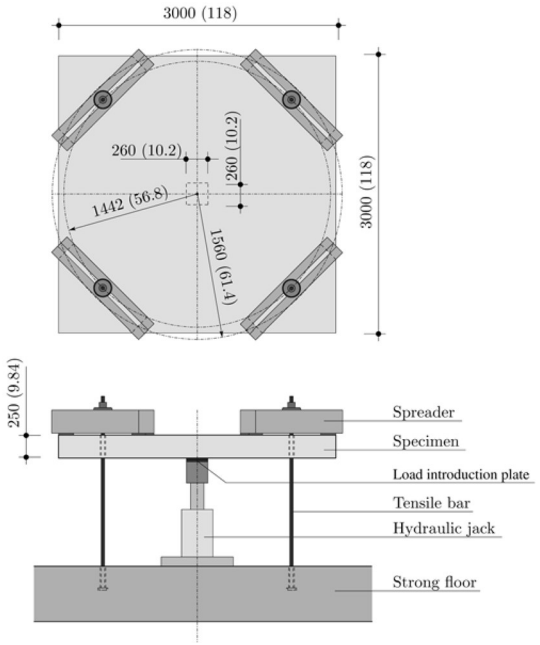

Testing Setup of the experimental program

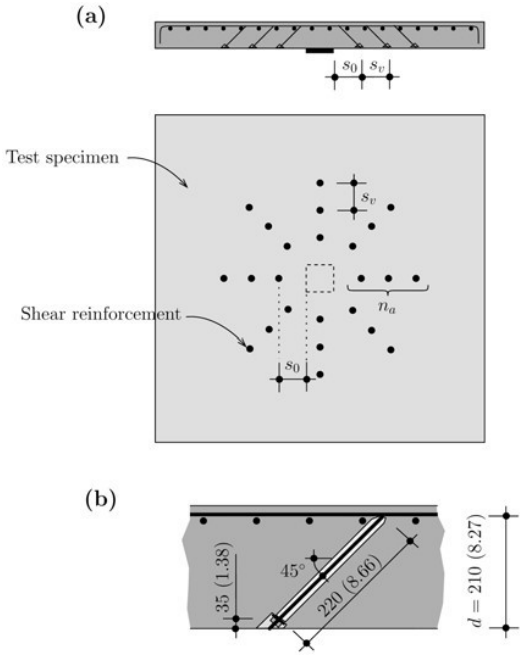

The layout of the post installed inclined shear reinforcement (a) the view of cross section and plan (b) dimension of shear reinforcement

Figure 1.4.8 The testing setup and the layout of the post-installed inclined shear reinforcement (Ruiz et al. 2010)

(Binici and Bayrak 2005) performed a study that presents the findings of an experimental program on upgrading reinforced concrete slab–column connections that were subjected to monotonic shear and unbalanced moment transfer. The connections were subjected to both monotonic shear and unbalanced moment transfer. The connections were tested under conditions where there was an unbalanced transfer of moment. This study presents the findings of an experimental program on upgrading reinforced concrete slab–column connections that were subjected to monotonic shear and unbalanced moment transfer. The connections were tested under conditions where there was an unbalanced transfer of moment. The experimental setup and specimen details are shown in **Figure 1.4.9**. Stirrups made of carbon fiber-reinforced polymer (CFRP), which were installed externally and acted as shear reinforcement around the slab–column connection area, were used in conjunction with two different patterns of CFRP arrangements. Shear reinforcement was not present in two of the four specimens, while carbon fiber reinforced plastic (CFRP) was used to strengthen the other two specimens. One control specimen (CC), without strengthening, was loaded concentrically, and the other (CE) was loaded eccentrically. It was decided to use patterns A and B of strengthening (details are provided in

Figure 1.4.10) with four CFRP perimeters, and the resulting specimens were designated with the names A4E and B4E, respectively. **Figure 1.4.11** depicts the behaviors of the test specimens with regard to the complete load versus the central deflection. It was discovered that the proposed method led to punching shear capacity increases of up to sixty percent in comparison to the specimen without any strengthening being applied. The use of carbon fiber reinforced plastics (CFRPs) as shear reinforcement was successful in preventing punching shear failure in some applications. The punching shear strength provisions of ACI 318-02 and yield line analyses for the test specimens were utilized to determine the capacities of the test specimens. In order to determine the capacities of the test specimens, punching shear strength provisions of ACI 318-02 and yield line analyses were used.

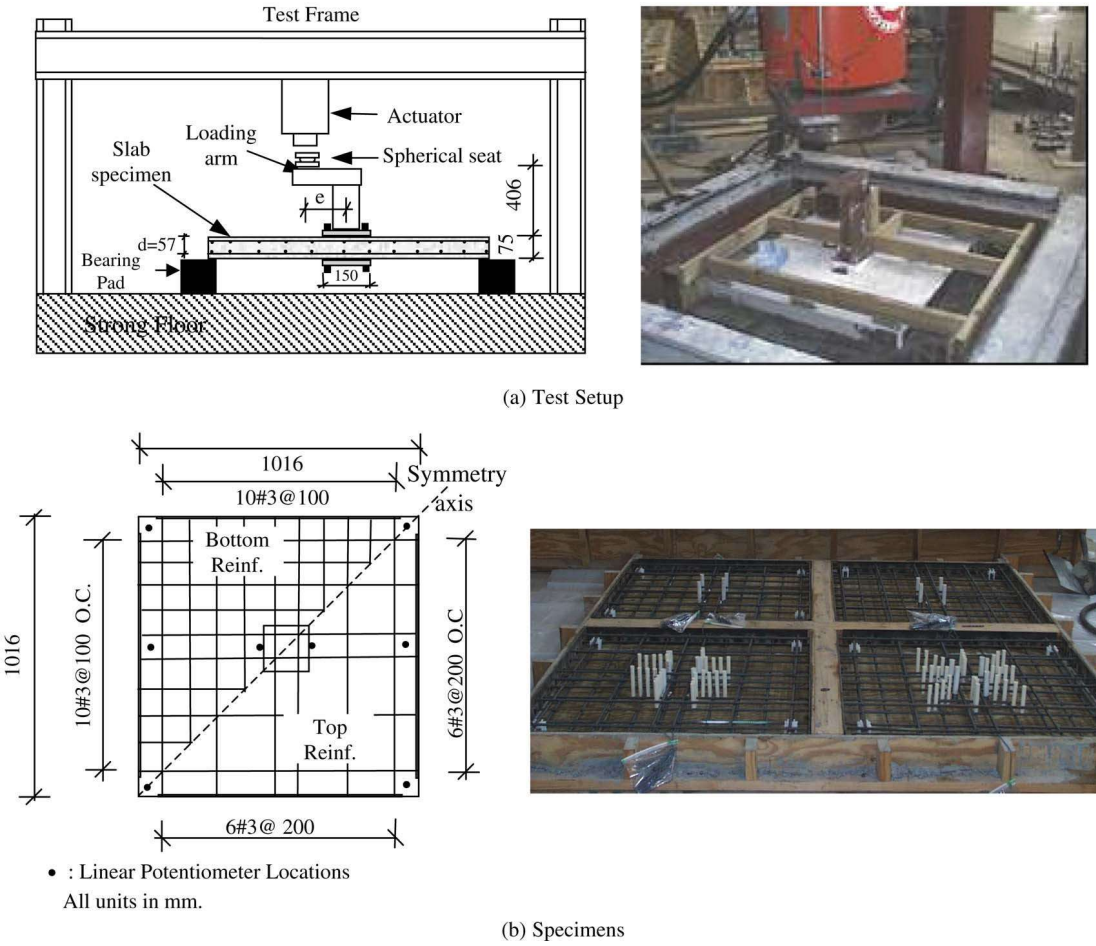

Figure 1.4.9 Setup of the experiments and details of the specimen using CFRP stirrups (Binici and Bayrak 2005)

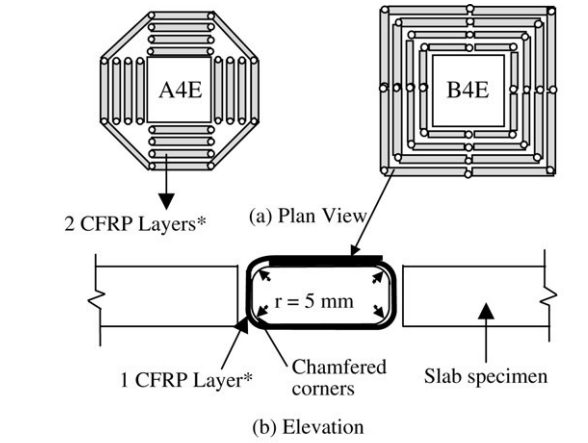

Figure 1.4.10 The external CFRP stirrups installation (Binici and Bayrak 2005)

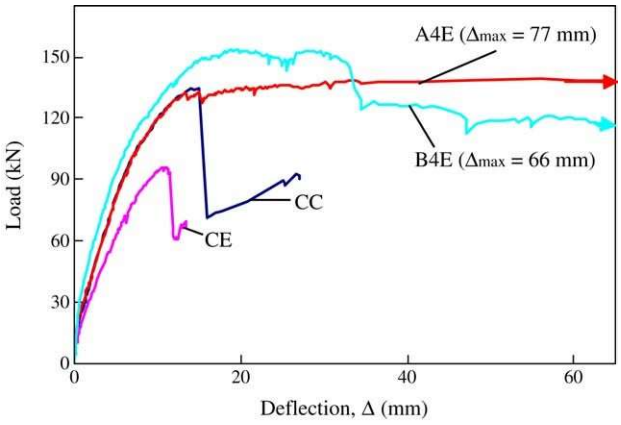

Figure 1.4.11 The load vs deflection behavior of the specimens using CFRP stirrups (Binici and Bayrak 2005)

In 2008, Lawler (Lawler and Polak 2011b) conducted experiments on slab-column connections that were strengthened with shear bolts made of glass fiber-reinforced polymer (GFRP). He concluded that fiber-reinforced plastic (FRP) could be a useful reinforcement material for the retrofit of slab-column joints against punching shear failure subjected to static and seismic loadings. In comparison to the slab-column joints (Bu and Polak 2009) tested that were retrofitted with steel bolts, the FRP connections demonstrated a lower level of strength; however, they also demonstrated less pinching, which led to a higher level of energy dissipation. This occurred because the GFRP bolts were not secured against the slab surface with an adequate level of tightness. This made it possible for cracks to open up within the slab, and the friction that developed between the crack faces as a result of the cyclic loading led to a greater loss of energy. The formation of cracks was another factor that contributed to a weaker connection overall compared to those that were reinforced with steel bolts.

(Ebead and Marzouk 2002) Ebead and Marzouk presented a method for strengthening two-way slabs by utilizing steel plates and steel bolts. The efficiency of two distinct arrangements of steel plates as well as four distinct configurations of steel bolts was analyzed and compared. Around the column, the reinforcing steel plates were extended to a depth that was twice as deep as the slab, and they acted as a drop panel with a concrete depth that was equivalent. The use of steel bolts was implemented in order to provide vertical shear reinforcement. It was sufficient to use only eight bolts in order to transfer the horizontal forces from the steel plates to the concrete, as well as to the confining concrete that was sandwiched between the steel plates. The specimens were loaded with 50% of the control's ultimate failure load, then released. This stage represents a damaged slab in an existing building that must be strengthened by removing live loads and jacking. On the other hand, a specimen was moved away from the loading frame. After strengthening and curing, the specimens were loaded with a central concentric load until failure. Five specimens were tested where C acted as the control specimen and A1 to A4 were strengthened using different configurations as shown in **Figure 1.4.12**. A layout of the strengthened plate is shown in **Figure 1.4.13**. The reinforced slabs demonstrated an increase in both their stiffness and their capacity to absorb energy. In addition to that, the ductility was enhanced to a small degree. The control specimen's load-carrying capacity was increased by 56.55, 57.76, and 64.56 percent when compared to that of the strengthened slabs, which had slabs that had eight, 12, and 16 bolts, respectively, as shown in **Figure 1.4.14**. The findings of this study present a concept for strengthening that can be utilized to strengthen two-way slabs in multi-storey structures. The test results were very consistent with the findings of a straightforward method that was founded on the yield line theory.

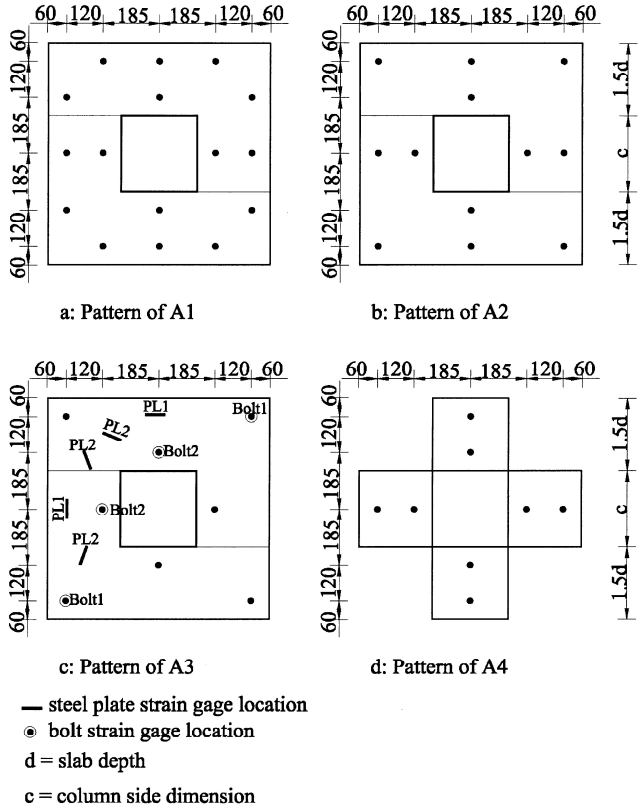

Figure 1.4.12 The configuration of bolt and pattern of the steel plate (Ebead and Marzouk 2002)

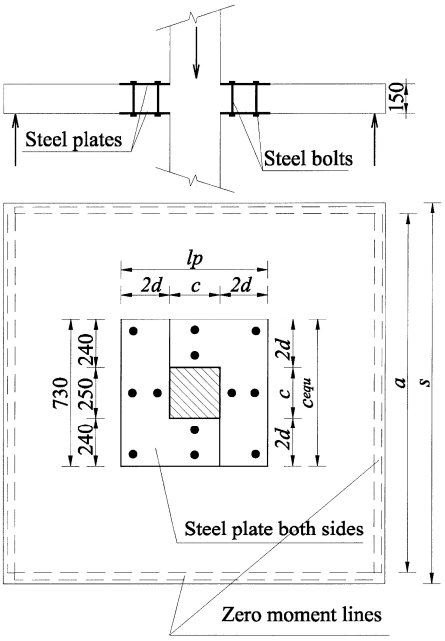

Figure 1.4.13 The layout of the strengthened plate (Ebead and Marzouk 2002)

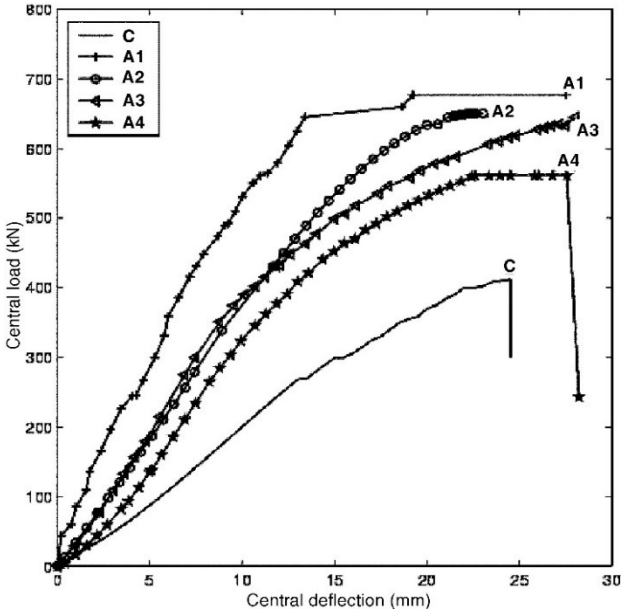

Figure 1.4.14 The load vs drift relationship of the tested specimens (Ebead and Marzouk 2002)

In the research that has been done on flat plate systems, a wide variety of different strengthening techniques have been presented. Nonetheless, because of the complexity of the work, material supply, and low cost of human resources, modern retrofitting techniques are frequently difficult to implement in developing countries. Furthermore, there is little to no guidance for strengthening flat plate structures built with low-strength concrete, which must perform not only to ensure the performance of flat plate-column connections but also to increase the lateral resistance of the entire structure. The majority of the earlier studies concentrate their attention primarily on reducing the risk of punching shear failure behind the lateral resistance of the column to improve seismic performance. Aside from that, the research is quite limited when it comes to low-strength concrete under seismic loading conditions, with a particular emphasis on developing countries, and when it comes to increasing the lateral resistance of columns. In order to improve the overall performance of the structure, developing countries should think about ways to boost the lateral resistance of independent columns that are already in place. Thus, this research, conducted a couple of experimental series to investigate the seismic performance of existing flat plate-column connections following the seismic strengthening scheme using wing walls and drop panels. In addition, the behavior of RC flat plate-column connections built with low-strength concrete and subjected to the proposed strengthening method was investigated. The purpose of the wing wall retrofit method is to improve the seismic performance of existing buildings by transforming the independent columns into columns that are equipped with wing walls. Previously, an improvement in the performance of the connections under seismic loading conditions was verified after this wing wall installation scheme was applied to substandard beam-column joints (Li and Sanada 2017; Li et al. 2019;

Wardi et al. 2020). As mentioned in the literature, the application of RC wing walls in developing countries is relatively easy and cost-effective. On the other hand, although the drop panel is a conventional method for preventing punching shear failure; however, in this study, its effectiveness was investigated with low-strength concrete under seismic loading conditions using post-installed bonded anchors. Buildings that do not need additional lateral resistance of the column but do need to resist the punching shear failure under deformability of the structure are good candidates for the post-installed drop panels. These panels will be effective in meeting this requirement due to their construction simplicity and cost-effectiveness.

1.5 Research Objectives

The main objective of this study is to propose a methodology to evaluate the seismic performance of flat plate structures often found in Asian developing countries such as Bangladesh and to introduce two retrofit schemes for seismic up-gradation. Therefore, as an initial effort, the authors conducted a couple of experimental series to investigate the seismic performance of the existing flat plate-column joint and strengthening with wing walls and drop panel. We proposed a simplified seismic evaluation methodology with its strengthening schemes based on the experimental findings. In the course of the research process, several stages were carried out as follows:

1. To perform experimental investigations on an interior flat plate-column joint constructed using low-strength concrete that is often found in Bangladesh for the identification of the essential characteristics of existing flat plate column joints.
2. To conduct experimental investigations on strengthening an interior flat plate-column joint using post-installed RC wing walls for the feasibility of its effectiveness with the application.
3. To carry out experimental research on the subject of strengthening an interior flat plate-column joint using post-installed RC drop panel, with the goal of determining the feasibility of its effectiveness with the application.
4. To introduce a simplified seismic evaluation methodology for flat plate structures, based on the experimental investigation, simulating the low-strength concrete that is typically used in Bangladesh.
5. To introduce a seismic retrofit strategy for flat plate structures based on the experimental investigations using the abovementioned post-installed wing wall and drop panel.
6. Application of the proposed seismic evaluation and retrofit methodology to a flat plate building located in Dhaka to illustrate how the seismic evaluation of existing buildings and its retrofit strategy can be applied

1.6 Outline of the thesis

This thesis consists of seven chapters organized as follows.

Chapter 1 presents the background, scope, literature review regarding the seismic evaluation and past retrofit strategy, and objectives of this research. This chapter also contains a brief introduction of the outline of each chapter.

Chapter 2 discusses the experimental investigations on a series of two half-scaled interior flat plate-column joints constructed using low-strength concrete often found in Bangladesh. Through this experimental study, the basic characteristics of existing flat plate column joints were identified. In addition, low-strength concrete was used because it is often found in Bangladesh, which leads to the vulnerability of the existing buildings. This chapter briefly explains the effect of low-strength concrete and how to evaluate the punching shear capacity when the existing building is constructed using low-strength concrete.

Chapter 3 discusses the experimental investigations on a series of two half-scaled interior flat plate-column joints strengthened using wing walls. This experimental study investigated the effectiveness and feasibility of post-installed wing walls. Wing walls were attached along the longitudinal direction for one specimen, while the direction was along with the transverse direction for the other specimen. The post-installed RC wing walls enlarged the critical section of the column, which increased the punching shear resistance resulting in an increase in the lateral resistance. The design concept of a critical section was introduced through this study.

Chapter 4 discusses the experimental investigations on a series of three half-scaled interior flat plate-column joints strengthened using drop panel. This exploratory study investigated the effectiveness and feasibility of a post-installed drop panel as a strengthening scheme. The ultimate objective of installing drop panel is to prevent brittle punching shear failure by expecting ductile flexure of the plate. This experimental study was principally conducted to examine whether the drop panel's size was adequate with enough anchorage connected with the existing structures made with low-strength concrete.

Chapter 5 introduces a simplified seismic evaluation methodology for flat plate structures, based on the experimental investigation described in chapter 2, simulating the low-strength concrete commonly used in Bangladesh. Based on the experimental investigations, the Japanese seismic evaluation procedure was modified to include the flat plate structure in the scope of application. The evaluation procedure was proposed based on the Japanese seismic evaluation method with simplified modifications in calculating *C*-index and *F*-index. The proposed seismic evaluation procedure was

applied to an example building to illustrate how the seismic evaluation strategy of existing buildings can be applied.

Chapter 6 introduces a seismic retrofit methodology for flat plate structures using wing walls and drop panels based on the experimental investigations described in chapters 3 and 4. A significant number of flat slab buildings require seismic strengthening against punching. There are various reasons for this, including design or construction errors, poor quality materials, failure to comply with new code provisions, and an increase in vertical load. Therefore, some appropriate strengthening techniques should be implemented to minimize the probability of this type of brittle structural failure. Based on the experimental findings a retrofit strategy for flat plate structure is introduced. The proposed seismic retrofit procedure was applied to an example building to illustrate how the seismic retrofit strategy of existing buildings can be applied.

Finally, Chapter 7 summarizes the findings of this research and presents the conclusions of this research. Moreover, further research needs related to the seismic evaluation and strengthening of flat plate structures and the limitation of this investigation were recommended.

CHAPTER 2

Experimental Study on an Interior Flat Plate-Column Joints Using Low-strength Concrete

2.1 General

This chapter explains experimental investigations on seismically vulnerable existing RC interior flat plate-column joints, considering low-strength concrete. Experimental research on a series of two half-scaled interior plate-column joints was conducted to explore the characteristics of the existing flat plate structure and analyze the joints' punching shear capacity. It focuses on typical existing flat plate structures that are constructed using low-strength concrete and are commonly found in Bangladesh. The two specimens were investigated in two countries with identical dimensions using local materials with different concrete strengths. The first specimen, FP-1, was investigated in Japan, while the other specimen, FP-2, which was investigated in Bangladesh, simulated low-strength concrete. Static cyclic vertical displacements with increasing amplitude were applied to the ends of the slabs to represent inter-storey drift under seismic action. The experimental results will be an excellent source to calibrate the seismic performance and behavior of existing flat plate buildings, representing the most vulnerable conditions in Asian developing countries like Bangladesh.

2.2 Target Building of Interests

This study focuses on an interior flat plate-column connection representing the subassembly of a typical prototype structure, as shown in **Figure 2.2.1**. The span and thickness of the flat plate were 6 m between the two columns and 150 mm, respectively. The target building is one of the typical flat plate structures constructed using low-strength concrete in Bangladesh, which is extremely vulnerable to seismic action compared to similar structures in other Asian countries because of the use of brick chips as coarse aggregates and inappropriate construction management. Brick aggregate concrete was applied to the test specimens to simulate low-strength concrete, representing existing vulnerable building conditions. **Figure 2.2.2** presents the result of the compressive strength test performed on a drilled concrete core obtained from an existing building in Dhaka city. The concrete core sample was collected to identify an approximation of the measurement of low-strength concrete. Thus, a concrete strength of approximately 7 N/mm^2 was used to design the test specimen of FP-1. Similar low-strength concrete with a compressive strength lower than 10 N/mm^2 is common ((JICA) 2015; Public Works Department (PWD) 2015; Wardi et al. 2020). Thus, a concrete strength of approximately 10 N/mm^2 was used to design the test specimens of FP-2. It was intentionally designed the concrete strength around 7-10 N/mm^2 to identify and compare the basic characteristics of existing plate column connections under

seismic loading conditions. The variation of concrete strength possibly may give a better recommendation for identifying the existing capacity.

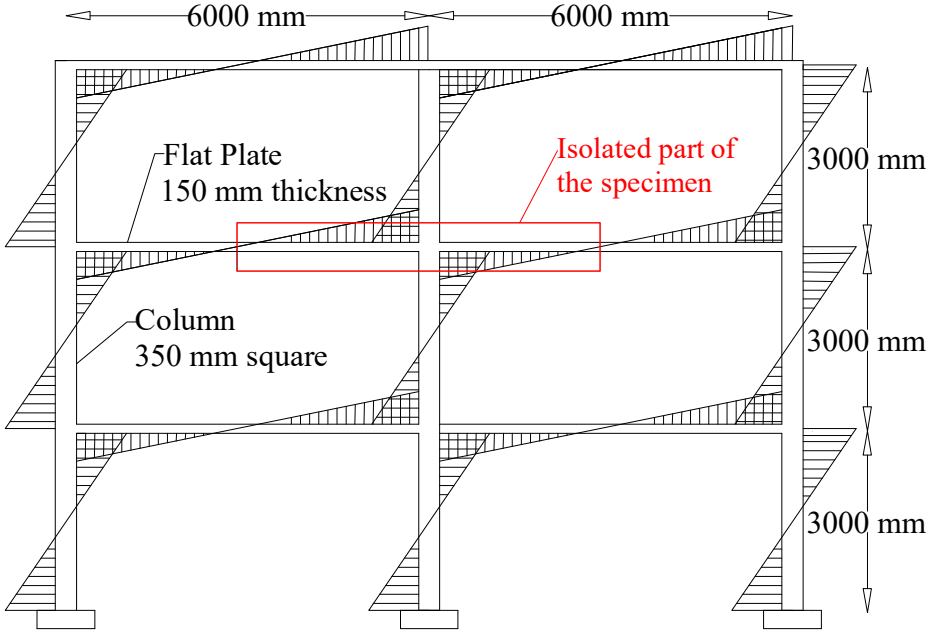

Figure 2.2.1 Building of interest: Focused flat plate-column joint

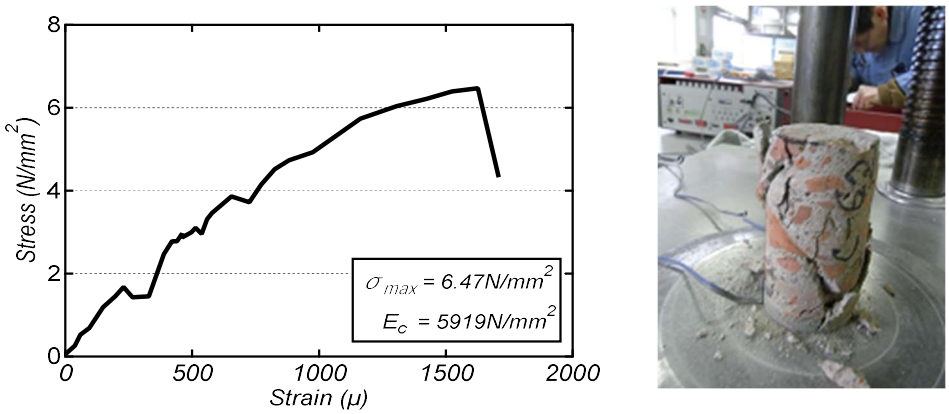

Figure 2.2.2 The typical result obtained from the test performed on a cylinder core

2.3 Specimen design/details

Experimental research on a series of two half-scaled interior flat plate-column joints was conducted mainly to investigate the seismic capacity of existing connections with low-strength concrete. These specimens can be regarded as part of a prototype structure in which the flat plate spans 6m between columns to columns, as shown in **Figure 2.2.1**. The slab thickness is 150 mm. The specimens represent interior plate-column connections which are isolated specimens with dimensions corresponding to the lines of contra flexure under vertical loads. The dimensions of both specimens

were the same, except for some of their reinforcing detailing because the specimens were constructed and tested in two different countries considering local materials.

2.3.1 *Specimen FP-1*

The specimen FP-1 was constructed and tested at Daido University concrete structure lab, Japan. **Figure 2.3.1** shows the details of the specimen. The plate dimensions were 1500 mm × 1100 mm × 75 mm in length × width × thickness and based on a model at half scale. Two layers of deformed bars with a nominal diameter of 6 mm were arranged for the plate at a spacing of 75 mm in the longitudinal and transverse directions. The column was located at the centroid of the plate with a cross-section of 175 mm × 175 mm. In total, eight 16 mm deformed bars were arranged as the main reinforcement, and 6 mm deformed bars with 135° hooks were provided at a spacing of 50 mm for shear reinforcement in the column. However, no column shear reinforcement was provided to the plate-column connections. A column bottom stub with dimensions of 400 mm × 400 mm × 300 mm in width × depth × height, respectively, was constructed with the existing structure to ensure perfect fixing with the loading frame.

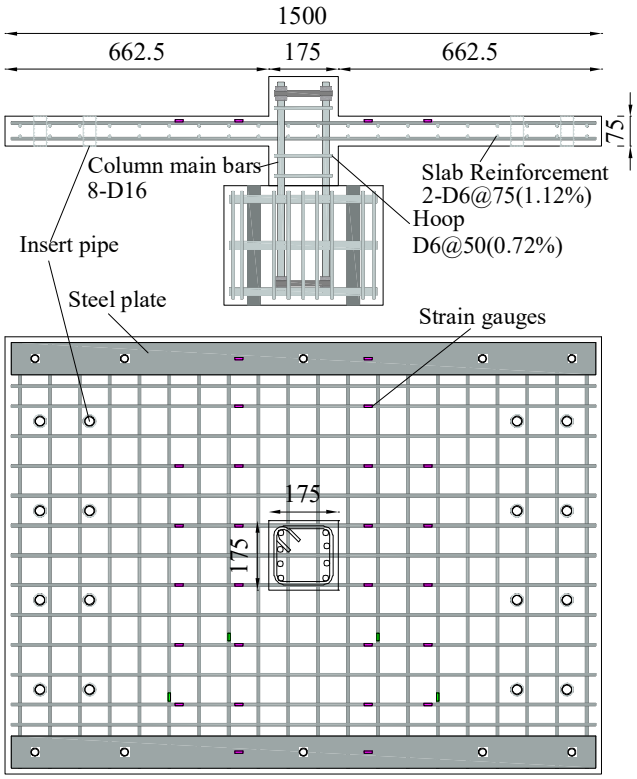

Figure 2.3.1 Details of the specimen FP-1

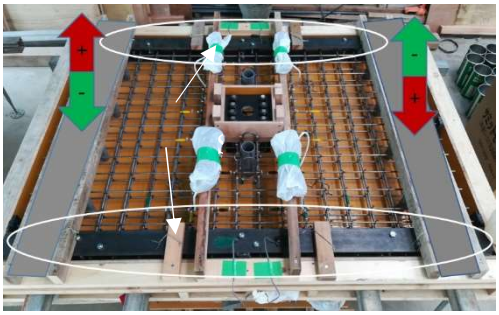

Figure 2.3.2 Placement of steel plates



Figure 2.3.3 Installation of studs

Moreover, two steel plates having a thickness of 6 mm and width of 80 mm (SS400 steel plate: according to the Japanese Industrial Standard (JIS)) were embedded on the top and bottom surfaces on both sides of the plate, as shown in **Figures 2.3.2** and **2.3.3**, to increase the flexural strength of the plate, resulting in prior punching shear failure. Ten studs with a diameter of 8 mm were installed on the steel plates for better integration between the steel plates and concrete, as shown in **Figure 2.3.3**. As a result, the designed ultimate flexural strength of the plate was sufficiently higher than the designed punching shear strength. In specimen FP-1, steel plates were used to ensure the punching shear failure before other failures.

2.3.2 *Specimen FP-2*

The specimen FP-2 was constructed in Bangladesh using local materials to represent actual Bangladeshi conditions. **Figure 2.3.4** shows the specimen details. The plate measurements were 1500 mm x 1100 mm x 75 mm in length, width, and thickness, respectively, considering the half-scaled specimen. For the plate with double layers, deformed bars with a nominal diameter of 8 mm were arranged with a spacing of 125 mm in both the longitudinal and transverse directions. The column was positioned with a cross-section of 175 mm square on the center of the plate. As column main reinforcement, 4-D16 and 4-D20 deformed bars were arranged, and 8 mm deformed bars with 90º hooks with 50 mm spacing were used for shear reinforcement in the column. There is no shear reinforcement placed on the slab near the plate-column joint. The reinforcement detailing couldn't keep the same as specimen FP-1 due to the unavailability of the D6 rebars in Bangladesh. As a result, the spacing between rebars is varies from that of specimen FP-1, but the reinforcement ratio is the same.

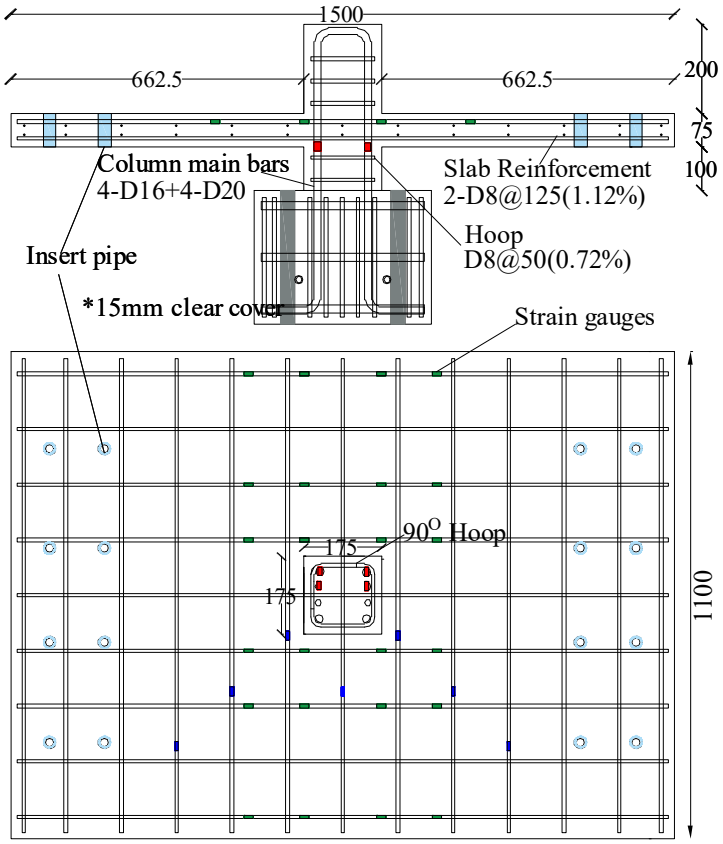

Figure 2.3.4 Details of the specimen FP-2

2.4 Material mechanical properties of concrete and steel

2.4.1 *Specimen FP-1*

The concrete mixture was designed based on a target concrete compressive strength of 7 N/mm^2, which was derived from the compressive strength of low-strength concrete commonly found in Bangladesh (**Figure 2.2**). Portland cement was used with mountain sand acting as fine aggregate and brick chips acting as coarse aggregate with a maximum aggregate size of 15 mm was used to simulate the low-strength concrete characteristics used in Bangladesh for the existing parts of the specimens. A cement and $CaCO_3$: sand: brick chips volumetric ratio was designed as 1 (=0.7+0.3): 2: 4. However, 30% of the cement was replaced by $CaCO_3$ to reduce the concrete strength. The ratio of water to the sum of cement and $CaCO_3$ was 60%. **Table 2.1** lists the concrete mixture by weight for the existing parts of the specimens. The concrete used for the existing parts was mixed in a mixing machine. The casting of the specimens was conducted in two phases. In the first phase, the bottom stub was cast by using ready-mixed concrete. In the second phase, the slab and column (existing structure) were cast using a concrete mixer machine in the laboratory after 1 week of finishing the first phase. A normal ready-mixed concrete with a design strength of 30 N/mm^2 with stone chips acting as coarse aggregates with a maximum size of 15 mm was used for the bottom stubs.

Concrete cylinders were prepared from the same concrete mixtures used during the casting of concrete into the specimens. According to the Japan Industrial Standards (JIS), concrete strength and elastic modulus were obtained through standard cylinder tests. For specimen FP-1, 3 concrete cylinder samples were obtained. The average properties of concrete determined from the cylindrical compression tests are listed in **Table 2.2.** The steel grades used in this study were SD295 (deformed rebar with a nominal yield stress of 295 N/mm^2) for the D6 reinforcement and SD345 (deformed rebar with a nominal yield stress of 345 N/mm^2) for the D16 reinforcement. The average material properties of the reinforcements determined from the tensile tests are listed in **Table 2.3**.

Table 2.1 Concrete mixture in kg/m^3

	W/(cement + $CaCO_3$)	Water	Cement	$CaCO_3$	Sand	Brick
FP-1	60%	212	248	88	596	959

Table 2.2 Material properties of concrete

Type	Compressive strength (N/mm^2)	Elastic modulus (N/mm^2)	Strain at compressive strength (μ)
FP-1	6.93 (brick chips)	8450	1829

*Elastic modulus is defined by $E = (F_c/3\text{-}f_2)/(\varepsilon_1\text{-}\varepsilon_2)$

(E: elastic modulus; F_c: compressive strength of concrete; f_2: stress at 50x10^{-6} strain; ε_1; strain at $F_c/3$; ε_2: 50x10-6 (JISA 1149 2010)

Table 2.3 Material properties of steel

	Type	Cross section of Bar (mm^2)	Yield stress (N/mm^2)	Elastic modulus (kN/mm^2)	Tensile strength (N/mm^2)
FP-1	D6 (D295A)	28.27	346	185	517
	D16 (SD345)	201.06	432	245	566

2.4.2 *Specimen FP-2*

Bangladeshi local materials were used for constructing this specimen. The target of the concrete compressive strength for the test specimens was designed as 10 N/mm^2. Ordinary Portland cement was used with locally called Sylhet sand as fine aggregates and brick chips as coarse aggregates with a

maximum aggregate size of 15 mm to simulate the low-strength concrete in Bangladesh. The average properties of the concrete from the cylindrical compression tests are summarized in **Table 2.4**. In order to simulate the low-strength concrete used in Bangladesh, brick chips were used as coarse aggregate for the specimen construction. **Table 2.5** shows a concrete mixture by weight. A cement and vita sand: sand: brick chips volumetric ratio was designed as 1(0.8: 0.2): 2: 4, where 20% of cement was replaced by vita sand to reduce the concrete strength considering practice in Bangladesh. Locally called vita sand is finer in size; FM varies from 0.8 to 1.2. In Bangladesh, many older buildings were constructed using Vita sand as fine aggregate (another name is local sand). The ratio of water to the sum of cement and vita sand was 60%.

The grades of steel were 400W (deformed rebar with the nominal yield stress of 400 N/mm^2) for D8 reinforcement and 500W (deformed rebar with the nominal yield stress of 500 N/mm^2) for D16 and D20reinforcements, respectively. The averaged material properties of reinforcement from the tensile tests are shown in **Table 2.6.**

Table 2.4 Material properties of concrete

Type	Compressive strength (N/mm^2)	Elastic modulus (N/mm^2)	Strain at compressive strength (μ)
FP-2	11.3 (brick chips)	17053	1899

*Elastic modulus is defined by $E = (F_c/3\text{-}f_2)/(\varepsilon_1\text{-}\varepsilon_2)$

(E: elastic modulus; F_c: compressive strength of concrete; f_2: stress at 50x10^{-6} strain; ε_1; strain at $F_c/3$; ε_2: 50x10-6 (JISA 1149 2010)

Table 2.5 Concrete mixture in kg/m^3

W/(cement + vita sand)	Water	Cement	Vita sand	Sand	Brick
60%	212	283	62	596	960

Table 2.6 Material properties of steel

	Type	Cross section of Bar (mm^2)	Yield stress (N/mm^2)	Elastic modulus (kN/mm^2)	Tensile strength (N/mm^2)
FP-2	D8 (400W)	50.27	407	267	537
	D16 (500W)	201.06	561	202	670
	D20 (500W)	314.16	556	212	675

2.5 Loading and Measurement Methods

2.5.1 *Experimental setup of the specimen*

A schematic view of the experimental setup of the flat plate specimen is shown in **Figure 2.5.1**. The specimen FP-1 was tested using a static loading system in the concrete structure laboratory at Daido University, while FP-2 was tested in the Housing and Building Research Institute (HBRI) laboratory. A bottom stub supported the plate and column and was bolted to the base beam of the loading frame. Various continuous measurement systems, including load cells, linear variable differential transducers (LVDTs), and strain gauges, were implemented to extract the data. The loading system, which was supported by the top beam of the loading frame, consisted of two vertical jacks with a capacity of 500 kN each. The jacks were connected to the ends of the plate via steel channels (125 × 65 × 12). Thus, the loads were uniformly distributed to the plate ends through the channels. Additionally, two load cells (300 kN capacity each) were installed in the vertical jacks to measure the absolute applied loads on the specimens. The vertical jacks were manually controlled using hydraulic pumps, so that drift could be controlled easily. **Figure 2.5.2** shows the photograph of the loading setup during the experimental investigation.

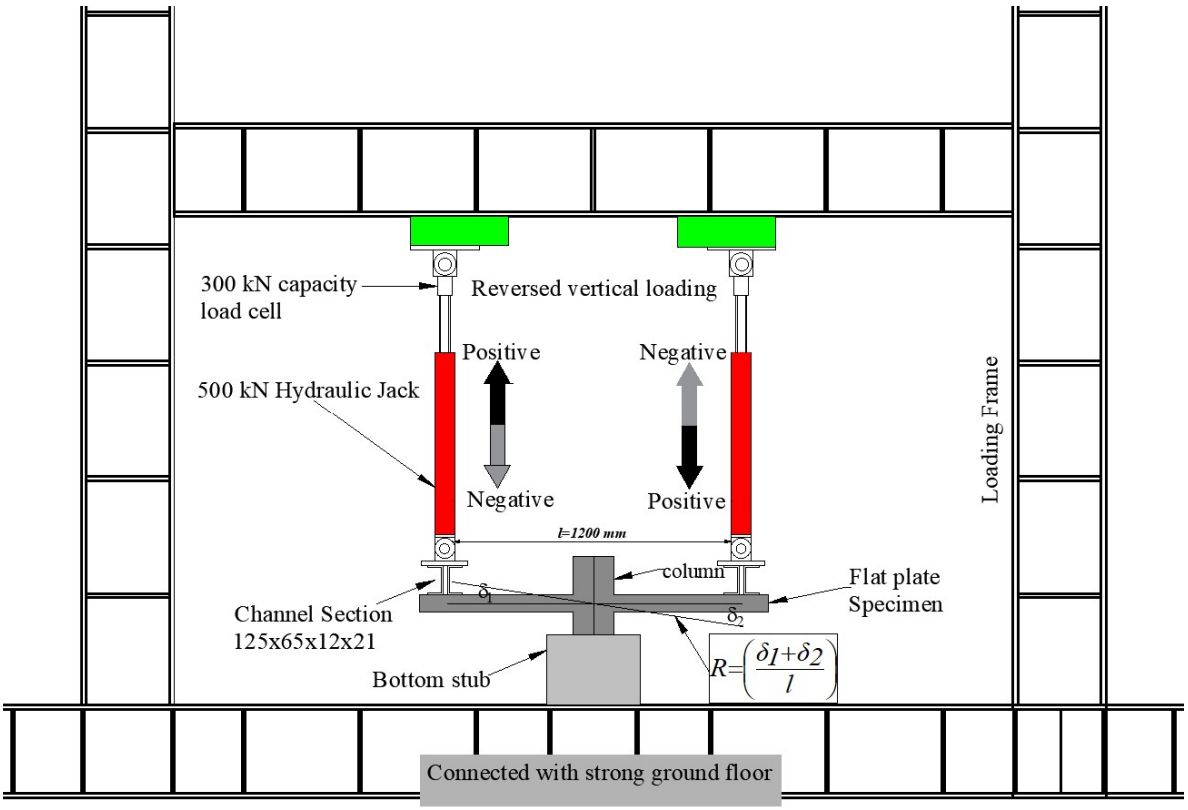

Figure 2.5.1 Loading setup of the experimental program

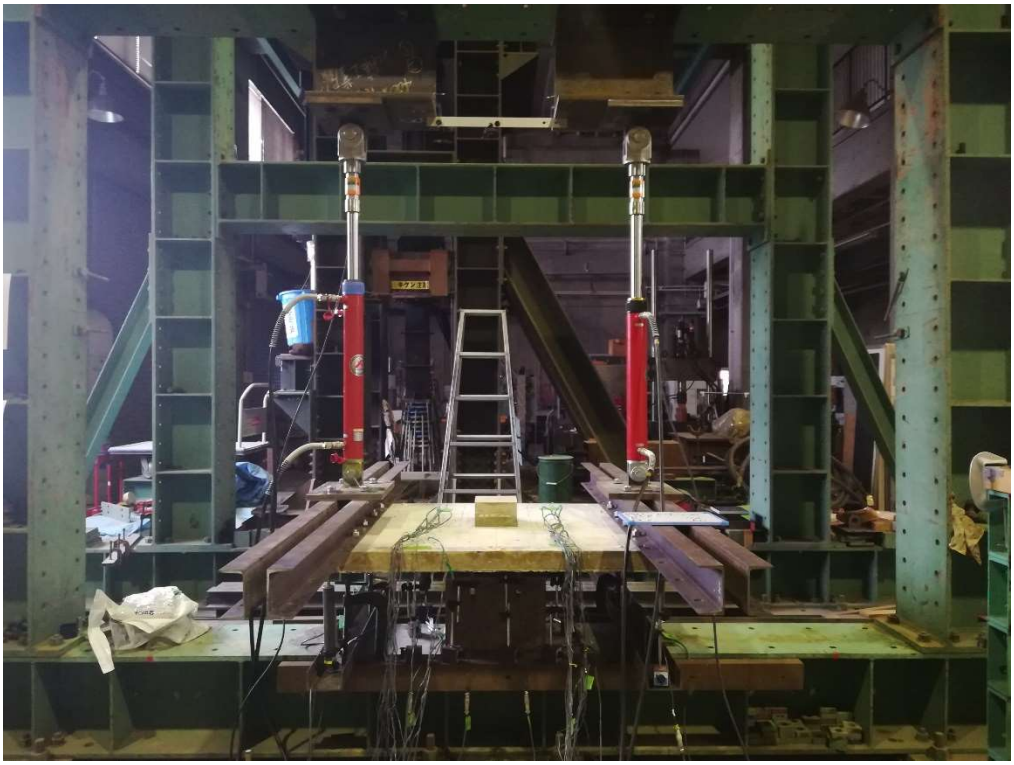

Figure 2.5.2 Photograph of the loading setup during the experiment

Vertical reversed cyclic loads with increasing amplitude were applied to the plate ends, which represented the bending moment distribution near the plate and column junction under earthquake loading (refer to **Figure 2.5.1**). The hydraulic jacks were manually operated so that the displacements δ_1 and δ_2 shown in **Figure 2.5.3,** were almost equal at each step of the loading process during the experiment. The loading of the specimen was given using two vertical hydraulic jacks in the following manner: the right hydraulic jack pushed the specimen while the left hydraulic jack pulled simultaneously during the positive loading direction, and the right hydraulic jack pulled the specimen while the left hydraulic jack pushed simultaneously during the negative loading direction. Four CDP-100 (D1, D2, D15, and D16) LVDTs were installed underneath the four corners of the plate for deflection measurements, as shown in **Figure 2.5.3**. Loading was controlled by the drift angle *R,* which was defined by Equation (1) (also refer to **Figure 2.5.3**):

$$R = \left(\frac{\delta_1+\delta_2}{l}\right) = \{\frac{(D_1+D_2)/2+((D_{15}+D_{16})/2)}{l}\}. \qquad \textbf{(2.5.1)}$$

The symbols used in this equation are defined in the LVDT setup shown in **Figure 2.5.3**, where δ_1 and δ_2 are the drift angle on the right and left sides of the plate, respectively; *l* is the distance between the loading points on both sides of the plate; D1, D2, D15, D16 are the displacements at designated points.

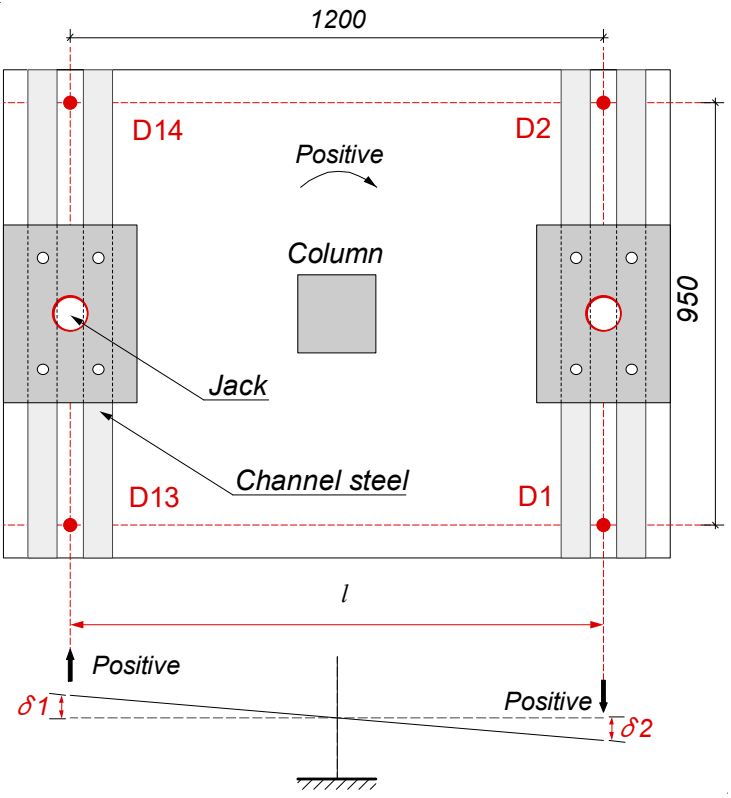

Figure 2.5.3 Position of LVDT and definition of *R*

The loading protocol with one cycle for each incremental amplitude was applied to the specimen, as illustrated in **Figure 2.5.4**. The loading cycle started from an initial cycle of R = 0.0167% rad, followed by one cycle of each in both positive and negative loading of R = 0.025% rad, 0.033% rad, 0.05% rad, 0.1% rad, 0.167% rad, 0.25% rad, 0.33% rad, 0.5% rad, 0.667% rad, 1.0 % rad, 1.33% rad, 1.67% rad, 2% rad, 2.5% rad, 3.3% rad, 4.17% rad and 5.0% rad, as shown in following figure.

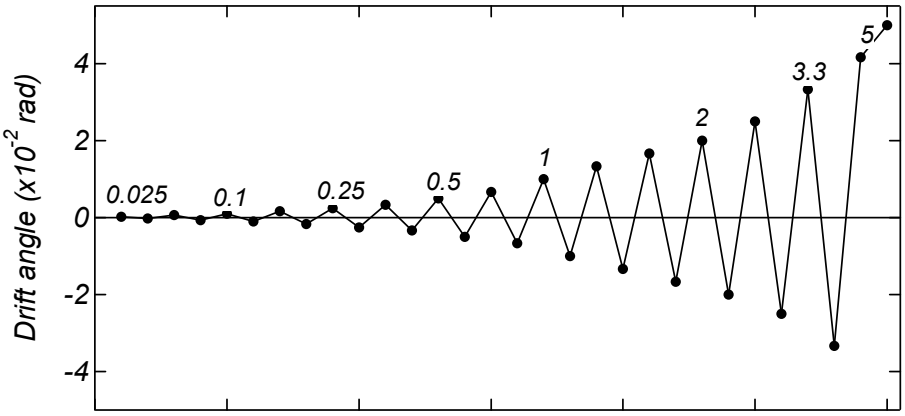

Figure 2.5.4 Loading history

2.5.2 *Instrumentation measurements*

In order to track the test of the specimen's response during the experiment, extensive measuring devices were assembled both externally and internally. The data acquisition system includes the following: a) two load cells connected to the vertical hydraulic jacks to measure the shear force on the slab; b) linear variable differential transducers (LVDTs) placed underneath the slab, to get the deformation as well as to measure the drift angle; c) strain gauges in reinforcements of the slab, and column reinforcement, to get the displacement and yield of reinforcement. All the data of load, strain, and displacement were monitored on the computer through a data logger. For each specimen, a total of 50 data channels were active during the testing process. Two load cells with 300kN capacity were used to record the applied reversed vertical load at the end of both sides of the plate. A total of 14 LVDTs that 4 with 100 mm, 6 with 50mm, and 4 with 25 mm travel was installed underneath the plate in order to record vertical displacement of the plate at each loading step. The LVDT with 100mm travel was mainly used to measure the vertical drift with the corresponding applied force, as shown in **Figure 2.5.5**. In order to measure the rebar's strain responses, 34 strain gauges were installed at various prescribed locations where 30 strain gauges in the slab rebars, 4 strain gauges in the column rebars, and their measuring values were listed in the **Appendix A-1**.

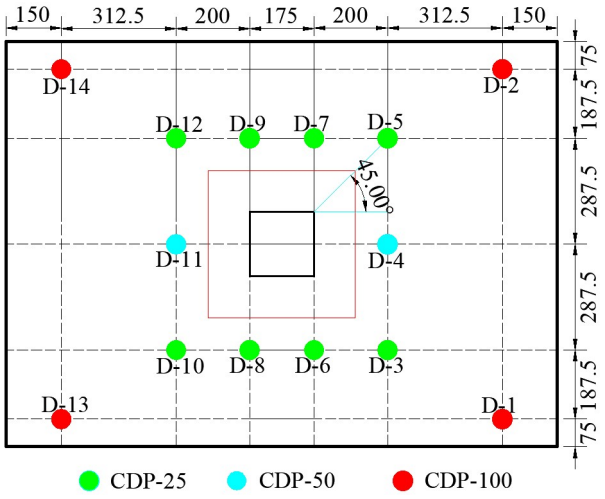

Figure 2.5.5 Position of displacement transducers of both specimens

An LVDT sensor is a type of displacement transducer used explicitly in measuring linear displacement. To monitor the deformations on each specimen, displacement transducers were installed at different places on the slab. The absolute displacement transducers D1, D2, D15, and D16 for both specimens were placed underneath the slab to measure the vertical drift *R*. The vertical drift *R* was used to measure the drift ratio (as explained in **Figure 2.5.3**) during the experiment, which is the main factor to control the vertical loading. A total of three types (CDP-25, CDP-50, CDP-100) of displacement

transducers LVDT were used during the experiment. The measurement detail for the displacement transducers on each specimen is shown in **Figure 2.5.5** (for details, see **Appendix B-1**). **Figure 2.5.5** shows the LVDT placement under the slab.

2.6 Experimental results

The nodal moments measured to the specimens were determined as a summation of bending moments by multiplying the vertical forces applied to the slab by the distance from the application point to the 600 mm column center. The nodal moment vs. vertical drift ratio relationship of the specimens is compared in the following section, in which the nodal moment was calculated by multiplying the average of absolute applied loads by both jacks by the shear span (l=1,200 mm in Fig. 3). Cracks occurred on the bottom surface slab, and the ultimate damage was drafted. Cracks were taken to observe the progression of cracking on the upper slab surface due to shear and moment transfer near the connection region of the specimens throughout the tests. Furthermore, the raised parts of concrete at punching failure are highlighted by thick black lines in the crack pattern drawing. The strain distributions of plate reinforcement parallel to the loading direction in different cycles was illustrated.

2.6.1 *Specimen FP-1*

The relationship between the nodal moment and drift ratio of this specimen is shown in **Figure 2.6.1 A**. An initial flexural crack occurred at the corner of the column at $R = -0.33\%$ rad. Subsequently, flexural cracks appeared and radially extended from the corners of the column with an angle of 45° relative to the loading direction at an R-value of +0.5% rad, as shown in **Figure 2.6.2**. The maximum strength in the positive direction was 7.3 kNm during the cycle to +2.35% rad with an increase in the diagonal cracks. The maximum strength in the negative direction was 6.1 kNm during the cycle to 2.0% rad. Thereafter, the strength started to decrease as the concrete surface lifted due to punching shear failure. The punching shear failure was fully visible at an R-value of 3.33% rad during positive loading. The ultimate damage to the top surface of the slab is shown in **Figure 2.6.1 B**. The detailed failure process and crack patterns at different drift levels are shown in **Figure 2.6.2**, where the damage on the top surface of the slab at punching shear failure is marked by a thick black line. The top surface of the concrete peeled up to 175 mm from the edge of the column in the loading direction. The failure mode of this specimen was classified as brittle punching shear failure. The maximum strength of 7.3 kNm was smaller than the calculated punching shear strength of 9.9 kNm according to AIJ standards (AIJ 2018) (defined as M_0 later in **Eq. 2.7.3**).

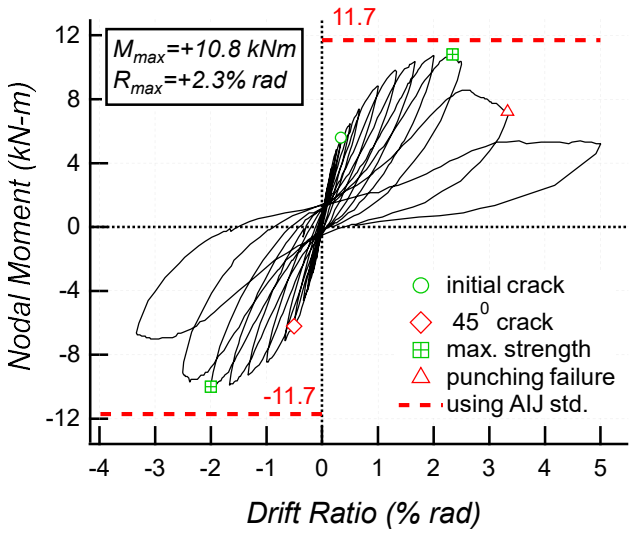

(A)



(B)

Figure 2.6.1 (A) Relationship of the nodal moment versus the drift ratio (Specimen FP), and (B) damage after punching shear failure

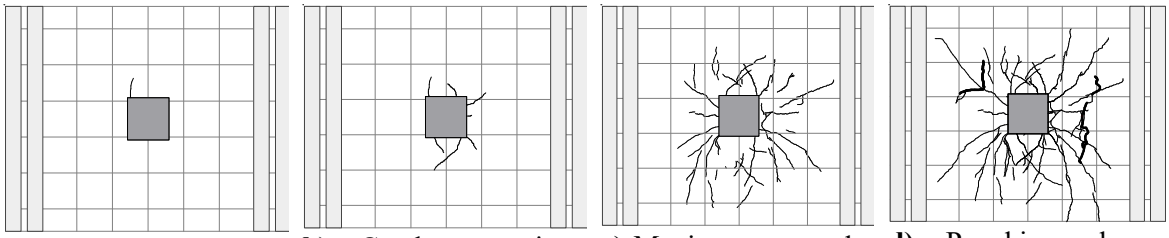

a) Initial cracks at R = -0.33%

b) Crack extension with an angle of 45^0 at R = 0.5%

c) Maximum strength at R = 2.5%

d) Punching shear failure at R = 3.33%

Figure 2.6.2 Crack pattern comparison in different cycles

The strains were obtained from the strain gauges installed on the top reinforcing bars of the slab along the loading direction. Although many strain gauges were installed in the slab reinforcement (as shown before in **Figure 2.3.1**), the major strain responses during the positive loading are discussed in the following section. The reinforcements were highlighted based on two categories, where A (blue-line) was defined as the exterior side in which the reinforcements were located 150 mm apart from the side surface of the column, as shown in **Figure 2.6.3**. For the other category, B (green-line) was defined as the interior side located approximately along the side surface of the column, as shown in the same figures. Comparing the strains of the reinforcing bars along with A and B, those on the interior side became larger with increasing drift angles for all specimens. The strain responses were much higher in the critical sections shown in these figures. These strain responses demonstrated that the plate was not only deformed in bending but also torsion around the column. It was identified that there were no strain

gauges yielded up to the peak load, as shown in **Figure 2.6.3**, showing punching shear failure before flexural yielding of the plate as designed.

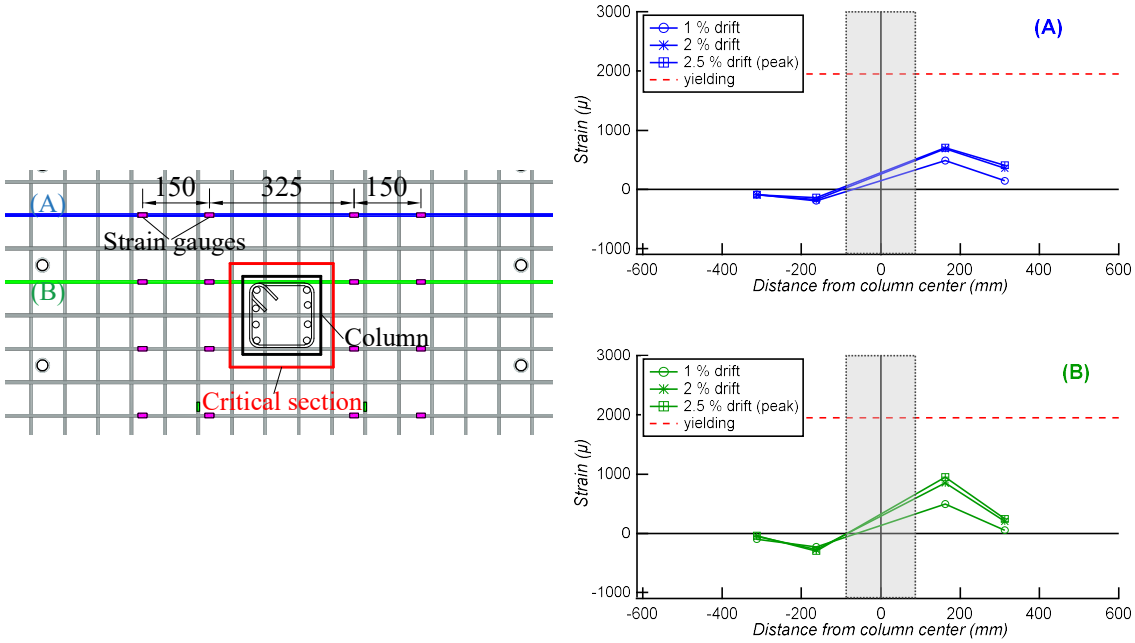

Figure 2.6.3 Comparison of the transitions of the strain distributions under different cycles for specimen FP-1

2.6.2 *Specimen FP-2*

The relationship between the nodal moment and drift ratio of this specimen is shown in **Figure 2.6.4 A**. Specimen FP-2 was tested as a benchmark specimen. An initial flexural crack appeared at the corner of the column at *R* of 0.33% rad. The maximum strength of 10.8 kN.m was observed in the cycle to 2.34 % rad during the positive loading, while 10.0 kN.m was observed in the cycle to 2% rad during the negative loading. Thereafter, the strength decreased with the raising up of the surface concrete due to punching shear failure. The maximum strength was close to the punching shear strength estimated by the AIJ standards (AIJ 2018), as explained later in section 2.7. The detailed failure process and crack patterns at different drift levels are shown in **Figure 2.6.5**, where the damage on the top surface of the slab at punching shear failure is marked by a thick black line. Punching shear failure occurred and was fully visible at *R* of 3.3% rad. The ultimate damage to the bottom surface of the slab with punching shear failure is shown in **Figure 2.6.4 B**.

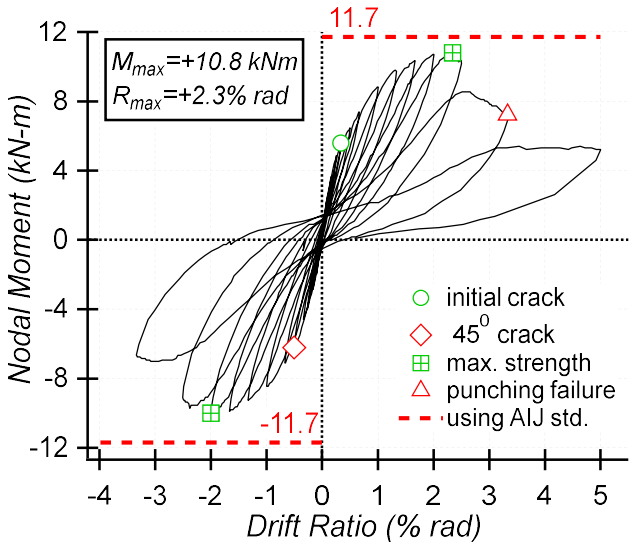

(A)



(B)

Figure 2.6.4 (A) Relationship of the nodal moment versus the drift ratio (Specimen FP-2), and (B) damage after punching shear failure

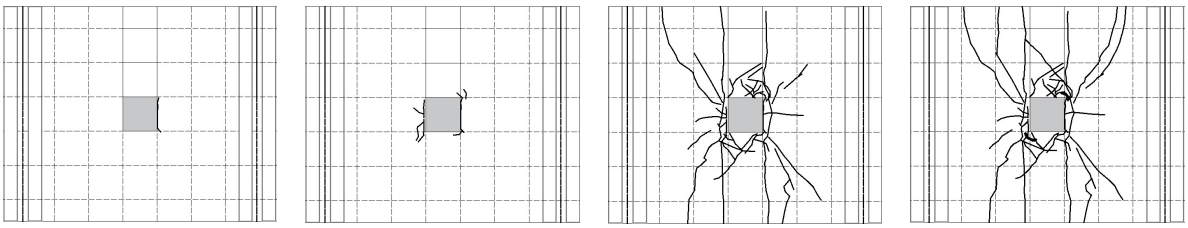

a) Initial cracks at R = -0.33%

b) Crack extension with an angle of 45^0 at R = 0.5%

c) Maximum strength at R = 2.5%

d) Punching shear failure at R = 3.33%

Figure 2.6.5 Crack pattern comparison in different cycles

The strains were obtained from the strain gauges installed on the top reinforcing bars of the slab along the loading direction. Although many strain gauges were installed in the slab reinforcement (as shown before in **Figure 2.6.6**, the major strain responses during the positive loading are discussed in the following section. The reinforcements were highlighted based on two categories, where A (red-line) was defined as the exterior side in which the reinforcements were located 150 mm apart from the edge of the column, as shown in **Figure 2.6.6**. For the other category, B (blue-line) was defined as the interior side located approximately along the side surface of the column, as shown in the same figures. Comparing the strains of the reinforcing bars along with A and B, those on the interior side became larger with increasing drift angles for all specimens. The strain responses were much higher in the critical sections shown in these figures for all the specimens. These strain responses demonstrated that the plate was not only deformed in bending but also torsion around the column. For this specimen, no

strain gauges yielded up to the peak load, as shown in **Figure 2.6.6**, showing punching shear failure before flexural yielding of the plate as the designed target. The behavior of strain gauges is almost similar responses to the specimen FP-1.

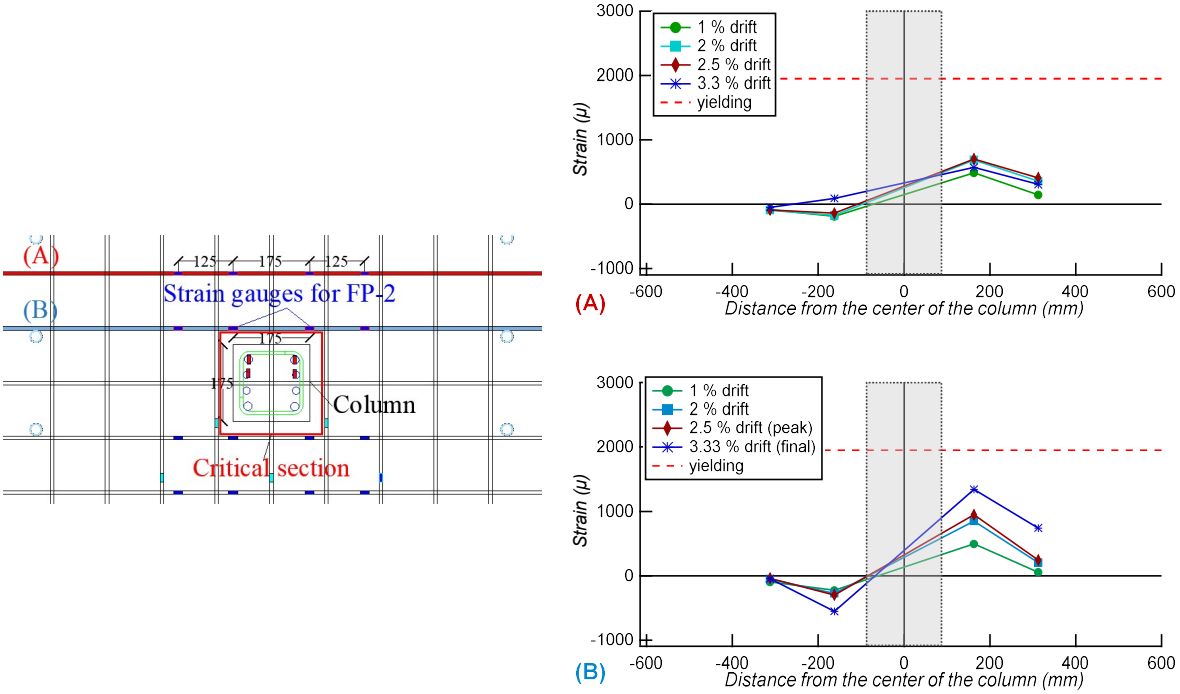

Figure 2.6.6 Comparison of the transitions of the strain distributions under different cycles for specimen FP-2

2.7 Strength estimation of the specimen

It is preferable to evaluate the capacity of each specimen before subjecting it to the testing procedure. Load cells are dependent on the capacity of specimens due to the selection of the hydraulic pump/jack capacity. During the capacity estimation of each specimen, the material parameters were assumed to be the same as the actual values. The bending moment diagrams of the specimens under static seismic loads are shown in **Figure 2.7.1**, which assume that the inflections are at the midpoints of the span of the plate. The ultimate strength of all the specimens was evaluated during the design stage. The ultimate strength of specimen M_u represents the joint nodal moment and failure mode, which are evaluated by **Eq. 2.7.1**:

$$M_u = min[_n M_y , M_{0,c} M_u] \quad \textbf{(2.7.1)}$$

where ${}_nM_y$ is the nodal moment at the plate-column connection when the plate yielded in flexure (N-mm), M_0 is the punching shear capacity at the critical section of the column (N-mm), ${}_cM_u$ is the nodal moment at the joint when the column yielded (N-mm).

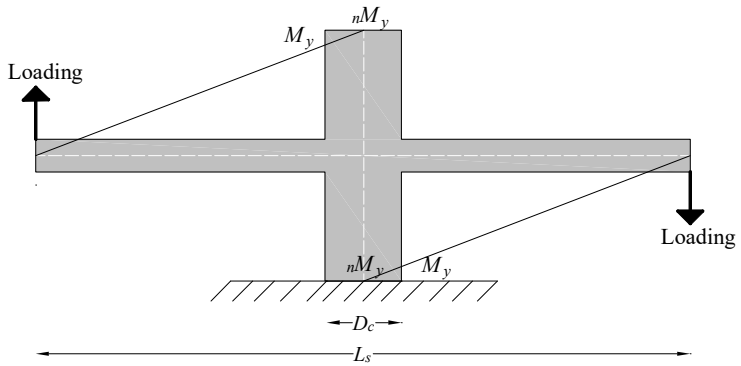

Figure 2.7.1. Moment diagram for both specimens

The capacity of the flexural strength of the plate (M_y) is obtained by flexural section analysis, where the following assumptions are used:

- The strain distribution in the cross-section is linear.
- The stress-strain relationship of the reinforcement is assumed to be a bilinear model in which the yield stress and elastic modulus are shown in **Tables 2.3 and 2.6** are used.
- The stress-strain relationship of concrete is assumed by using the model proposed by Hognestad et al. (Hognestad E, Hanson NW 1955) where the strain at the compressive stress is $2\sigma_B/E$ and the stress at 0.38% strain is $0.85\sigma_B$ (σ_B is the compressive stress of concrete).

The conversion of M_y into the nodal moment of joint ${}_nM_y$ is defined by **Eq. 2.7.2** for both specimens (refer to **Figure 2.7.1**):

$$nM_y = 2M_y \frac{L_s/2}{L_s/2 - D_c/2} \quad \textbf{(2.7.2)}$$

The designed punching shear capacity of the specimens was calculated based on the AIJ standard (AIJ 2018). The punching shear strength (M_0) was calculated according to the following equations (**Eqs. 2.7.3, 2.7.4, 2.7.5, and 2.7.6)** from the AIJ standard for RC structures. However, low-strength concrete was originally beyond the scope of these equations. Thus, this research investigates the applicability of these equations for specimens made with low-strength concrete. According to the AIJ standard, as shown in **Figure 2.7.2**, the moment resistances due to the bending, shearing, and twisting of concrete in the critical cross-section around the column were summed in **Eq. 2.7.3**:

$$M_0 = M_f + M_s + M_t \tag{2.7.3}$$

$$M_f = 0.9a_{0t}\sigma_y d\frac{c_2 + d}{x_t} + 0.9a_{0b}\sigma_y d\frac{c_2 + d}{x_b} \tag{2.7.4}$$

$$M_S = \tau_u(c_2 + d)d(c_1 + d) \tag{2.7.5}$$

$$M_t = \tau_{tu}\frac{d^2}{2}\{(c_1 + d) - \frac{d}{3}\}2 \tag{2.7.6}$$

where a_{0t} and a_{0b} are the cross-sectional areas of the top of the plate and bottom rebar (mm^2), respectively; x_t and x_b are the spacings of the top and bottom rebar (mm), respectively; σ_y is the yield stress of the rebar (N/mm^2); d is the effective depth of the plate (mm), c_1 is the column depth in the loading direction (mm); c_2 is the column width in the direction orthogonal to the loading direction (mm); τ_u is the direct shear strength of concrete (N/mm^2), where $\tau_u = 0.335\sqrt{\sigma_B}$; σ_B is the compressive strength of concrete (N/mm^2); and τ_{tu} is the torsional shear strength of concrete (N/mm^2), where $\tau_{tu} = 6\tau_u$. The critical sections are assumed to be at a distance $d/2$ from the column shown in **Figure 2.7.2**.

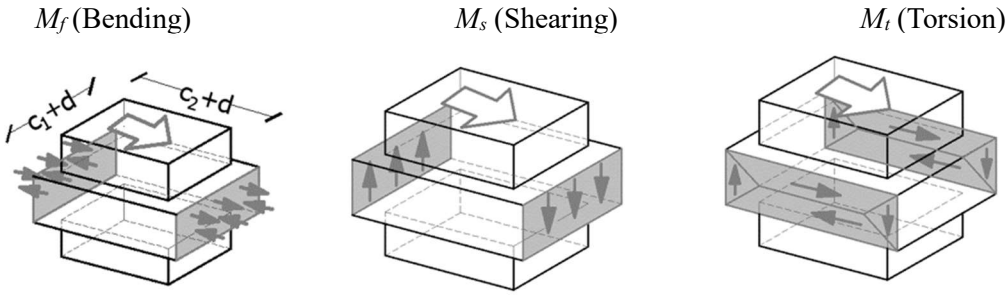

Figure 2.7.2 Punching shear mechanism due to bending, shearing, and twisting

In addition to the normal application of Equations (**2.7.3**) to (**2.7.6**) above, some modifications were applied in the present study to consider the low-strength concrete. The punching shear strength considering the low-strength concrete (M_{0l}) was computed by **Eq. 2.7.3**; however, the bending resistance of the plate (M_f) was evaluated using section analysis in the critical zone in the same manner that M_y was evaluated, and the shearing resistance (M_s) and twisting resistance (M_t) of the plate were computed by applying the direct shear strength (τ_u) formula of **Eq. 2.7.7** (Miyauchi et al. 2009) considering low-strength concrete (without confinement) to **Eqs. 2.7.5 and 2.7.6**.

$$\tau_u = 0.38(\sqrt{13.5}/13.5)\sigma_B \quad \textbf{(2.7.7)}$$

The capacities of the flexural strength of the column ($_cM_u$) was obtained by flexural section analysis in the same manner that M_y was obtained.

Flexural strength of a column

The ultimate flexural strength of a column without wing walls is calculated by **Eq. 2.7.8**. In the calculation, the effect of the slab reinforcement and the intermediate reinforcement in the column with the multi-layered arrangement of the flexural reinforcement shall be considered in principle.

$$M_u = 0.8 \sum a_t \, \sigma_y d \quad \textbf{(2.7.8)}$$

where:

a_t = cross sectional area of the tensile reinforcing bars (mm^2).

σ_y = yield strength of the tensile reinforcing bars (N/mm^2).

d = effective depth of the column (the distance between the center of gravity of the tensile reinforcement and the extreme fiber of compressive zone).

According to the above calculations, the expected failure mode was estimated to be punching failure for both specimens. The details of the calculated results and experimental strengths are tabulated in **Table 2.7.1**. A discussion will be given in the following section.

Table 2.7.1 Calculated ultimate strengths compared to the ultimate strengths obtained from the experimental data

Specimen no.	Experi-mental strengths M_{exp} (kN·m)	Flexural strength of the slab $_nM_y$ (kN·m)	Flexural Strength of column M_u (kN.m)	Calculated strength by AIJ M_0 (kN·m) [M_{exp}/M_0]	Calculated strength considering low-strength concrete M_{0l} (kN·m) [M_{exp}/M_{0l}]	Experimental failure mode
FP-1	7.3	15.8	39.81	9.85 [0.74]	8.3 [0.88]	Punching shear failure
FP-2	10.8	21.8	55.7	11.7 [0.92]	11.1 [0.97]	Punching shear failure

2.8 Experimental discussion

The backbone curve of the nodal moment vs drift angle relationship is shown in **Figure 2.8.1**. Both specimens showed similar characteristics and failure mode with brittle punching shear failure. Although the maximum strengths of both specimens were different due to the application of different concrete strengths (6.93 MPa for FP-1 and 11.5 MPa for FP-2) in **Figure 2.8.1**, both specimens showed similar deformability of approximately 2% drift angle in the negative loading, as shown in the figure. According to the AIJ RC standard, the punching shear strength was close to the experimental value when the low-strength concrete was considered. The experimental strengths were compared with the design calculations, as listed in Table 2.7.1. The maximum experimental strengths of all the specimens were lower than the design strengths according to the AIJ standards. In particular, the maximum punching shear capacity of FP-1 was 26% lower than the calculated value while it was 8% lower for specimen FP-2. This was probably caused by the utilization of low-strength concrete in the specimens. Therefore, the previous section presented two modifications: the application of sectional bending analysis and the direct shear strength equation proposed by Miyauchi et al. (2009). Consequently, the estimate of the punching shear strength for specimen FP-1 was improved by approximately 12%, while it was 3% for FP-2. The comparison of the component of AIJ punching shear strength estimation is shown in **Figure 2.8.2**. In this study, it was confirmed that the estimate of the punching shear strength was acceptable for both specimens. However, further research, including finite element modelling and analysis, is necessary, particularly to validate these equations in terms of the failure mechanism of flat plate structures constructed using low-strength concrete.

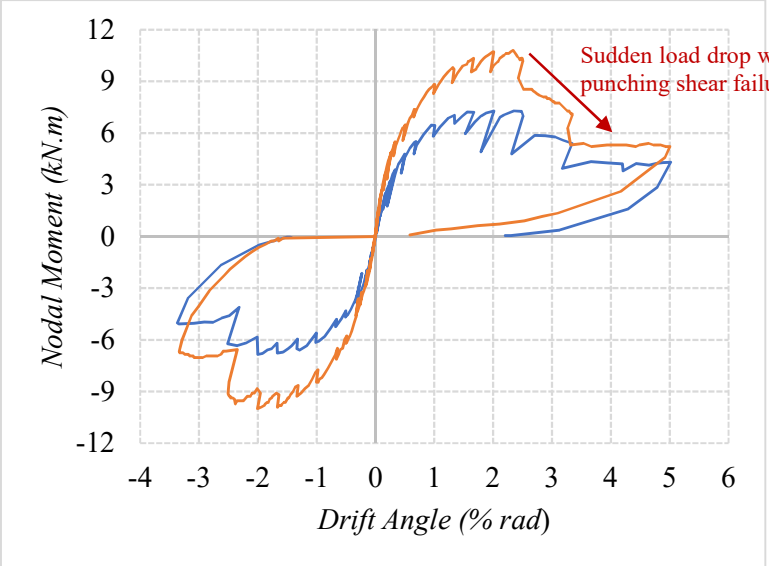

Figure 2.8.1 Backbone curve of both specimens

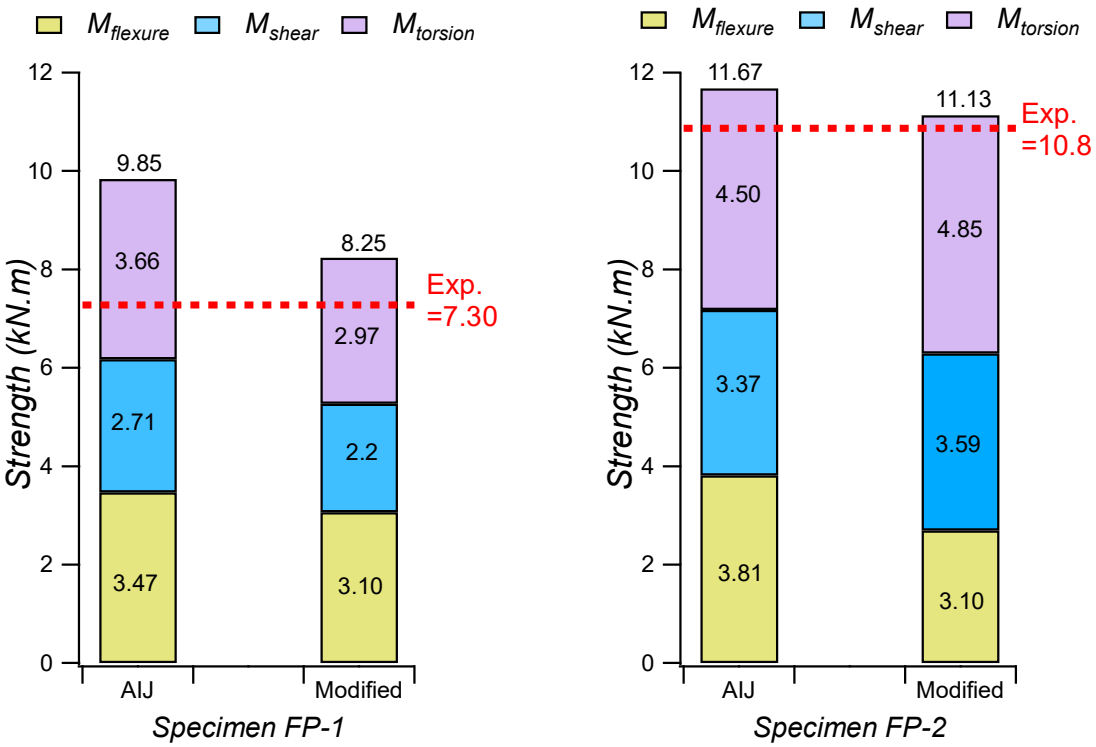

Figure 2.8.2 Comparison of the component of the punching shear estimation using AIJ standard

2.9 Summary

A series of experimental studies of two half-scaled interior flat plate-column connection specimens were conducted mainly to evaluate the seismic behavior and performance. The two specimens were constructed and tested in two different countries with different concrete strengths. Based on the results obtained from the tests and their strength estimations, the following conclusions can be drawn:

1) Experimental investigations were conducted with two interior flat plate column connections to identify the structural characteristics, which were constructed using low-strength concrete representing the most vulnerable concrete conditions in Bangladesh.
2) In the experiments, both specimens showed punching shear failure as intended in their design stage, Flexural cracks were prolonged in the 45° direction from the column surface, whereas punching cracks extended radially from the column/wing wall surface. Finally, the surface concrete peeled due to punching shear failure.
3) The maximum strength was 7.3 kNm for specimen FP-1 while 10.8 kNm was for specimen FP-2 at the same drift level of 2.3% rad in the positive loading direction. Thereafter the load was dropped immediately due to punching shear failure. The deformation capacity of both specimens in the negative loading direction was 2%.

4) The punching shear strength estimated based on the AIJ standards overestimated the maximum capacity using low-strength concrete. According to the AIJ standard, the maximum capacity of FP-1 was 26% lower than the calculated result of the punching shear strength whereas the maximum capacity of FP-2 was 12% lower than the calculated result of the punching shear strength. The lower the concrete strength increased the overestimation.
5) According to the AIJ standard, the punching shear strength was close to the experimental value when the low-strength concrete was considered. Consequently, the estimate of the punching shear strength for specimen FP-1 was improved by approximately 10%, while it was 3% for FP-2. Therefore, from this study, it is recommended to consider the low strength issue while the structure is constructed using low-strength concrete.

CHAPTER 3

Experimental Study on Strengthening of the Interior Flat Plate-column Joint Using Post-installed RC Wing Walls

3.1 General

The previous chapter investigated that RC flat plate structures were tremendously vulnerable to the progressive punching shear collapse near the plate-column joint under seismic loading conditions. Therefore, an appropriate strengthening technique should be implemented to minimize the probability of this type of brittle structural failure in addition to the increase of column lateral strength. Thus, the focus of this chapter emphasizes a new strengthening scheme for seismically vulnerable flat plate-column connections in existing structures. An experimental investigation on a series of two half-scaled interior plate-column connections was conducted in order to evaluate the effectiveness of the proposed seismic strengthening method using post-installed RC wing walls and to analyze the punching shear capacity of the connections. In this investigation, we seek to investigate the typical existing flat plate structures, which are constructed using low-strength concrete in Bangladesh. To strengthen the existing specimens, we implemented wing walls that employed two principal directions, namely, the loading direction and the orthogonal direction. Specimen FP-1 was described in that previous chapter which served as a control specimen for comparisons between the cases with and without wing walls. Static cyclic vertical displacements with increasing amplitude were applied to the ends of the slabs to represent inter-storey drift under seismic action.

3.2 Wing Wall

In this study, wing wall is selected and proposed as a retrofitting technique. A wing wall is a small wall panel that may not be considered a shear wall with a boundary column. This retrofit method intends to increase the seismic performance of existing buildings by changing the existing independent columns to columns with wing walls by upgrading their strength. The objective of this method is to increase the lateral resistance of the columns under lateral loads. Another advantage of the wing wall, it can carry the axial load of a column and eliminate the problem of second-class prime elements, whose failure leads to building collapse (JBDPA 2005). For example, installing a wing wall in the direction of lateral load concerned to increase its strength is an effective retrofitting method when they are extremely brittle columns. Wing walls are not new as a strengthening technique of reinforced concrete structures, But it's a typical new concept in RC flat plate structures. A typical layout of installing wing wall is in reinforced concrete flat plate structures is shown in **Figure 3.2.1**. Installing RC wing walls were introduced in the Japanese standard for normal moment-resisting structure.

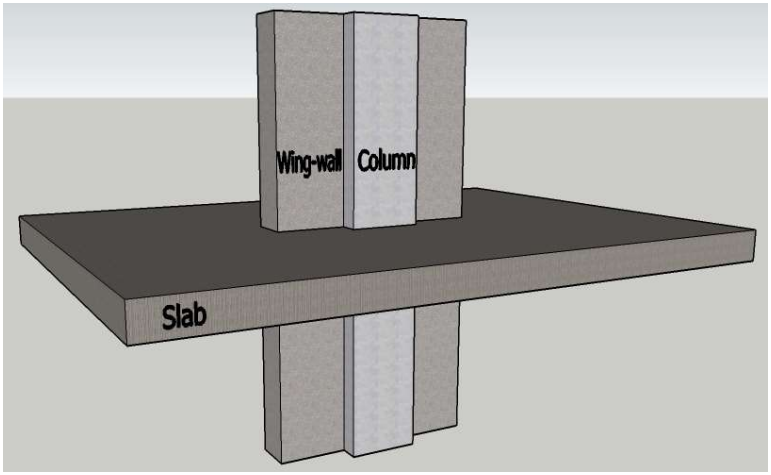

Figure 3.2.1 Seismic retrofit by RC flat plate-column joint by installing post-installed wing walls

3.3 Specimen design/details

A series of experiments involving two half-scaled interior flat plate-column connections with strengthened specimens by RC wing walls were conducted primarily to investigate the effectiveness of this technique as well as to evaluate the seismic behavior and performance. The specimen FP-1 (described in the previous chapter) was constructed without wing walls and served as a control specimen to compare the cases with and without retrofitting. Wing walls were attached along the longitudinal direction for specimen FP-W1, while the direction was along with the transverse direction for specimen FP-W2. The layout of all specimens is shown in **Figure 3.3.1**.

The plate dimensions were 1500 × 1100 × 75 in length × width × thickness. 2-D6@75 was used for slab reinforcement in both longitudinal and transverse directions. The column was on the centroid of the plate with a cross section of 175 mm square. 8-D16 bars were used as main reinforcement, and 2-D6@50 was used for hoop reinforcement of the column. There is no shear reinforcement on the slab near the slab-column connection. Wing walls were attached along the longitudinal direction for specimen FP-W1, while the direction was along with the transverse direction for specimen FP-W2. The dimensions of wing walls were 175 × 100 in length × width, respectively. 4-D6 (U-shaped) vertical rebar and 2-D6 @155mm horizontal rebar were used in the wing walls. The details of both specimens are shown in **Figure 3.3.1**. However, the existing component of both strengthened specimens was designed and constructed the same as the specimen FP-1 described in chapter 2.

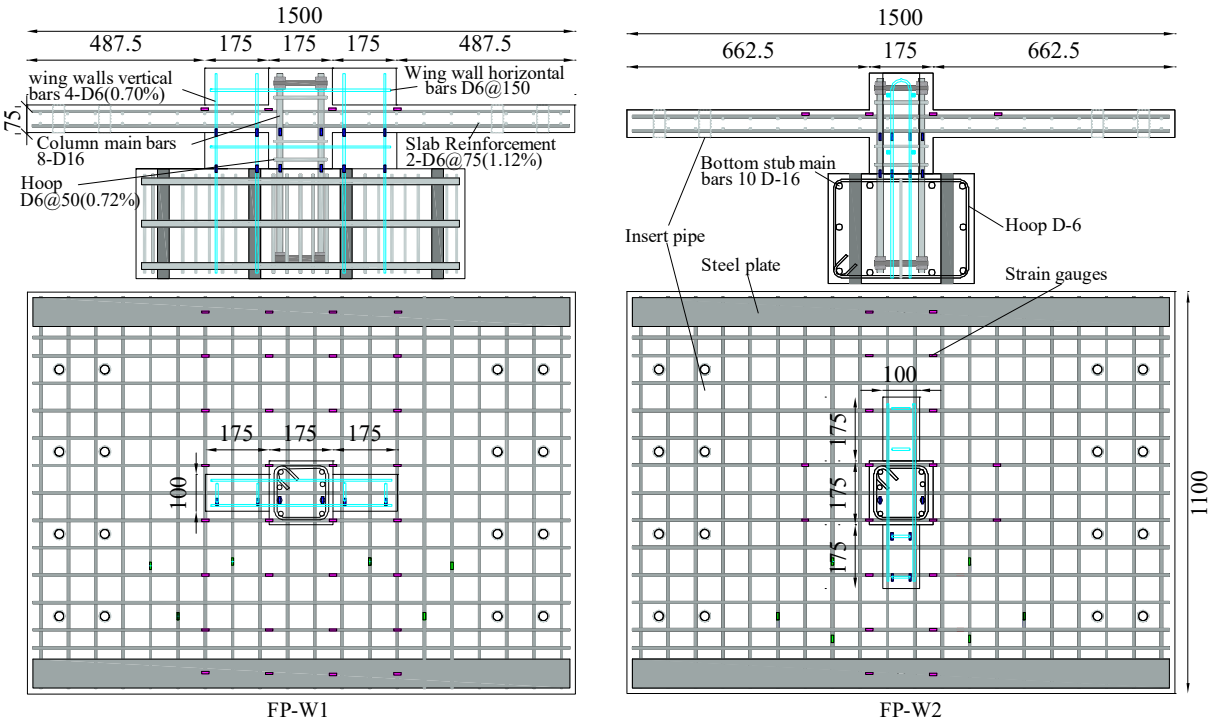

Figure 3.3.1 Details of the strengthening specimens using wing walls

3.4 Material mechanical properties of concrete and steel

The concrete mixture was designed based on the target concrete compressive strength of 7 N/mm^2 which was from that of low-strength concrete commonly found in Bangladesh. Portland cement was used with mountain sand as fine aggregate and brick chips as coarse aggregate with a maximum aggregate size of 15 mm to well simulate the low-strength concrete in Bangladesh for the existing parts of the specimens. A cement and $CaCO_3$: sand: brick chips volumetric ratio was designed as 1 (=0.7+0.3): 2: 4, where 30% of cement was replaced by $CaCO_3$ mainly to decrease the concrete strength. The proportion of water to the sum of cement and $CaCO_3$ was 60%. **Table 3.1** shows a concrete mixture by weight for the existing parts of the specimens. The concrete for the existing parts was mixed with a concrete mixture machine. On the other hand, a normal ready-mixed concrete of design strength of 30 N/mm^2 with stone chips as coarse aggregate, of which the maximum size was 15 mm, was used for the wing walls and the bottom stubs. The average properties of the concrete from the cylindrical compression tests are summarized in **Table 3.2**. The grades of steel were SD295 (deformed rebar with the nominal yield stress of 295 N/mm^2) for D6 reinforcement and SD345 (deformed rebar with the nominal yield stress of 345 N/mm^2) for D16, respectively. The averaged material properties of reinforcement from the tensile tests are shown in **Table 3.3**.

Table 3.1 Concrete mixture in kg/m^3

	W/(cement + $CaCO_3$)	Water	Cement	$CaCO_3$	Sand	Brick
FP-1	60%	212	248	88	596	959

Table 3.2 Material properties of concrete

Type	Compressive strength (N/mm^2)	Elastic modulus (N/mm^2)	Strain at compressive strength (μ)
FP-W1	7.16 (brick chips)	8672	1694
FP-W2	7.20 (brick chips)	8741	1586
Wing Wall	37.04 (stone chips)	30929	1956

*Elastic modulus is defined by $E = (F_c/3\text{-}f_2)/(\varepsilon_1\text{-}\varepsilon_2)$

(E: elastic modulus; F_c: compressive strength of concrete; f_2: stress at 50x10^{-6} strain; ε_1; strain at $F_c/3$; ε_2: 50x10-6 (JISA 1149 2010)

Table 3.3 Material properties of steel

	Type	Cross section of Bar (mm^2)	Yield stress (N/mm^2)	Elastic modulus (kN/mm^2)	Tensile strength (N/mm^2)
FP-W1, FP-W2	D6 (D295A)	28.27	381	201	505
	D16 (SD345)	201.06	369	198	536

3.5 Loading and Measurement Methods

3.5.1 *Experimental set-up*

Figure 3.5.1 shows the photograph of the experimental setup of the flat plate specimen that strengthened with the wing wall. The test setup and loading protocol were the same as those shown in **Figures 2.5.1 and 2.5.4**. These specimens were also tested using a static loading system at Daido University Concrete Structure Lab. The arrangement of LVDT to determine the drift ratio R is shown in **Figure 3.5.2**. The loading history of both specimens is shown in **Figure 3.5.3**; however, the increasing amplitude kept the same. The loading was given up to 2.5% cycle for high specimen FP-W1

while it was continued until 8.3% cycle for specimen FP-W2 due to high deformation capacity compared to the former specimen.



Figure 3.5.1 Photographic view of the experimental setup

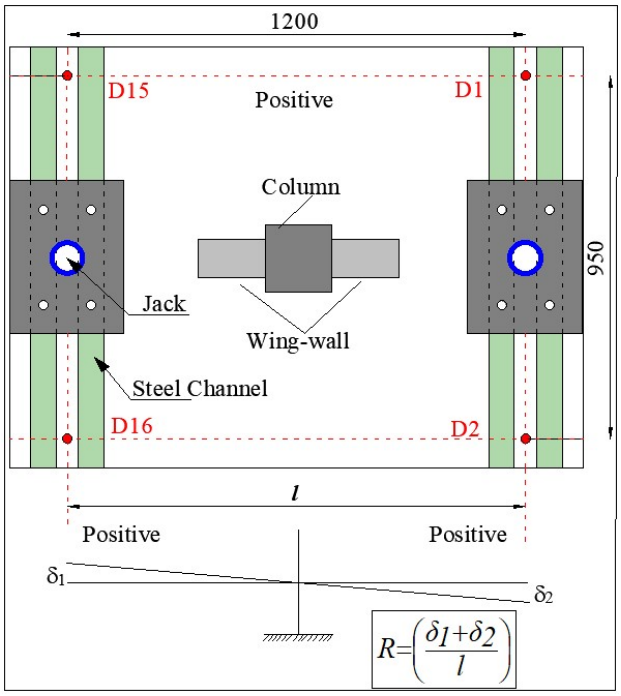

Figure 3.5.2 Arrangement of LVDTs and the definition of R

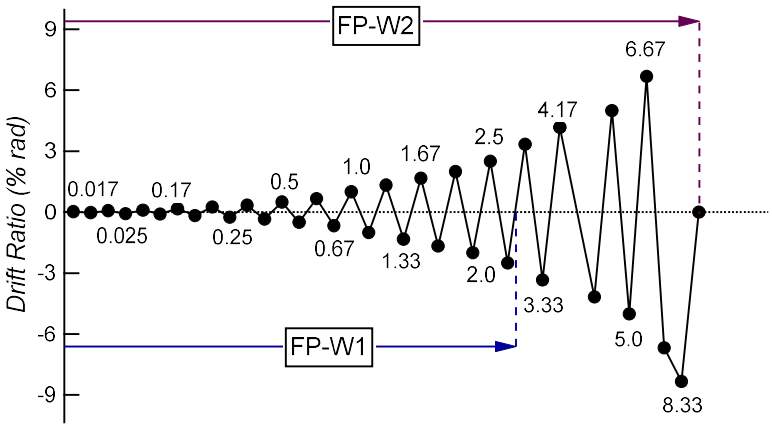

Figure 3.5.3 Loading history

3.5.2 *Instrumentation measurements*

Extensive measuring devices were assembled both externally and internally to track the test of the specimen's response during the experiment as already described in chapter 2. The overall view of the picture of data acquisition system is shown in **Figure 3.5.4**. For each specimen, a total of 69 data channels were active during the testing process. Two load cells with 300kN capacity were used to record the applied reversed vertical load at the end of both sides of the plate. A total of 16 LVDTs that 4 with 100 mm, 6 with 50mm, and 4 with 25 mm travel was installed underneath the plate in order to record vertical displacement of the plate at each loading step. **Figure 3.5.5** shows the LVDTs placement under the slab. The LVDT with 100mm travel was mainly used to measure the vertical drift with the corresponding applied force, as shown in **Figure 3.5.5**. In order to measure the rebar's strain responses, 39 strain gauges were installed at various prescribed locations where 31 strain gauges in the slab rebars, 12 strain gauges in the column/wing walls rebars, and their measuring values were listed in the **Appendices A-1 and A-2**.



Figure 3.5.4 Picture of data acquisition system during testing

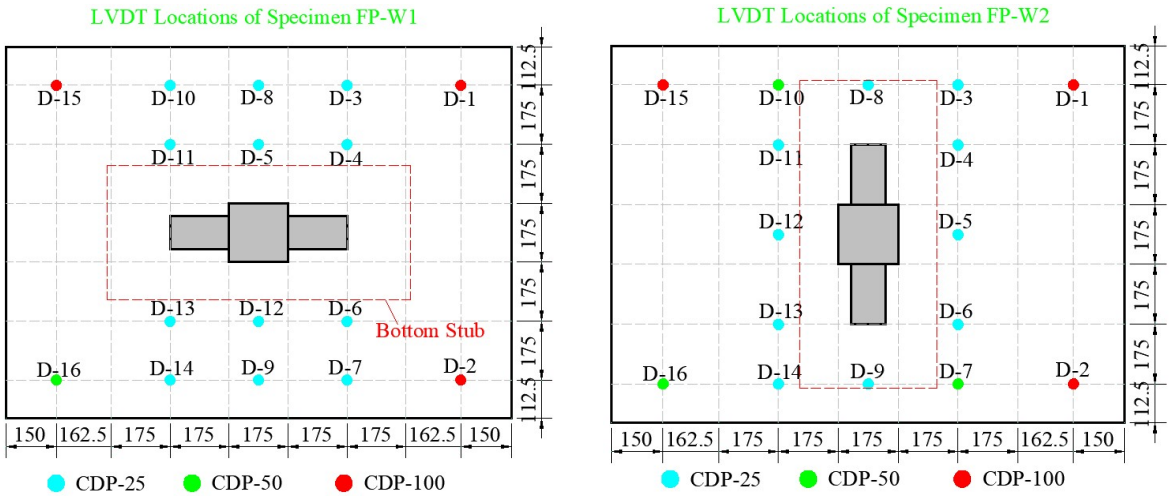

Figure 3.5.5 Position of displacement transducers

3.6 Experimental results

The nodal moment versus drift angle relationships of the specimens are explained in this section. The nodal moments applied to the specimens were calculated as the summation of bending moments obtained by multiplying the absolute vertical forces applied to the slab by both hydraulic jacks by 600 mm and the distance from the application point to the center of the column, as shown in **Figure 3.5.2**.

3.6.1 *Specimen FP-W1*

Specimen FP-W1, which was strengthened with post-installed wing walls that were installed along the loading direction of the column, showed higher stiffness and strength, and lower deformation capacity. The relationship between the nodal moment and drift ratio R of the specimen is shown in **Figure 3.6.1 A**. An initial flexural crack occurred at the corner of the wing wall at an R value of 0.167% rad in the positive cycle. Afterward, the cracks radially extended approximately 45° relative to the loading direction from the corners of the wing wall at an R-value of 0.5% rad. The maximum strength was 19.9 kNm during the positive and negative loading in the cycle at 1.33% rad. Subsequently, the strength decreased as the concrete surface lifted due to punching shear failure. The ultimate damage to the specimen is shown in **Figure 3.6.1 B**. The detailed failure process and crack patterns for different cycles are shown in **Figure 3.6.2**, where the ultimate damage due to punching failure on the top surface of the slab is marked by thick black lines. Punching shear failure was observed at the top and bottom surfaces of the slab. It was observed that the top concrete surface peeled up by approximately 160 mm far from the edge of the wing wall in the loading direction. Additionally, brittle punching shear failure was observed in this specimen, as intended in the design stage. The maximum strength was 19.9 kNm, which was close to the calculated punching shear strength of 20.5 kNm according to the AIJ standards (M_0 in **Eq. 2.7.3**).

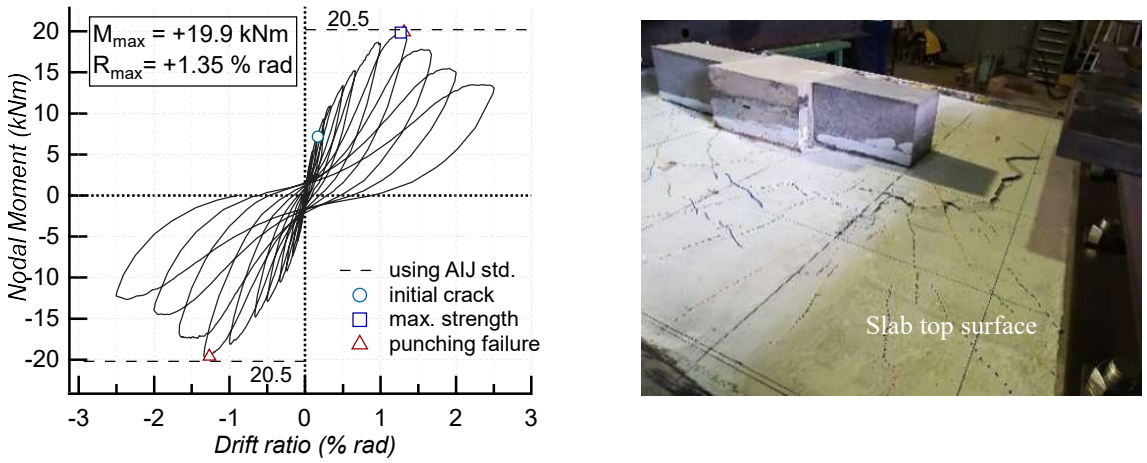

Figure 3.6.1 (A) Nodal moment versus drift ratio relationship (specimen FP-W1) and (B) damage after punching shear failure

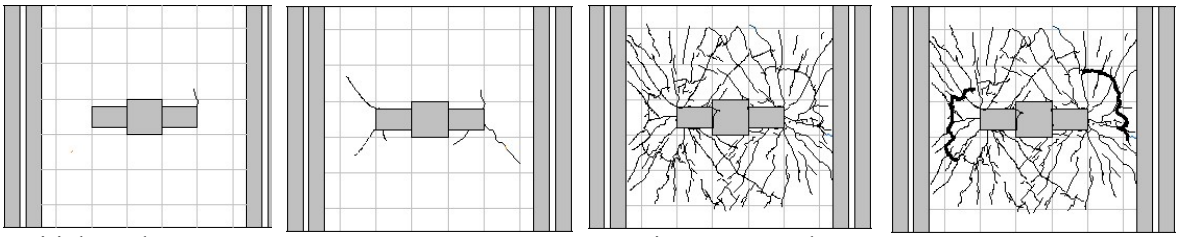

Initial cracks at R = +0.167%

Cracks extension at an angle of 45° at R = 0.5%

Maximum strength at R = 1.33%

Punching shear failure at R = 3.33%

Figure 3.6.2 Failure process on the top surface of the plate of specimen FP-W1

3.6.2 *Specimen FP-W2*

Specimen FP-W2, which was strengthened with post-installed wing walls along the orthogonal loading direction of the column, showed higher strength but did not exhibit higher initial stiffness compared to the benchmark specimen FP-1. The relationship between the nodal moment and drift ratio for this specimen is shown in **Figure 3.6.3A**. An initial flexural crack occurred at the corner of the wing wall at an *R*-value of +0.5% rad. Then, the cracks extended approximately 45° relative to the loading direction from the corners of the column during the negative cycle at an *R*-value of 0.67% rad. The maximum strength was 14.7 kNm during positive loading in the cycle at 4.82% rad. The maximum strength in the negative loading direction was 14.1 kNm at 4.74% rad, but the strength did not decrease significantly as *R* increased to 6% rad. Subsequently, the bottom surface of the concrete peeled up slightly from the edge of the column in the loading direction at approximately 200 mm. In this specimen,

punching shear failure was observed on the bottom surface of the slab, as shown in **Figure 3.6.3B**. Additionally, from the strain gauges, it was observed that the plate rebar started to yield at an *R*-value of 4.2%, indicating that flexural yielding occurred in the plate before punching damage was observed (described later in section 3.6.3). Consequently, the failure mode of this specimen was categorized as a ductile flexural failure, followed by punching shear failure. The detailed failure process and crack patterns at different cycles are shown in **Figure 3.6.4**. The maximum strength of 14.7 kNm was smaller than the calculated punching shear strength of 20.2 kNm according to the AIJ standard (M_0 in **Eq. 3.7.3**).

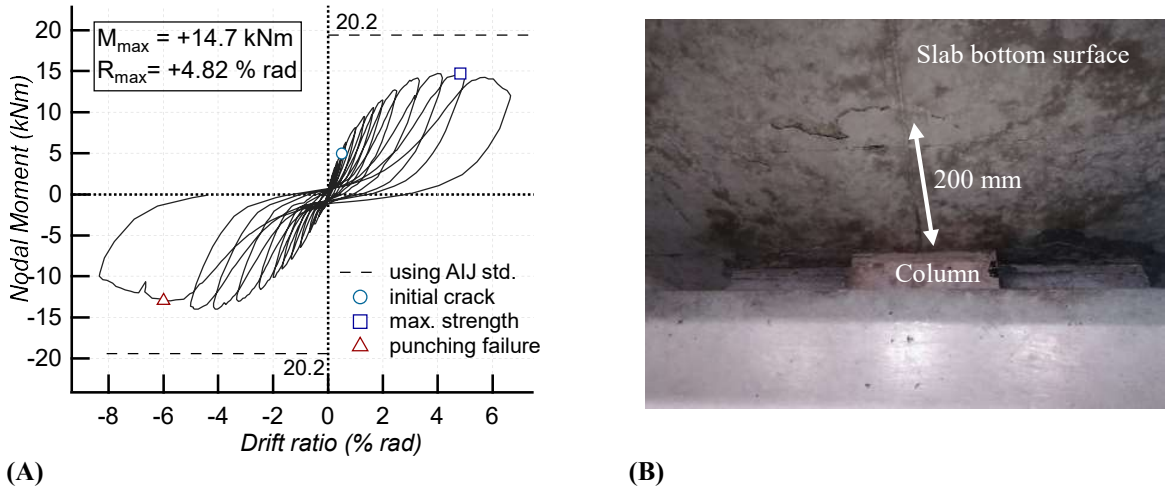

Figure 3.6.3 (A) Nodal moment versus drift ratio relationship (specimen FP-W2) and (B) damage after punching shear failure

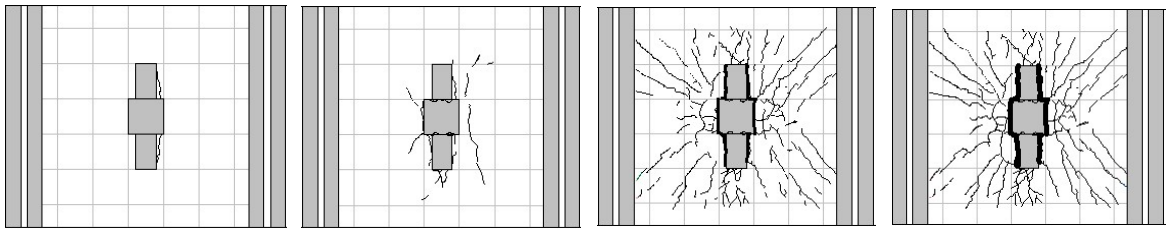

Initial cracks at R = +0.5% | Cracks extension at an angle of 45° at R = -0.67% | Maximum strength at R = 5.0% | Punching shear failure at R = 6.0%

Figure 3.6.4 Failure process on the top surface of the plate of specimen FP-W2

3.6.3 *Strain Distribution of the Slab Reinforcement*

The strains were obtained from the strain gauges installed on the top reinforcing bars of the slab along the loading direction. Although many strain gauges were installed in the slab reinforcement, the major strain responses during the positive loading are discussed in the following section. The reinforcements were highlighted based on two categories, where A (blue-line) was defined as the exterior side in which the reinforcements were located 150 mm apart from the side surface of the column, as shown in **Figures 3.6.5 and, 3.6.6** for specimens FP-W1, and FP-W2, respectively. For the other category, B (green-line) was defined as the interior side located approximately along the side surface of the column, as shown in the same figures. Comparing the strains of the reinforcing bars along A and B, those on the interior side became larger with increasing drift angle for all specimens. The strain responses were much higher in the critical sections shown in these figures for all the specimens. These strain responses demonstrated that the plate not only deformed in bending but also in torsion around the column. For specimens FP-W1, no strain gauges yielded up to the peak load, as shown in **Figure 3.6.5**, showing punching shear failure before flexural yielding of the plate as the design target. For specimen FP-W2, one strain gauge yielded before the specimen reached its maximum strength due to the flexural behavior of the plate near the column surface at R of 4.2% rad, as shown in **Figure 3.6.6**. Later, other strain gauges also started to yield with the increase in the drift ratio. The strain responses were different from those of FP-1 and FP-W1. This indicates that the failure process of FP-W2 was different from that of the other two specimens, as described in previous sections.

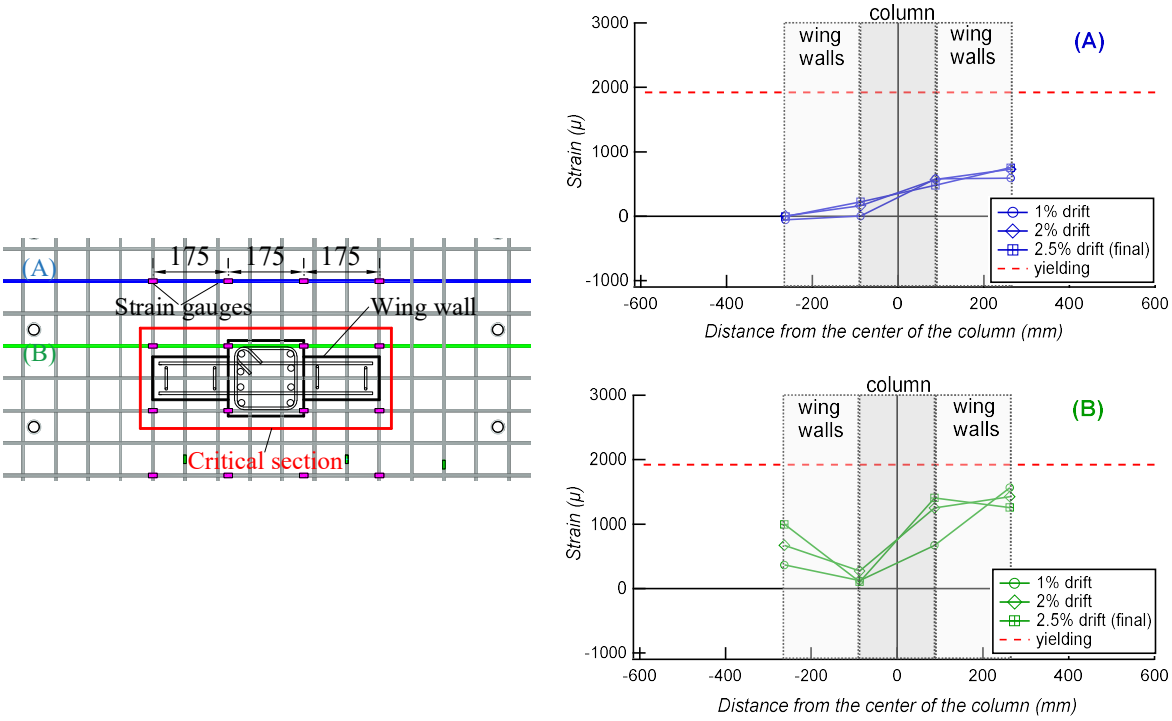

Figure 3.6.5 Comparison of strain distribution transitions under different cycles for specimen FP-W1

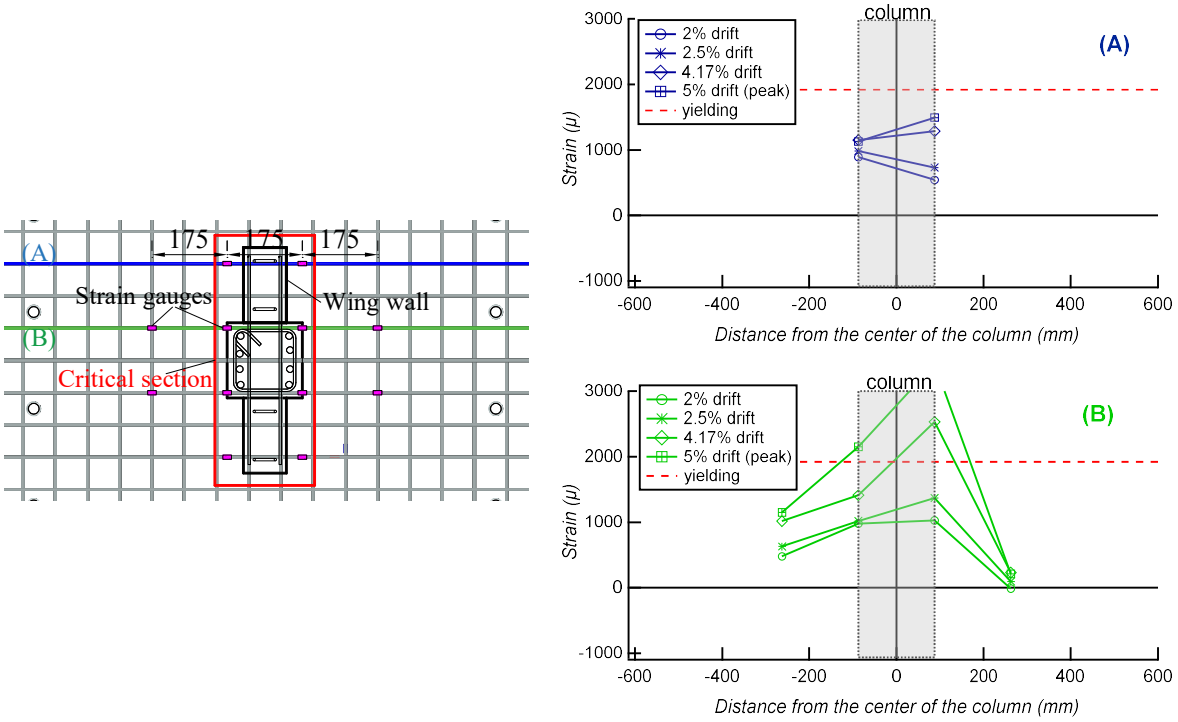

Figure 3.6.6 Comparison of strain distribution transitions under different cycles for specimen FP-W2

3.7 Strength estimation of the specimens

The bending moment diagrams of the specimens under static seismic loads are shown in **Figure 3.7.1** and **Figure 3.7.2**, which assume that the inflections are at the midpoints of the span of the plate. The ultimate strength of all the specimens was evaluated during the design stage. The ultimate strength of specimen M_u represents the joint nodal moment and failure mode, which are evaluated by **Eq. 3.7.1**:

$$M_u = min[{}_n M_y, M_0, {}_c M_u, {}_{cw} M_u] \quad \textbf{(3.7.1)}$$

where ${}_nM_y$ is the nodal moment at the plate-column connection when the plate yielded in flexure (N-mm), M_0 is the punching shear capacity at the critical section of the column (N-mm), ${}_cM_u$ is the nodal moment at the joint when the column yielded (N-mm) for FP-W2, and ${}_{cw}M_u$ is the nodal moment at the joint when the column with a wing wall yielded (N-mm) for FP-W1.

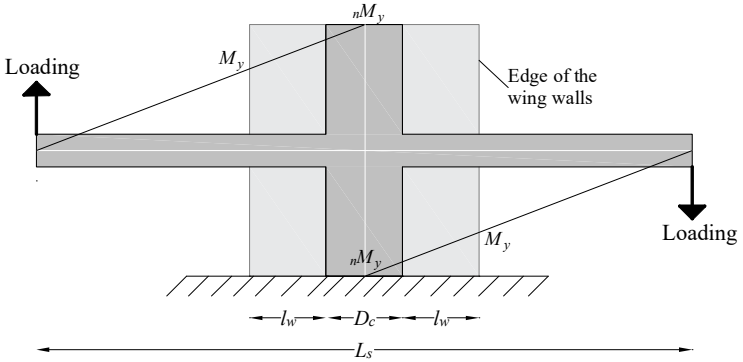

Figure 3.7.1 Moment diagram of specimen FP-W1

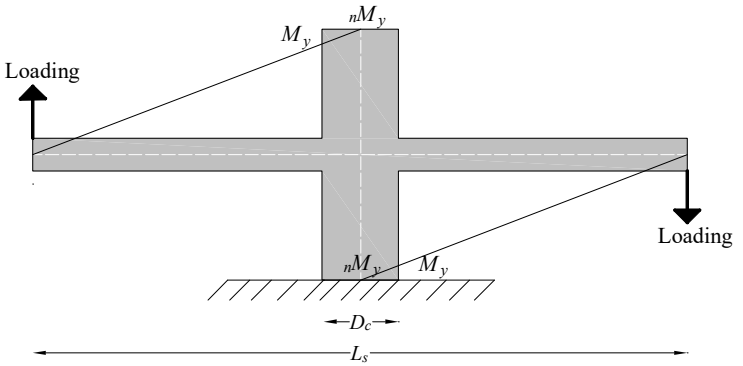

Figure 3.7.2 Moment diagram for specimen FP-W2

The capacity of the flexural strength of the plate (M_y) is obtained by flexural section analysis, as described in the section 2.7 of previous chapter.

The conversion of M_y into the nodal moment of joint ${}_nM_y$ is defined by **Eq. 3.7.2** for specimens FP-W1 and **Eq. 3.7.3** for specimen FP-W2 (refer to **Figures. 3.7.1 and 3.7.2**):

$$nM_y = 2M_y \frac{L_s/2}{L_s/2 - D_c/2 - l_w} \quad \textbf{(3.7.2)}$$

$$nM_y = 2M_y \frac{L_s/2}{L_s/2 - D_c/2} \quad \textbf{(3.7.3)}$$

The designed punching shear capacity of the specimens was calculated based on the AIJ standard (AIJ 2018). The punching shear strength (M_0) was calculated the same as the section 2.7 according to the following equations (**Eqs. 2.7.3, 2.7.4, 2.7.5, and 2.7.6)** from the AIJ standard for RC structures. However, their critical section is assumed and proposed based on the experimental findings. The punching shear strength component is assumed as the following mechanism as shown in **Figures 3.7.3 and 3.7.4** for specimens FP-W1, and FP-W2, respectively. The critical section was assumed d/2

distance from the column/wing wall edge, as shown in **Figure 3.7.5**. Therefore, the critical section is assumed from the edge of the wing wall surface for specimen FP-W1.

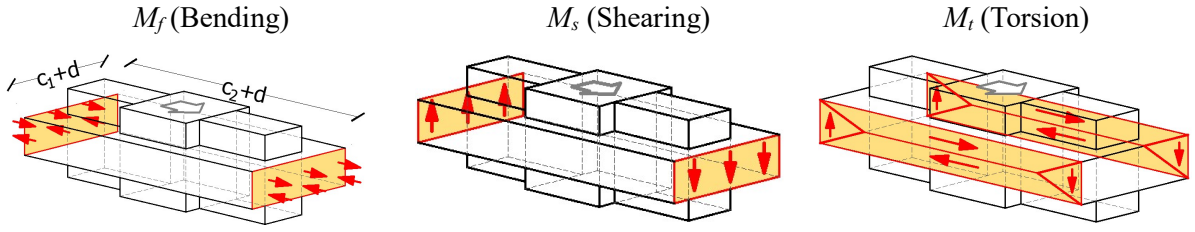

Figure 3.7.3 Punching shear mechanism due to bending, shearing, and twisting for specimen FP-W1

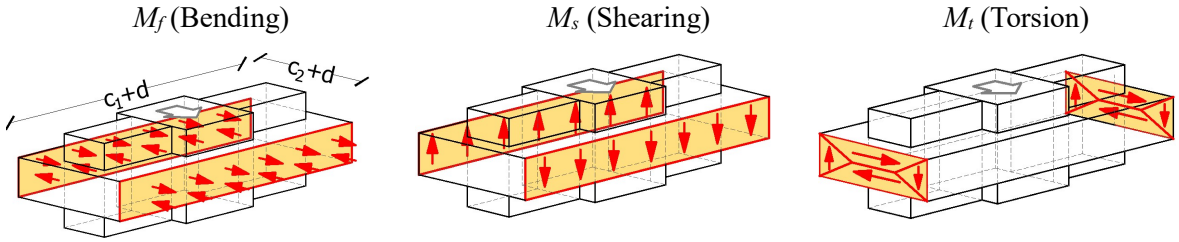

Figure 3.7.4 Punching shear mechanism due to bending, shearing, and twisting for specimen FP-W2

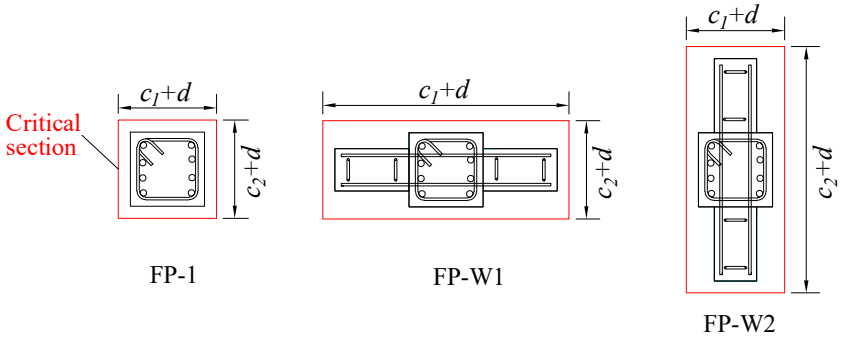

Figure 3.7.5 Assumed critical section

Flexural strength of column with wing walls

The ultimate flexural strength of a column with wing wall is calculated by the **Eq. 3.7.4.** In the calculation, the effect of the wing walls reinforcement and the intermediate reinforcement in the column with the multi-layered arrangement of the flexural reinforcement shall be considered in principle.

$$M_u = a_{te}\sigma_y(b - 0.5x_n) \qquad \textbf{(3.7.4)}$$

where, σ_y is *the* yield stress of column bar, b is the distance between, and a_{te} is defined by the following equation

$$a_{te} = a_t + a_t{}' \frac{\sigma_y{}'}{\sigma_y} \quad \ldots. \quad \textbf{(3.7.5)}$$

where a_t = total tensile reinforcement area of column

a_t' = total reinforcement area of wing walls

σ_y' = yield stress of column bar

and x_n is defined by the following equation.

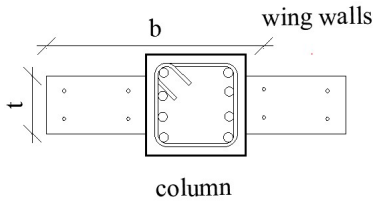

$$x_n = \frac{a_{te}\sigma_y}{0.85F_c t} \quad (3.8)$$

F_c= compressive strength of concrete (N/mm^2).

t = wall thickness in the compression side (t =b in case of no wall) (mm).

According to the aforementioned calculations, the expected failure mode was estimated to be punching failure for all specimens. However, specimen FP-W2 experienced prior flexural yielding, as described in Section 3.6. The details of the calculated results and experimental strengths are presented in **Table 3.7.1**.

Table 3.7.1 Calculated ultimate strengths compared to the ultimate strengths obtained from the experimental data

Specimen no.	Experimental strengths M_{exp} (kN·m)	Flexural strength of the slab ${}_nM_y$ (kN·m)	Calculated strength by AIJ M_0 (kN·m) [M_{exp}/M_0]	Calculated strength considering low-strength concrete M_{0l} (kN·m) [M_{exp}/M_{0l}]	Experimental failure mode
FP-1	7.3	15.8	9.85 [0.74]	8.3 [0.88]	Punching shear
FP-W1	19.9	26.1	20.5 [0.97]	17.2 [1.15]	Punching shear
FP-W2	14.7	17.2	20.2 [0.85]	18.0 [0.85]	Flexure followed by punching shear

3.8 Experimental discussion

The performance comparisons of the strengthened specimens and control specimens are shown in **Figure 3.8.1** using backbone curves. Punching shear failure occurred in the control specimen FP-1

at a drift ratio of 2.35%. The strengthened specimen FP-W1 exhibited a significant increase in strength by 2.7 times, showing higher stiffness than the control specimen while punching shear failure occurred at a drift ratio of 1.35%. However, the strengthened specimen FP-W2 exhibited a two-fold increase in strength. Therefore, it can be concluded that both strengthened specimens showed the effectiveness of the wing walls for improving the punching shear resistance of the flat plate-column connection.

The experimental strengths were compared with the design calculations, as listed in **Table 3.7.1**. The maximum experimental strengths of all the specimens were lower than the design strengths according to the AIJ standards. In particular, the maximum punching shear capacity of FP was 26% lower than the calculated value. This was probably caused by the utilization of low-strength concrete in the specimens. Therefore, the previous section presented two modifications: the application of sectional bending analysis and the direct shear strength equation proposed by Miyauchi et al. (2009). Consequently, the estimate of the punching shear strength for specimen FP-1 was improved by approximately 10%. Moreover, specimen FP-W1 strengthened with wing walls in the in-plane direction was conservative when considering low-strength conditions. However, for FP-W2 with wing walls in the out-of-plane direction, the estimate was 15% higher than the experimental value, which was likely caused by the flexural yielding of the flat plate, as described in the experimental results. In this study, it was confirmed that the estimate of the punching shear strength was acceptable for two flat plate specimens strengthened with and without using wing walls in the in-plane direction. However, further research, including finite element modeling and analysis, is necessary, particularly to validate these equations in terms of the failure mechanism of flat plate structures constructed using low-strength concrete.

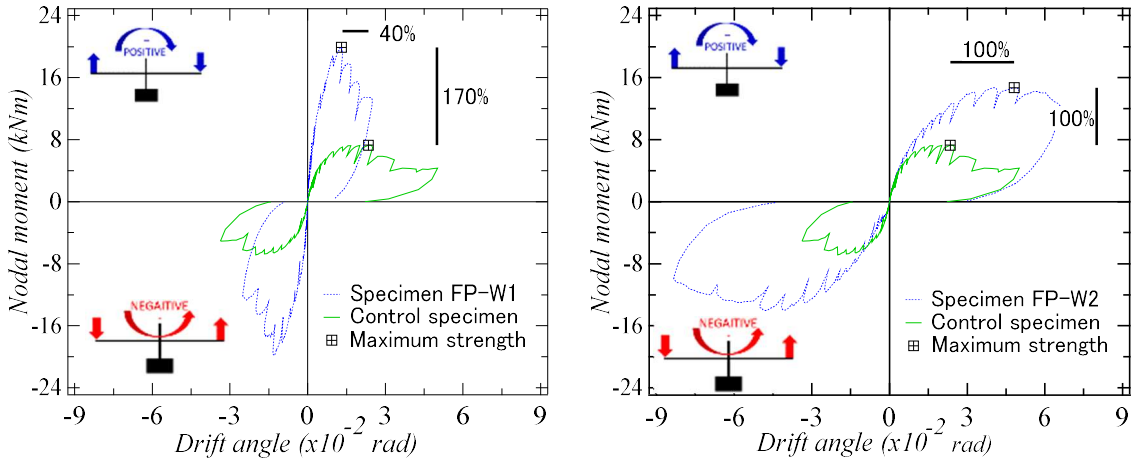

Figure 3.8.1 Performance comparisons of the strengthened specimens with that of the control specimen

3.9 Summary

In this investigation, a new strengthening scheme was proposed for the seismic retrofitting of an RC flat plate structure. A series of experiments was conducted involving three half-scaled interior flat plate-column connections with two specimens strengthened with RC wing walls to investigate the effectiveness of the proposed scheme and to evaluate the seismic behavior and performance. Based on the results obtained from the experiments, the following conclusions can be drawn:

1) In the experiments, specimens FP and FP-W1 showed punching shear failure as intended in their design, whereas FP-W2 showed plate rebar yielding followed by punching. Flexural cracks were prolonged in the 45° direction from the column/wing wall surface, whereas punching cracks extended radially from the column/wing wall surface. Finally, the surface concrete peeled due to punching shear failure.
2) The RC wing wall was effective in strengthening the flat plate structure. By applying in-plane direction strengthening for FP-W1, the maximum strength was 2.7 times larger than that of the control specimen FP. In the case of out-of-plane direction strengthening for FP-W2, the maximum strength was two times larger than that of the control specimen. Additionally, the former strengthening scheme contributed to stiffening the flat plate structure, but the latter scheme provided no additional stiffness.
3) Two slab reinforcements in the connection between slab and wing walls yielded at the peak load of specimen FP-W2, while no more reinforcements yielded until punching for specimen FP-1 and specimen FP-W1.
4) Punching shear failure occurred in FP-1 after attaining the maximum strength. On the other hand, punching shear failure occurred in FP-W1 at the maximum strength, while that occurred after the maximum strength of FP-W2.
5) The aforementioned increase in the resistance to punching shear failure by RC wing walls was attributed to the enlargement of the punching shear failure surface, which was considered in the punching shear strength estimations.
6) The punching shear strength estimated based on the AIJ standards overestimated the maximum capacity of the flat plate specimen using low-strength concrete. Thus, consideration of the low-strength concrete conditions improved the estimation but provided an overestimation of approximately 10%. However, the maximum capacity of the specimen strengthened with wing walls in the in-plane direction (FP-W1) was conservatively estimated by considering the low-strength conditions, whereas that of the specimen with wing walls in the out-of-plane direction (FP-W2) did not reach the estimated value because of prior flexural yielding of the flat plate.

As mentioned above, the proposed retrofitting scheme using RC wing walls was experimentally verified to be effective in upgrading flat plate-column connections constructed using low-strength

concrete. However, further investigations are recommended to evaluate the punching shear strength. In particular, finite element analysis may clarify the punching shear failure mechanism in flat plate structures with low-strength concrete. The present experimental data will be an excellent source for calibrating future studies using finite element analysis.

CHAPTER 4

Experimental Study on Strengthening of the Interior Flat Plate-column Joint using Post-installed RC Drop Panel

4.1 General

This chapter places an emphasis on an additional seismic strengthening scheme using post-installed drop panel for flat plate-column joints in existing structures that are seismically vulnerable. An experimental investigation on a series of three-scaled interior plate-column joints was conducted to explore the effectiveness of the seismic strengthening method using post-installed RC drop panel and to analyse the punching shear capacity of the plate column joint. It also focuses on typical existing flat plate structures constructed using low-strength concrete in Bangladesh. The series of three specimens with identical thickness and similar reinforcement details were constructed, varying in different dimensions of drop panel with proper anchorages. Post-installed bonded anchors were applied to connect the drop panel with the existing structure. Reversed static vertical loading was carried out with increasing amplitude up to the failure on both sides of the plate end same as Chapters 2 and 3.

4.2 Specimen design/details

Experimental testing has been performed with a set of three half-scaled specimens. One specimen, FP-2 (previously explained in chapter 2) was used as a benchmark specimen to compare the behaviour of the specimens with strengthening. Three specimens were designed, which were strengthened with a post-installed RC drop panel to investigate the feasibility of this method in the present study. The behavior of plate-column joints strengthened with the alternative size of post-installed drop panel installation was studied.

The existing component of all strengthened specimens was designed and constructed the same as the specimen FP-2 described in chapter 2. FP-D2 is a medium-type drop panel where the size was standardized by one-sixth of the shear span of slab, while other specimens, FP-D1 and FP-D3 marked as small and large type drop panel, respectively. The dimensions of the post-installed drop panels of FP-D1, FP-D2, and FP-D3 were 380 x 380 x 75 mm, 500 x 500 x 75 mm, and 620 x 620 x 75 mm in length x width x thickness, respectively. The dimension of small and large type drop panels were determined based on the medium type drop panel, smaller and bigger, with proper installation of anchorage. The thickness of the drop panel was assumed to be the same as the plate thickness of 75 mm to use the anchorage appropriately as per JBDPA standard (JBDPA 2005). The details of the drop panels were entirely the same between all specimens; nevertheless, the size was different.

The construction process was done based on three separate stages. A column bottom stub with dimensions of 400 mm x 400 mm x 300 mm in width x depth x height, respectively, was built to mount it to the bottom beam of the loading frame. RC bottom stub had eight holes at appropriate positions to mount the specimens on a frame base in the loading frame using steel PC bars. Firstly, the bottom stab was constructed to support the existing structure made with normal strength concrete. Two weeks later, existing structures were constructed using low-strength concrete. Then, after adequate curing of the concrete of the existing parts for 28 days, RC drop panels were installed along the column over the plate. The post-installed bonded anchor was applied to connect the strengthening part with the existing part considering the minimum thickness and spacing required in the Japanese guidelines of retrofit design of RC buildings (JBDPA) JBDPA2). The details of the specimens are shown in **Figure 4.2.1,** **Figure 4.2.2,** and **Figure 4.2.3** for specimens FP-D1, FP-D2, and FP-D3, respectively.

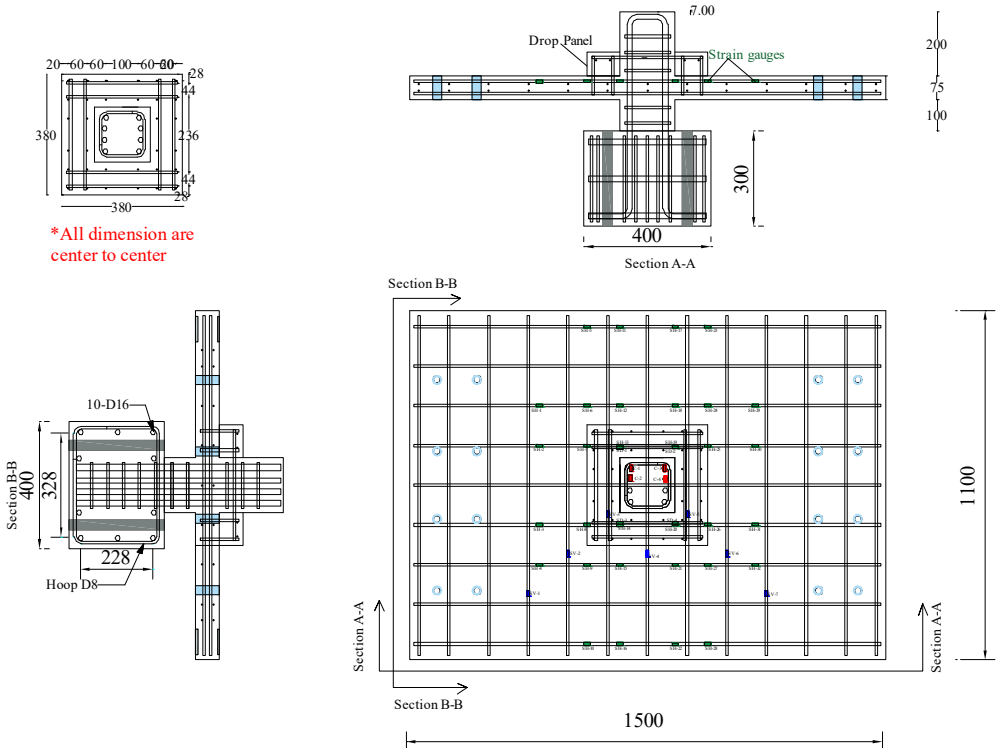

Figure 4.2.1 Details of the specimen FP-D1

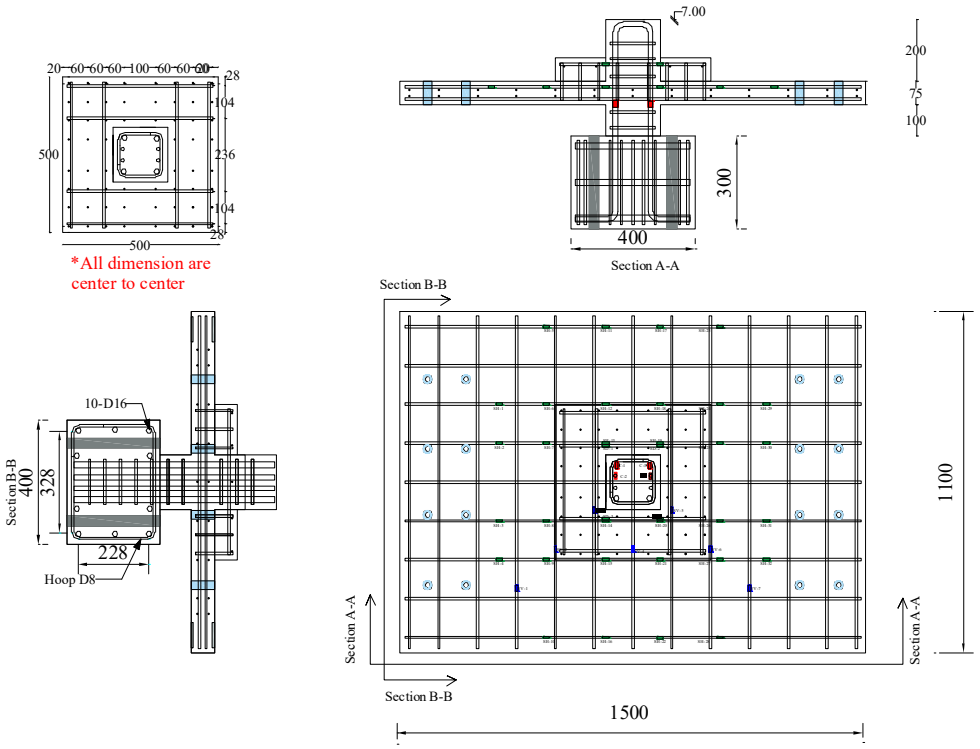

Figure 4.2.2 Details of the specimen FP-D2

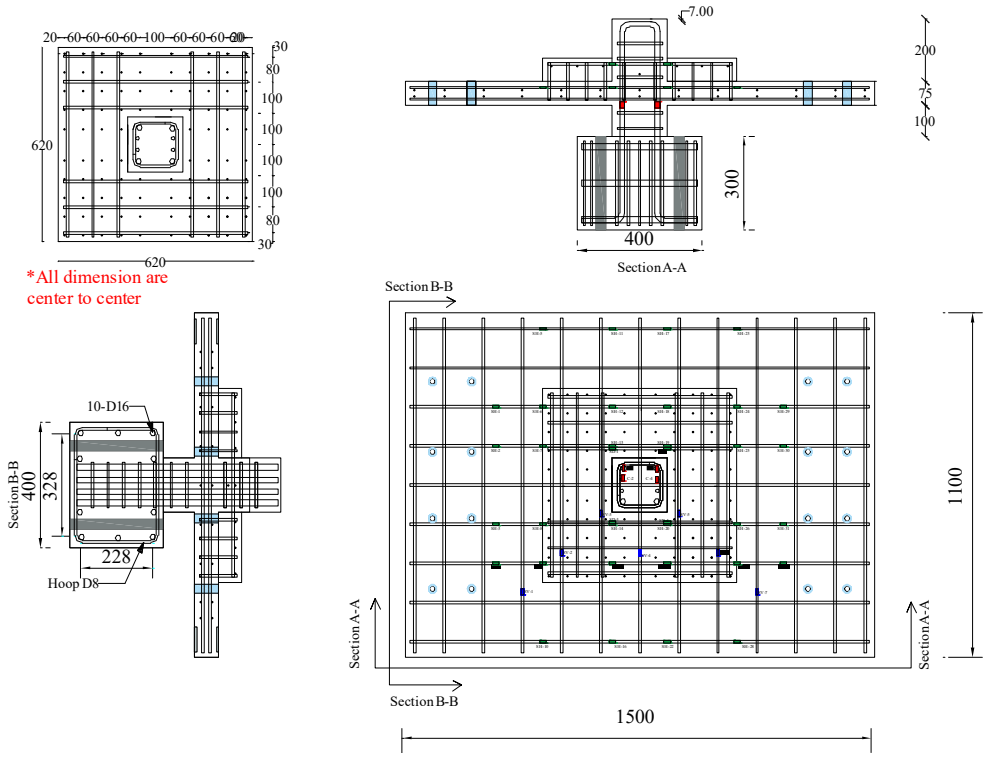

Figure 4.2.3 Details of the specimen FP-D3

4.3 Material mechanical properties of concrete and steel

The material properties were used the same as specimen FP-2, described in chapter 2. The concrete was mixed with a local mixing machine at the Housing and Building Research Institute (HBRI). However, the mixed concrete with a design strength of 30 N/mm^2 with stone chips as coarse aggregates, of which the maximum size was 15 mm, was used for the casting of the drop panel. The average properties of the concrete from the cylindrical compression tests are summarized in **Table 4.2**. The averaged material properties of the reinforcement from the tensile tests are referred to **Table 2.6 (chapter 2)**.

Table 4.1 Concrete mixture in kg/m^3

W/(cement + vita sand)	Water	Cement	Vita sand	Sand	Brick
60%	212	283	62	596	960

Table 4.2 Material properties of concrete

Type	Compressive strength (N/mm^2)	Elastic modulus (N/mm^2)
FP-D1	11.5 (brick chips)	15,998
FP-D2	13.6 (brick chips)	13,827
FP-D3	12.5 (brick chips)	13402
Drop Panel	47.0 (stone chips)	26,727

4.4 Experimental Program

4.4.1 *Experimental Setup*

Figure 4.4.1 shows the photograph of the experimental setup of the flat plate specimen that was strengthened with the drop panel. The test setup and loading protocol were the same as those shown in **Figures 2.5.1 and 2.5.4**. These specimens were also tested using a cyclic reversed static loading system at the structural laboratory of the Housing and Building Research Institute. The arrangement of LVDT to determine the drift ratio *R* is the same as shown in **Figure 2.5.3** in Chapter 2. The top and bottom surfaces of the specimens were inverted in this testing set-up. The loading history of all specimens is shown in **Figure 4.4.2**; however, the increasing amplitude kept the same. The loading was continued until 14% drift ratio for specimens FP-D1 and FP-D2 due to high deformation capacity. However, the test of the specimens FP-D2 and FP-D3 were conducted through an online platform system due to the coronavirus pandemic situation. There was an interrupt in the mid of the testing series; thus, it was decided to continue the test using the online platform. The overall image of the online platform is shown in **Figure 4.4.3**.



Figure 4.4.1 Photographic view of the experimental setup

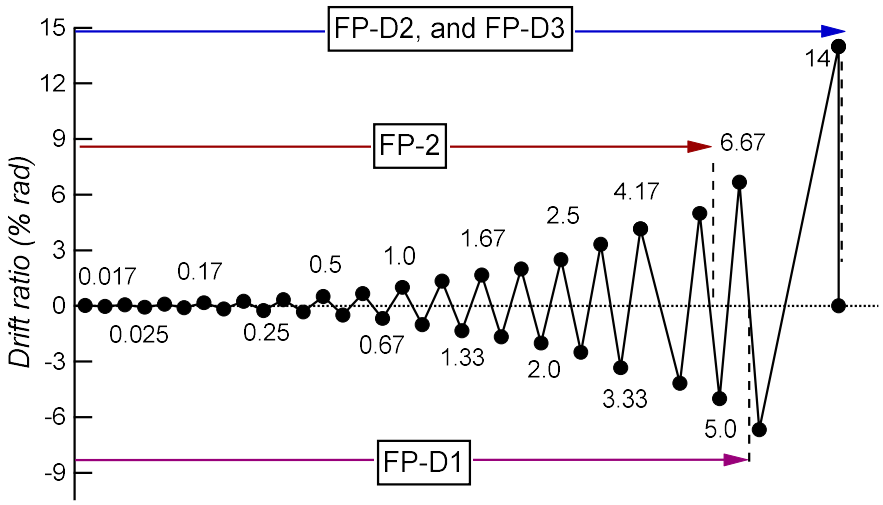

Figure 4.4.2 Loading history



Figure 4.4.3 Overall testing image through the online platform

4.4.2 *Instrumentation measurements*

Extensive measuring devices were assembled both externally and internally in the specimen so that we could monitor the response of the specimen as it was subjected to the experiment. During the process of testing, there were a total of 63 data channels that were active for each individual specimen. For the purpose of recording the applied reversed vertical load at the end of both sides of the plate, two load cells with a capacity of 300 kN each were utilized. A total of 14 LVDTs that 4 with 100 mm, 6 with 50mm, and 4 with 25 mm travel was installed underneath the plate in order to record vertical displacement of the plate at each loading step. In order to measure the strain responses of the rebar, a total of 40 strain gauges were installed at various prescribed locations. As shown in the **Figure 4.2.1, 4.2.2, and 4.23**, 39 strain gauges were installed in the plate rebars, 4 strain gauges were installed in the column rebars, and 4 strain gauges were installed in the drop panel rebars. All the installed LVDT's and strain gauges are listed in Appendices A-1 and A-2.

4.5 Experimental results

The nodal moments applied to the specimens were determined as a summation of bending moments by multiplying the absolute vertical forces applied to the slab by the distance from the application point to the 600 mm column center. In this particular configuration for the test, the top and bottom surfaces of the specimens were turned upside down.

4.5.1 *Specimen FP-D1*

Specimen FP-D1, which was strengthened by post-installed drop panel along with the plate and column connection, showed higher strength and deformation capacity. The relationship between the nodal moment and drift ratio *R* of the specimen is shown in **Figure 4.5.1 A**. An initial flexural crack occurred along with the drop panel and plate connection at *R* of -0.17% rad. The maximum strength of 28.1 kNm was observed during the positive loading in the cycle to 4.17% rad, while 26.7 kNm was observed in the cycle to 4.17% during negative loading. Subsequently, the strength decreased with the raising up of the surface concrete due to punching shear failure at *R* of 5% rad. **Figure 4.5.1 B** shows the punching shear failure observed on the top surface of the slab. It was observed that the top concrete surface peeled up by approximately 160 mm far from the edge of the drop panel in the loading direction. Additionally, brittle punching shear failure was observed in this specimen, as intended in the design stage. The crack pattern was drawn in **Figure 4.5.2**. The thick black line shows the punching shear failure. However, it was observed that some reinforcements were yielded which initiated from at *R* of 2.5% rad, as shown in **Figure 4.5.3**. The specimen started to yield the plate flexural yielding but meanwhile, it failed in punching shear failure after the drift started from 5%. The maximum strength was 28.2 kNm, which is close to the calculated punching shear strength of 28.1 kNm according to the AIJ standards (***M*₀ in Eq. 2.7.3**).

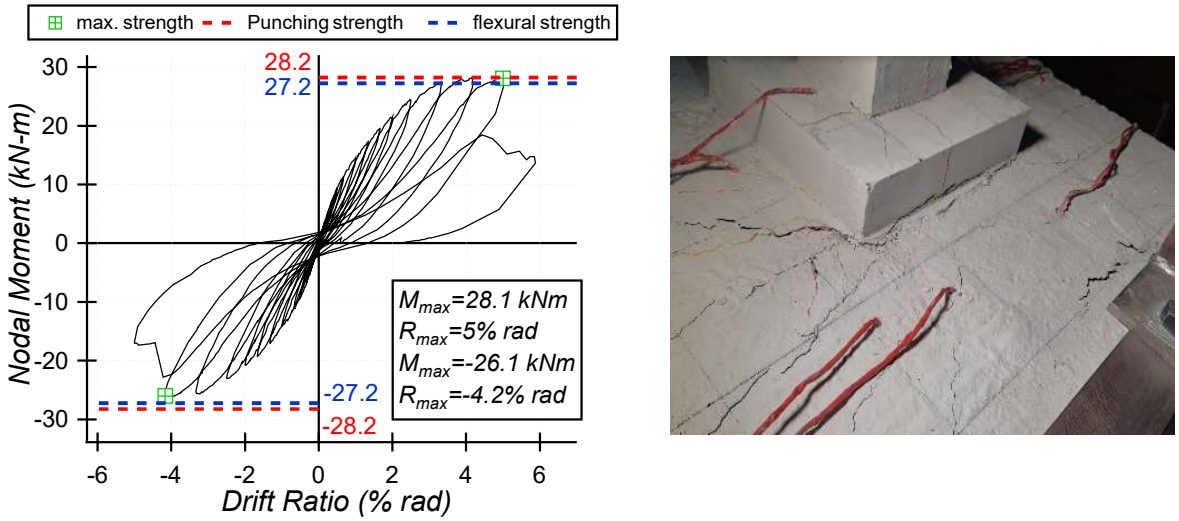

(A) **(B)**

Figure 4.5.1 (A) Nodal moment versus drift ratio relationship (specimen FP-D1) and (B) damage after punching shear failure

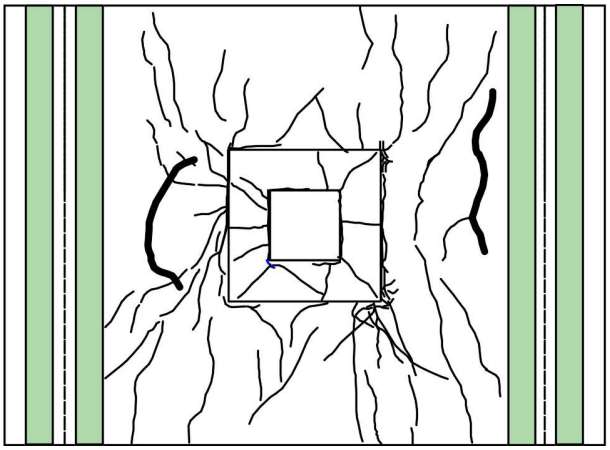

Figure 4.5.2 Crack pattern of specimen FP-D1

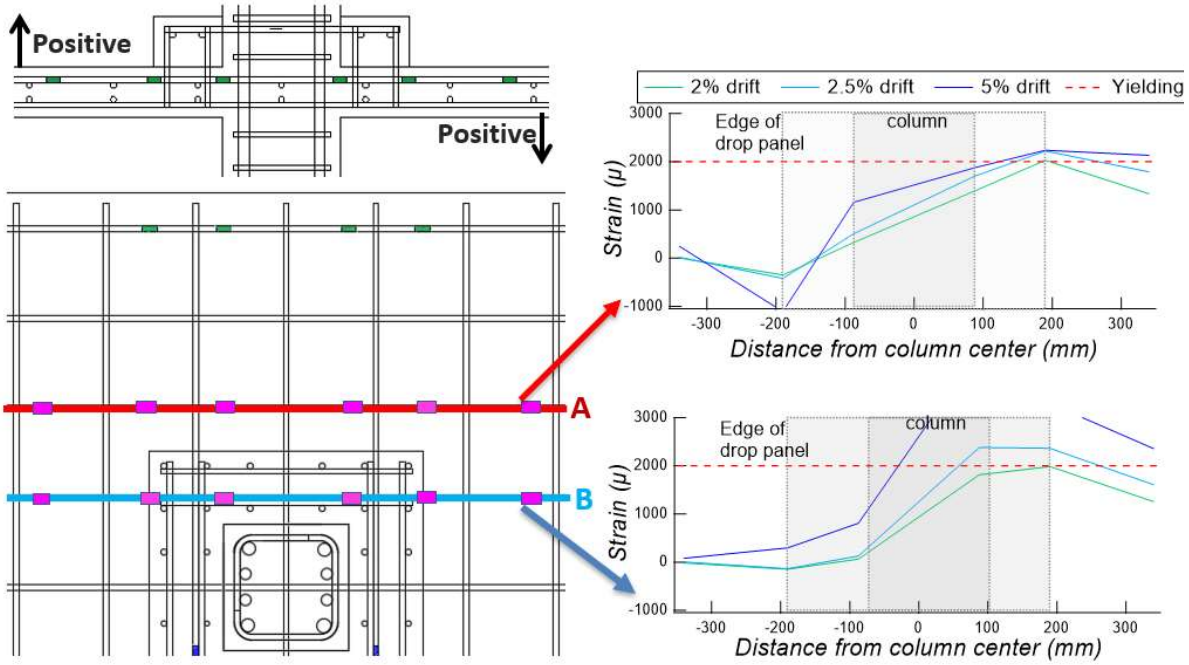

Figure 4.5.3 Comparison of strain distribution transitions under different cycles for specimen FP-D1

4.5.2 *Specimen FP-D2*

Specimen FP-D2 was strengthened by a medium-type post-installed drop panel along with the plate and column connection. The relationship between the nodal moment and drift ratio *R* of the specimen is shown in **Figure 4.5.4 A**. An initial flexural crack occurred parallel to the drop panel and slab edge at *R* of 0.25% rad. The maximum strength of 31.5 kNm was observed in the cycle to 5% rad during the positive loading while 28.5 kNm was observed in the cycle to -5% during negative loading.

Thereafter, the strength remained almost at the peak load with large slab displacement due to the plate flexure. **Figure 4.5.4 B** shows the observed damage on the bottom surface of the slab. Most of the substantial damages occurred near the edge of drop panel indicating the flexural yielding of the plate. The crack pattern was drawn on the top surface of the slab as shown in **Figure 4.5.5**, in which the thick black line shows the flexural yielding of the plate near the edge of drop panel. From the data of strain gauges, it was observed that some reinforcements started to yield at 4.2% drift, near the plate column joints, as shown in **Figure 4.5.6**. From the figure, it was noticed that the strain responses were higher on the outside of the edge of the drop panel and yielded the plate rebars. As a result, we are able to make assumptions about the critical section from outside of the critical section. The maximum strength 31.5 kNm, which was close to the calculated flexural strength of 31.6 kNm according to the AIJ standards. The punching shear strength of this specimen was larger than the plate flexural strength, which validated the intended design strength.

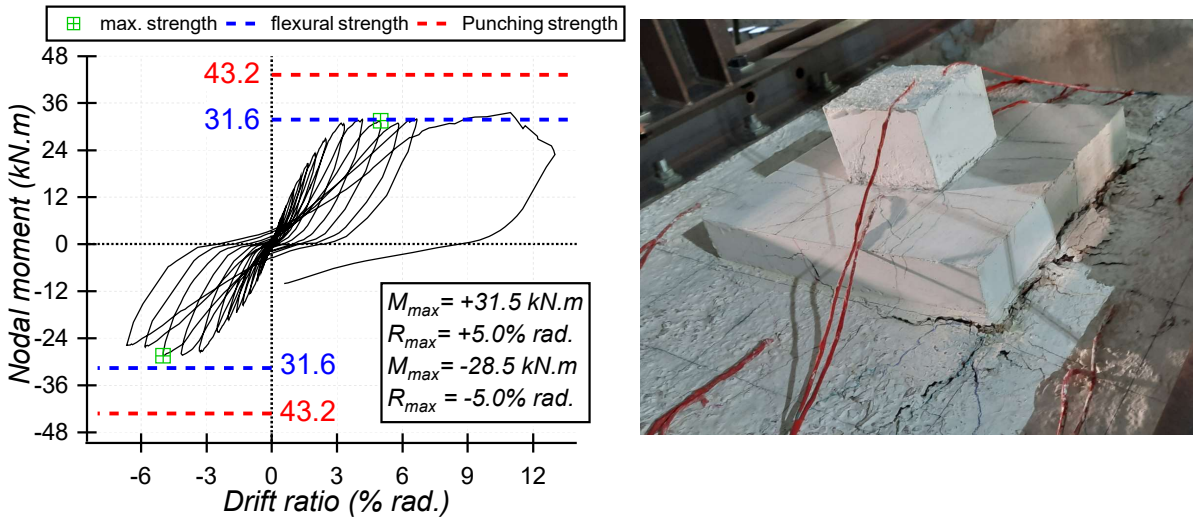

(A) **(B)**

Figure 4.5.4 (A) Nodal moment versus drift ratio relationship (specimen FP-D1) and (B) damage after punching shear failure

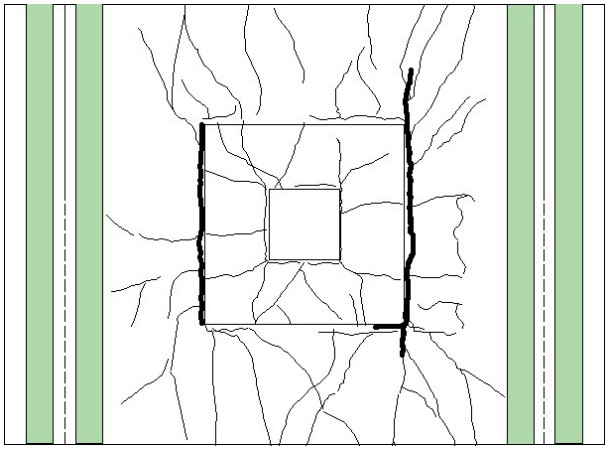

Figure 4.5.5 Crack pattern of specimen FP-D1

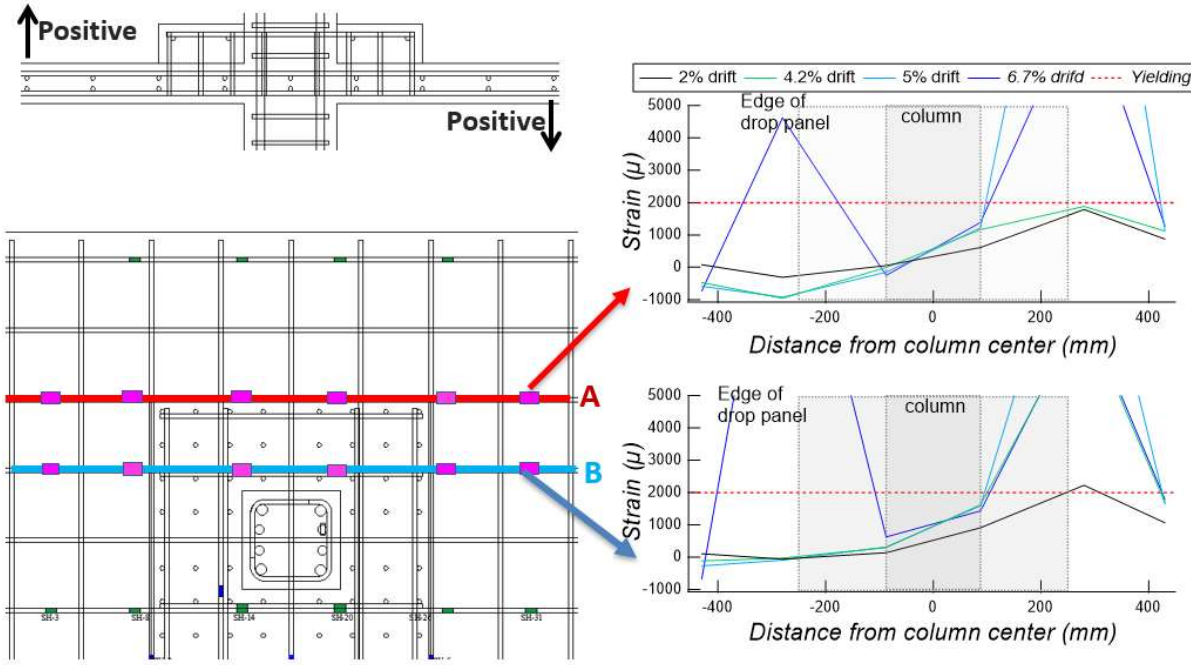

Figure 4.5.6 Comparison of strain distribution transitions under different cycles for specimen FP-D2

4.5.3 *Specimen FP-D3*

Specimen FP-D3, which was strengthened by a large-type post-installed drop panel, showed slightly higher strength but similar displacement behaviour as specimen FP-D2. The relationship between the nodal moment and drift ratio *R* of this specimen is shown in **Figure 4.5.7 A**. An initial flexural crack occurred along with the drop panel and plate connection at *R* of -0.33% rad. The maximum strength of 36.7 kNm was observed during the negative loading in the cycle to 4.2% rad. On the other hand, the maximum strength was 34.5 kNm in the positive loading cycle. The strength was

constant with the increasing drift ratio due to the large rebar yielding of the plate. **Figure 4.5.7 B** shows the plate flexure was observed on the bottom surface of the slab. The crack pattern was drawn on the bottom surface of the slab, in which it is noticeable that there is not so much substantial damage to the slab. The reinforcements started to yield, which initiated from *R* of 4.2% rad, as shown in **Figure 4.5.9**. From the figure, it was observed that the strain responses were higher and yielded for those located on the outside of the edge of the drop panel. Therefore, we can assume the critical section from the outside of the critical section. The maximum strength was 36.7 kNm, which was close to the calculated flexural strength of the slab strength of 28.1 kNm according to the AIJ standards (***M*₀ in Eq. 2.7.3**).

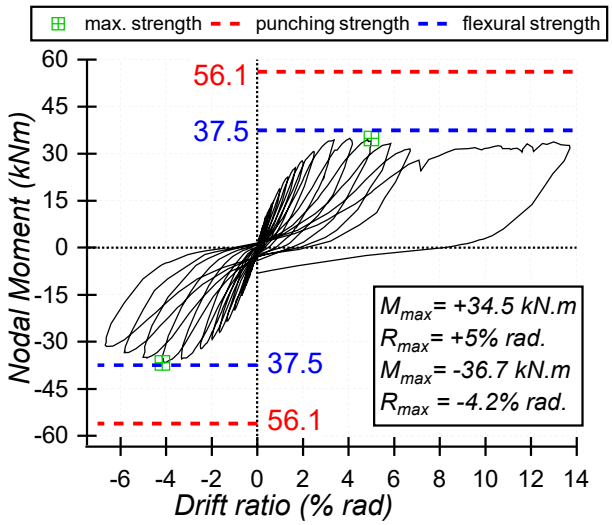

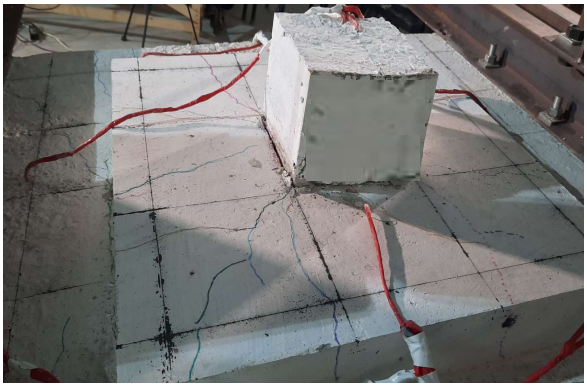

(A) **(B)**

Figure 4.5.7 (A) Nodal moment versus drift ratio relationship (specimen FP-D1) and (B) damage after punching shear failure

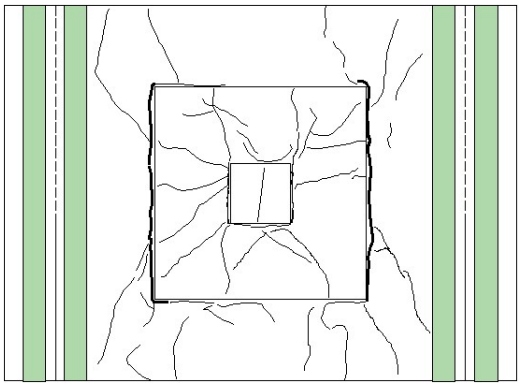

Figure 4.5.8 Crack pattern of specimen FP-D1

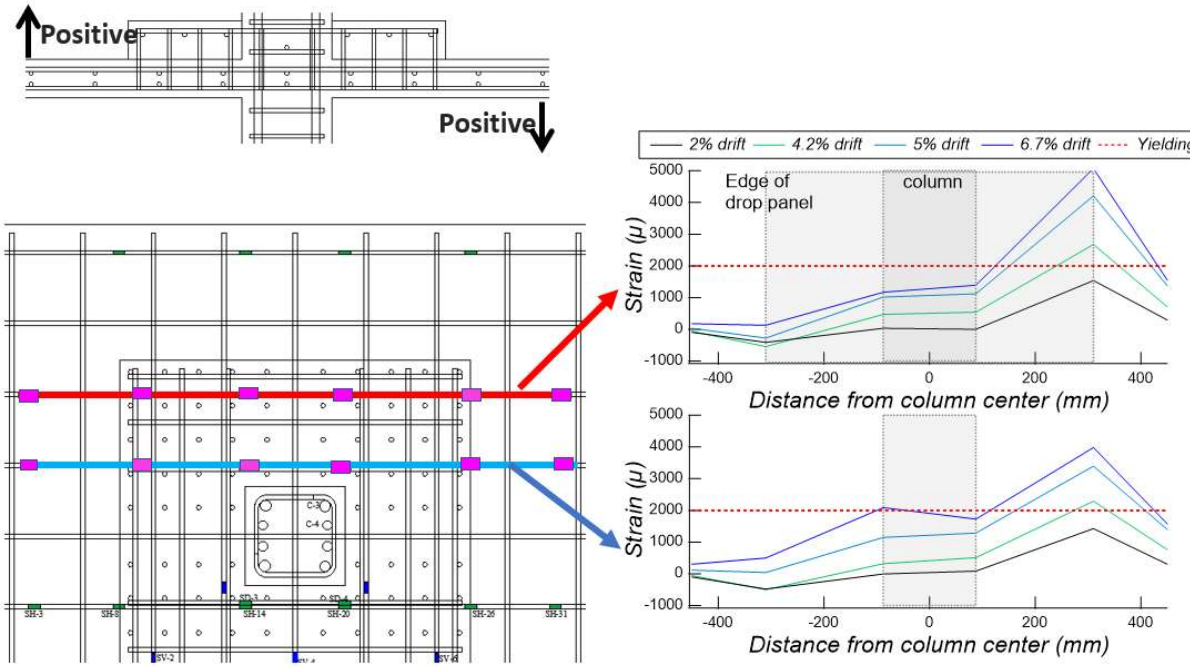

Figure 4.5.9 Comparison of strain distribution transitions under different cycles for specimen FP-D2

4.6 Strength estimation of the specimens

The bending moment diagrams of the specimens under static seismic loads are shown in **Figure 4.6.1**, which assume that the inflections are at the midpoints of the span of the plate. The ultimate strength of all the specimens was evaluated during the design stage. The ultimate strength of specimen M_u represents the joint nodal moment and failure mode, which are evaluated by **Eq. 4.6.1**:

$$M_u = min[{}_n M_y, M_{0,c} M_u] \quad \textbf{(4.6.1)}$$

where ${}_nM_y$ is the nodal moment at the plate-column connection when the plate yielded in flexure (N-mm), M_0 is the punching shear capacity at the critical section of the column (N-mm), ${}_cM_u$ is the nodal moment at the joint when the column yielded (N-mm).

The conversion of M_y into the nodal moment of joint ${}_nM_y$ is defined by **Eq. 4.6.2** for all specimens using drop panel (refer to **Figure 4.6.1**):

$$ {}_nM_y = 2M_y \frac{L_s/2}{L_s/2 - l_d/2} \tag{4.6.2} $$

According to the above calculations, the expected failure mode was estimated to be punching failure for specimen FP-D1. The details of the calculated results and experimental strengths are tabulated in Table 4.4. A discussion will be given in the following section. The critical section was assumed d/2 distance from the edge of drop panel based on the evidence described in the previous section (as shown in **Figures 4.5.3, 4.5.6,** and **4.5.9**), for calculating the punching shear strength according to AIJ standard, as shown in **Figure 4.6.2.**

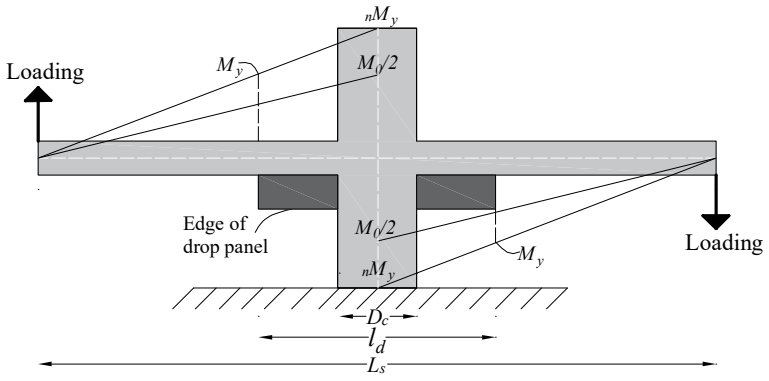

Figure 4.6.1 Moment diagram for specimens using drop panel

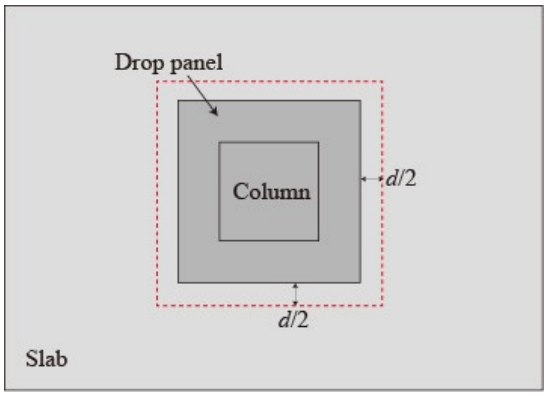

Figure 4.6.2 Assumed critical section of punching shear failure

Table 4.3 Calculated ultimate strengths compared to the ultimate strengths obtained from the experimental data

Specimen no.	Experimental strengths M_{exp} (kN·m)	Flexural strength of the slab ($_nM_y$) (kN·m)	Calculated strength by AIJ M_0 (kN·m)	Calculated strength considering low-strength concrete M_{0l} (kN·m)	Experimental failure mode
FP-D1	28.1	27.2	28.2	31.6	Punching
FP-D2	31.6	31.7	43.2	57.1	Flexure followed by punching
FP-D3	36.7	37.6	56.1	71.6	Slab flexure

4.7 Experimental discussion

The backbone curves are shown in **Figure 4.7.1** to illustrate the performance comparisons that were made between the benchmark specimen and the strengthened specimens. The maximum strength was increased by 270% to 340%, while the deformation capacity was enhanced with a large scale of all strengthened specimens using a drop panel compared to that of the benchmark specimen. The flexural crack initially started from the corner of the column/drop panel and extended approximately 45-degree direction, leading to the lifting of the surface concrete for specimen FP-D1. On the other hand, flexural cracks grew along the drop panel edge for specimens FP-D2 and FP-D3. The maximum capacity of all strengthened specimens showed flexural yielding of the plate as intended in their design stage, and the estimation was close to the theoretical prediction. However, the flexural yielding of the plate and punching shear strength estimations were close to each other for specimen FP-D1; thus, punching shear failure was fully visible from the damage to the specimen. The critical section was assumed at d/2 distance from the edge of the drop panel. The assumed critical section gave a good agreement with the calculation of punching shear strength estimation. The small type drop panel significantly increased both strength and deformation but not enough to prevent punching shear failure. The medium-sized drop panel FP-D2 had a good agreement with all perspectives. However, the damage to the connection between the drop panel and the plate was minimal for FP-D3 compared to FP-D2 because of the use of large drop panel with anchorage. It is possible to say that the strength and ductility of the plate improved in proportion to the size of the drop panel. The post-installed RC drop panel effectively changed the brittle punching shear failure to ductile flexural failure mode with the increase of flexural strength of the plate compared to that of the benchmark specimen.

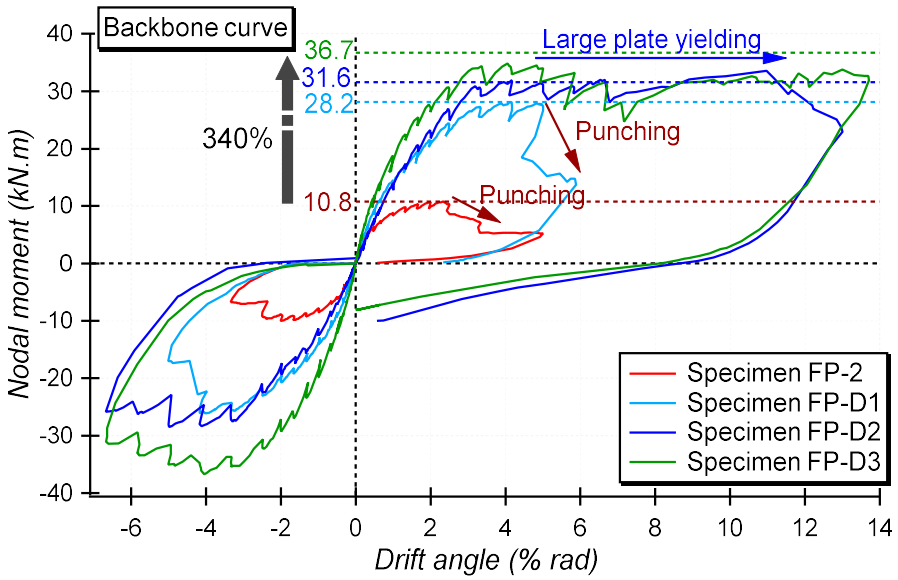

Figure 4.7.1 Performance comparison using backbone curve

4.8 Summary

An experimental investigation was carried out on a series of three-scaled interior plate-column joints in order to investigate the efficacy of the proposed seismic strengthening method utilizing post-installed RC drop panel and to investigate the punching shear capacity of the plate column joint. From the experimental results explained above, the following conclusions were obtained:

1) The maximum strength was increased by 270% to 340%, while the deformation capacity was enhanced with a large scale of all strengthened specimens using a drop panel compared to that of the benchmark specimen.
2) The flexural crack initially started from the corner of the column/drop panel and extended approximately 45-degree direction, leading to the lifting of the surface concrete for specimen FP-D1. On the other hand, flexural cracks grew along the drop panel edge for specimens FP-D2 and FP-D3.
3) The maximum capacity of all strengthened specimens showed flexural yielding of the plate as intended in their design stage, and the strength estimations of theoretical prediction were close to the experimental strengths. The assumed critical section gave a good agreement with the punching shear strength estimation calculation.
4) The small type drop panel significantly increased both strength and deformation but not enough to resist punching shear strength. The medium-sized drop panel FP-D2 had a good agreement with all perspectives. However, the damage to the connection between the drop panel and the plate was minimal for FP-D3 compared to FP-D2.

5) The post-installed RC drop panel effectively changed the brittle punching shear failure to ductile flexural failure mode with the increase of flexural strength compared to that of the benchmark specimen.
6) It was experimentally verified that installing the RC drop panel effectively upgraded flat plate-column connections with low-strength concrete under seismic loading by increasing the effective depth of the plate and periphery of the column critical section.

CHAPTER 5

Seismic Evaluation of Existing Flat Plate Structure

5.1 General

This chapter intends to introduce a simplified evaluation methodology for the seismic capacity of existing flat plate structures commonly used in Bangladesh, based on the Japanese seismic evaluation guideline concepts. Reinforced concrete (RC) flat plate structural systems have a very high risk of punching shear failure, which could lead to a risk of life safety and damage to property when there is an earthquake. Bangladesh has a large number of poorly constructed flat plate structures, and new structures are constantly being built without adequate seismic design. Therefore, the seismic evaluation and strengthening of the existing low-performance RC flat plate structures are required to avoid catastrophic damage from earthquakes. In addition, there was no standard for seismic evaluation of RC structures in Bangladesh until 2015. Strict adherence to the code, particularly the seismic provisions, came into practice very recently, as mandated by the "CNCRP Manual" (Public Works Department (PWD) 2015) in 2015 based on the Japanese Standard (JBDPA 2005). In contrast, this latest manual has not included the seismic evaluation of flat plate structures. Therefore, it is necessary to introduce the seismic evaluation of the existing flat plate structure. As a result, this chapter introduced an evaluation methodology for the seismic capacity of existing flat plate structures commonly used in Bangladesh, with simplified modifications to the abovementioned guidelines. The evaluation procedure was proposed based on the research evidence described in chapter 2 with the concept of simple modification and demonstrated in the following.

5.2 Scope

In Bangladesh, the typical flat plate structures often have beams in the perimeter frame, as shown in **Figure 5.2.1**. But the flat plate structures are flexible due to the absence of beams; thus, the exterior columns with beams on their perimeter shall be considered (explained in the following sections) to evaluate the seismic capacity of flat plate structures. Exterior columns connected with beams can be assessed in the same manner as the moment-resisting frame per the JBDPA Standard. The contributions of the columns with beams enclosed by the red circles are considered only focusing on the x-direction, as shown in **Figure 5.2.1**.

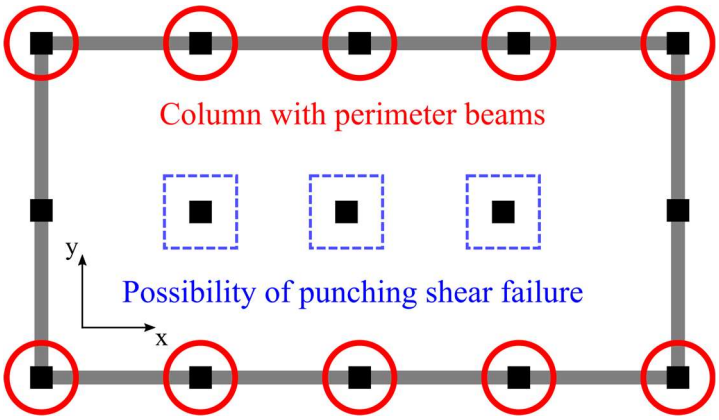

Figure 5.2.1 Conceptual image of the seismic evaluation for a typical floor plan

5.3 Seismic Evaluation Work-flow

The seismic evaluation workflow diagram is shown in **Figure 5.3.1**, where Q_{mu} is column shear resistance based on the flexural yielding of the column, Q_{su} is column shear resistance of column, Q_{slab} is column shear resistance based on the flexural yielding of the slab and Q_{punch} is column shear resistance based on the punching shear of the slab. The modification in the calculation of strength index C and ductility index F were briefly introduced in this evaluation procedure. The strength index C shall be calculated from the ultimate lateral load-carrying capacity (Q_{mu} or Q_{su}) of exterior columns with beams in principle described later in **section 5.5**. For example, the contributions of the columns with beams enclosed by the red circles are considered only focusing on the x-direction, as shown in **Figure 5.2.1**. However, the judgment of the interior column's failure mode is necessary to compute the ductility index F of exterior columns because the interior column is likely to fail in punching, which possibly leads to failure of the partial/overall structure. The detailed procedure of calculating the seismic index is the same as the JBDPA standard, except for the modification in the following sections.

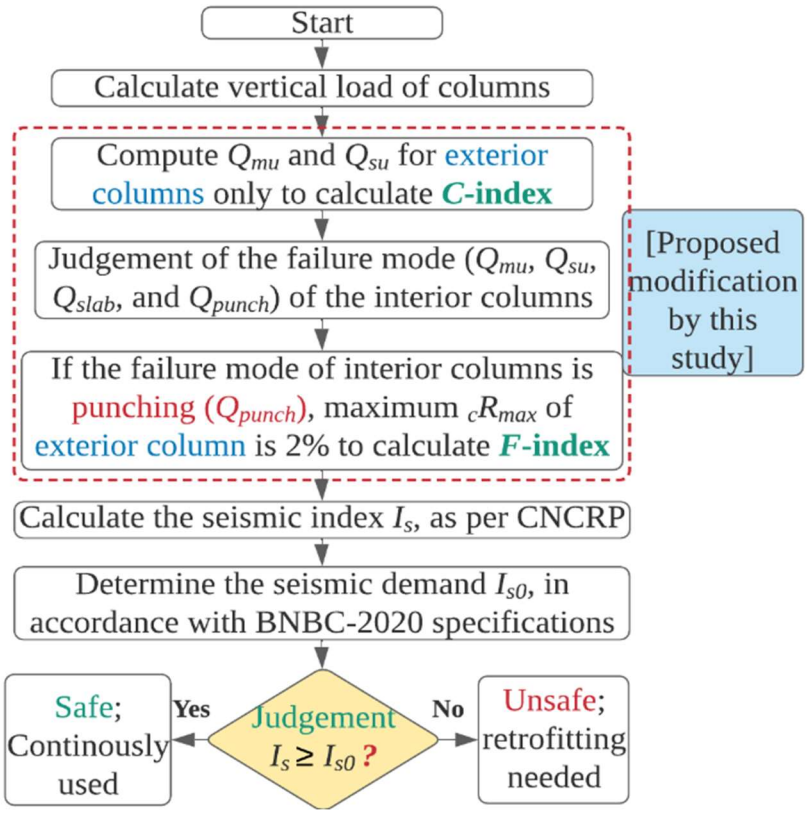

Figure 5.3.1 Flowchart of the seismic evaluation process

5.4 Column Failure Mechanism and Shear Resistance

The exterior columns with the beams on their perimeter are considered to evaluate the seismic capacity of flat structures, as shown in **Figure 5.4.1**. The following equation calculates the exterior column shear resistance ${}_eQ_u$ according to the JBDPA standard. The failure mode can be determined based on the computed strengths by taking the minimum value between Q_{mu} and Q_{su} as follows:

$$ {}_eQ_u = \min(Q_{mu}, Q_{su}) \tag{5.4.1} $$

For the exterior columns, two types of failure modes should be considered. The strength of each failure mechanism is calculated as the following.

(a) Q_{mu} : column shear resistance based on the flexural yielding of a column can be calculated as below (Public Works Department (PWD) 2015):

$$ Q_{mu} = \frac{2M_u}{h_0} \tag{5.4.2} $$

where M_u is flexural strength of column, calculated as the following and h_0 is clear height of column.

Flexural strength of columns shall be calculated in accordance with **Eqs. (5.4.3) -(5.4.6)**.

For columns with deformed longitudinal reinforcing bars:

In case of $N_{max} \geq N > 0.4bDF_c$,

$$M_u = \left(0.8a_t\sigma_y D + 0.12bD^2F_c\right)\left(\frac{N_{max}-N}{N_{max}-0.4bDF_c}\right)e_h \quad \textbf{(5.4.3)}$$

and in case of $0.4bDF_c \geq N > 0$,

$$M_u = 0.8a_t\sigma_y D + 0.5ND\left(1-\frac{N}{bDF_c}\right) \quad \textbf{(5.4.4)}$$

For columns with plain longitudinal reinforcing bars:

where $N_{max} \geq N > 0.4bDF_c$,

$$M_u = \left(0.8a_t\sigma_y D + 0.12bD^2F_c\right)\left(\frac{N_{max}-N}{N_{max}-0.4bDF_c}\right)e_h e_p \quad \textbf{(5.4.5)}$$

and where $0.4bDF_c \geq N > 0$,

$$M_u = \left(0.8a_t\sigma_y D + 0.5ND\left(1-\frac{N}{bDF_c}\right)\right)e_p \quad \textbf{(5.4.6)}$$

where

$e_h = (N/bDF_c + 0.2) / 0.6$

e_p= 0.8 for $F_c \leq$13.5 MPa and 1.0 for F_c>13.5MPa

M_u: flexural strength of column

a_t: total area of tensile longitudinal reinforcement

σ_y: yield strength of longitudinal reinforcing bars in column

N_{max}: maximum axial strength of column

N_{min}: minimum axial strength of column

N: axial load of column

e_h: strength enhancement factor for high axial load

F_c: concrete compressive strength

b: width of column

D: depth of column

(b) Q_{su}: column shear resistance of a column can be calculated as below (Public Works Department (PWD) 2015):

$$Q_{su} = K_r\left\{\frac{0.053p_t^{0.23}(18+F_c)}{M/(Q\cdot d)+0.12} + \alpha_L 0.85\sqrt{p_w\sigma_{wy}} + 0.1\sigma_0\right\}bj \quad \textbf{(5.4.7)}$$

where $K_r = 0.244 + 0.056F_c$ (reduction factor for low-strength concrete ($F_c < 13.5$MPa));

F_c is concrete strength; $\alpha_L = 0.038\sigma_B \leq 0.85$;

p_t: tensile reinforcement ratio (%)

d: effective depth of column. D – 50 mm shall be applied.

M/Q: Shear span length. $h_0/2$ shall be applied. $1.0 \leq M/Qd \leq 3.0$

j: distance between centroids of tension and compression forces, $0.8D$ shall be applied.

p_w: transverse reinforcement ratio

σ_{wy}: yield strength of transverse reinforcing bars in column

σ_0: axial stress in column, not exceeding 8.0MPa

α_L: reduction factor for low-strength concrete

h_0: clear height of column

For the interior columns, additional two types (**Figure 5.4.1**) of failure modes (Q_{slab} and Q_{punch}) should be considered for the shear resistance ${}_iQ_u$, due to the absence of beams. However, the contribution of interior columns that are connected without beam is not accounted for the building strength, and the failure mode is identified to mainly calculate the ductility index of the exterior column, as described later. The strength under each failure mechanism is calculated as the following.

$$ {}_iQ_u = \min(Q_{mu}, Q_{su}, Q_{slab}, Q_{punc}) \quad \textbf{(5.4.8)} $$

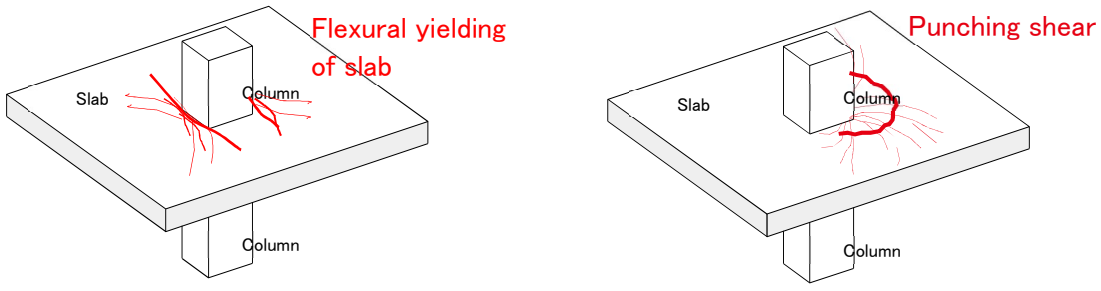

Figure 5.4.1 Failure mechanisms governed from the slab

(c) Q_{slab} : Column shear resistance based on the flexural yielding of slab, calculated by the following equation:

$$Q_{slab} = \frac{M_{slab}}{h_0} \tag{5.4.9}$$

The bending moment of slab can be assumed as an antisymmetric bending moment, and M_{slab} is the nodal flexural capacity of slab. The M_{slab} is calculated by **Eq. 5.4.10**, assuming the moment diagram as shown in **Figure 2.4.2**.

$$M_{slab} = \frac{{}_lM_{slab}}{l_l/2} \times \left(\frac{l_l}{2} + \frac{D_c}{2}\right) + \frac{{}_rM_{slab}}{l_r/2} \times \left(\frac{l_r}{2} + \frac{D_c}{2}\right) \tag{5.4.10}$$

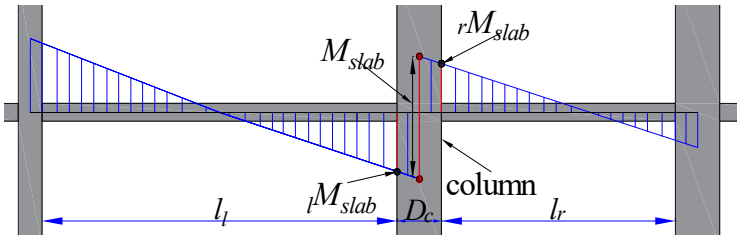

Figure 5.4.2 Assumed moment diagram

The notations are shown in **Figure 5.4.2**, and ${}_lM_{slab}$ or ${}_rM_{slab}$ is the flexural capacity of slab by **Equation 5.4.11** (AIJ 2018), in which full slab width is assumed to be effective.

$${}_lM_{slab}\ or\ {}_rM_{sla} = 0.9 \sum a_t\, \sigma_y\, d \tag{5.4.11}$$

where,

a_t is the cross-sectional area of tensile rebar,

σ_y is yield stress of rebar,

d is the effective depth of slab.

(d) Q_{punch}: column shear resistance based on the punching shear failure can be calculated as below (AIJ 2018):

$$Q_{punch} = \frac{M_u}{h_0} = (1 - \frac{V_u}{V_0})\frac{M_0}{h_0} \tag{5.4.12}$$

where

M_u is bending moment at the ultimate state

V_u is vertical load at the ultimate state

M_0 is capacity of the bending moment

V_0 is the capacity of the vertical load

In the Japanese design standard (AIJ 2018), column and flat plate joint capacity is assumed to be consumed by the applied vertical load and bending moment. The capacity to vertical load V_0 is the

capacity of connection under vertical load only. Therefore, (1-V_u/V_0) in Eq. 5.4.12 is the ratio of the capacity used by the applied vertical load V_u. Similarly, the capacity to bending moment M_0 is the capacity of the connection when it is consumed by the bending moment only. Therefore, (1-V_u/V_0)M_0 is the capacity that can be consumed by bending moment under V_u. The capacity of vertical load V_0 can be calculated as the product of the shear strength of concrete and the area of the critical section. The critical section is located $d/2$ distance away from the column edge, as shown in **Figure 5.4.3**. The punching shear strength (M_0) was calculated according to the following equations (**Eqs. 2.7.3, 2.7.4, 2.7.5,** and **2.7.6)** from the AIJ standard for RC structures.

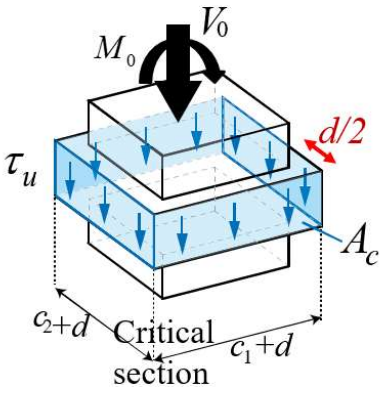

Figure. 5.4.3 Induced vertical load and moment with assumed critical section

5.5 Calculation of *C*-index

This section introduces the calculation of the *C*-index that was modified based on the experimental findings. The following equation calculates the *C*-index of an exterior column that is connected with beams only.

$$C = {}_eQ_u / \sum W \qquad \textbf{(5.5.1)}$$

where

${}_eQ_u$ the shear resistance of exterior columns

$\sum W$: total weight supported by the story concerned

This study recommends that the column's contribution to the column's shear resistance without being connected with beams should be ignored for the seismic resistance of flat plate structures under conservative estimation. According to the first level screening of the JBDPA standard, the shear resistance of an independent column is assumed to be 0.4%, which corresponds to F=1. Thus, based on previous experimental investigations explained in chapter 2, the shear resistance of the existing column is conservatively measured at 0.4% to identify the flexibility of the flat plate structure. Flat plate structures were found to be flexible; thus, it should be carefully estimated. **Figure 5.5.1** shows the

experimental results in which the applied nodal moment of Specimen FP-1 at a drift of 0.4 % was 2.0 kNm. Assuming a storey height of 1.5 m considering the half-scaled model, the shear force of the column at a drift of 0.4% was 2.66 kN (= 1.98 kNm x 2/1.5 m) under double curvature. The column size in this experiment was 175 mm x 175 mm; thus, the shear stress was 0.086 MPa (= 2.66 kN/(175 mm x 175 mm) which was less than 10 % of the value assumed in the first level screening at the same drift level. Therefore, the shear resistance for calculating the *C*-index of an interior column that is connected without beams can be ignored; namely, this study recommends that the contribution of the column without connected with beams should be ignored for the seismic resistance of flat plate structure.

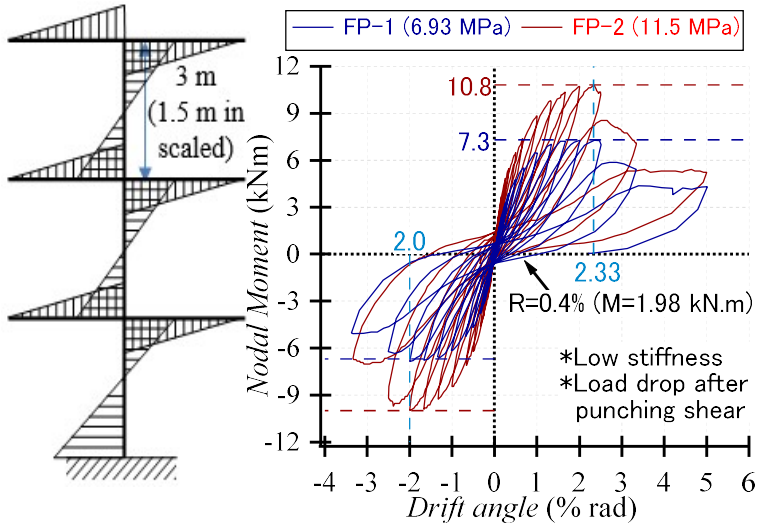

Figure 5.5.1 Experimental flat plate-column joint capacity

5.6 Calculation of *F*-index

According to the JBDPA, the *F*-index of an exterior column can be determined. The following equation calculates the *F*-index of an exterior column connected with beams.

$$F = \frac{\sqrt{2R_{mu}/R_y - 1}}{0.75(1+0.05\ mu/R_y)} \leq 3.2;\ for\ R_{mu} > R_y \qquad \textbf{(5.6.1)}$$

where R_{mu} is the drift angle at ultimate strength, R_y is the drift at yielding, and R_{250} is the standard inter-storey drift.

From the experimental studies, as shown in **Figure 5.5.1**, it was observed that the flat plate specimens exhibited a lower stiffness to flexural yielding than typical beams and a sudden load drop immediately after the punching shear failure. Although the maximum strengths of both specimens were different due to the application of different concrete strengths (6.93 MPa for FP-1 and 11.5 MPa for

FP-2) in **Figure 5.5.1**, both specimens showed similar deformability of approximately 2% drift angle in the negative loading, as shown in the figure. Based on the experimental results, an upper bound of ${}_cR_{max}$ is recommended at 2% for the *F*-index of exterior columns (the flat plate structure) when any interior column is expected to show punching shear failure to collapse. Under seismic action during an earthquake along with its gravity load, punching may cause the partial/overall structure to fail, so an upper bound is required to prevent punching failure. However, the *F*-index of interior columns is not necessary for the seismic evaluation because its contribution is neglected due to the minimal resistance, as mentioned in the previous section.

5.7 Judgment of the evaluation

The seismic index is a numerical representation of the seismic performance of a building based on its strength and ductility. In the seismic evaluation of the existing building, it is desirable to compare the capacity of a structure against seismic demand. The seismic safety of any structure shall be judged by **Eq. 5.7.1** as per the JBDPA standard, comparing the seismic index I_s and the seismic demand index I_{s0}.

$$I_s \geq I_{s0} \text{ (Safe)} \qquad \textbf{(5.7.1)}$$

where, I_s is the seismic index of the structure defined for each story and in each principal direction of the structure, which is based on the JBDPA standard. The minimum acceptable performance level for an existing structure is defined as the structure maintaining a small margin from collapse when subjected to the maximum probable earthquake. Seismic demand index I_{s0} is determined as per the requirement of the Bangladesh National Building Code.

$$I_{s0} =\geq 0.8 \times \frac{2}{3} \times Z \times I \times C_s \qquad \textbf{(5.7.2)}$$

where Z is the seismic zone coefficient, I is the structural importance factor, and C_s is the normalized acceleration response spectrum. (BNBC 2020). The minimum acceptable performance level for an existing structure is defined as the structure maintaining a small margin from collapse when subjected to the maximum probable earthquake. And, I_{s0} is the seismic demand index, determined by Eq. 16, as per the requirement of the Bangladesh National Building Code (BNBC-2020).

Seismic demand index

Seismic demand index I_{s0} is determined as per the requirement of BNBC 2020. It is briefly introduced in the following:

$$I_{S0} = \frac{0.8*2}{3}.Z.I.C_s \qquad \textbf{(5.7.2)}$$

Where:

Z : Seismic zone coefficient, as defined in **Section 2.5.4.2** of BNBC (2020)

I : Structure importance factor, as defined in **Section 2.5.5.1** of BNBC (2020)

C_S: Normalized acceleration response spectrum, which is a function of structure (building) period and soil type (site class), as defined by **Eqs. 6.2.35a to 6.3.35d** of BNBC (2020)

Z: 0.2 (zone coefficient)

I : 1.0

5.8 Example of application

The process for seismic evaluation is demonstrated in this section using a flat plate structure as an illustration. By conducting a detailed seismic evaluation, it will be possible to estimate the flat plate building's seismic capacity and compare it to the required seismic capacity as specified by BNBC 2020. A typical Bangladeshi flat plate structure is introduced by showing **Figure 5.8.1**, where it has beams in the perimeter frame, and the interior columns are not connected with beams. The summary of the building materials is tabulated in Table 5.1. The building is six storied residential building located in Dhaka. The height and weight of each building floor are 3 m and 1746 kN, respectively. The column schedule of the existing building is shown in **Figure 5.8.2**. The proposed seismic evaluation methodology was applied in this example building. The failure mode of the interior columns of this building was evaluated to be punching.

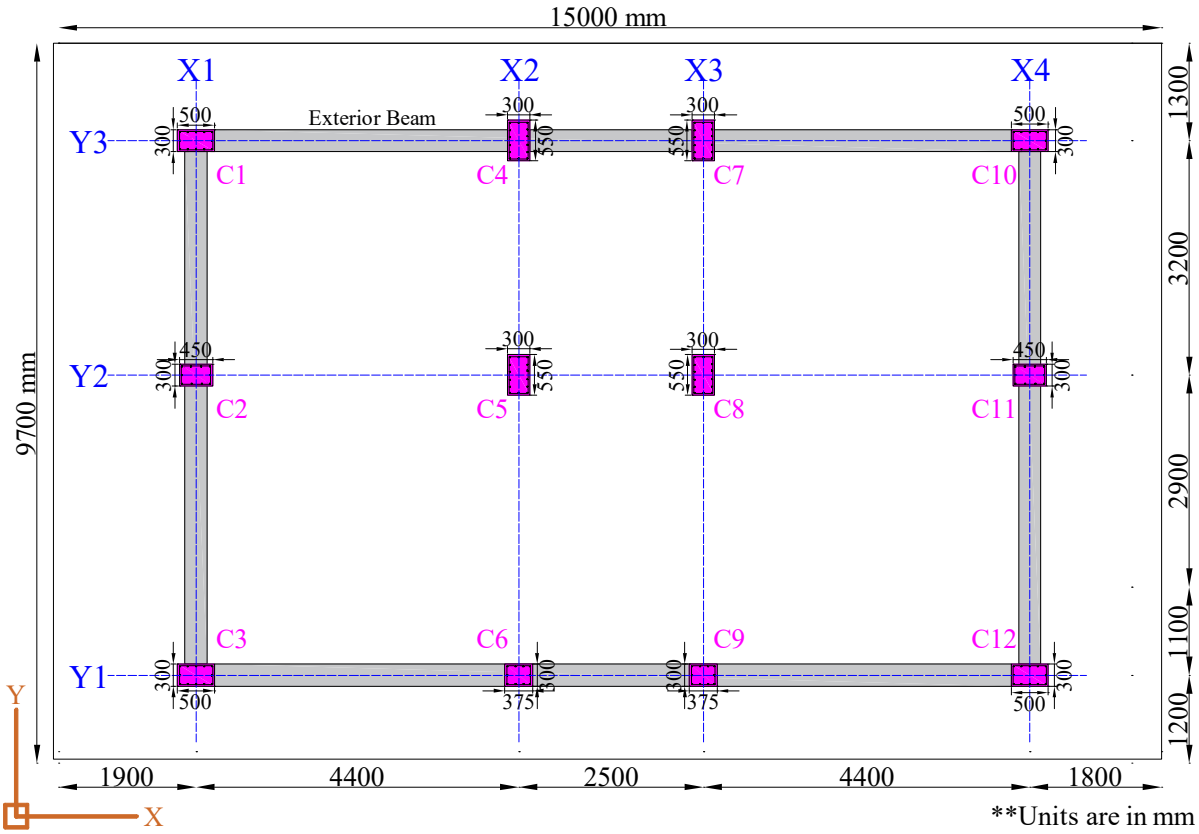

**Slab thickness = 200mm

**12mm @ 100 mm C/C STR top bar

**12mm @ 200 mm C/C STR bottom bar

**Clear cover at bottom 25mm, top 18mm

Figure 5.8.1 Typical floor layout with exterior beams

Characteristics of the building

Some of the important specifications of the building are listed below:

1) A typical flat plate structure
2) No earthquake resisting design performed
3) Exterior beams exist

Table 5.1 Summary of materials

Concrete Strength	24 (N/mm^2) for column and 20 (N/mm^2) for slab
Rebar yield stress	400 (N/mm^2)
Type of rebar	Deformed

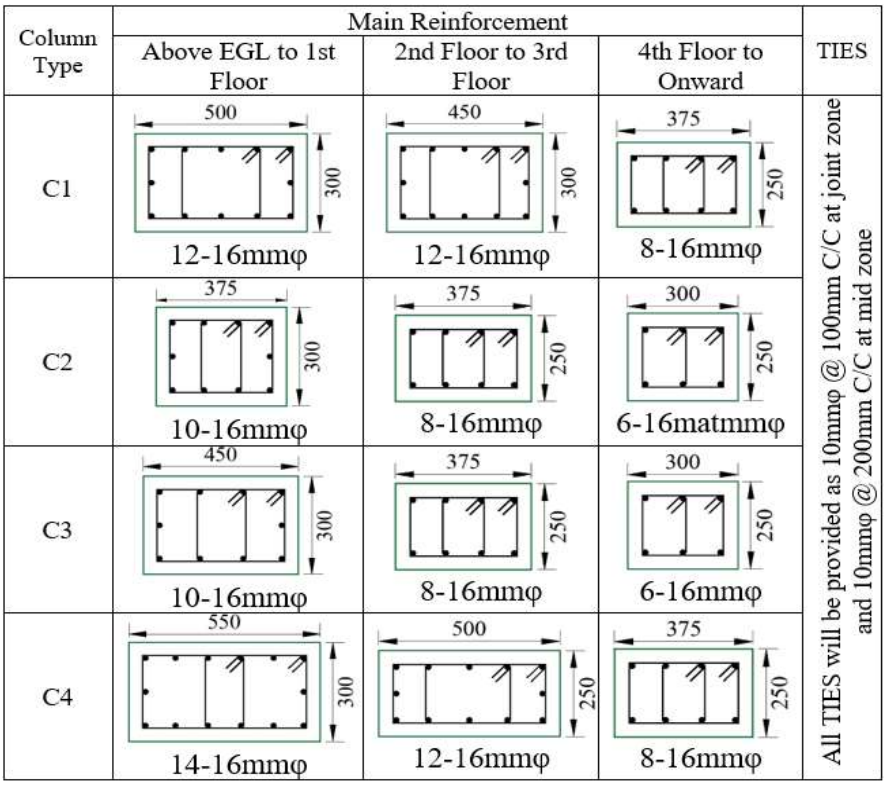

Figure 5.8.2 Column schedule of the existing structure

The procedures of the sample calculations in detail are shown in **Appendix A3**. The seismic evaluation results are summarized in **Table 5.2** and **Figure 5.8.3** for each principal direction and each floor. The seismic demand I_{s0} is computed according to CNCRP Manual, as 0.36 for buildings located in Dhaka based on soil type SD of BNBC-2020. It was evaluated that the seismic index of this existing building didn't satisfy the seismic demand, and the building was not safe in any direction. It demonstrates the vulnerable conditions of the flat plate buildings in Bangladesh and the necessity of seismic retrofit. Therefore, it is desirable to establish some retrofit plans that will ensure I_s>0.36 on each floor and in each direction.

Table 5.2 Summary of the seismic evaluation

Storey	Seismic demand I_{s0}	X-direction			Y-direction		
		Seismic capacity, I_s	Corresponding ductility index	Judgement	Seismic capacity, I_s	Corresponding ductility index	Judgement
6	0.36	0.405	2.6	OK	0.330	2.6	Not OK
5		0.279	2.6	Not OK	0.215	2.6	Not OK
4		0.239	2.6	Not OK	0.179	2.6	Not OK
3		0.310	2.6	Not OK	0.222	2.6	Not OK
2		0.305	2.6	Not OK	0.214	2.6	Not OK
1		0.303	2.6	Not OK	0.189	2.6	Not OK

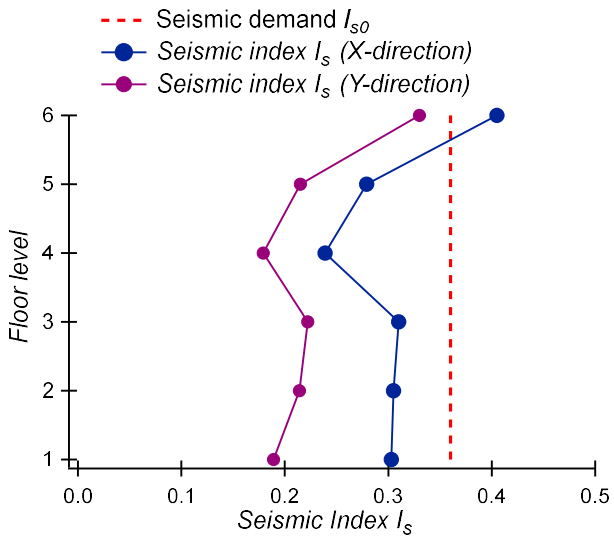

Figure 5.8.3 Comparison between seismic demand and capacity

In this example building, the interior columns were likely to fail in punching; therefore, retrofit techniques should be used to prevent the punching shear failure. In addition, the performance of the building has very low seismic performance. Hence, strengthening should be carried out, either installing by wing walls or drop panel, or shear wall as much as needed and possible.

5.9 Summary

This study presented a simpler evaluation approach for the seismic capacity of existing flat plate structures that are extensively used in Bangladesh, which is based on the concepts of the Japanese seismic evaluation guideline.

1) A simplified seismic evaluation methodology for flat plate structures is proposed in this study to include in the scope of application based on our research findings as discussed in Chapter 2.
2) The evaluation procedure was proposed based on the Japanese seismic evaluation method with simplified modifications in calculating *C*-index and *F*-index by conservative estimation based on the experimental investigations.
3) The interior plate-column connection exhibited very low shear resistance with punching failure; thus, the shear resistance of the interior column was neglected, and the upper bound of ${}_cR_{max}$ was recommended to prevent punching failure.
4) The proposed seismic evaluation and retrofit were applied to an example flat plate structure in Dhaka. The example building exhibited poor performance with the punching shear failure in the interior columns. Therefore seismic retrofit is recommended using proposed retrofit schemes that are investigated in chapters 3 and 4 of this thesis.

5) The seismic evaluation of flat plate structures can be evaluated using the proposed simple evaluation process, which leads to the further strengthening of existing structures to ensure the safety of the structures.

CHAPTER 6

Seismic Retrofit of Flat Plate Structure

6.1 General

Seismic retrofit refers to the process of strengthening a structure in order to make it more resistant to earthquake-induced tremor and damage. Many seismically vulnerable buildings exist in Asian developing countries, and seismic retrofitting is required to strengthen these already-constructed structures. Implementing an effective and appropriate retrofit scheme for the existing building is required to meet the seismic performance requirements by increasing the strength or ductility of the structure in this situation. In this context, appropriate, reliable, effective, and low-cost retrofitting is challenging for the existing low-performance RC buildings in developing countries. The existing structure can be upgraded in a variety of ways, including one that is strength-oriented, one that is ductility-oriented, or one that is a combination of both strength-oriented and ductility-oriented, as shown in **Figure 6.1.1**. Therefore, this study emphasizes two strengthening schemes for seismically vulnerable flat plate-column connections in existing structures. Through this study, two retrofitting schemes are proposed, both of which have been proven to be effective and feasible through this study, as explained in chapters 3 and 4. The wing wall could be considered a strength-oriented retrofit method, whereas the drop panel could be considered a ductility-oriented retrofit method. Afterward, the retrofit measures were demonstrated with a practical example of how they could be applied effectively.

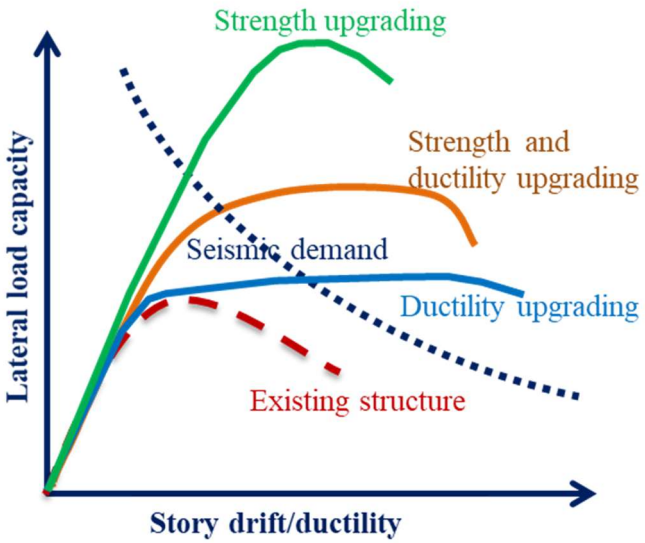

Figure 6.1.1 Basic concept of seismic up-gradation

6.2 Scope

This section introduces the seismic retrofit of existing RC structures with flat plate-column joints, following the seismic evaluation according to the JBDPA standard. Therefore, the scope of application is existing RC structures with flat column joints which also have beams on their perimeter, as explained in chapter 5. The evaluation procedure before and after retrofit will follow as per chapter 5. As explained in chapters 3 and 4, this study proposes two retrofitting schemes using wing wall and drop panel, both of which have been shown to be effective and feasible throughout the course of this research, as explained before. Installing wing walls on a flat-plate structure can be an effective way to increase the lateral resistance of the structure while also preventing punching shear failure. Drop panel can be applied to prevent the flat plate-column joint from punching shear failure. However, the columns connected without beams that have been retrofitted with drop panels do not contribute to the lateral load-carrying capacity and therefore are not taken into consideration.

6.3 Strengthening Strategy

Figure 6.3.1 presents a flowchart for seismic retrofit of existing RC flat plate structures.

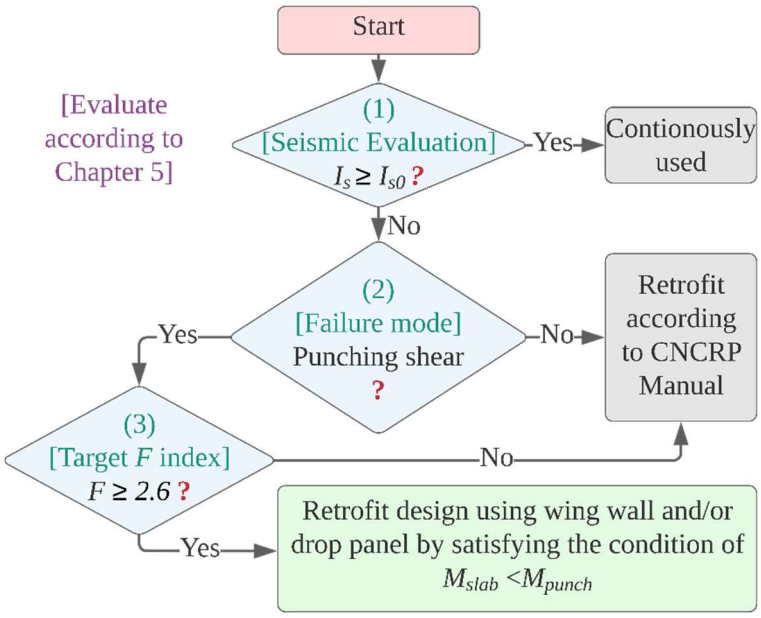

Figure 6.3.1 Proposed flowchart of seismic retrofit

The following illustrates the flowchart step by step.

1) The seismic retrofit is required when the seismic index (I_S) is insufficient to meet the seismic demand (I_{S0}). As explained in Chapter 5 on seismic evaluation, when the seismic index is calculated

for a structure flat plate-column structures, the strength contribution of columns without beam, namely columns that have flat plate-column joints, is completely ignored in the seismic evaluation.

2) The seismic retrofit design will be carried out in the same manner as the moment-resisting frame in accordance with the JBDPA standard if the punching shear failure is not expected.
3) The necessity of retrofitting the flat plate-column joints shall be considered based on a target *F*-index for the seismic retrofit. The punching shear failure will not happen if the target *F* index does not exceed 2.6 (corresponds to 2% drift angle); thus, the retrofitting of flat plate-column joints is not required. The conventional seismic retrofit design will be performed according to the CNCRP/JBDPA. On the other hand, the following sections shall be applied if the target index exceeds 2.6.

Figure 6.3.2 shows an example that represents a typical flat plate structure with perimeter beams, as described in chapter 5. Focusing on the seismic evaluation of x-direction, the contributions of the columns with beams enclosed by the red circles are taken into consideration, as shown in **Figure 6.3.2A**. **Figure 6.3.2B** shows the *C*-*F* relationship by the black lines and the red circle at $F = 3.2$ in the case that the flat plate-column joints enclosed by the blue squares do not fail in punching shear. In contrast, the blue circle at $F = 2.6$ in **Figure 6.3.2B** indicates the upper limit when the flat plate-column joints enclosed by the blue squares fail in punching shear. Then, the seismic indexes of the former and latter cases are 0.12*3.2 = 0.384 and 0.12*2.6 = 0.312, respectively. Therefore, if the seismic demand is between 0.312 and 0.384 (the red line in the figure), the seismic retrofit to prevent punching shear failure of the flat plate-column joints is effective in exceeding the demand. In this case, drop panel will be adopted for retrofit. If the seismic demand is greater than 0.384 (the green line in the figure), wing walls will be more effective because it contributes not only to preventing punching shear failure but also to increasing the strength.

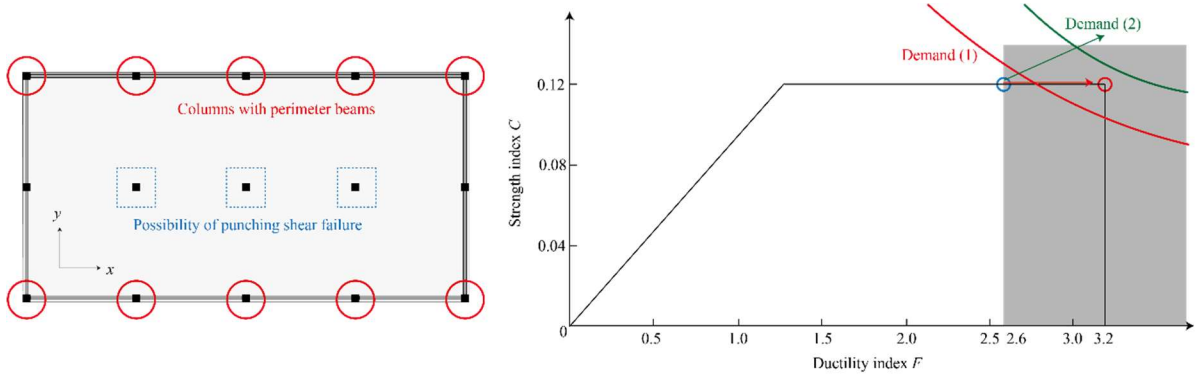

(A) Building plan (B) *C*-*F* relationship

Figure 6.3.2 An example of flat plate structure to which this section is applied

6.4 Seismic Retrofit using wing walls

The research is quite limited to low-strength concrete structures under seismic loading conditions, with a particular emphasis on developing countries. We, therefore, intended to conduct an experimental series to investigate the seismic performance of existing flat plate-column joints and to strengthen them by installing wing walls that had already been verified, as explained in Chapter 3. The purpose of this retrofit method is to improve the seismic performance of existing buildings by converting the existing independent columns to columns with wing walls and increasing their lateral strength. In chapter 3, it was concluded that the post-installed RC wing walls enlarged the critical section of the column, which increased the punching shear resistance resulting in an increase in the lateral resistance. The significant advantage of this retrofit method is that it increases not only the punching shear strength of the column by extending its critical section but also the lateral strength capacity. Moreover, a theoretical evaluation scheme of the ultimate flexural strength of the multi-storey column with wing walls was presented under seismic loading conditions for flat plate structures in this section.

Referring to the flat plate structure, we constructed two half-scaled interior plate-column joint specimens to verify the effectiveness of wing wall installation in the previous chapter 3. One specimen, FP-1 (explained in chapter 2), was designed without strengthening and used as a benchmark specimen to compare the effectiveness with and without retrofitting. The test results from chapters 2 and 3 are briefly summarized. The nodal moment vs drift angle relationships of both specimens was compared in **Figure 6.4.1 (a)**. The maximum capacity of specimen FP-W1 strengthened installing wing walls, which showed brittle punching shear failure as shown in **Figure 6.4.1 (b)**, was 2.7 times higher than that of the benchmark specimen FP-1. The failure area almost agreed with the critical section shown in **Figure 6.4.1 (a)**. We proposed a modified punching shear strength evaluation method for the column with wing walls using low-strength concrete based on the Japanese standard. After that, the maximum punching shear strength was conservatively estimated by 1.15 times using the proposed critical section as shown in **Figure 6.4.1 (b)**.

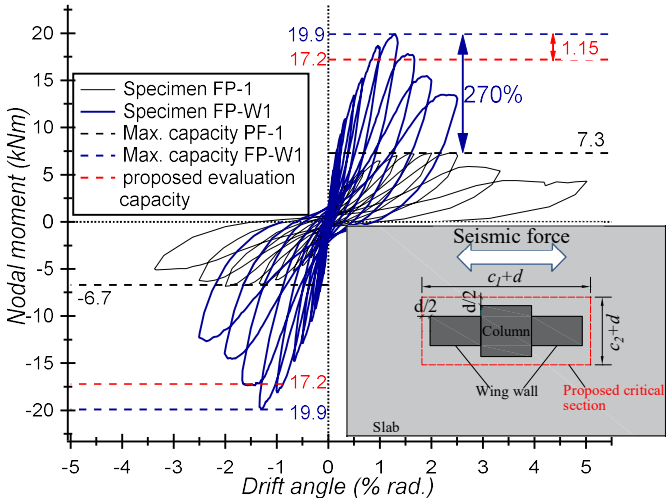

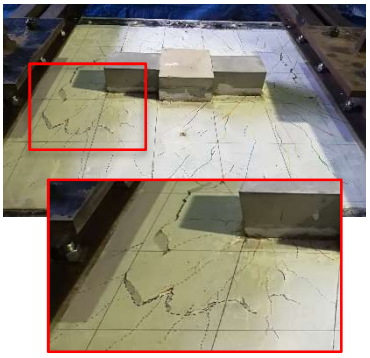

(a) Nodal moment vs drift angle relationship (b) Punching shear failure

Figure 6.4.1 Experimental results with the proposed critical section

Although the specimens were designed to exhibit punching shear failure precedes flexural yielding of the slab, it is possible in practical design to prevent punching shear failure by designing to precede flexural yielding of the plate. However, the post-installed wing walls strengthening scheme is new for flat plate structures; thus, the flexural strength evaluation should be carefully performed since flat plate structures are flexible in the absence of beams. Therefore, an evaluation method of the ultimate flexural strength of the column with wing walls in multi-storey flat plate structures is introduced in the following section.

The contribution of columns without beams retrofitted by wing walls can be considered in the lateral load-carrying capacity, therefore, strength index C and ductility index F are calculated according to the JBDPA standard, respectively. Application of the post-installed wing walls to the seismic retrofit is new for flat plate structures; thus, the flexural strength evaluation should be carefully performed since flat plate structures are flexible in the absence of beams. Therefore, an evaluation method of the ultimate flexural strength of the column with wing wall in multi-storey flat plate structures is introduced. For upgrading, not only their strength but also deformability, the punching shear failure of the plate-column connection will be prevented by satisfying a condition of $M_{slab} < M_{punch}$. Thus, the lateral load-carrying capacity Q_u of a column retrofitted using wing wall(s) fails in flexure is evaluated by **Eq. 6.4.1**.

$$Q_u = \frac{cM_w}{h} = \frac{cM_w + N \cdot M_{slab}}{H} \leq \frac{2_cM_w}{H} \qquad \textbf{(6.4.1)}$$

where ${}_cM_w$ is the flexural capacity of a column with wing wall(s) calculated as per JBDPA Standard (JBDPA 2005), h is an equivalent inflection height from the bottom of wing wall, N is the number of stories installed wing walls, H is the total height of column with wing walls, M_{slab} is the nodal flexural capacity of slab.

Equation 6.4.1 represents the lateral load-carrying capacity of the column retrofitted by wing walls at an overall yielding mechanism with flexural hinging at the bottom and slab ends, as shown in **Figure 6.4.2**. As shown in the figure, **Eq. 6.4.1** is derived assuming uniform shear force distribution along with the height for conservative estimation of the base shear; thus, the obtained Q_u is constant over the multi-stories concerned (namely, the first to fifth stories in **Figure 6.4.2**). However, Q_u cannot exceed $2_cM_w/H$ with a hinging at the top of the column with wing walls.

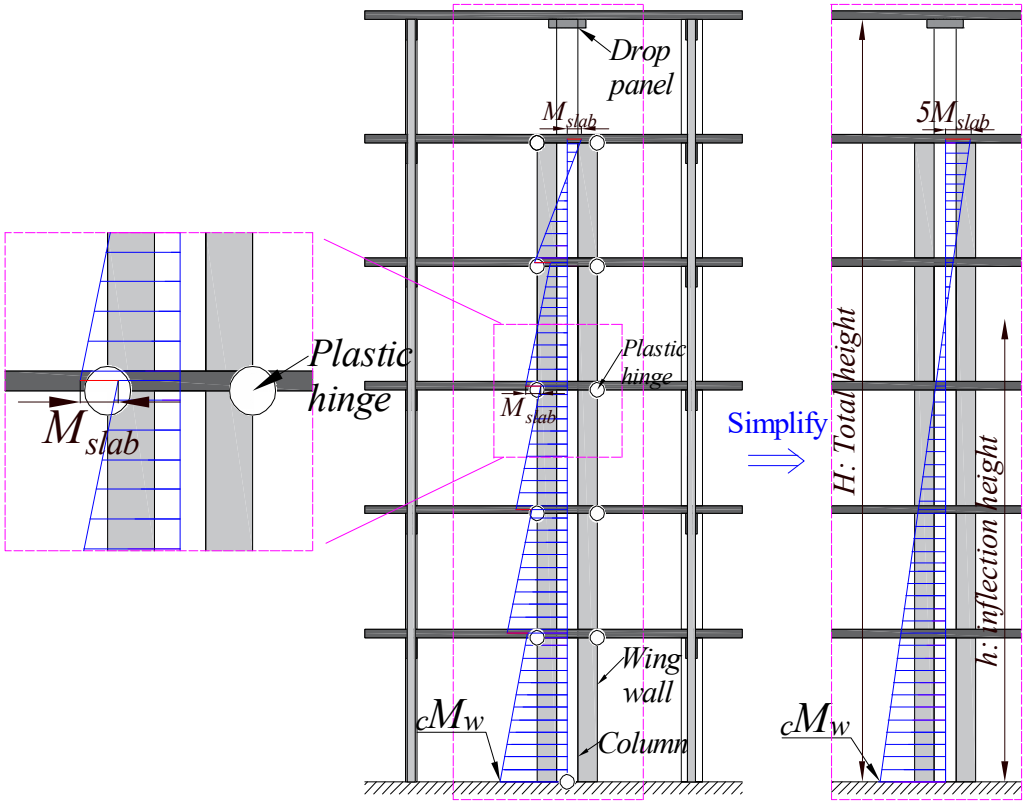

Figure 6.4.2 Moment diagram image of the column retrofitted by wing walls for Eq. (6.4.1)

The nodal flexural capacity of slab (M_{slab}) and the punching shear capacity (M_{punch}) (AIJ 2018) shall be compared to prevent punching shear failure. The nodal flexural capacity of slab (M_{slab}) is calculated by **Eq. 6.4.2**, assuming the moment diagram as shown in **Figure 6.4.3.**

$$M_{slab} = \frac{{}_lM_{slab}}{l_l/2} \times \left(\frac{l_l}{2} + l_w + \frac{D_c}{2}\right) + \frac{{}_rM_{slab}}{l_r/2} \times \left(\frac{l_r}{2} + l_w + \frac{D_c}{2}\right) \quad \textbf{(6.4.2)}$$

where the notations are shown in **Figure 6.4.3**.

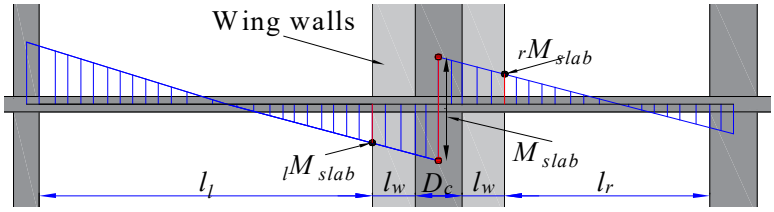

Figure 6.4.3 Assumed moment diagram with wing walls

Strength index C shall be calculated by $C = Q_u / \Sigma W$, where Q_u is calculated from **Eq. 6.4.1** and ΣW is the weight of the building including live load for seismic calculation supported by the storey concerned. Ductility index F shall be calculated according to Section 5.6 which follows the Japanese guidelines. In the Japanese guidelines, the ductility index F of a column with wing walls is limited to $F < 2$, which is smaller than the upper limit due to punching shear failure in this proposed evaluation method. However, the length of wing walls will be decided in accordance with preventing punching shear failure, as described in the following section. In the case of wing walls installed on columns with beams to satisfy the seismic demand, the contribution of columns with beams retrofitted by wing walls can be evaluated according to the JBDPA standards.

6.4.1 *Design concept using wing wall*

The flowchart shown in **Figure 6.4.4** should be followed to avoid punching shear failure of the flat plate-column joint. The wing walls are designed in the first step, which includes determining the size of the wing walls as well as the reinforcing detail in the wing walls. The second step is the construction of the wing walls. The nodal moments at the flexural capacity of the slab (M_{slab}) and punching shear capacity (M_{punch}) must be compared in order to prevent punching shear failure. The punching shear capacity (M_{punch}) is calculated in accordance with the procedures detailed in the following section. The installation of wing walls is intended to prevent punching shear failure, so if M_{punch} is smaller than M_{slab}, the design of the wing walls must be redesigned.

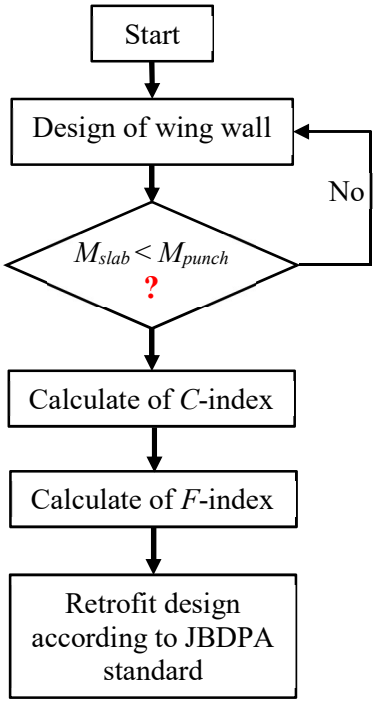

Figure 6.4.4 Flowchart of seismic retrofit of existing RC flat plate-column joint by wing walls

The punching shear capacity (M_{punch}) is calculated according to the following section. If M_{punch} is smaller than M_{slab}, go back to the design of wing walls because the purpose of the installation of wing walls is to prevent punching shear failure.

In the case of the interior column (C5) shown in Section 5.8 in the previous chapter, which is expected to fail in punching shear failure, the wing walls of 300 mm length (equal to the column depth) can prevent the column from punching shear failure (**Figure 6.4.5**). The punching shear capacity (M_{punch}) of the column before retrofitting was 278 kNm whereas the nodal moment at the flexural yielding of slab was 301(=105+196) kNm, as shown in **Figure 6.4.6A**. After retrofitting by wing walls, the punching shear capacity of the column with wing walls was improved to be 579 kNm. Although the nodal moment at the flexural yielding of the slab also increased by the installation of wing walls because the slab yields at the face of the wing walls, as shown in **Figure 6.4.6B**, that of 374(=144+230) kNm was smaller than the punching shear capacity. It has been identified that installing wing walls can significantly increase the punching shear capacity. The detailed calculation procedure is referred to in appendix **Appendix A3.**

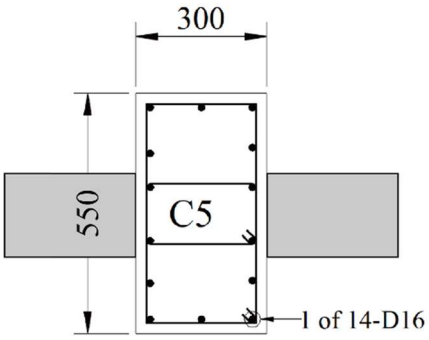

Figure 6.4.5 Column with wing walls

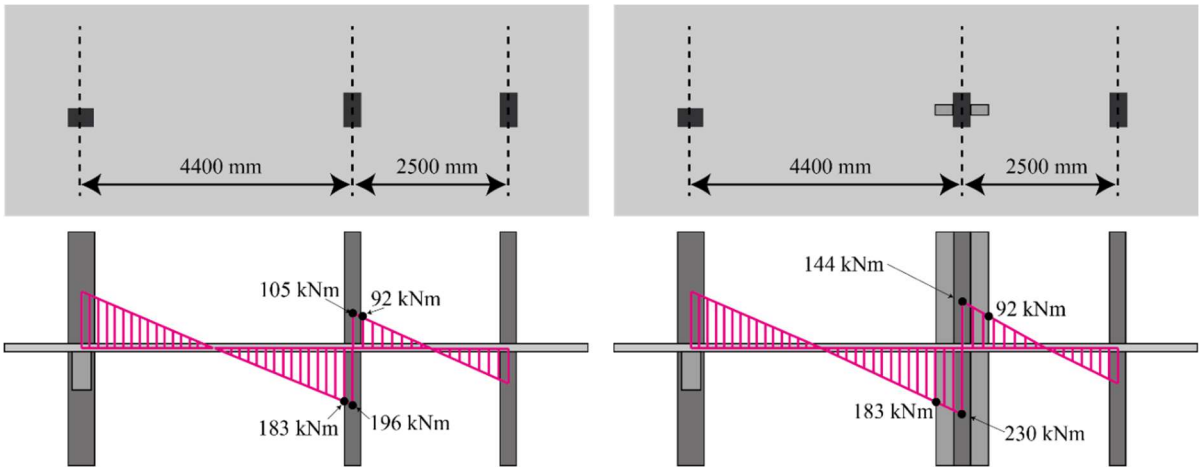

(A) Moment diagram before retrofit **(B)** Moment diagram after retrofit

Figure 6.4. The nodal moment at the flexural yielding of slab

6.5 Seismic Retrofit using drop panel

The ultimate objective to install drop panel is to prevent brittle punching shear failure by expecting ductile flexural deformability of the plate, as verified in Chapter 4. The test results are briefly summarized here. The nodal moment vs. drift angle relationships of both specimens is compared in **Figure 6.5.1**. The maximum capacity of specimen FP-D1 strengthened by installing drop panel, which showed brittle punching shear failure after ductile flexural failure yielding, was 2.6 times higher than that of the benchmark specimen FP-2. According to **Eqs. (2.7.3) to (2.7.8)** by AIJ RC standard, the maximum punching shear capacity was estimated well by assuming the critical section shown in **Figure 6.5.1**. The punching shear failure of the plate-column connection must be prevented by satisfying the condition of $M_{slab} < M_{punch}$, in which M_{slab} is evaluated by the following equation assuming the moment diagram shown in **Figure 6.5.2**.

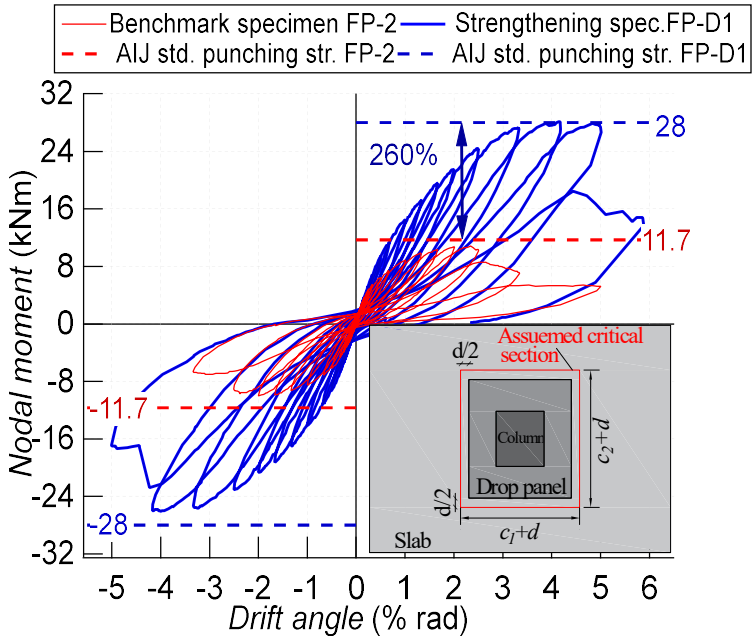

Figure 6.5.1 Experimental results on the contribution of drop panel

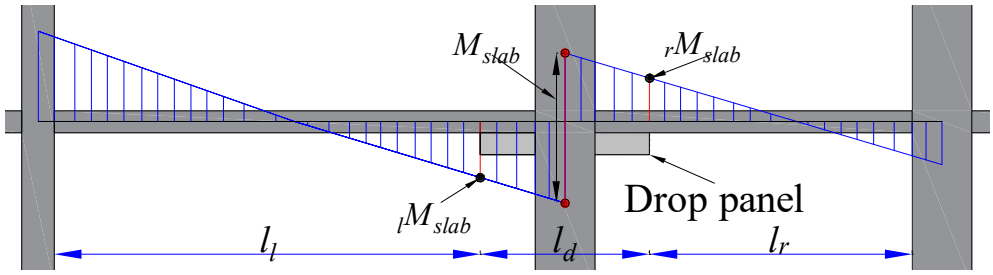

Figure 6.5.2 Assumed moment diagram with drop panel

To prevent the punching shear failure of flat plate-column joint, the flowchart shown in **Figure 6.5.3** is applied. First, drop panel is designed; the dimensions of drop panel and the reinforcing detail in drop panel are planned. To identify the failure mode, the flexural capacity of slab (M_{slab}) and punching shear capacity (M_{punch}) are compared. The flexural capacity of slab (M_{slab}) is calculated by assuming the moment diagram shown in **Figure 6.5.2**.

$$M_{slab} = \frac{{}_lM_{slab}}{l/2} \times \left(\frac{l}{2} + \frac{l_d}{2} \right) + \frac{{}_rM_{slab}}{l/2} \times \left(\frac{l}{2} + \frac{l_d}{2} \right) \qquad \textbf{(6.5.1)}$$

where, the calculation of ${}_lM_{slab}$ and ${}_rM_{slab}$ are shown in **Figure 6.5.2**.

6.5.1 *Design concept using drop panel*

The punching shear capacity (M_{punch}) is calculated according to the following section. If M_{punch} is smaller than M_{slab}, go back to the design of drop panel because the purpose of the installation of drop panel is to prevent punching shear failure.

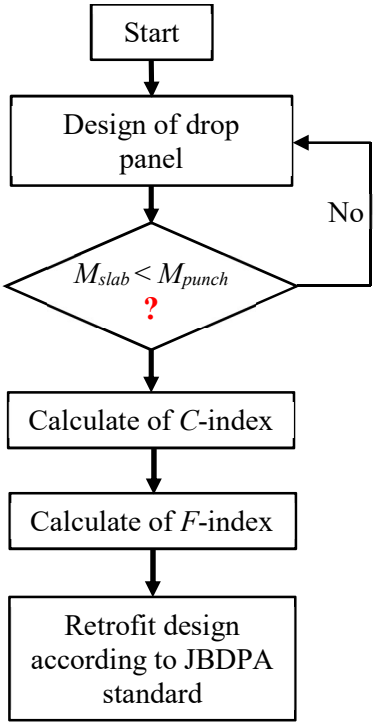

Figure 6.5.3 Flowchart of seismic retrofit of existing RC flat plate-column joint by drop panel

In the case of the interior column (C5) shown in Section 5.8 in the previous chapter, which was expected to fail in punching shear failure, the drop panel of 700×700×75 mm in length × width × thickness, respectively, can prevent the column from punching shear failure (**Figure 6.5.4**). The punching shear capacity (M_{punch}) of the column before retrofitting was 215.1 kNm, whereas the nodal moment at the flexural yielding of slab was 267.7(=92.6+175.1) kNm, as shown in **Figure 6.5.4 A**. After retrofitting by drop panel, the punching shear capacity of the column with drop panel was improved to be 442.9 kNm. Although the nodal moment at the flexural yielding of the slab also increased by the installation of drop panel because the slab yields at the face of the drop panel, as shown in **Figure 6.5.4 B**, that of 306(=113.2+192.8) kNm was smaller than the punching shear capacity. It has been identified that installing drop panel can significantly increase the punching shear capacity. The detailed calculation procedure is referred to in **Appendix A3**.

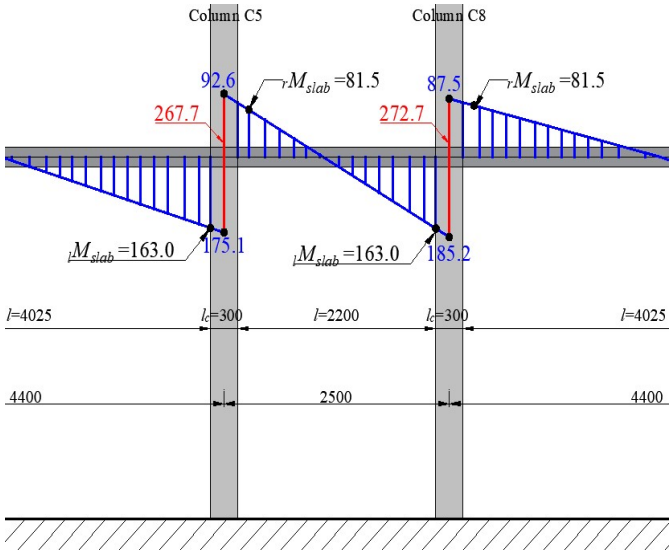

(A) Moment diagram before retrofit

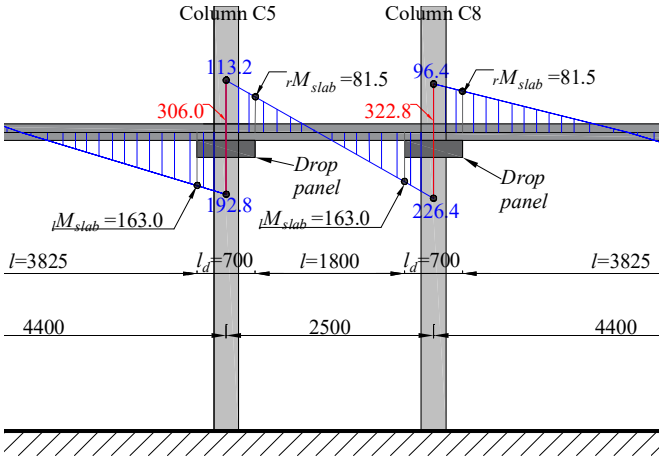

(B) Moment diagram after retrofit

Figure 6.5.4 The nodal moment at the flexural yielding of slab (before retrofit) (Grid Y2)

6.6 Example of application

The procedures of the sample calculations in detail are shown in **Appendix A3.** The seismic evaluation results are summarized in **Table 6.6.1** for each principal direction and each floor. The seismic demand I_{s0} is computed according to CNCRP Manual (Public Works Department (PWD) 2015), as 0.36 for buildings located in Dhaka based on soil type SD of BNBC-2020 (HBRI 2020). It was evaluated that the seismic index of this existing building didn't satisfy the seismic demand, and the building was not safe in any direction. It demonstrates the vulnerable conditions of the flat plate buildings in Bangladesh and the necessity of seismic retrofit. Therefore, it is desirable to establish some retrofit plans that will ensure I_s>0.36 on each floor and in each direction.

Table 6.1 Summary of the seismic evaluation

Storey	Seismic demand index, I_{s0}	X-direction			Y-direction		
		Seismic capacity, I_s	Corresponding ductility index	Judgement	Seismic capacity, I_s	Corresponding ductility index	Judgement
6	0.36	0.405	2.59	Safe	0.330	2.59	Unsafe
5		0.279	2.59	Unsafe	0.215	2.59	Unsafe
4		0.239	2.59	Unsafe	0.179	2.59	Unsafe
3		0.310	2.59	Unsafe	0.222	2.59	Unsafe
2		0.305	2.59	Unsafe	0.214	2.59	Unsafe
1		0.303	2.59	Unsafe	0.189	2.59	Unsafe

In **Figure 6.6.1,** a layout of wing walls and drop panels is presented for the seismic retrofit. The wing walls were planned to be installed to increase the *C* index showing a strength-type retrofit design. The wing walls were installed from the 1st to 5th-floor levels of the building, and the drop panels were installed on the 6th floor only because it was sufficient to increase the seismic index in both X & Y-directions. The detailed design of the wing wall and drop panel was performed based on the JBDPA (JBDPA 2005) and BNBC(HBRI 2020) guidelines, respectively. Thereafter, the building was re-evaluated using the proposed evaluation scheme for the existing building after retrofitting with a combination of wing wall and drop panel installations. Subsequently, the building was considered satisfactory after retrofitting using wing walls up to the 5th-floor levels and using drop panels on the 6th floor, as shown in **Table 6.2** and **Figure 6.6.2**.

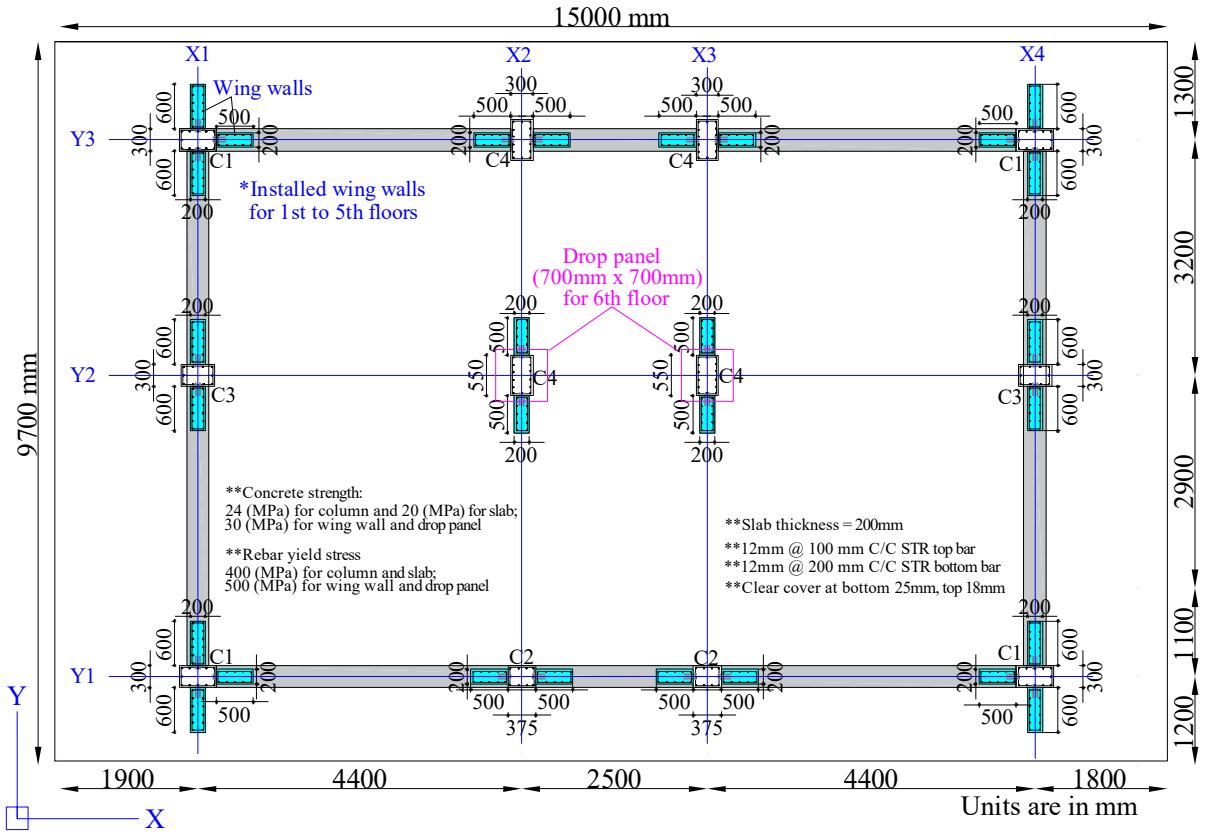

Figure 6.6.1 The plan of existing columns with an arrangement of post-installed wing walls and drop panels

Table 6.2 Summary of the seismic evaluation using wing wall and drop panel

Storey	Seismic demand index I_{s0}	X-direction			Y-direction			Remarks (retrofit scheme)
		Seismic capacity I_s	Corresponding ductility index	Judge-ment	Seismic capacity I_s	Corresponding ductility index	Judge-ment	
6	0.36	0.484	3.1	Safe	0.408	3.1	Safe	Drop panel
5		0.590	2.0	Safe	0.729	2.0	Safe	Wing wall
4		0.456	2.0	Safe	0.534	2.0	Safe	Wing wall
3		0.459	2.0	Safe	0.496	2.0	Safe	Wing wall
2		0.403	2.0	Safe	0.438	2.0	Safe	Wing wall
1		0.371	2.0	Safe	0.375	2.0	Safe	Wing wall

In this example building, the interior columns were likely to fail in punching; however, both retrofit techniques can prevent the punching shear failure by extending the critical section as described in section 3. Drop panels typically improve the ductility of the structure by preventing the brittle punching shear failure of the interior slab, but they do not increase the lateral resistance of the column. Increasing the ductility of exterior columns fulfilled the requirement of seismic demand at the 6th floor

only. Consequently, wing walls were incorporated into the retrofit design of the building from 1st to 5th-floor level to improve its seismic performance in both directions by preventing punching shear failure.

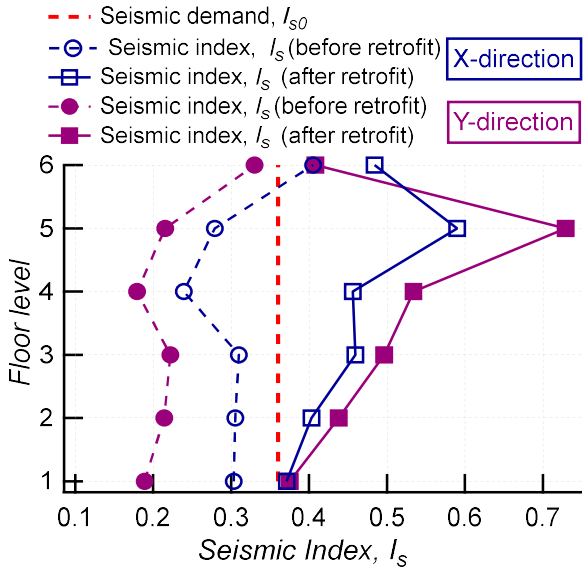

Figure 6.6.2 Comparisons between the seismic demand and capacity before/after retrofit

6.7 Summary

The seismic strengthening of the existing flat plate building stock is essential for the implementation of immediate earthquake disaster mitigation measures. As a result, this chapter describes a strategic retrofit procedure for strengthening an existing building by incorporating post-installed wing walls and drop panels into the design. This research demonstrates how to achieve the desired characteristics of a flat plate structure when it is subjected to an earthquake. These characteristics include sufficient strength with stiffness and/or ductility to withstand the shaking of a moderate-intensity or base motion. The following conclusions can be drawn from the discussion and recommendations contained in this chapter.

1. The post-installed wing walls and drop panels were proposed as retrofitting techniques that were experimentally verified and might effectively measure earthquake mitigation.
2. Referred to the experimental results in chapter 3, a conservative estimation was introduced for the theoretical evaluation of the ultimate flexural strength of multi-storey RC columns with wing walls in RC flat plate structures.

3. According to this study, the contribution of columns without beams retrofitted by wing wall can be considered in the lateral load-carrying capacity, while the columns with beams retrofitted by wing wall can be evaluated according to the JBDPA standard.
4. Drop panel can be applied to prevent the flat plate-column joint from punching shear failure. The contribution of columns without beams retrofitted by drop panel cannot be considered in the lateral load-carrying capacity. The upper limit of ductility index F can be removed by preventing flat plate-column joint from punching shear failure.
5. The post-installed drop panels will be effective for buildings that don't need additional lateral resistance of the column but need to resist the punching shear failure under deformability of the structure.
6. The proposed seismic retrofit method was applied to an example flat plate structure in Dhaka. The existing building exhibited poor performance; however, the building was satisfactorily upgraded after retrofitting with wing walls and drop panels. The wing walls were effective to mainly increase the strength as used from the 1st to 5th floors, and the drop panels were effective for the target that is not needed additional lateral resistance but is needed to prevent the punching shear failure for increasing ductility as used in the 6th floor.

CHAPTER 7

Conclusions and Recommendations

7.1 General

The outcomes of the research presented in this thesis are outlined and discussed in this chapter, along with recommendations for further investigations. A brief description of the summary and conclusions drawn from the experimental results can be found later in this chapter. This chapter also provides an overview of the seismic evaluation and retrofit strategy and its conclusions.

Many reinforced concrete (RC) flat plate structural systems, particularly in Asian developing countries, are at serious risk of punching shear failure around the plate-column connection when subjected to lateral loads like seismic activity. Therefore, a reliable estimate of the seismic load-carrying capacity and the deformation capacity of existing reinforced concrete (RC) flat plate structures is required for seismic strengthening in order to avoid catastrophic damage from earthquakes. In addition, many flat slab buildings require seismic strengthening to prevent punching failures from occurring. This can be attributed to a number of factors, including design or construction flaws, low-quality materials, failure to comply with new code provisions, and an increase in vertical load. Therefore, the seismic strengthening of the existing building stock is essential for implementing immediate earthquake disaster mitigation measures.

The research is quite limited, and seismic evaluation and retrofit of poorly constructed flat plate structures are not well established in the code for some particular zones in Asian developing countries such as Bangladesh. So, the focus of this research is on a typical existing flat plate structure constructed of low-strength concrete in Bangladesh, which represents one of the most seismically vulnerable flat plate structures in Asian developing countries. Based on the results of the experiments, the purpose of this study is to develop a method for seismic evaluation and retrofitting that can be applied to already-existing vulnerable RC flat plate structures. Thereafter the findings from this study are briefly summarized in the following section.

7.2 Summary

Firstly, we performed experiments on a series of two half-scaled specimens to evaluate the seismic performance of an existing interior flat plate-column joints that were constructed using low-strength concrete. In the experimental tests, the brick aggregate concrete was used to construct the specimens with low strength, which was typical of Bangladeshi building construction. In order to simulate the inter-storey drifts that can occur as a result of seismic action, static cyclic vertical

displacements with increasing amplitudes were applied to the ends of the slabs, and their behaviors were observed. Both specimens exhibited poor seismic performance showing brittle punching shear failure near the plate-column joints. The punching shear strength estimated based on the AIJ standards overestimated the maximum capacity using low-strength concrete. According to the AIJ standard, the maximum capacity of FP-1 was 26% lower than the calculated result of the punching shear strength whereas the maximum capacity of FP-2 was 12% lower than the calculated result of the punching shear strength. On the other hand, the punching shear strength was close to the experimental value when the low-strength concrete was considered. Consequently, the estimate of the punching shear strength for specimen FP-1 was improved by approximately 12%, while it was 3% for FP-2.

Consequently, this study emphasized two strengthening schemes for seismically vulnerable flat plate-column connections in existing structures. The experimental investigation (in Japan) on a series of two half-scaled interior plate-column connections was conducted to explore the effectiveness of the proposed seismic strengthening method using post-installed RC wing walls and analyze the punching shear capacity of the connections. Two specimens using wing walls were employed in two principal directions, i.e., along the loading direction and orthogonal direction. Both specimens were constructed by simulating low-strength concrete and tested in Japan. Specimen FP-1 which was described in chapter 2, was constructed and tested without wing walls and served as a benchmark specimen for comparisons between the cases with and without strengthening. The maximum strength of FP-W1 was 2.7 times greater than that of the control specimen FP-1 as a result of the application of wing walls in-plane direction. The out-of-plane direction strengthening applied to FP-W2 resulted in a maximum strength that was twice as high as that of the control specimen. In addition, the former strengthening scheme contributed to stiffening the flat plate structure, whereas the latter scheme did not contribute any additional stiffness. . Both strengthened specimens successfully showed higher resistances to punching shear failure; thus, the test results experimentally verified that installing RC wing walls was a feasible method of upgrading flat plate-column joints, even with low-strength concrete, thereby preventing collapse under seismic action. Appropriate application of wing walls of existing RC flat plate column connections will result in a change of brittle punching shear failure to the ductile flexural failure mode.

Another experimental investigation (in Bangladesh) on a series of three half-scaled interior plate-column connections was conducted to explore the effectiveness of the proposed seismic strengthening using post-installed RC drop panel. Chapter 4 of this thesis describes an experimental study on existing flat plate column joints that were strengthened using RC drop panels. Standard design practices and locally available materials were selected for the test specimens to represent typical RC buildings constructed earlier in Bangladesh. A series of three specimens with identical thickness and similar reinforcement details were constructed with RC drop-panel varying in different dimensions. Post-installed bonded anchors were applied to connect the drop panel with the existing structure. All the

specimens were constructed and tested in Bangladesh while the specimen FP-2 which was described in chapter 2, served as a benchmark specimen for comparisons between the cases with and without strengthening. It was experimentally verified that installing the RC drop panel effectively upgraded flat plate-column connections with low-strength concrete under seismic loading by increasing the effective depth of the plate and/or periphery of the column critical section.

To avoid catastrophic damage from earthquakes, it is essential to identify a reliable estimate of the seismic load-carrying capacity and the deformation capacity of existing reinforced concrete flat plate structures in earthquake-prone areas and to use that information to design seismic strengthening. Therefore, chapter 5 intended to introduce a simplified evaluation methodology for the seismic capacity of existing flat plate structures that are often found in Bangladesh, based on the Japanese seismic evaluation guideline concepts. Based on the experimental findings in chapter 2, the evaluation methodology of existing seismically vulnerable flat plate structures was introduced with slight modifications to the Japanese standard. The evaluation procedure was proposed based on the Japanese seismic evaluation method with simplified modifications in calculating *C*-index and *F*-index by conservative estimation based on the experimental investigations. The interior plate-column connection exhibited very low shear resistance with punching failure; thus, the shear resistance of the interior column was neglected, and the upper bound of ${}_cR_{max}$ was recommended to prevent punching failure. A practical example of how the evaluation procedures could be applied effectively was then used to demonstrate the procedures following that.

The implementation and retrofit strategy were briefly introduced in chapter 6. An effective and appropriate retrofit scheme for the existing building is required to meet the seismic performance requirements in this situation. This can be accomplished by increasing either the strength or ductility of the structure, as appropriate. Therefore, this study emphasizes two strengthening schemes for the up-gradation of seismically vulnerable flat plate-column connections in existing flat plate structures. Through this study, two retrofitting schemes are proposed, both of which have been proven to be effective and feasible through this study, as explained in chapters 3 and 4. The post-installed wing walls will be effective for buildings that need additional lateral resistance of the columns by increasing the *C* index showing a strength-type retrofit design and preventing punching shear failure. A theoretical evaluation scheme was proposed to evaluate the column with wing wall. Drop panel can be applied to prevent the flat plate-column joint from punching shear failure, while the contribution of columns without beams retrofitted by drop panel cannot be considered in the lateral load-carrying capacity. The upper limit of ductility index F can be removed by preventing flat plate-column joint from punching shear failure. Afterward, the retrofit measures were demonstrated with a practical example of how they could be applied effectively.

7.3 Conclusions

The major conclusions were drawn from this thesis as follows:

Chapter 2 discussed the experimental investigations on a series of two half-scaled interior flat plate-column joints constructed using low-strength concrete often found in Bangladesh. Through this experimental study, the basic characteristics of existing flat plate column joints were identified. This chapter briefly explained the effect of low-strength concrete and how to evaluate the punching shear capacity when the existing building is constructed using low-strength concrete.

Chapter 3 discussed the experimental investigations on a series of two half-scaled interior flat plate-column joints strengthened with wing walls. This experimental study investigated the effectiveness and feasibility of post-installed wing walls. The post-installed RC wing walls enlarged the critical section of the column, which increased the punching shear resistance resulting in increase in the lateral resistance of independent columns.

Chapter 4 discussed the experimental investigations on a series of three half-scaled interior flat plate-column joints strengthened using drop panels. This exploratory study investigated the effectiveness and feasibility of a post-installed drop panel as a strengthening scheme. This experimental study was principally conducted to examine whether the size of the drop panel was adequate with enough anchorage connected with the existing structures made with low-strength concrete.

Chapter 5 presented a simplified seismic evaluation methodology for flat plate structures, based on the experimental investigation described in chapter 2, simulating the low-strength concrete commonly used in Bangladesh. Based on the experimental investigations, the Japanese seismic evaluation procedure was modified to include the flat plate structure in the scope of application.

Chapter 6 proposed a seismic retrofit methodology for flat plate structures using wing walls and drop panels based on the experimental investigations described in chapters 2 and 3. Based on the experimental findings a retrofit strategy for flat plate structure was briefly outlined. The proposed seismic retrofit procedure was applied to an example building to illustrate how the seismic retrofit strategy of existing buildings can be applied.

7.4 Limitations and Recommendations

Field investigations can be carried out to identify whether there are any other possible causes of punching shear failure besides low-strength concrete and improper construction management practices in Asian developing countries.

The current study was conducted for focusing on the low-strength concrete, however, more specimens with moderate to high-strength concrete for both retrofitted and non-retrofitted is recommended.

As discussed in chapter 3, the proposed retrofitting scheme using RC wing walls was experimentally verified to be effective in upgrading flat plate-column connections constructed using low-strength concrete. The system that is being presented was developed for slab retrofitting with low-strength concrete; however, it can be predicted that the same principle can also be used for the construction of structures made out of moderate to high-strength concrete. It is anticipated that the installation of this strengthening method can be used in both the long and short directions of the slab simultaneously, if necessary and appropriate; however, more research can be carried out and recommended. More variables (steel ratio of vertical reinforcement of wing walls, wing walls size, etc.) and more specimens should be considered to investigate the effect on improving punching shear capacity more precisely. A full-scale model may be investigated to get the effects of wing walls on punching shear capacity more accurately. However, further investigations are recommended to evaluate the punching shear strength. In particular, finite element analysis may help to clarify the mechanism of punching shear failure in flat plate structures made of low-strength concrete. For future studies involving finite element analysis, the current experimental data will serve as an excellent source of calibration.

Drop panel is a popular and conventional method for preventing punching shear failure, and it is already included in the code provisions for new building designs. The drop panel should be connected to the existing component by means of a post-installed bonded anchorage, which should be carefully designed, as suggested by this study. More variables (steel ratio of drop panel, size of drop panel, etc.) and more specimens, and full-scale model can be considered to investigate the effect on improving punching shear capacity of low-strength flat plate structure more precisely. In particular, finite element analysis has the potential to assist in elucidating the punching shear failure mechanism in flat plate structures made of low-strength concrete.

Pure flat plate structure (beamless) was out of scope in the application for seismic evaluation recommended by this study. However, it is acceptable to occupy well-designed structures that have been constructed in accordance with the most recent design provisions, because the most recent code permitted the use of pure flat plate structures with proper design by increasing shear capacity and/or by preventing the punching shear failure near the plate column joint. Beam members can be installed in the perimeter frame for a pure flat plate structure if that is required; however, additional research is recommended. Therefore, this study was focused on the old buildings that are most vulnerable to future seismic events. Computer-aided analysis can be done to validate this evaluation and retrofit methods.

References

(JICA) JICA (2015) Project for capacity development on natural disaster-resistant techniques of construction and retrofitting for public buildings in the people's republic of Bangladesh (CNCRP)

Abbas H, Hwee TK (2014) Advanced construction technologies : selected, peer reviewed papers from the 2014 4th International Conference on Structures and Building Materials (ICSBM 2014), March 15-16, 2014, Guangzhou, China

ACI 318-08 (2008) ACI Committee, and International Organization for Standardization. "Building code requirements for structural concrete and commentary."

Adetifa B, Polak MA (2005) Retrofit of slab column interior connections using shear bolts. ACI Struct J 102:. https://doi.org/10.14359/14278

AIJ (2018) AIJ Standard for Structural Calculation of Reinforced Concrete Structures, revised 2010; 2010 (in Japanese)

Al zaman MA, Jahan Monira N (2017) A Study of Earthquakes in Bangladesh and the Data Analysis of the Earthquakes that were generated In Bangladesh and Its' Very Close Regions for the Last Forty Years (1976-2016). J Geol Geophys 6:

Alam E (2019) Importance of long-term earthquake, tsunami and tropical cyclone data for disaster risk reduction in Bangladesh. Prog Disaster Sci 8:100121

Alam E, Dominey-Howes D (2016) A catalogue of earthquakes between 810BC and 2012 for the Bay of Bengal. Nat Hazards 81:. https://doi.org/10.1007/s11069-016-2174-7

Binici B, Bayrak O (2005) Upgrading of slab-column connections using fiber reinforced polymers. Eng Struct 27:97–107. https://doi.org/10.1016/j.engstruct.2004.09.005

BNBC (2020) Bangladesh National Building Code-2020

Bu W, Polak MA (2009) Seismic retrofit of reinforced concrete slab-column connections using shear bolts. ACI Struct J 106:514–522

Durucan C, Anil Ö (2015) Effect of opening size and location on the punching shear behavior of interior slab-column connections strengthened with CFRP strips. Eng Struct 105:. https://doi.org/10.1016/j.engstruct.2015.09.033

Ebead U, Marzouk H (2002) Strengthening of two-way slabs using steel plates. ACI Struct J 99:23–31

El-Salakawy EF, Polak MA, Soudki KA (2003) New shear strengthening technique for concrete slab-column connections. ACI Struct J 100:297–304

Elbakry HMF, Allam SM (2015) Punching strengthening of two-way slabs using external steel plates. Alexandria Eng J 54:. https://doi.org/10.1016/j.aej.2015.09.005

Ghali A, Sargious MA, Huizer A (1974) Vertical prestressing of flat plates around columns. In: American Concrete Institute, ACI Special Publication

HBRI (1993) Bangladesh National Building Code, 1993rd edn. Housing and Building Resaerch Institute, Ministry of Housing and Public Works, Dhaka, Bangladesh

Hognestad E, Hanson NW MD (1955) Concrete stress distribution in ultimate strength design. ACI J Proc 52:455–480

Hossain A, Adhikari TL, Ansary MA, Bari QH (2015) Characteristics and consequence of Nepal earthquake 2015: A review. Geotech Eng J SEAGS AGSSEA 46:

Islam R, Islam MN, Islam MN (2016) Earthquake risks in Bangladesh: causes, vulnerability, preparedness and strategies for mitigation. ARPN J Earth Sci 5:75–90

Jafarian N, Mostofinejad D, Naderi A (2020) Effects of FRP grids on punching shear behavior of reinforced concrete slabs. Structures 28:. https://doi.org/10.1016/j.istruc.2020.10.061

JBDPA (2005) Standard for Seismic Evaluation of Existing Reinforced Concrete Buildings, 2001, Guidelines for Seismic Retrofit of Existing Reinforced Concrete Buildings, 2001 and Technical Manual for Seismic Evaluation and Seismic Retrofit of Existing Reinforced Concre

Lawler N, Polak MA (2011a) Development of FRP Shear Bolts for Punching Shear Retrofit of Reinforced Concrete Slabs. J Compos Constr 15:591–601

Lawler N, Polak MA (2011b) Development of FRP Shear Bolts for Punching Shear Retrofit of Reinforced Concrete Slabs. J Compos Constr 15:. https://doi.org/10.1061/(asce)cc.1943-5614.0000188

Li Y, Sanada Y (2017) Seismic strengthening of existing RC beam-column joints by wing walls. Earthq Eng Struct Dyn 46:1987–2008

Li Y, Sanada Y, Maekawa K, et al (2019) Seismic strengthening and rehabilitation of RC frame structures with weak beam-column joints by installing wing walls. Bull Earthq Eng 17:2533–2567

Miyauchi Y, Fukuhara T, Kei T (2009) Experimental study on seisimic performance of retrofitted reinforced concrete member with low-strength concrete. Japan Concr Institute, Japan 31:1015-1020 (in Japanese)

Mokhtar AS, Ghali A, Dilger W (1985) Stud shear reinforcement for flat concrete plates.. J Am Concr Inst 82:676–683

Public Works Department (PWD) (2015) Manual for seismic evaluation of existingreinforced concrete buildings, Manual for seismic retrofit design of existingreinforced concrete buildings, Manual for seismic design of existing rein-forced concrete buildings (CNCRP manual). Dhaka, Bangladesh

Rahman MZ, Siddiqua S, Kamal ASMM (2020) Seismic source modeling and probabilistic seismic hazard analysis for Bangladesh. Nat Hazards 103:. https://doi.org/10.1007/s11069-020-04094-6

Ruiz MF, Muttoni A, Kunz J (2010) Strengthening of flat slabs against punching shear using post-installed shear reinforcement. ACI Struct J 107:434–442

Saleh H, Abdouka K, Al-Mahaidi R, Kalfat R (2018) Strengthening of slab–column connections against punching shear using FRP materials: state-of-the-art review. Aust J Struct Eng 19:188–206. https://doi.org/10.1080/13287982.2018.1462901

Shiddiqi HA, Tun PP, Kyaw TL, Ottemöller L (2018) Source study of the 24 August 2016 Mw 6.8 Chauk, Myanmar, earthquake. Seismol Res Lett 89:1773–1785

Steckler M, Stein S, Akhter S, Seeber L (2018) The Wicked Problem of Earthquake Hazard in Developing Countries. Eos (Washington DC) 99:. https://doi.org/10.1029/2018eo093625

The Daily Star (2007) Savar Spectra sweater factory failure: Institute of Engineers Bangladesh (IEB) Investigation Report. Dly. Star

The daily Star (Photo courtesy of SK Enamul Haq) (2005) 9-storey Garment Building Crumbles at Savar. Dly. Star Vol. 5, Num 312

The New York Times (photo courtesy of Abir Abdullah) (2015) Bangladesh Police Charge 41 With Murder Over Rana Plaza Collapse (Published 2015)

Topuzi D, Polak MA, Narasimhan S (2017) A new technique for the seismic retrofit of Slab-Column connections. ACI Struct J 114:. https://doi.org/10.14359/51689500

Walkner R, Spiegl M, Feix J (2021) Concrete screws as a post-installed punching shear reinforcement. Struct Concr 22:. https://doi.org/10.1002/suco.202000427

Wardi S, Sanada Y, Saha N, Takahashi S (2020) Improving integrity of RC beam-column joints with deficient beam rebar anchorage. Earthq Eng Struct Dyn 49:234–260

Widianto, Bayrak O, Jirsa JO, Tian Y (2010) Seismic rehabilitation of slab-column connections. ACI Struct J 107:237–247

Wood JGM (2003) Pipers Row Car Park, Wolverhampton." Quantitative study of the causes of the partial collapse on 20th March (1997). UK

Wörle P (2014) Enhanced shear punching capacity by the use of post installed concrete screws. Eng Struct 60:. https://doi.org/10.1016/j.engstruct.2013.12.015

Appendix A1

Position of strain gauges on reinforcing bars and their strain responses for each specimen

The appendix explains the experimental results for the various items that are covered in Chapters 2, 3, and 4. This section contains a description of the findings of strain gauges.

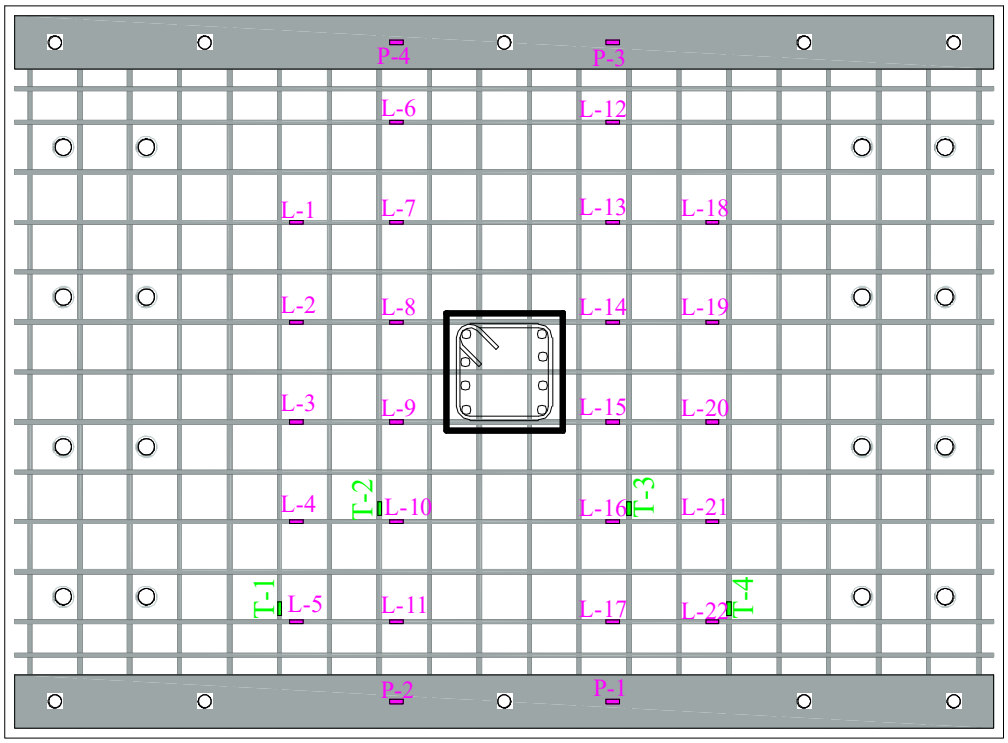

Figure A1.1 Position of strain gauges (specimen FP-1)

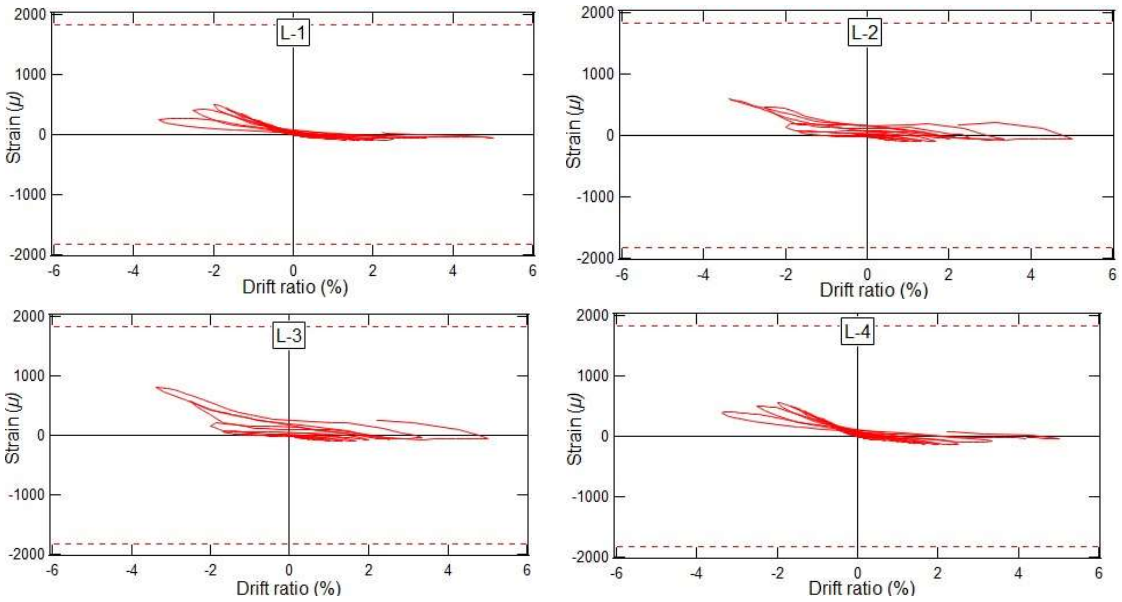

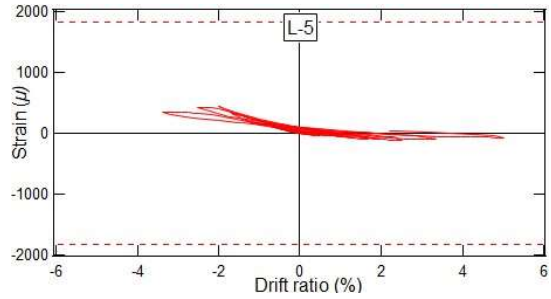
L-5
Strain (μ)
Drift ratio (%)

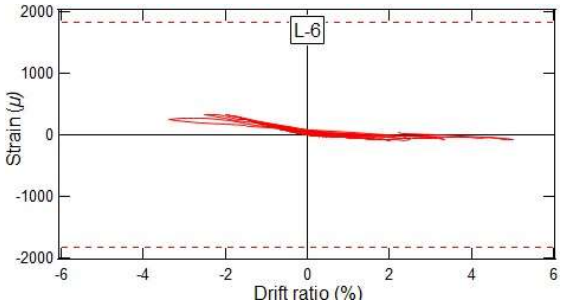
L-6
Strain (μ)
Drift ratio (%)

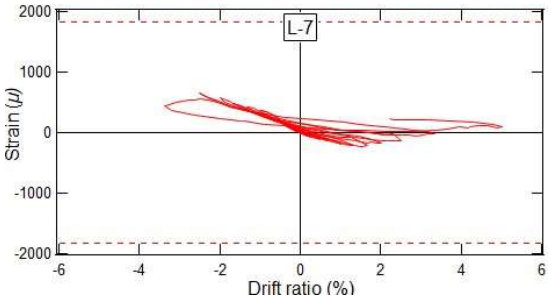
L-7
Strain (μ)
Drift ratio (%)

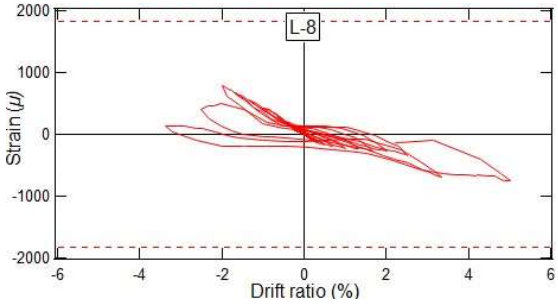
L-8
Strain (μ)
Drift ratio (%)

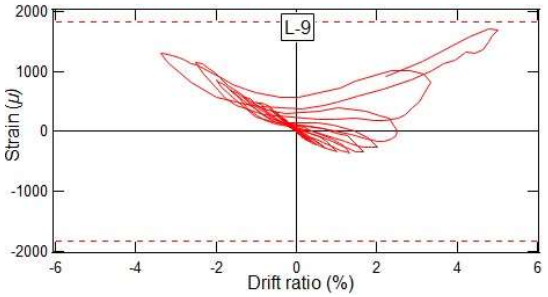
L-9
Strain (μ)
Drift ratio (%)

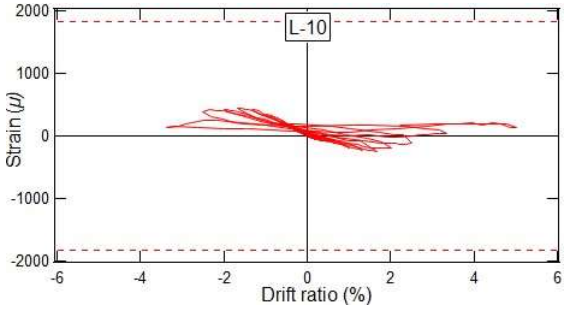
L-10
Strain (μ)
Drift ratio (%)

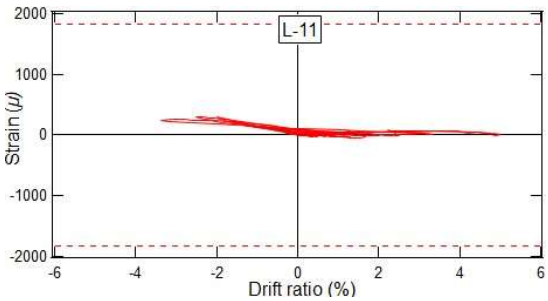
L-11
Strain (μ)
Drift ratio (%)

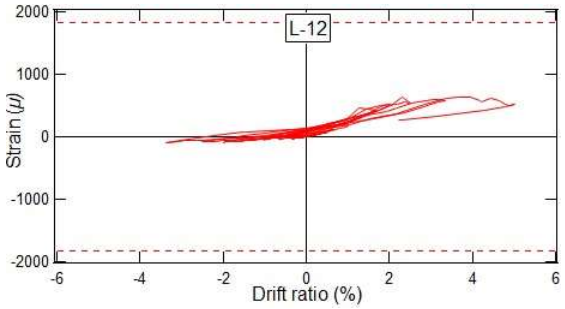
L-12
Strain (μ)
Drift ratio (%)

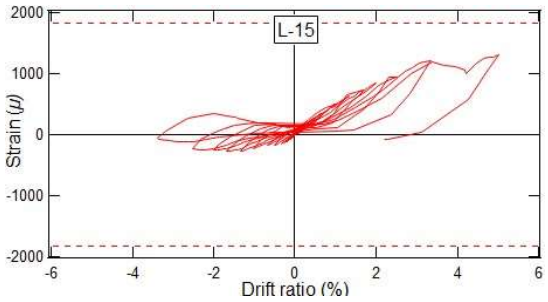
L-15
Strain (μ)
Drift ratio (%)

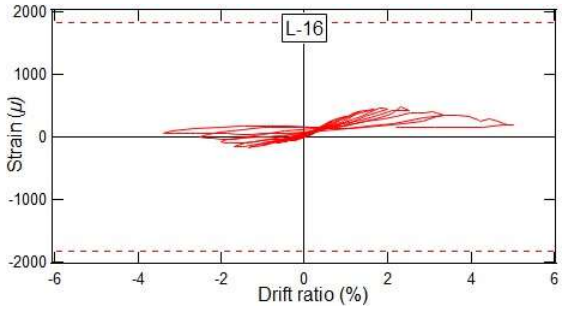
L-16
Strain (μ)
Drift ratio (%)

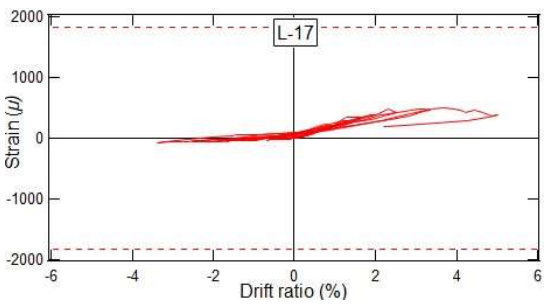
L-17
Strain (μ)
Drift ratio (%)

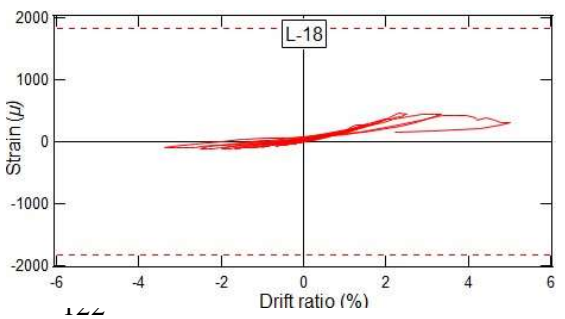
L-18
Strain (μ)
Drift ratio (%)

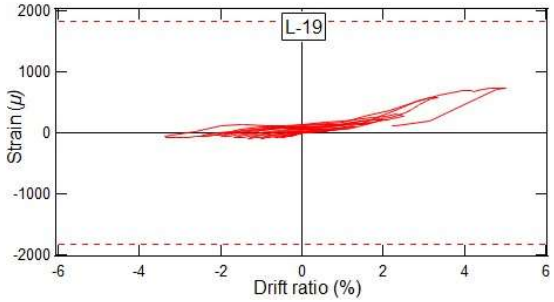
L-19
Strain (μ)
Drift ratio (%)

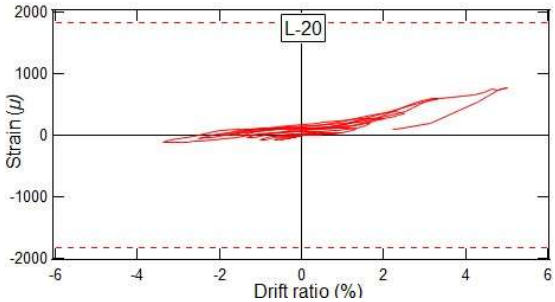
L-20
Strain (μ)
Drift ratio (%)

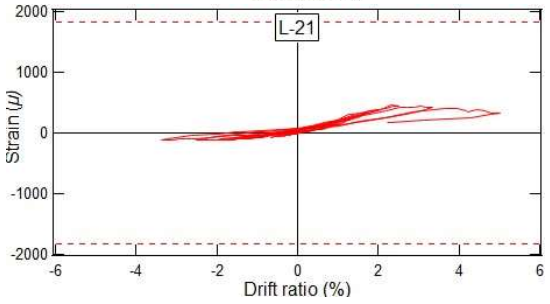
L-21
Strain (μ)
Drift ratio (%)

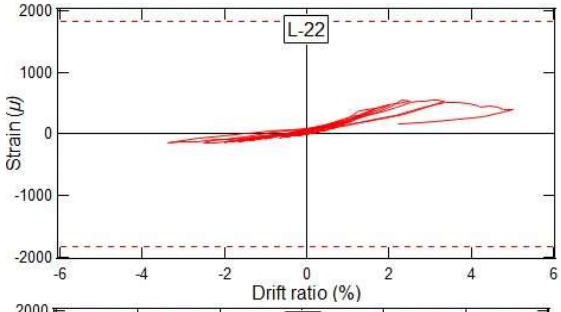
L-22
Strain (μ)
Drift ratio (%)

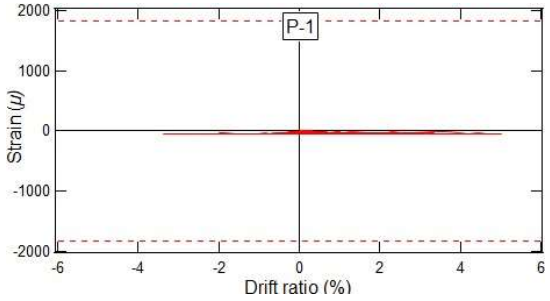
P-1
Strain (μ)
Drift ratio (%)

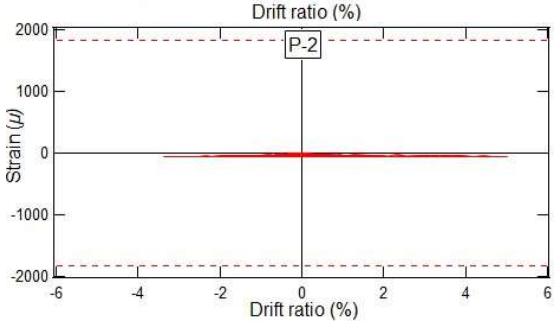
P-2
Strain (μ)
Drift ratio (%)

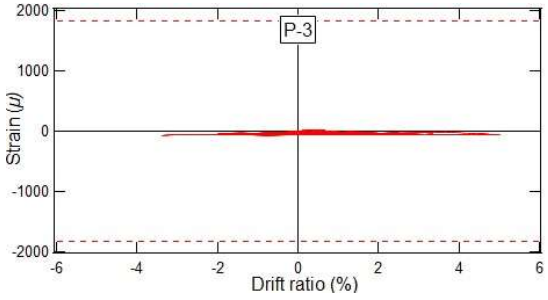
P-3
Strain (μ)
Drift ratio (%)

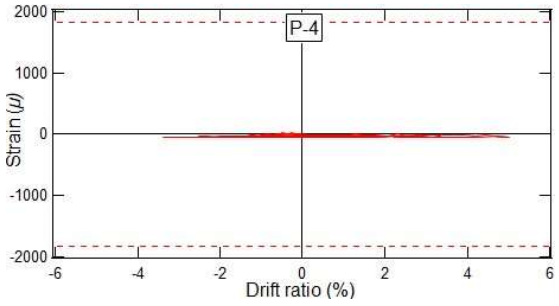
P-4
Strain (μ)
Drift ratio (%)

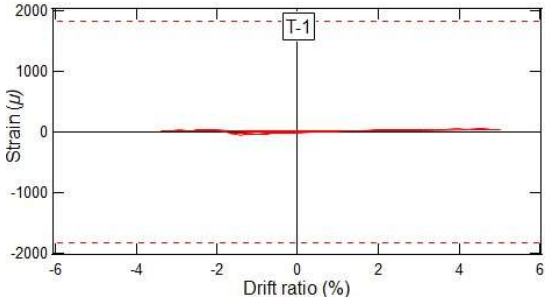
T-1
Strain (μ)
Drift ratio (%)

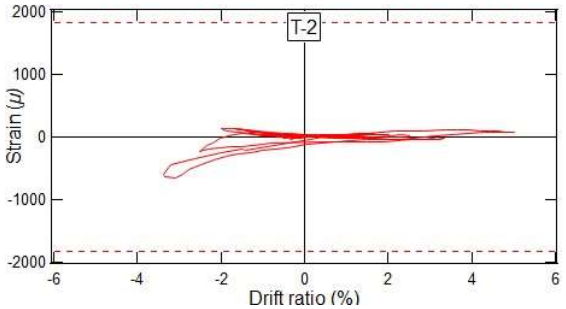
T-2
Strain (μ)
Drift ratio (%)

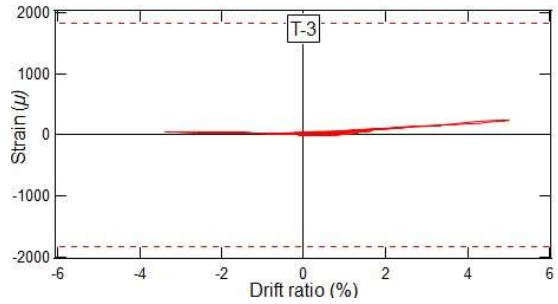
T-3
Strain (μ)
Drift ratio (%)

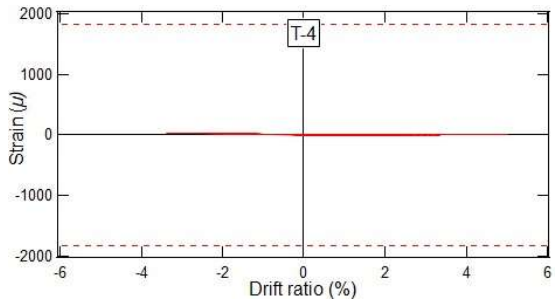
T-4
Strain (μ)
Drift ratio (%)

Figure A1.2 Strains of reinforcing bars for each strain gauge (specimen FP-1)

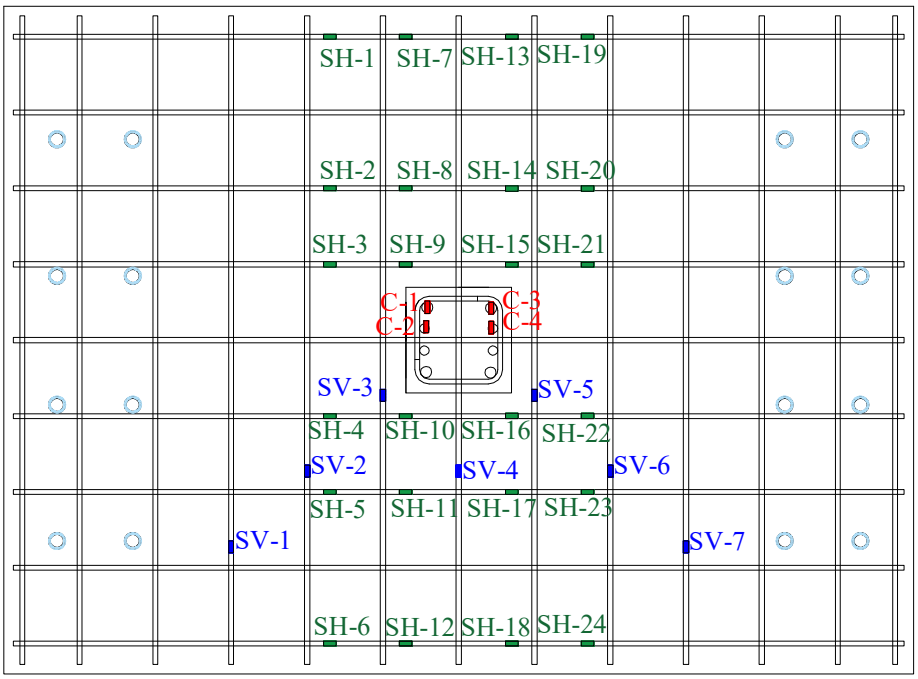

Figure A1.3 Position of strain gauges (specimen FP-2)

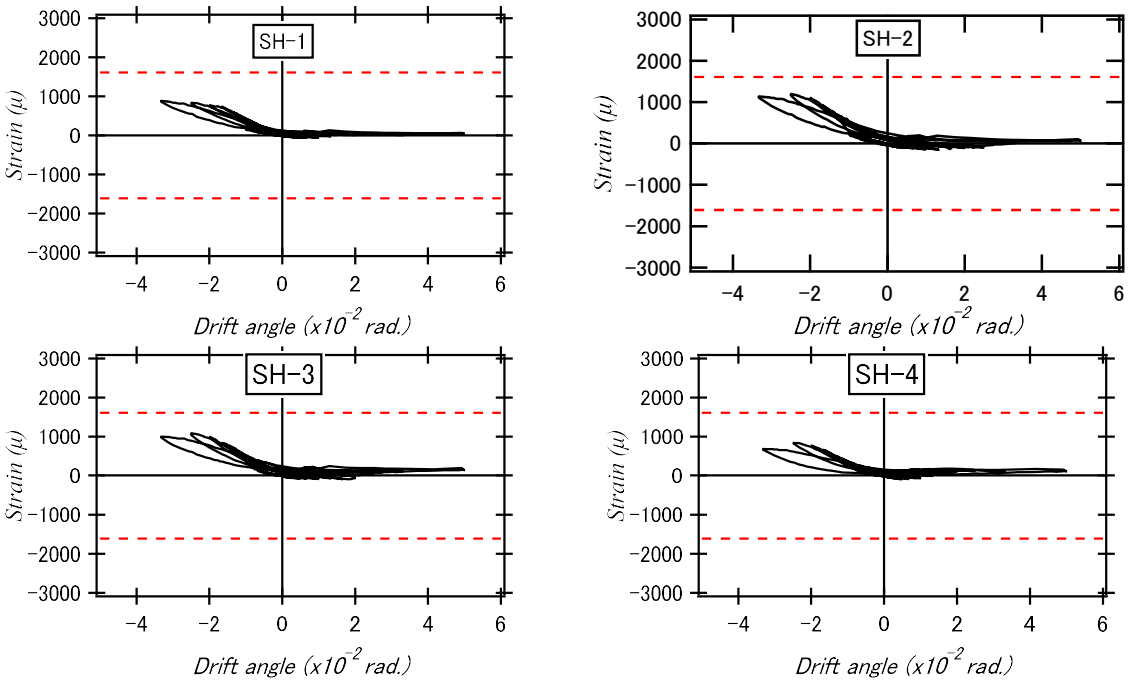

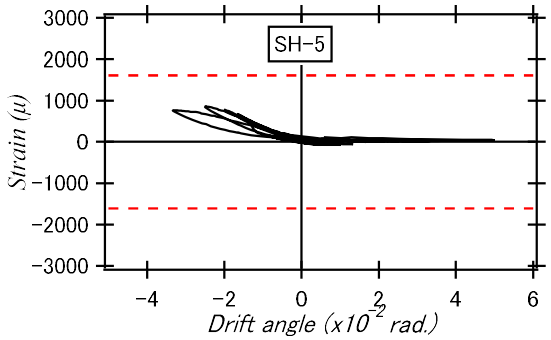
SH-5
Strain (μ)
Drift angle (x10⁻² rad.)

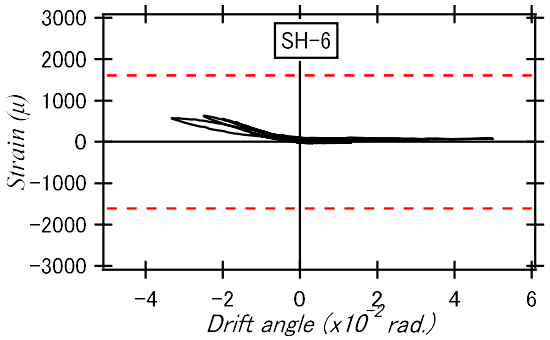
SH-6
Strain (μ)
Drift angle (x10⁻² rad.)

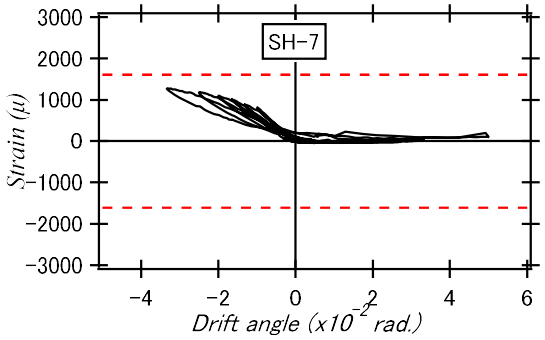
SH-7
Strain (μ)
Drift angle (x10⁻² rad.)

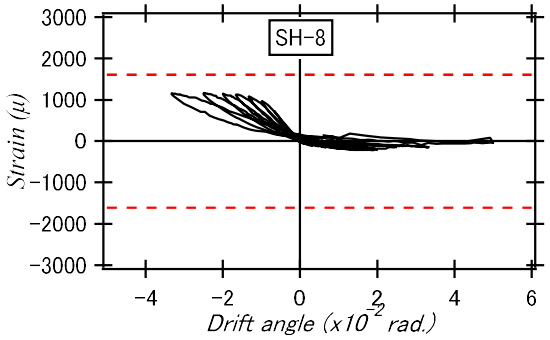
SH-8
Strain (μ)
Drift angle (x10⁻² rad.)

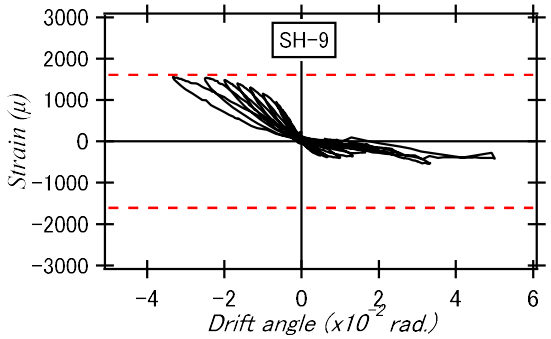
SH-9
Strain (μ)
Drift angle (x10⁻² rad.)

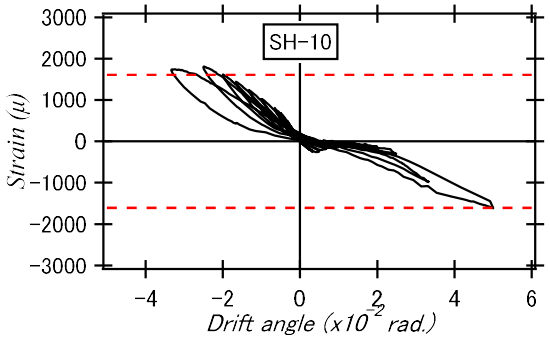
SH-10
Strain (μ)
Drift angle (x10⁻² rad.)

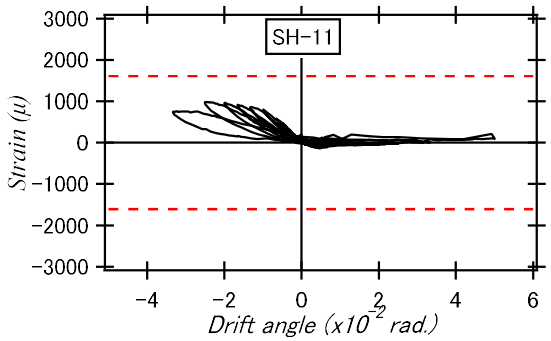
SH-11
Strain (μ)
Drift angle (x10⁻² rad.)

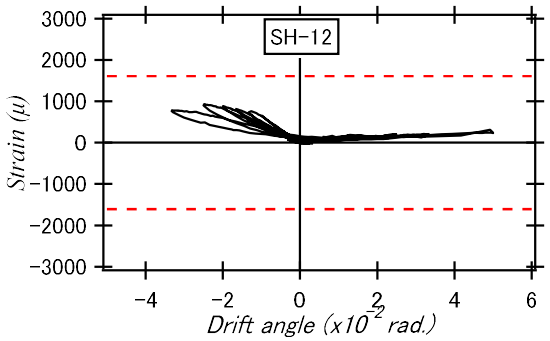
SH-12
Strain (μ)
Drift angle (x10⁻² rad.)

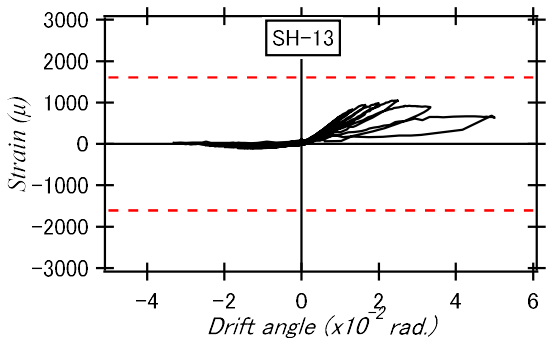
SH-13
Strain (μ)
Drift angle (x10⁻² rad.)

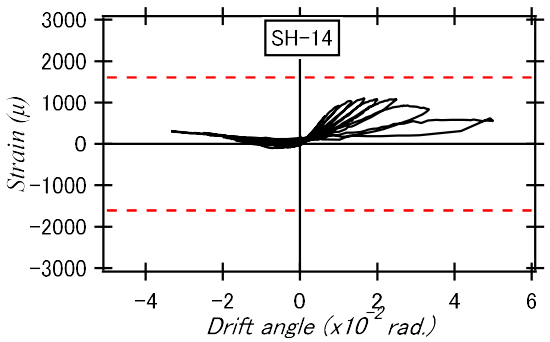
SH-14
Strain (μ)
Drift angle (x10⁻² rad.)

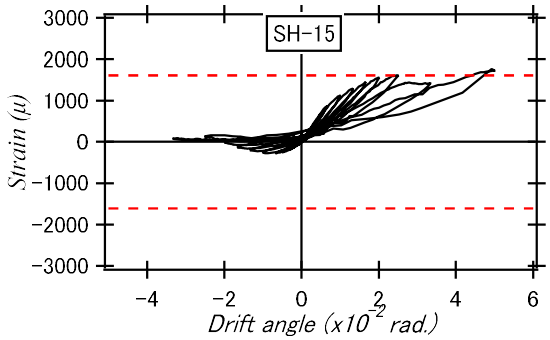
SH-15
Strain (μ)
Drift angle (x10⁻² rad.)

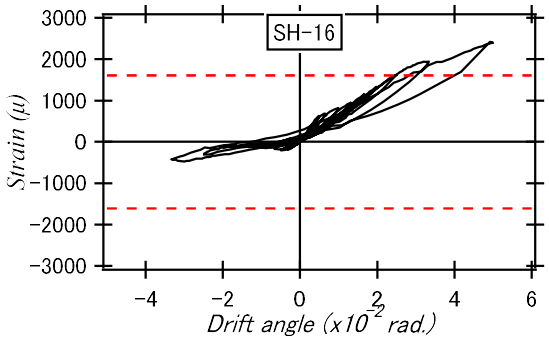
SH-16
Strain (μ)
Drift angle (x10⁻² rad.)

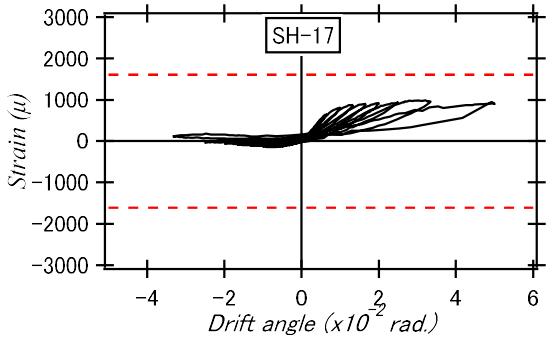
SH-17
Strain (μ)
Drift angle (x10⁻² rad.)

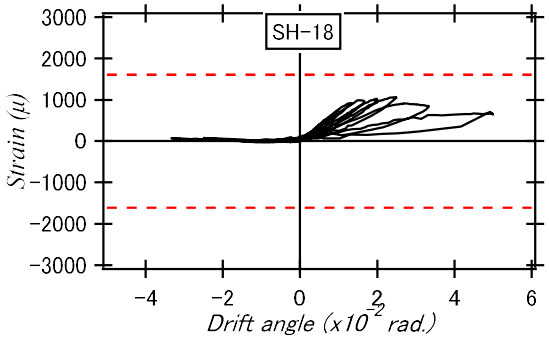
SH-18
Strain (μ)
Drift angle (x10⁻² rad.)

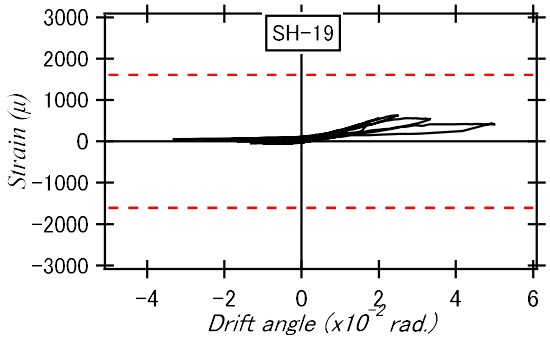
SH-19
Strain (μ)
Drift angle (x10⁻² rad.)

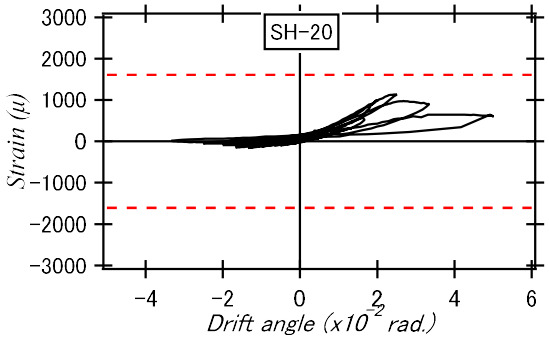
SH-20
Strain (μ)
Drift angle (x10⁻² rad.)

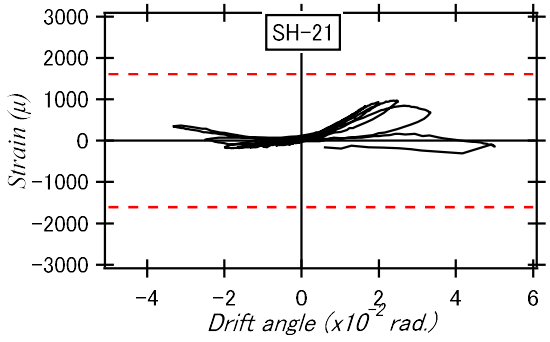
SH-21
Strain (μ)
Drift angle (x10⁻² rad.)

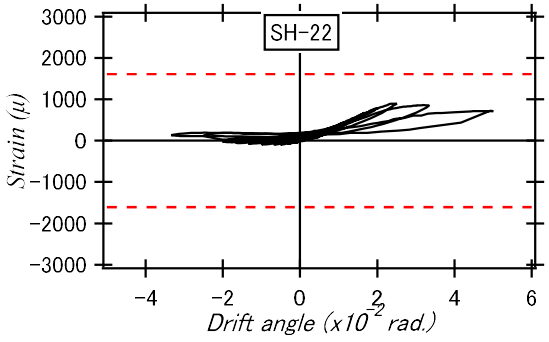
SH-22
Strain (μ)
Drift angle (x10⁻² rad.)

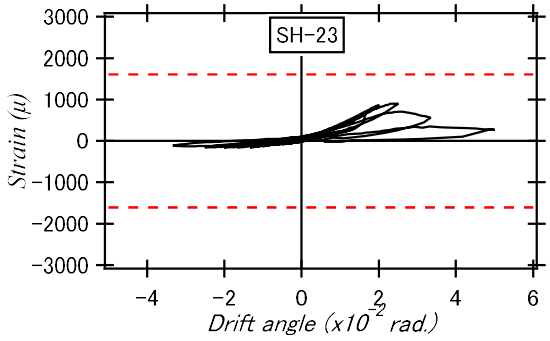
SH-23
Strain (μ)
Drift angle (x10⁻² rad.)

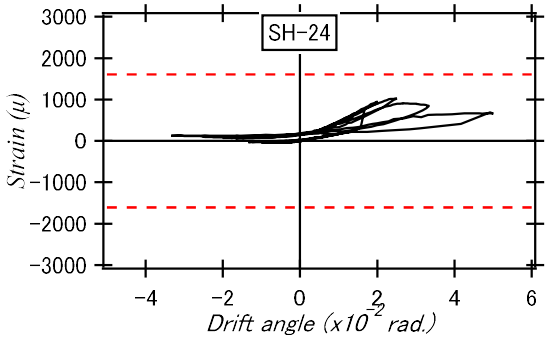
SH-24
Strain (μ)
Drift angle (x10⁻² rad.)

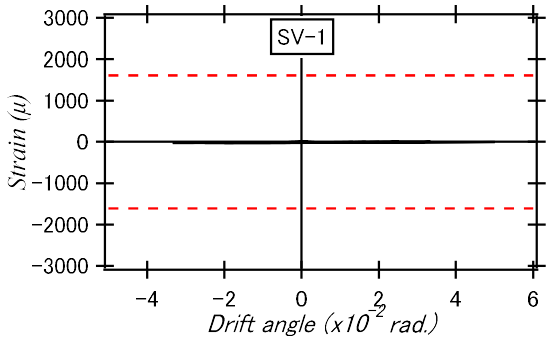
SV-1
Strain (μ)
Drift angle (x10^-2 rad.)

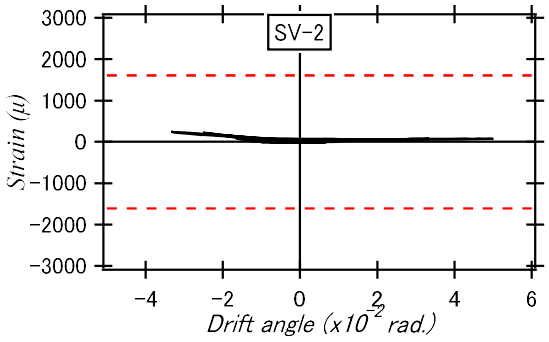
SV-2
Strain (μ)
Drift angle (x10^-2 rad.)

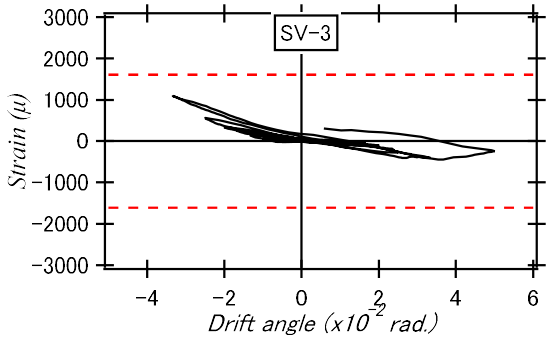
SV-3
Strain (μ)
Drift angle (x10^-2 rad.)

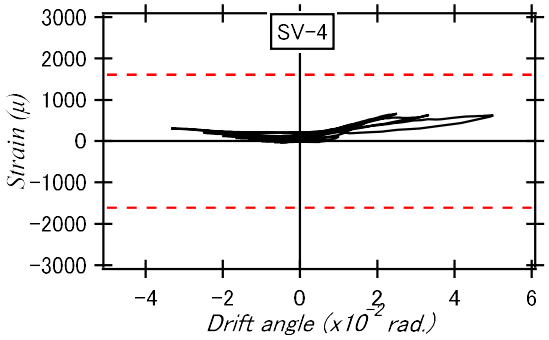
SV-4
Strain (μ)
Drift angle (x10^-2 rad.)

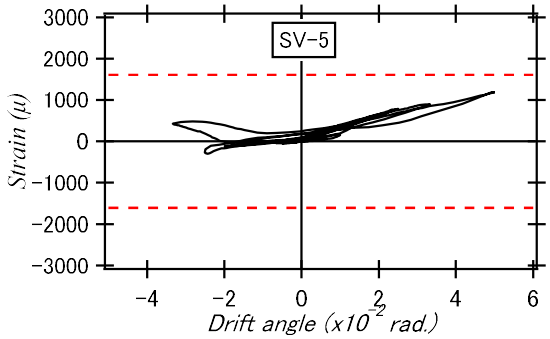
SV-5
Strain (μ)
Drift angle (x10^-2 rad.)

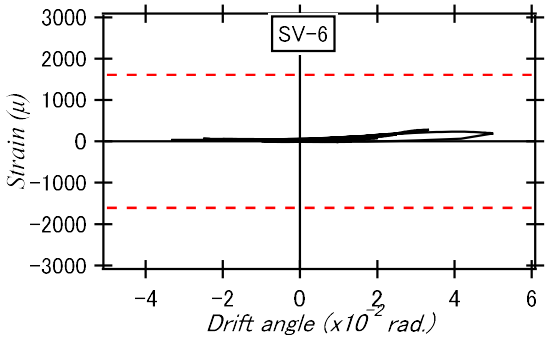
SV-6
Strain (μ)
Drift angle (x10^-2 rad.)

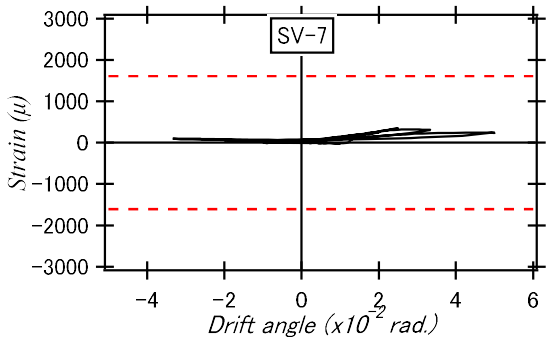
SV-7
Strain (μ)
Drift angle (x10^-2 rad.)

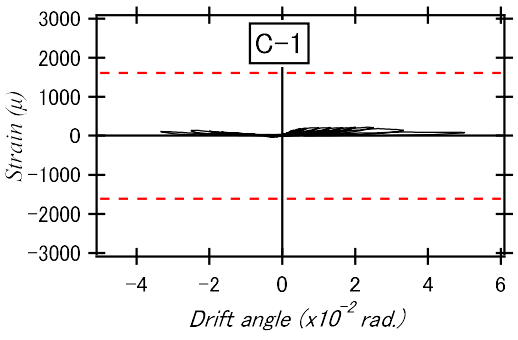
C-1
Strain (μ)
Drift angle (x10^-2 rad.)

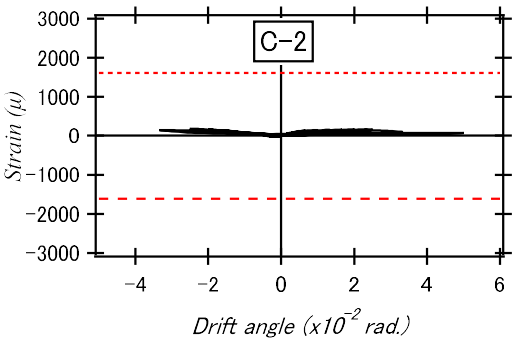
C-2
Strain (μ)
Drift angle (x10^-2 rad.)

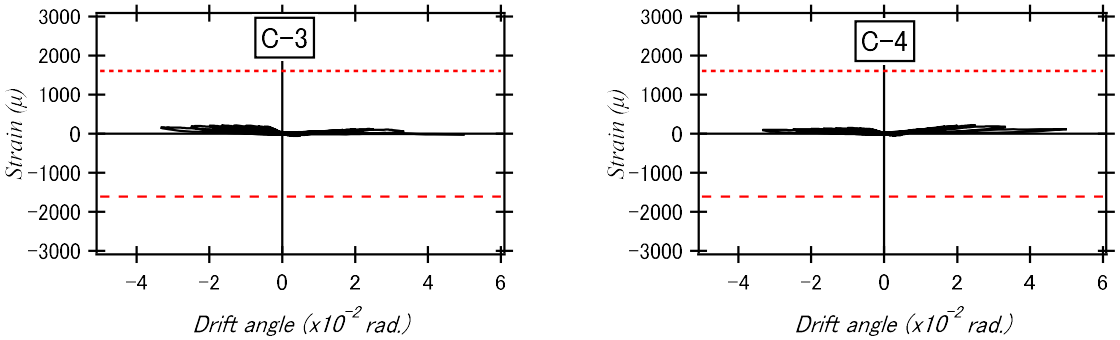

Figure A1.4 Strains of reinforcing bars for each strain gauge (specimen FP-2)

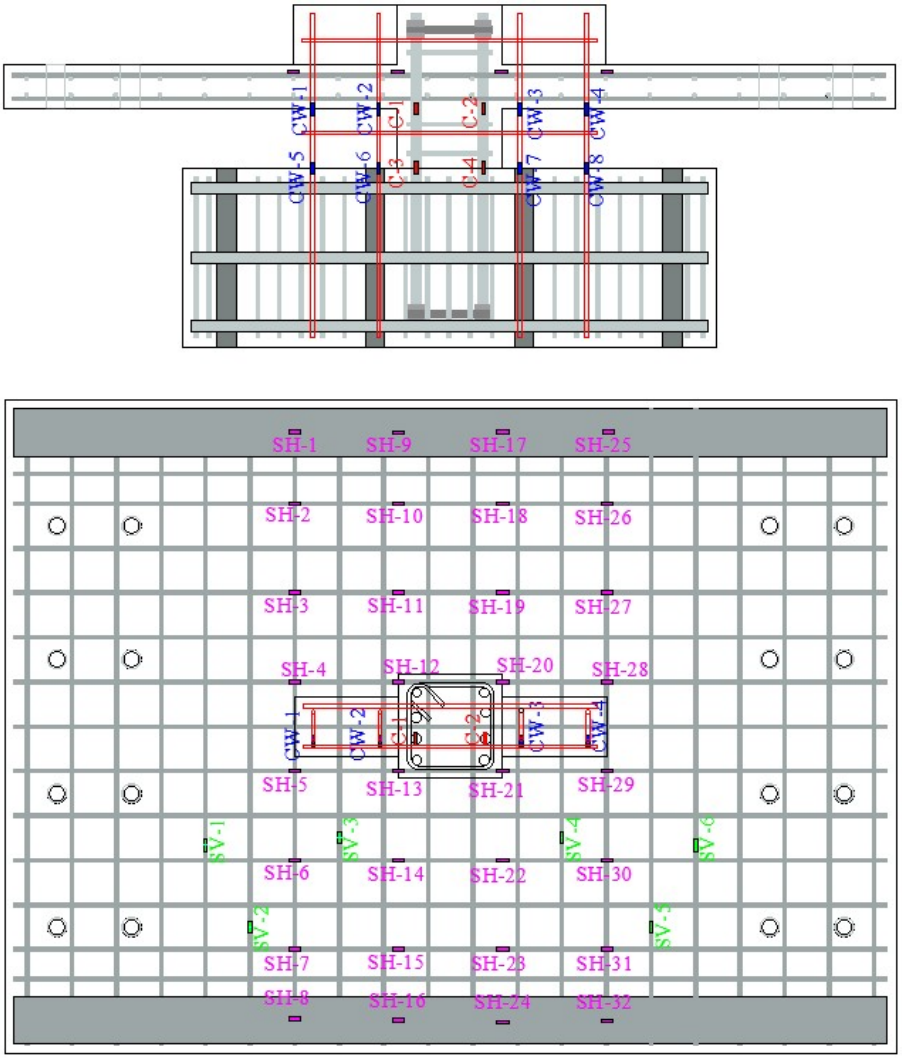

Figure A1.5 Position of strain gauges (specimen FP-W1)

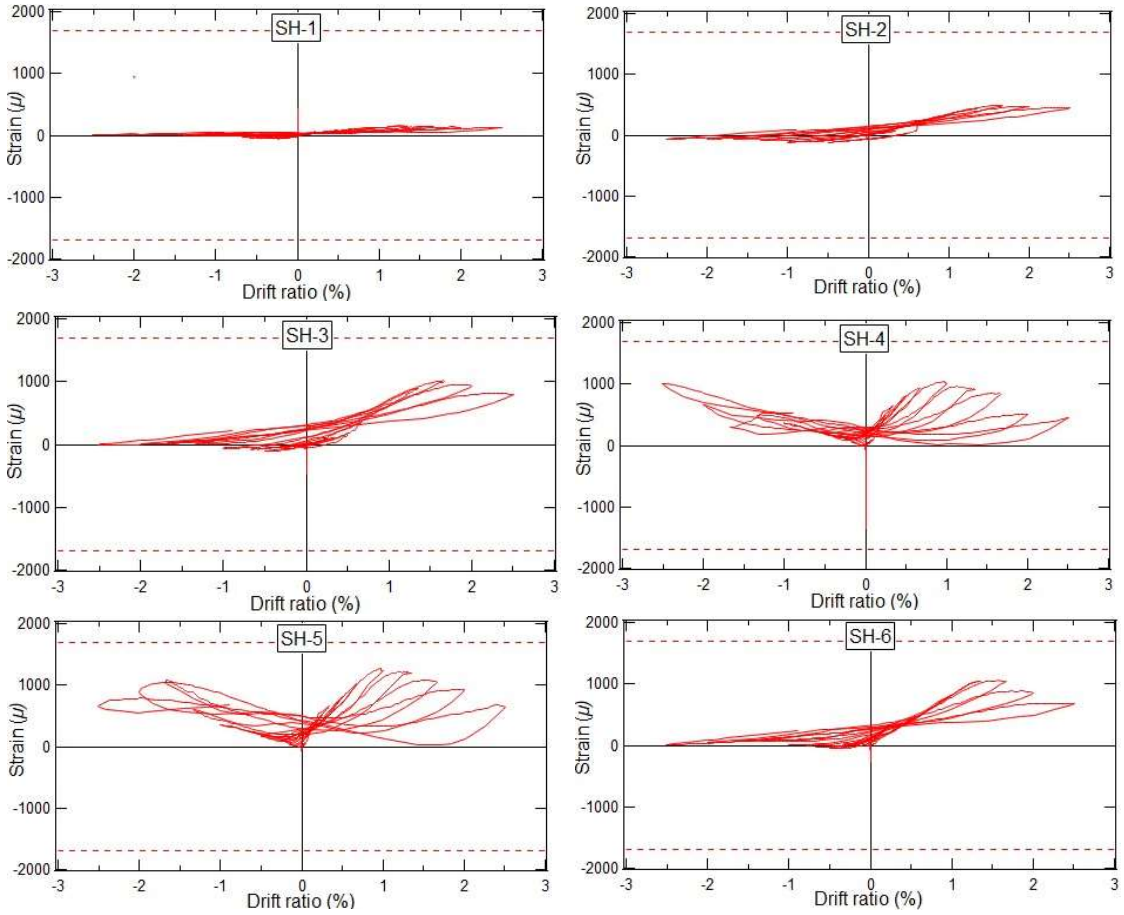
SH-1
SH-2
SH-3
SH-4
SH-5
SH-6
Strain (μ)
Drift ratio (%)
2000
1000
0
-1000
-2000
-3
-2
-1
0
1
2
3

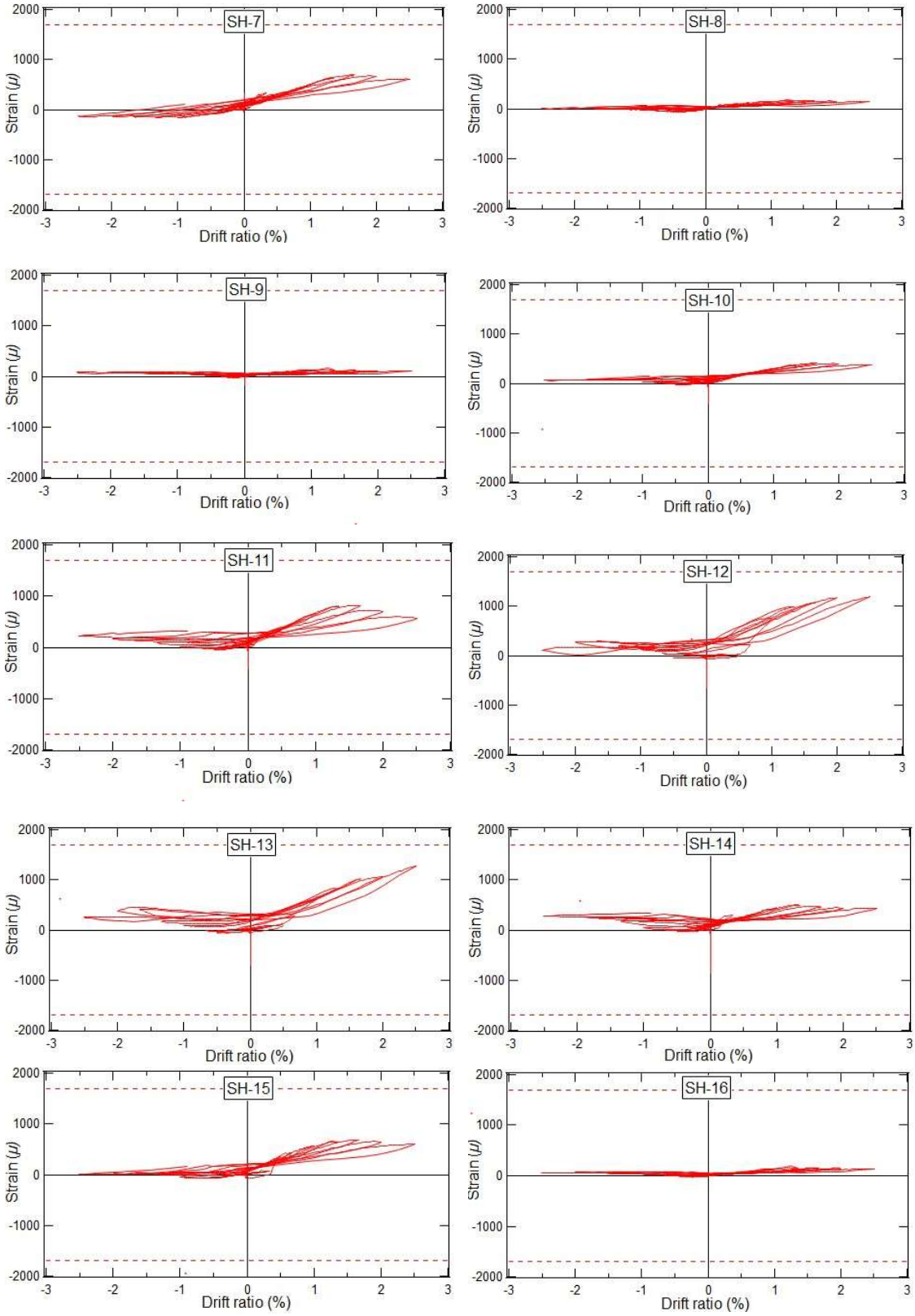
SH-7
SH-8
SH-9
SH-10
SH-11
SH-12
SH-13
SH-14
SH-15
SH-16
Strain (μ)
Drift ratio (%)
2000
1000
0
-1000
-2000
-3
-2
-1
0
1
2
3

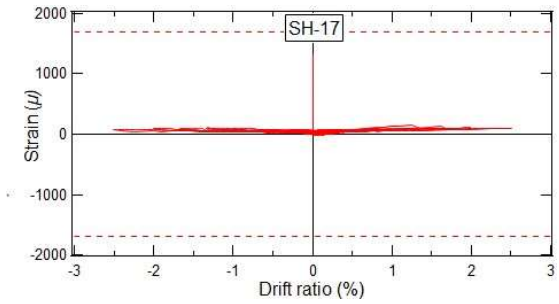
SH-17
Strain (μ)
Drift ratio (%)

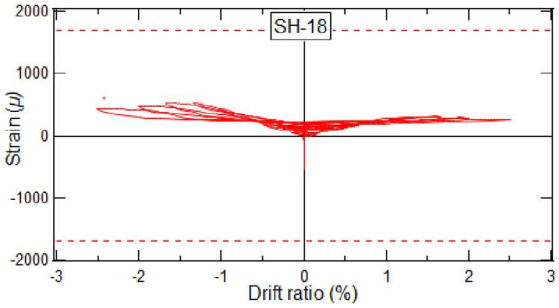
SH-18
Strain (μ)
Drift ratio (%)

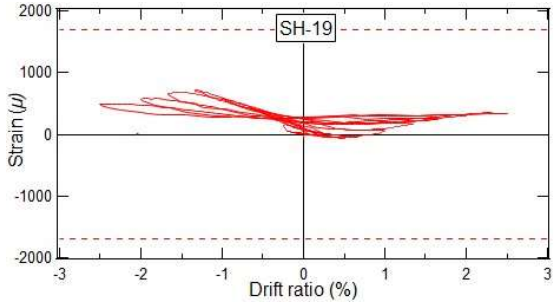
SH-19
Strain (μ)
Drift ratio (%)

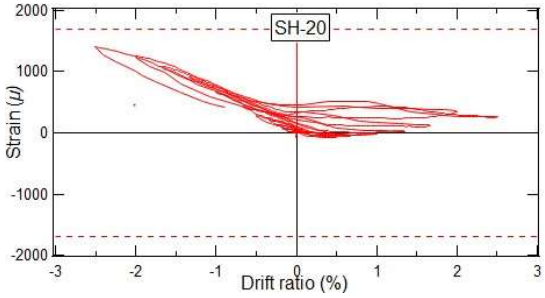
SH-20
Strain (μ)
Drift ratio (%)

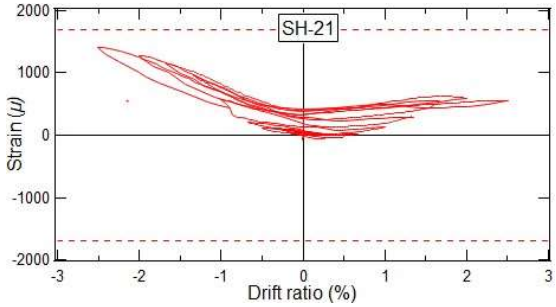
SH-21
Strain (μ)
Drift ratio (%)

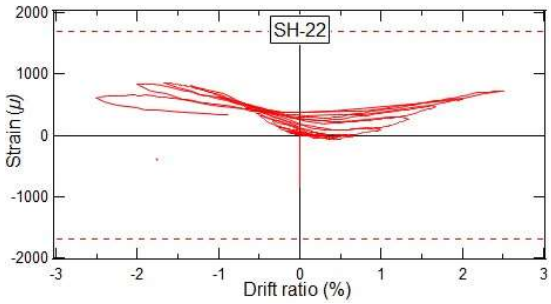
SH-22
Strain (μ)
Drift ratio (%)

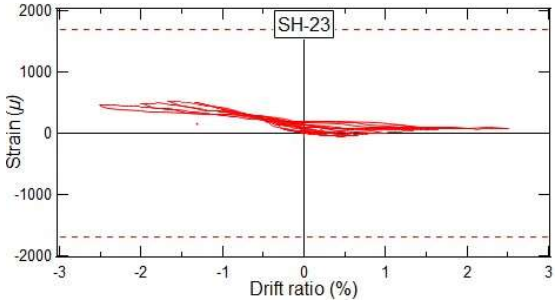
SH-23
Strain (μ)
Drift ratio (%)

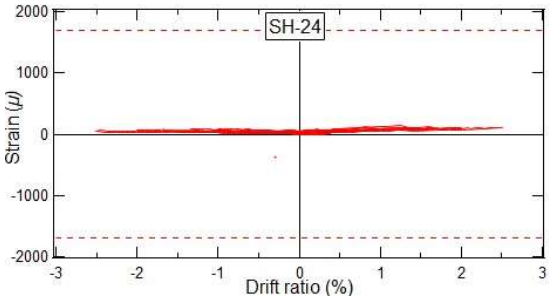
SH-24
Strain (μ)
Drift ratio (%)

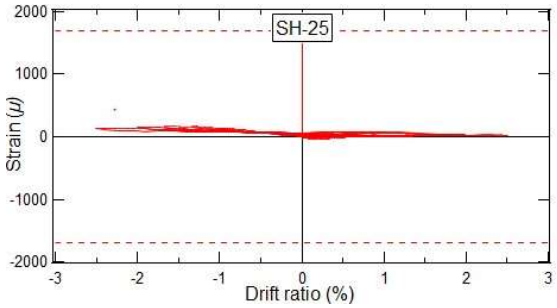
SH-25
Strain (μ)
Drift ratio (%)

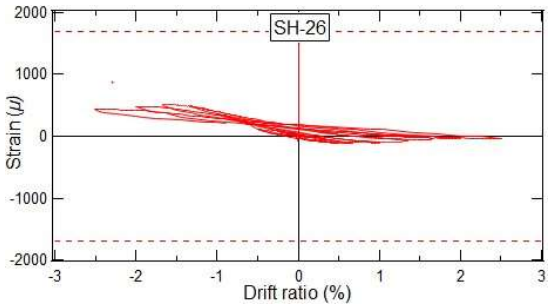
SH-26
Strain (μ)
Drift ratio (%)

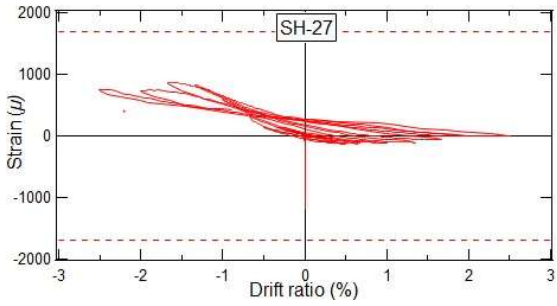
SH-27
Strain (μ)
Drift ratio (%)

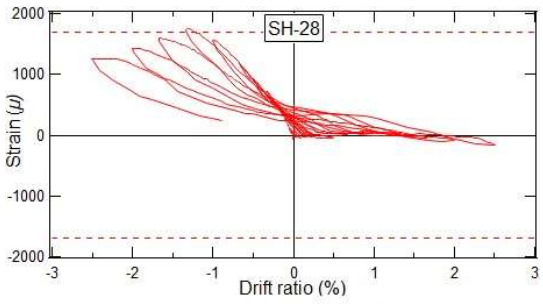
SH-28
Strain (μ)
Drift ratio (%)

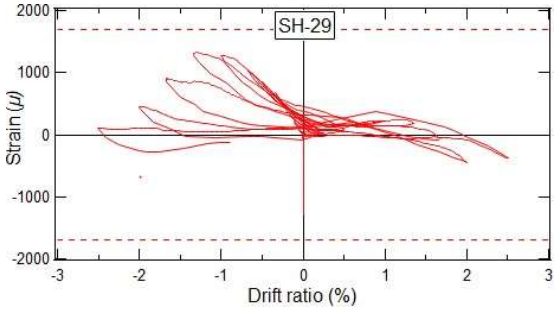
SH-29
Strain (μ)
Drift ratio (%)

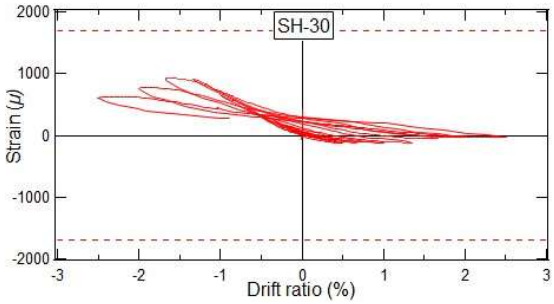
SH-30
Strain (μ)
Drift ratio (%)

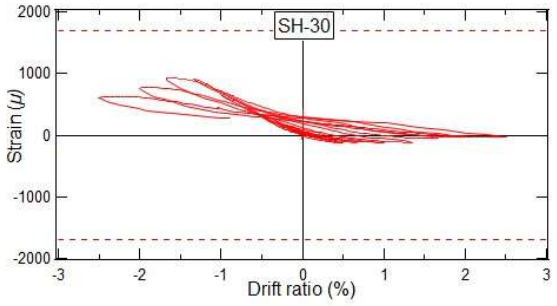
SH-30
Strain (μ)
Drift ratio (%)

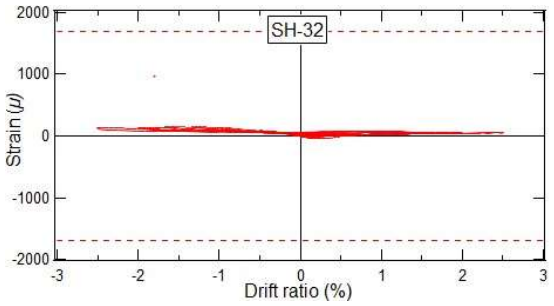
SH-32
Strain (μ)
Drift ratio (%)

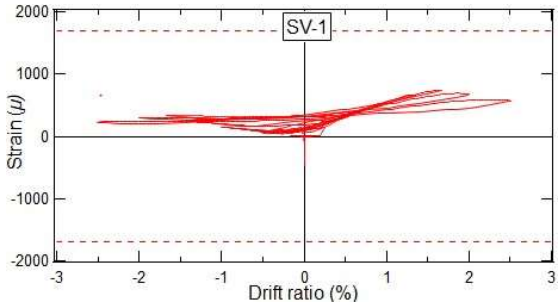
SV-1
Strain (μ)
Drift ratio (%)

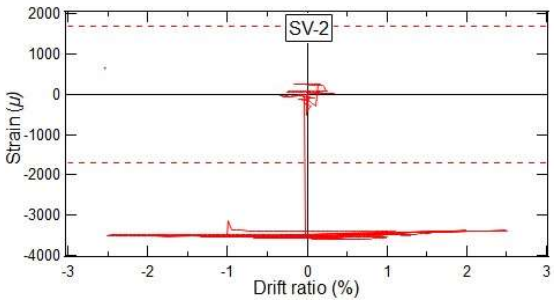
SV-2
Strain (μ)
Drift ratio (%)

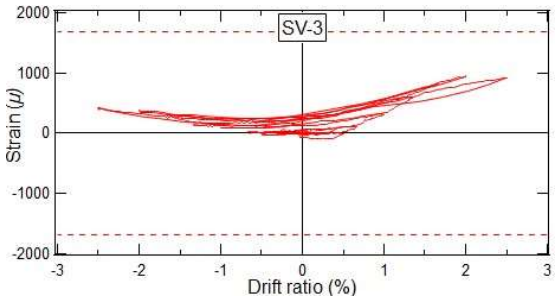
SV-3
Strain (μ)
Drift ratio (%)

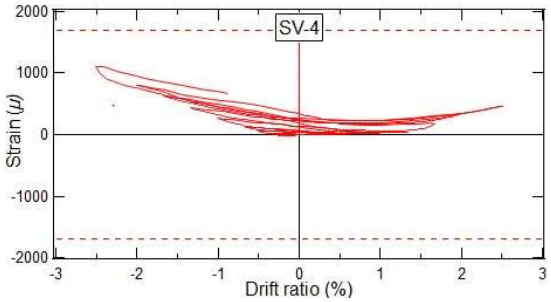
SV-4
Strain (μ)
Drift ratio (%)

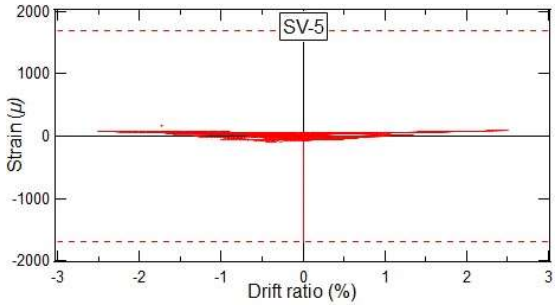
SV-5
Strain (μ)
Drift ratio (%)

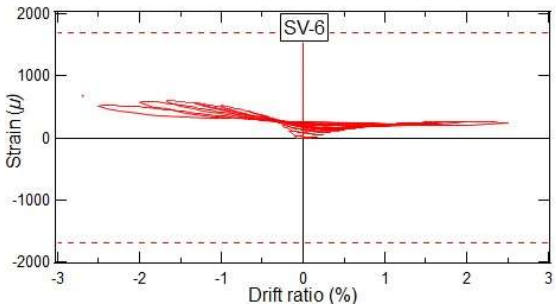
SV-6
Strain (μ)
Drift ratio (%)

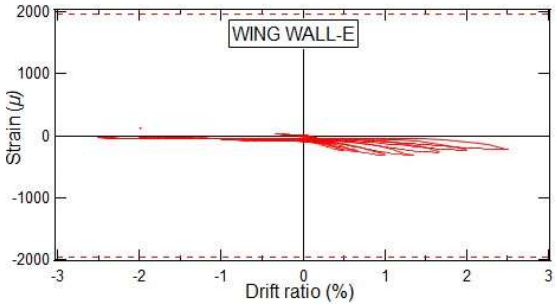
WING WALL-E
Strain (μ)
Drift ratio (%)

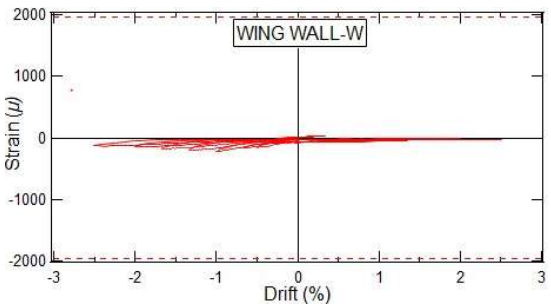
WING WALL-W
Strain (μ)
Drift (%)

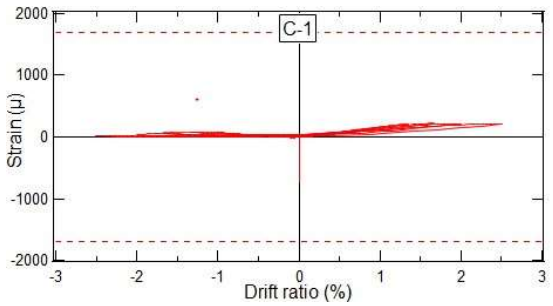
C-1
Strain (μ)
Drift ratio (%)

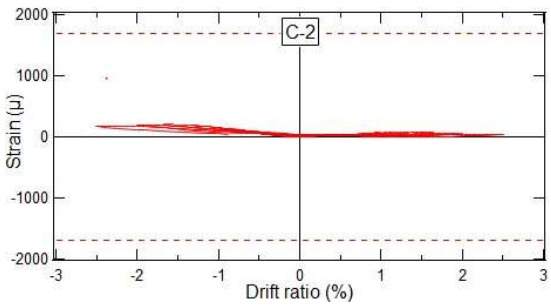
C-2
Strain (μ)
Drift ratio (%)

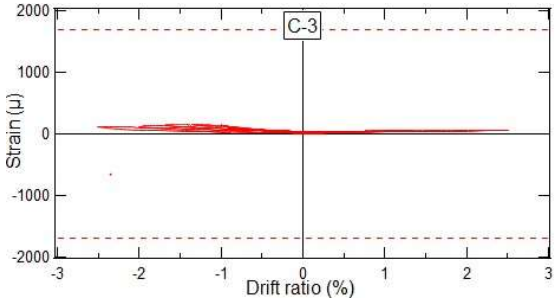
C-3
Strain (μ)
Drift ratio (%)

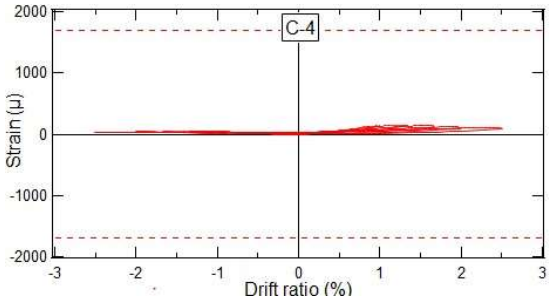
C-4
Strain (μ)
Drift ratio (%)

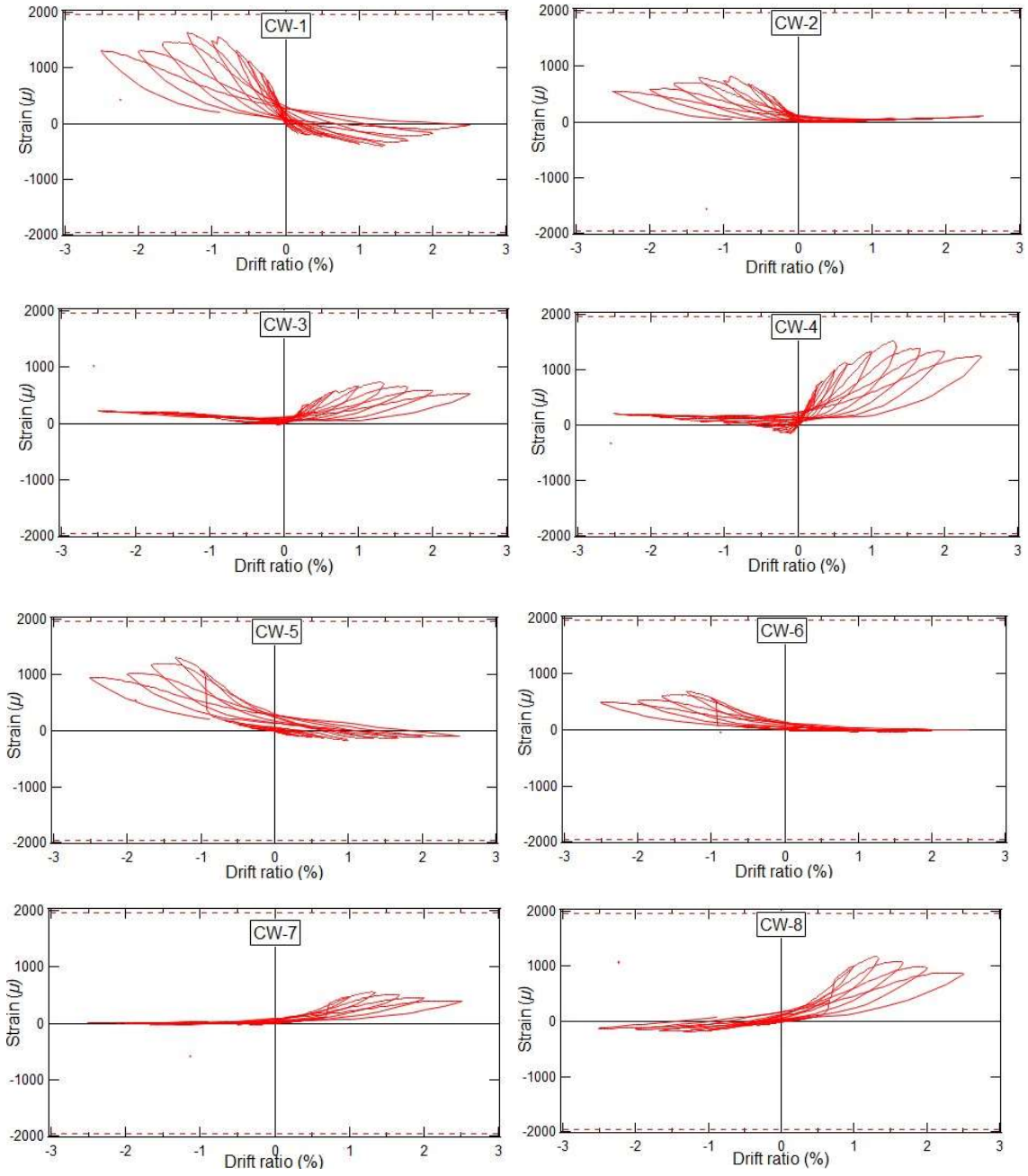

Figure A1.6 Strains of reinforcing bars for each strain gauge (specimen FP-W1)

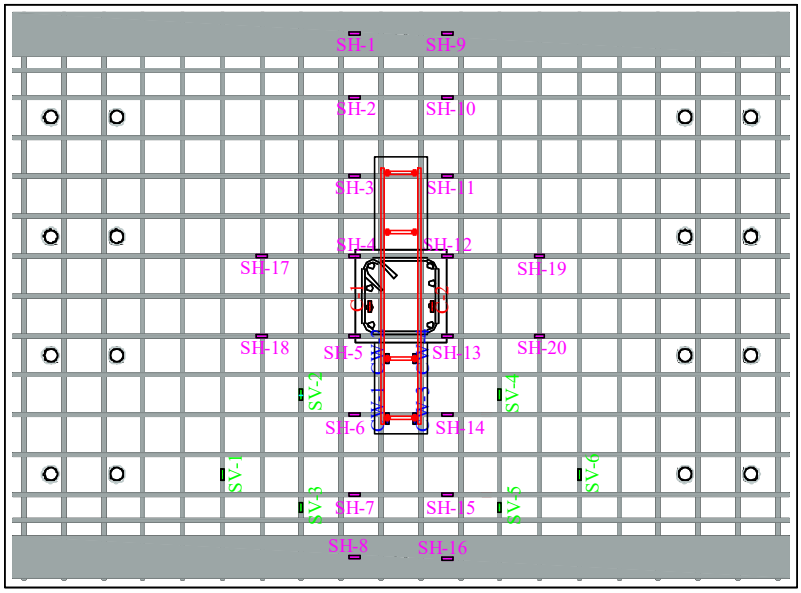

Figure A1.7 Position of strain gauges (specimen FP-W2)

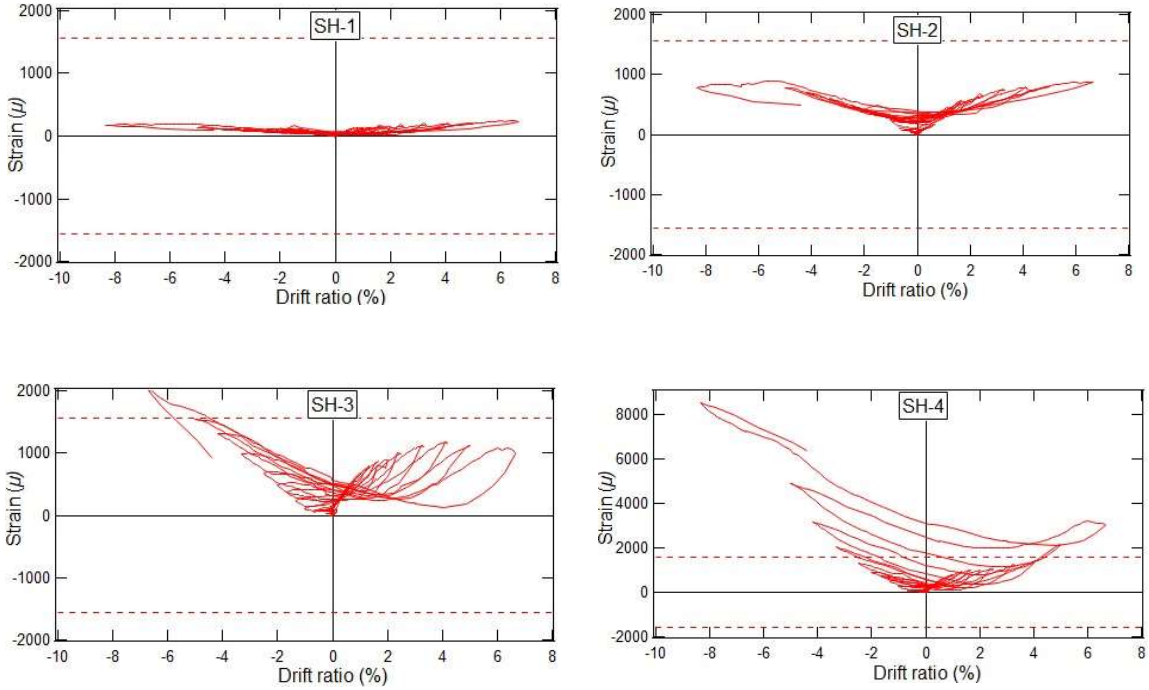

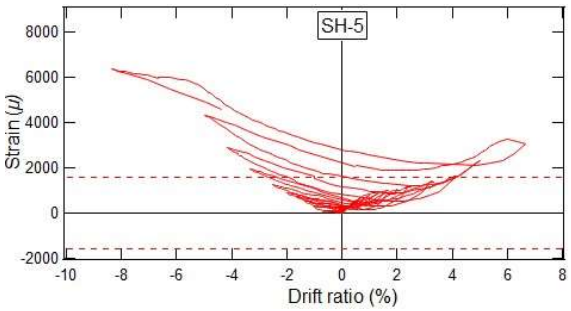
SH-5
Strain (μ)
Drift ratio (%)

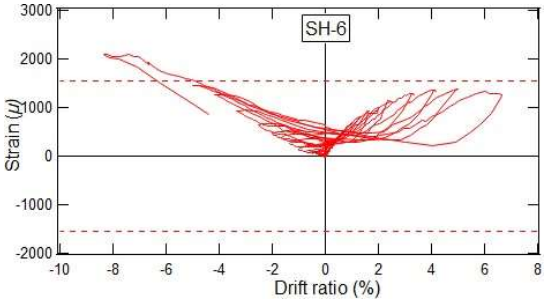
SH-6
Strain (μ)
Drift ratio (%)

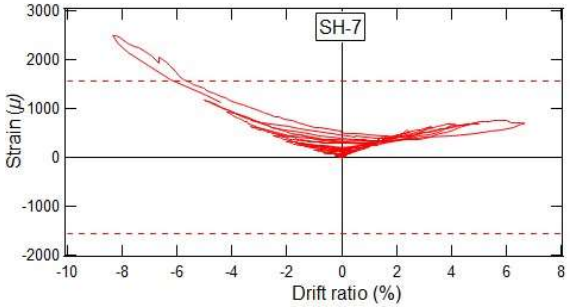
SH-7
Strain (μ)
Drift ratio (%)

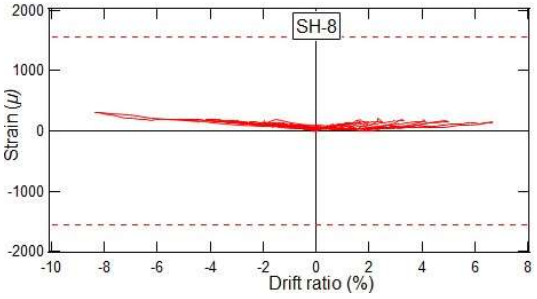
SH-8
Strain (μ)
Drift ratio (%)

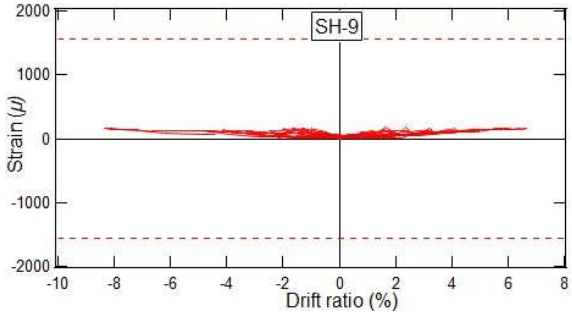
SH-9
Strain (μ)
Drift ratio (%)

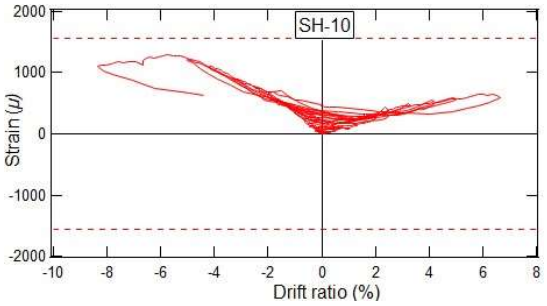
SH-10
Strain (μ)
Drift ratio (%)

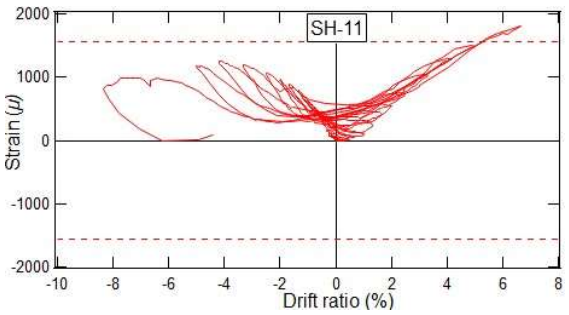
SH-11
Strain (μ)
Drift ratio (%)

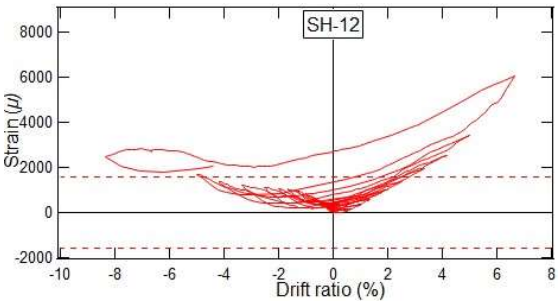
SH-12
Strain (μ)
Drift ratio (%)

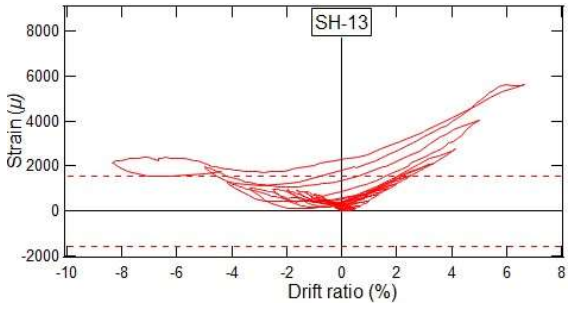
SH-13
Strain (μ)
Drift ratio (%)

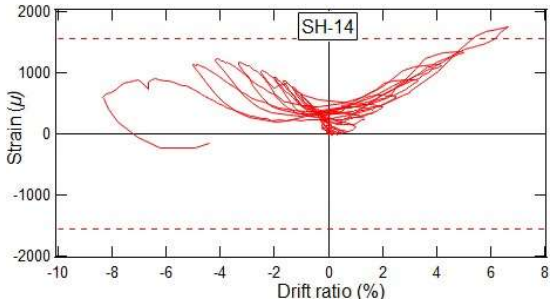
SH-14
Strain (μ)
Drift ratio (%)

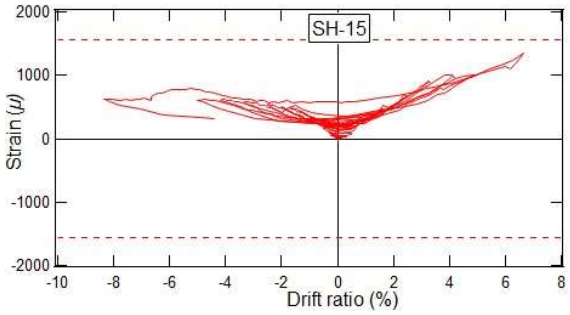
SH-15
Strain (μ)
Drift ratio (%)

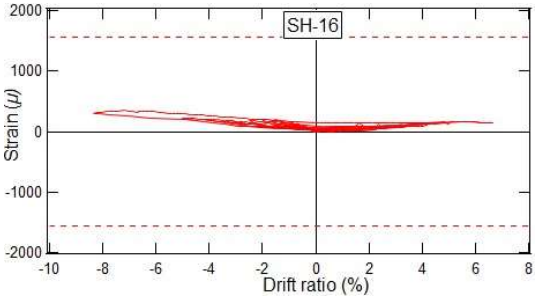
SH-16
Strain (μ)
Drift ratio (%)

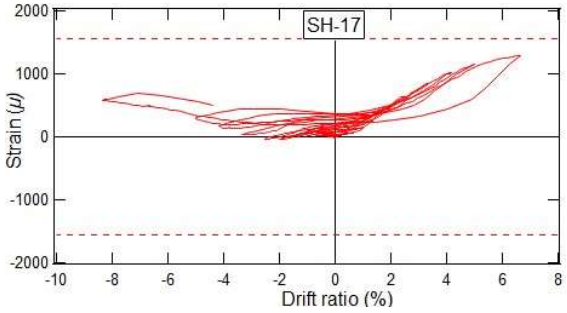
SH-17
Strain (μ)
Drift ratio (%)

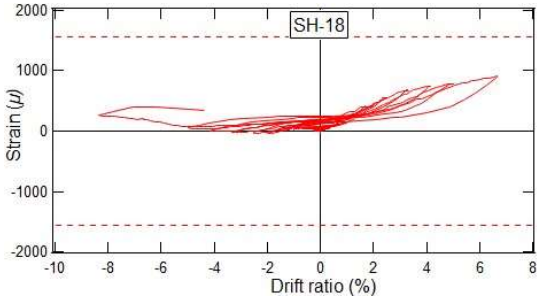
SH-18
Strain (μ)
Drift ratio (%)

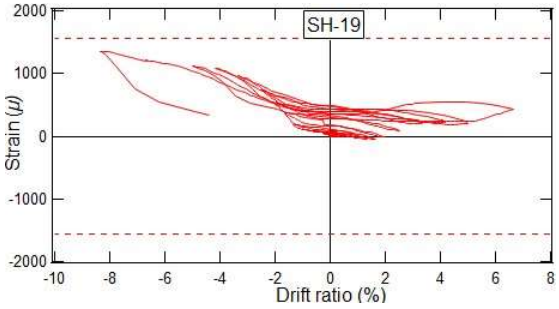
SH-19
Strain (μ)
Drift ratio (%)

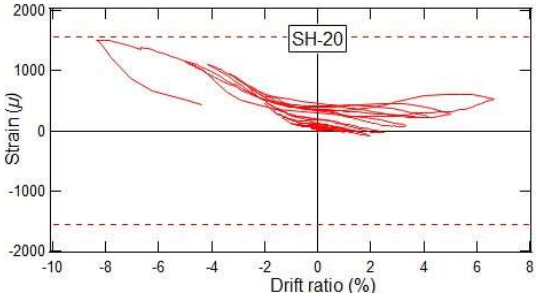
SH-20
Strain (μ)
Drift ratio (%)

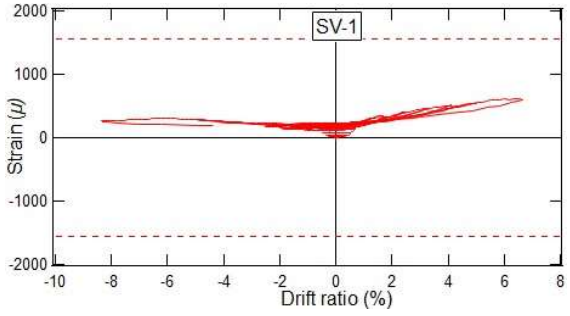
SV-1
Strain (μ)
Drift ratio (%)

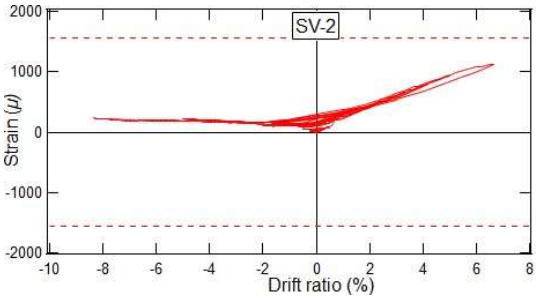
SV-2
Strain (μ)
Drift ratio (%)

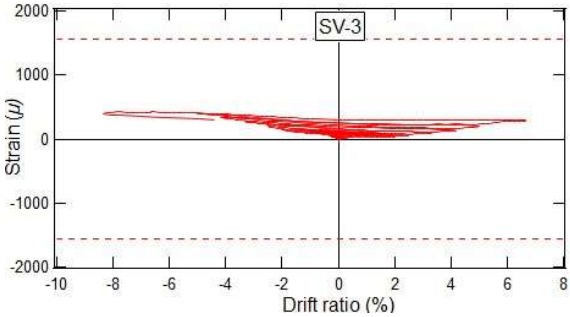
SV-3
Strain (μ)
Drift ratio (%)

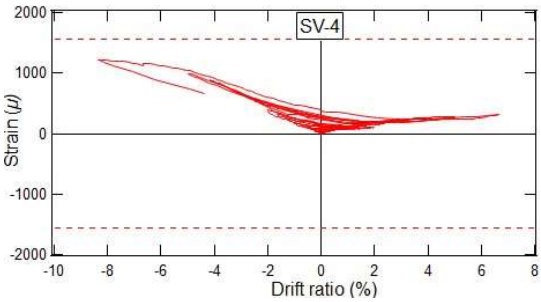
SV-4
Strain (μ)
Drift ratio (%)

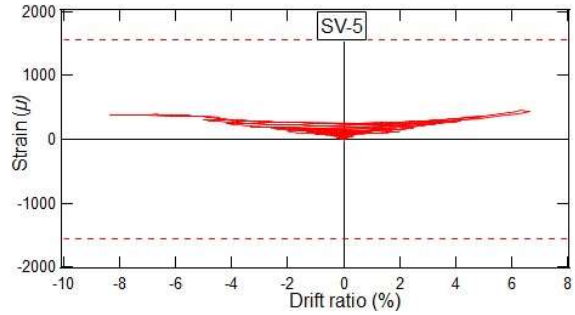
SV-5
Strain (μ)
Drift ratio (%)

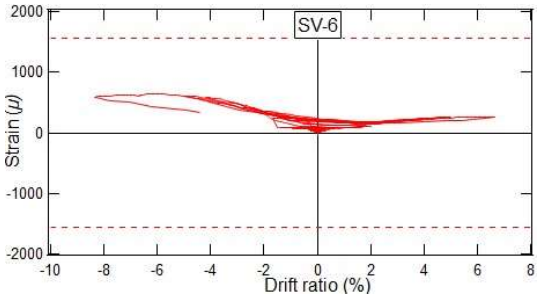
SV-6
Strain (μ)
Drift ratio (%)

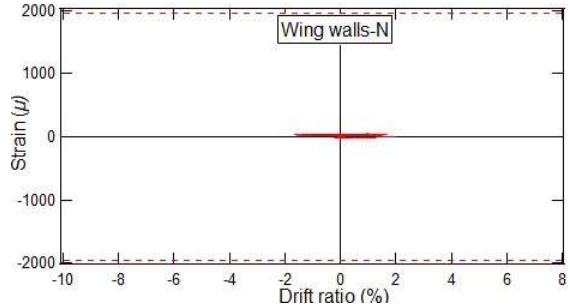
Wing walls-N
Strain (μ)
Drift ratio (%)

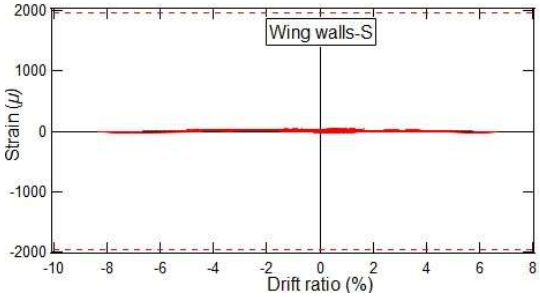
Wing walls-S
Strain (μ)
Drift ratio (%)

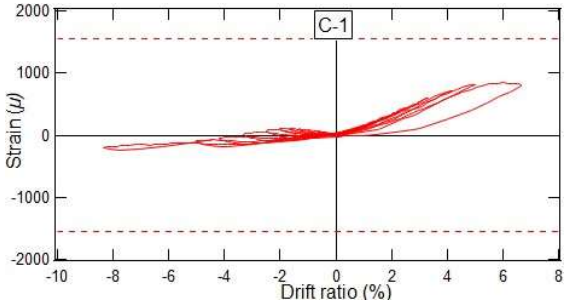
C-1
Strain (μ)
Drift ratio (%)

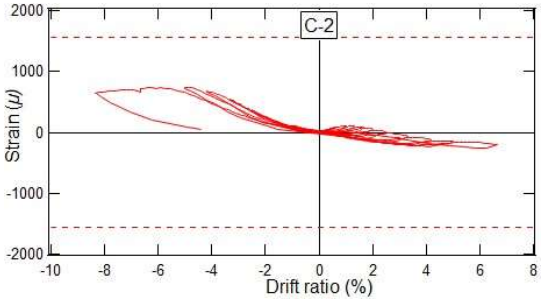
C-2
Strain (μ)
Drift ratio (%)

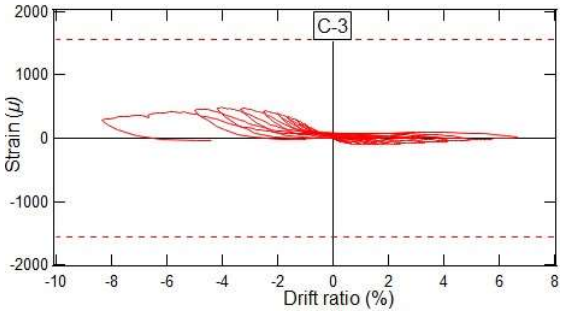
C-3
Strain (μ)
Drift ratio (%)

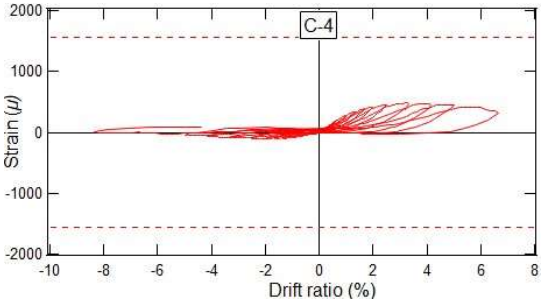
C-4
Strain (μ)
Drift ratio (%)

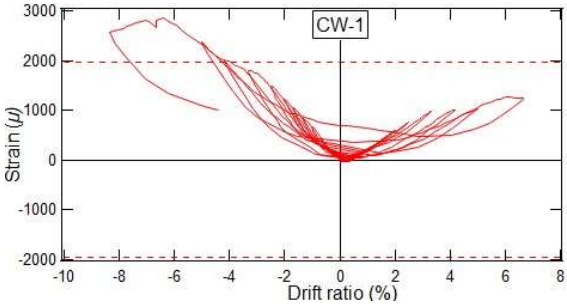
CW-1
Strain (μ)
Drift ratio (%)

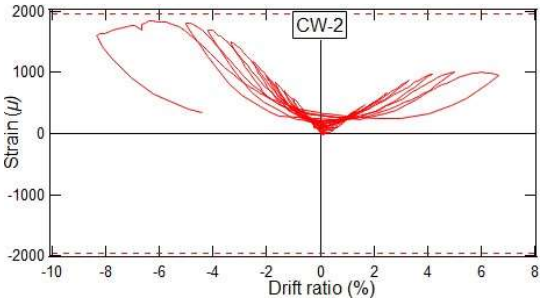
CW-2
Strain (μ)
Drift ratio (%)

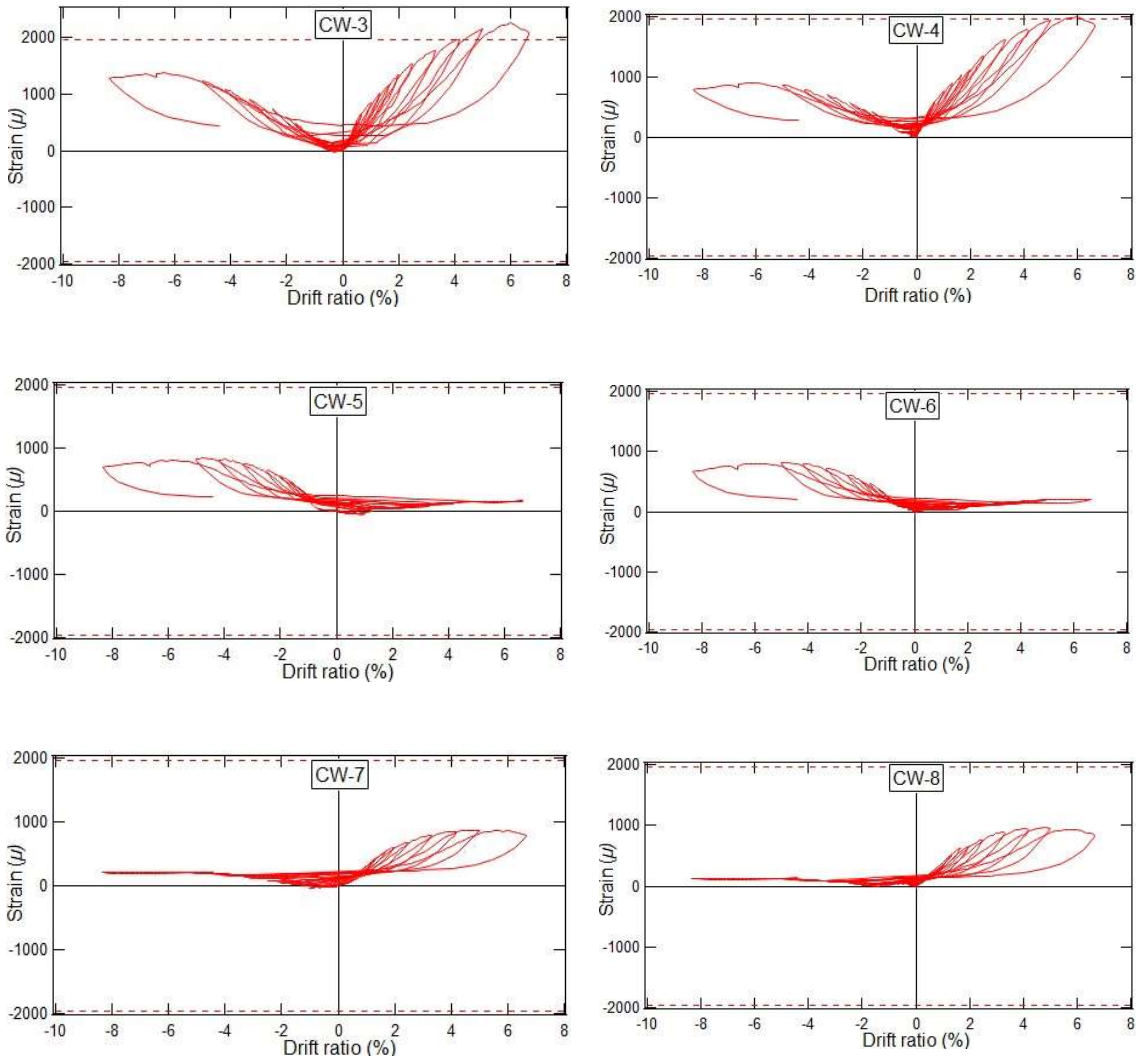

Figure A1.8 Strains of reinforcing bars for each strain gauge (specimen FP-W2)

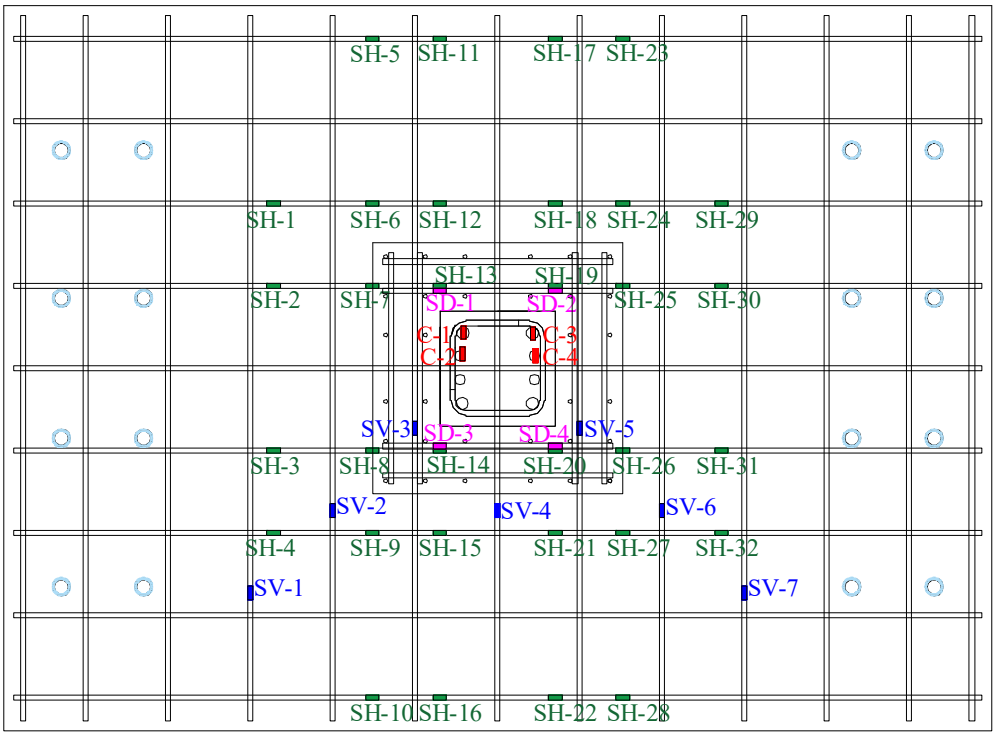

Figure A1.9 Position of strain gauges (specimen FP-D1)

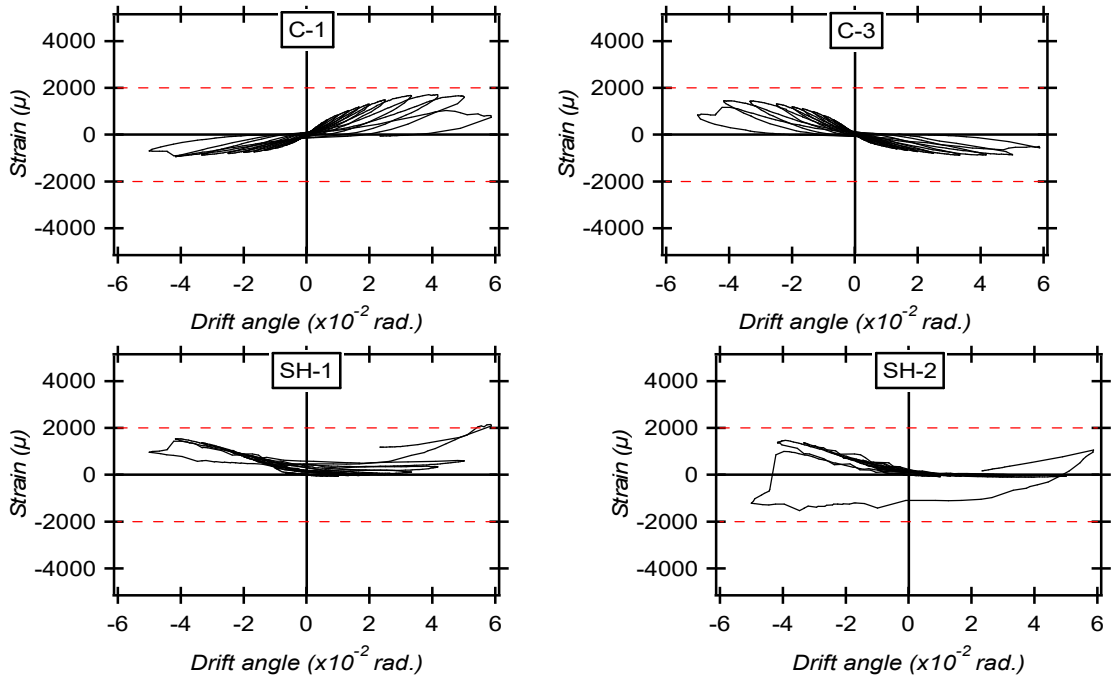

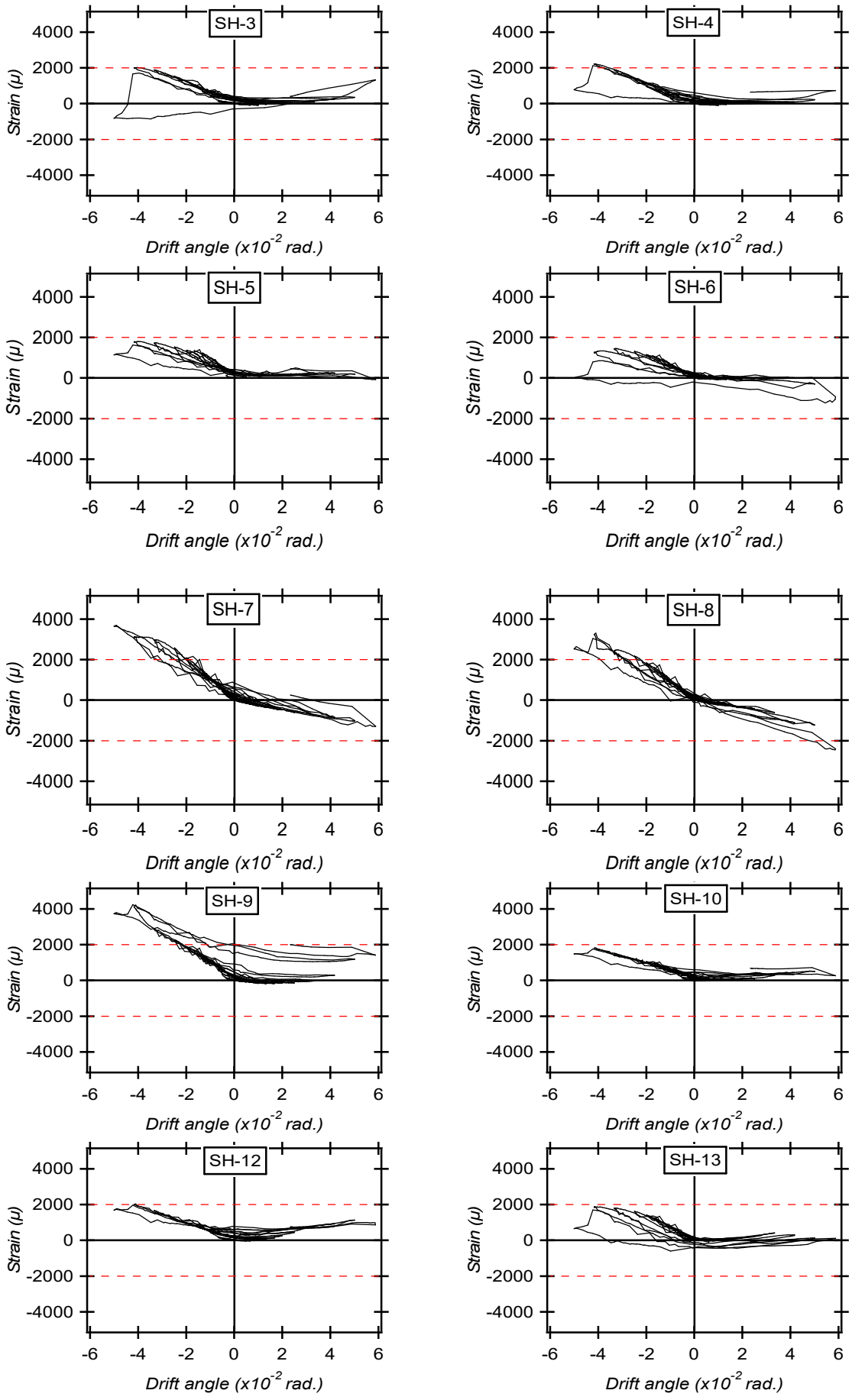
SH-3
SH-4
SH-5
SH-6
SH-7
SH-8
SH-9
SH-10
SH-12
SH-13
Strain (μ)
4000
2000
0
-2000
-4000
-6
-4
-2
0
2
4
6
Drift angle (x10-2 rad.)

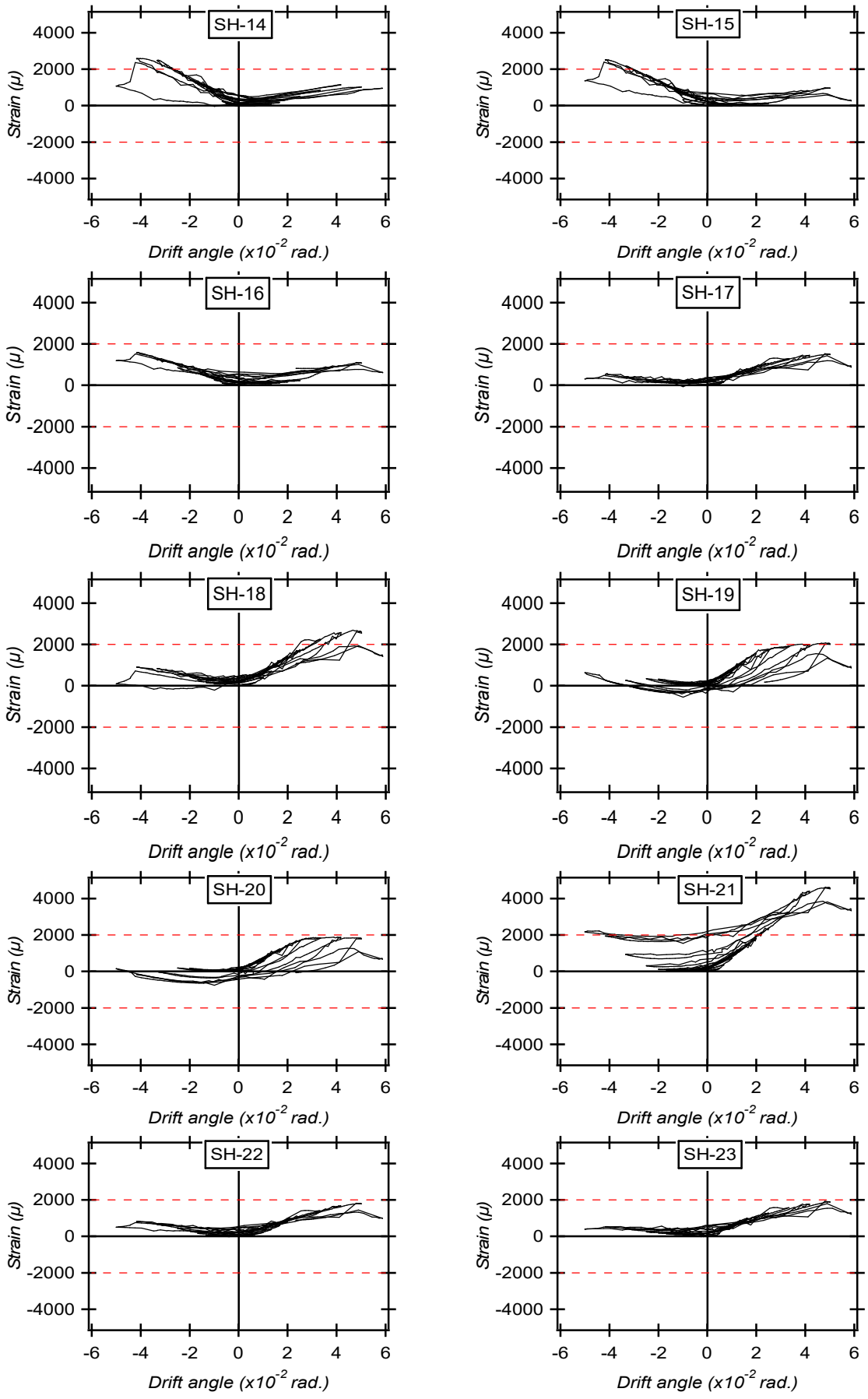
SH-14
SH-15
SH-16
SH-17
SH-18
SH-19
SH-20
SH-21
SH-22
SH-23
Strain (μ)
4000
2000
0
-2000
-4000
-6
-4
-2
0
2
4
6
Drift angle (x10-2 rad.)

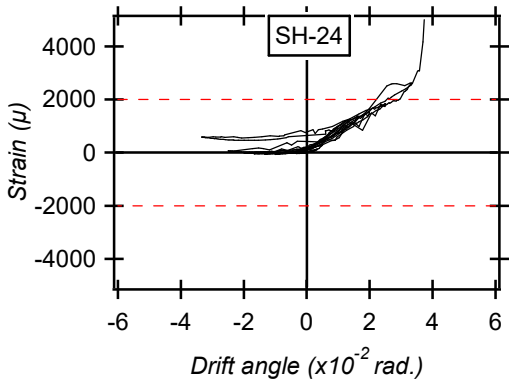
SH-24
Strain (μ)
4000
2000
0
-2000
-4000
-6 -4 -2 0 2 4 6
Drift angle (x10-2 rad.)

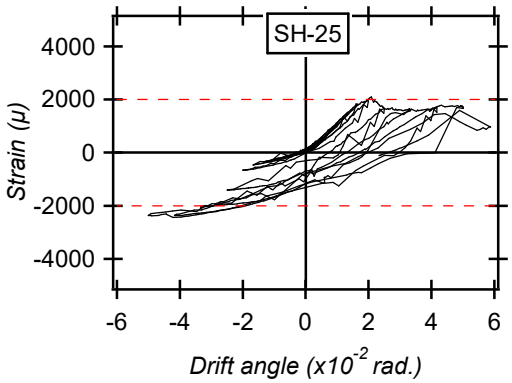
SH-25
Strain (μ)
4000
2000
0
-2000
-4000
-6 -4 -2 0 2 4 6
Drift angle (x10-2 rad.)

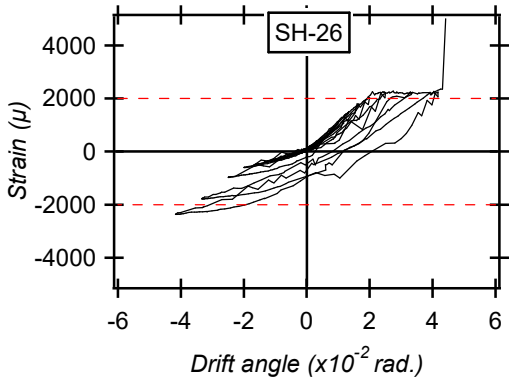
SH-26
Strain (μ)
4000
2000
0
-2000
-4000
-6 -4 -2 0 2 4 6
Drift angle (x10-2 rad.)

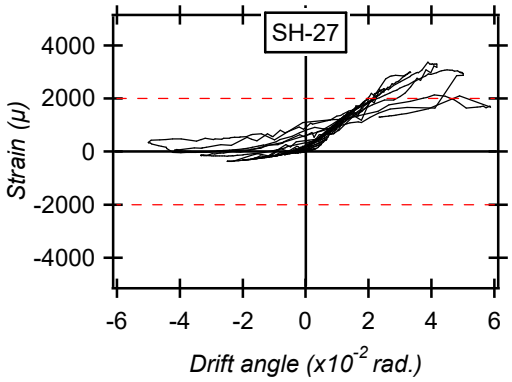
SH-27
Strain (μ)
4000
2000
0
-2000
-4000
-6 -4 -2 0 2 4 6
Drift angle (x10-2 rad.)

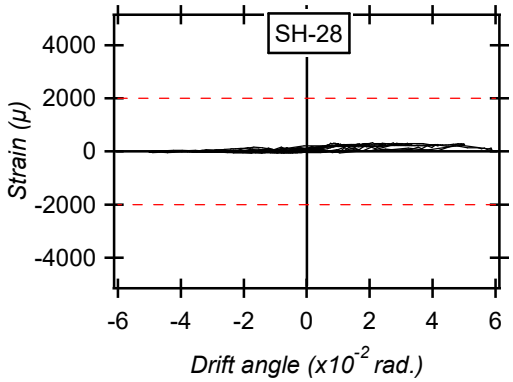
SH-28
Strain (μ)
4000
2000
0
-2000
-4000
-6 -4 -2 0 2 4 6
Drift angle (x10-2 rad.)

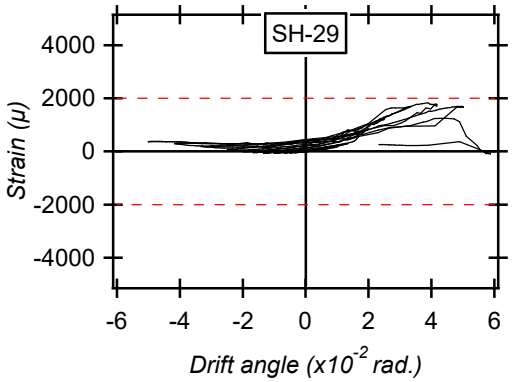
SH-29
Strain (μ)
4000
2000
0
-2000
-4000
-6 -4 -2 0 2 4 6
Drift angle (x10-2 rad.)

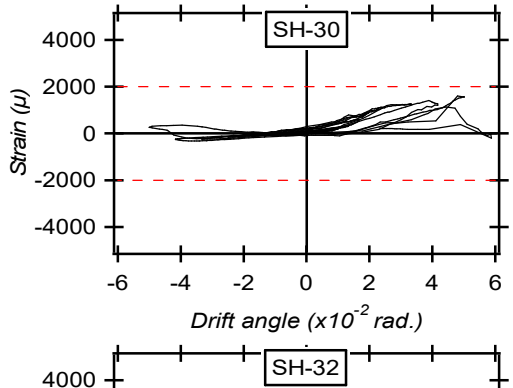
SH-30
Strain (μ)
4000
2000
0
-2000
-4000
-6 -4 -2 0 2 4 6
Drift angle (x10-2 rad.)

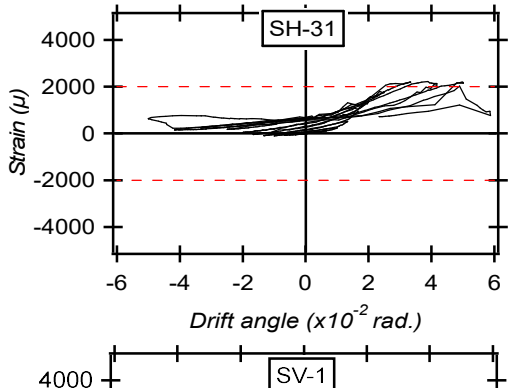
SH-31
Strain (μ)
4000
2000
0
-2000
-4000
-6 -4 -2 0 2 4 6
Drift angle (x10-2 rad.)

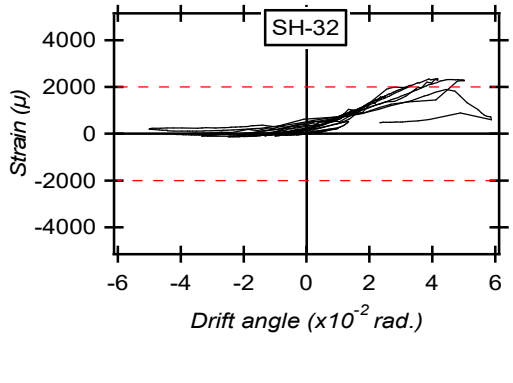
SH-32
Strain (μ)
4000
2000
0
-2000
-4000
-6 -4 -2 0 2 4 6
Drift angle (x10-2 rad.)

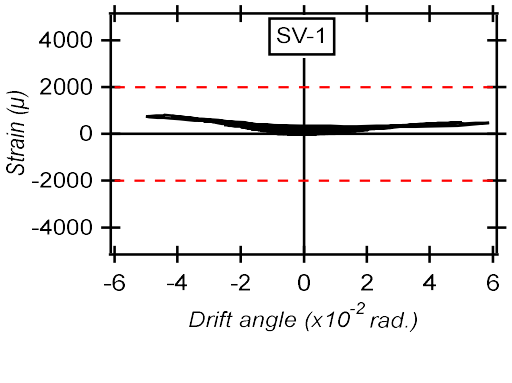
SV-1
Strain (μ)
4000
2000
0
-2000
-4000
-6 -4 -2 0 2 4 6
Drift angle (x10-2 rad.)

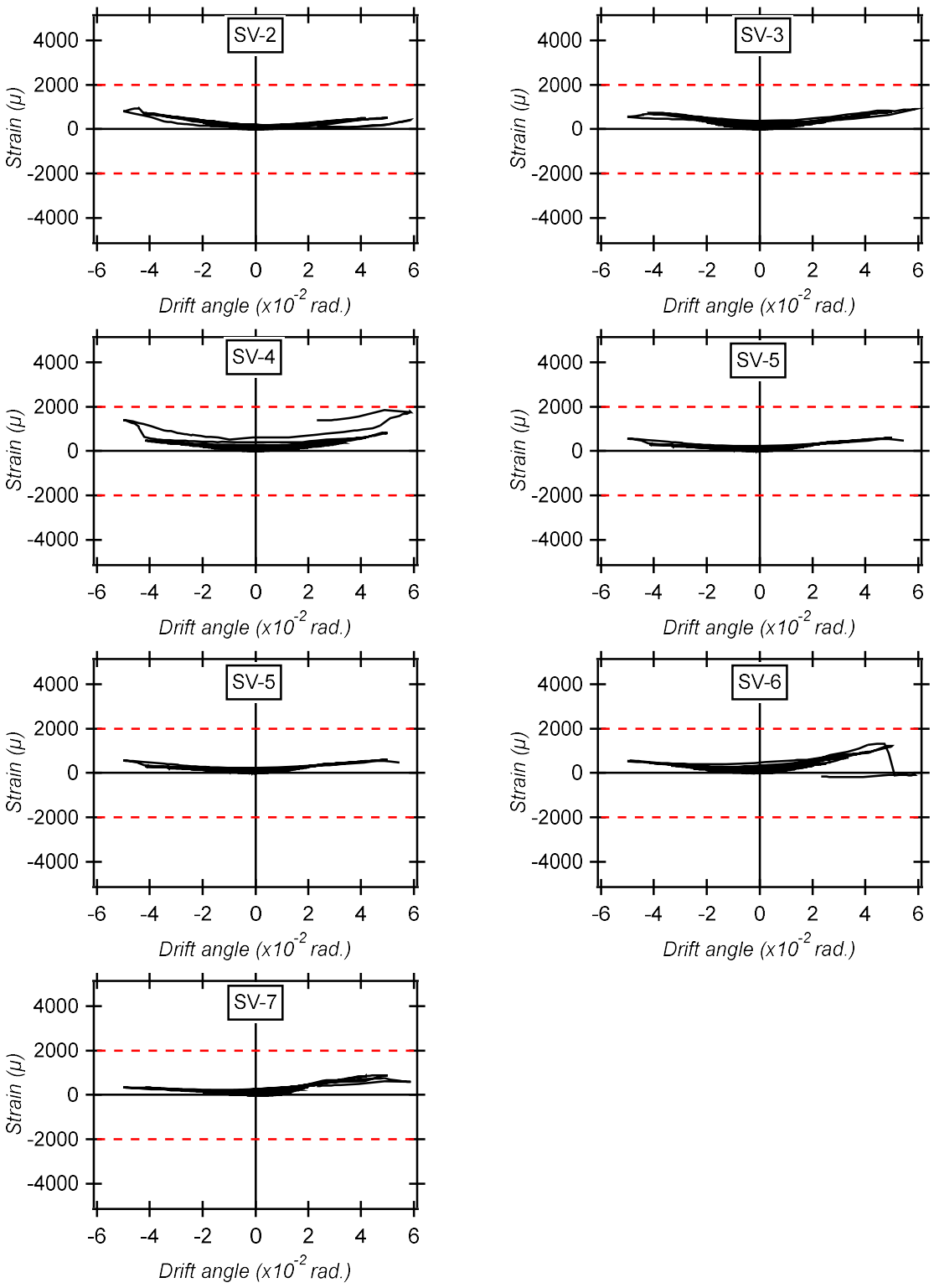

Figure A1.10 Strains of reinforcing bars for each strain gauge (specimen FP-D1)

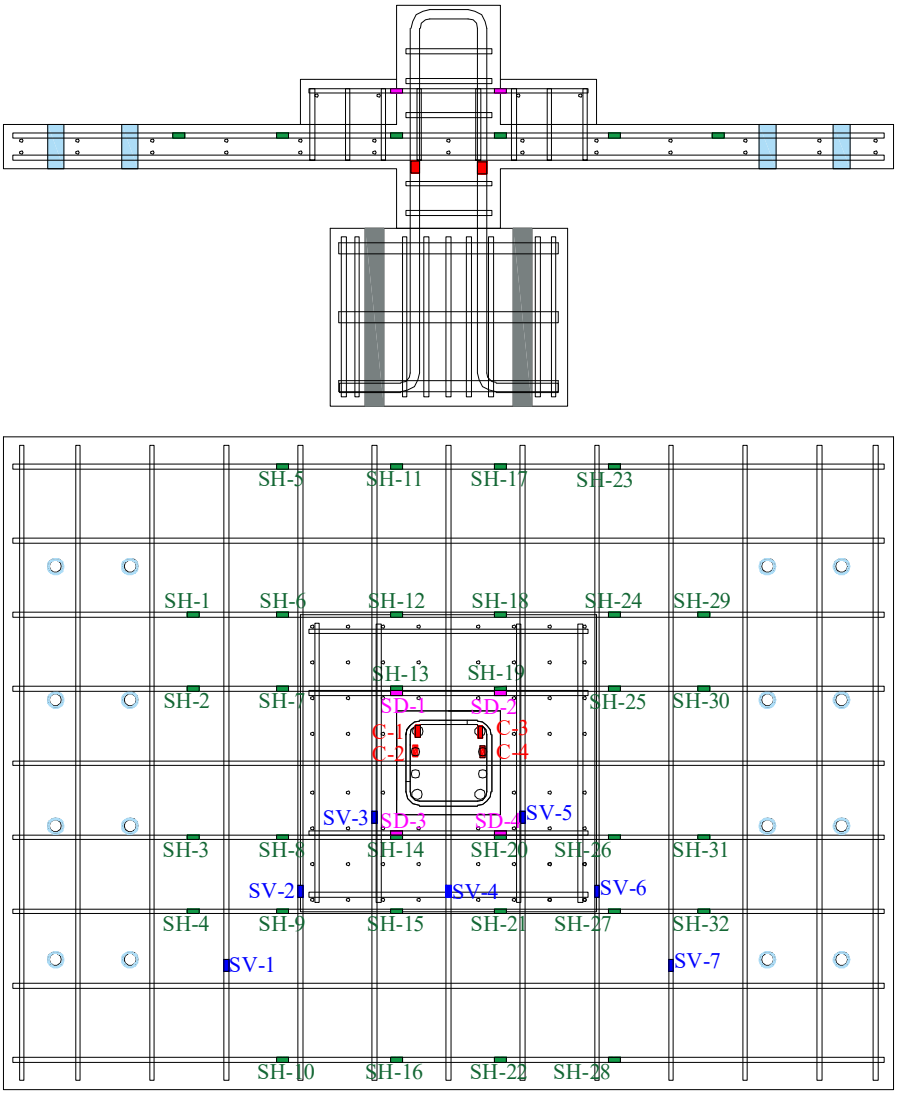

Figure A1.11 Position of strain gauges (specimen FP-D2)

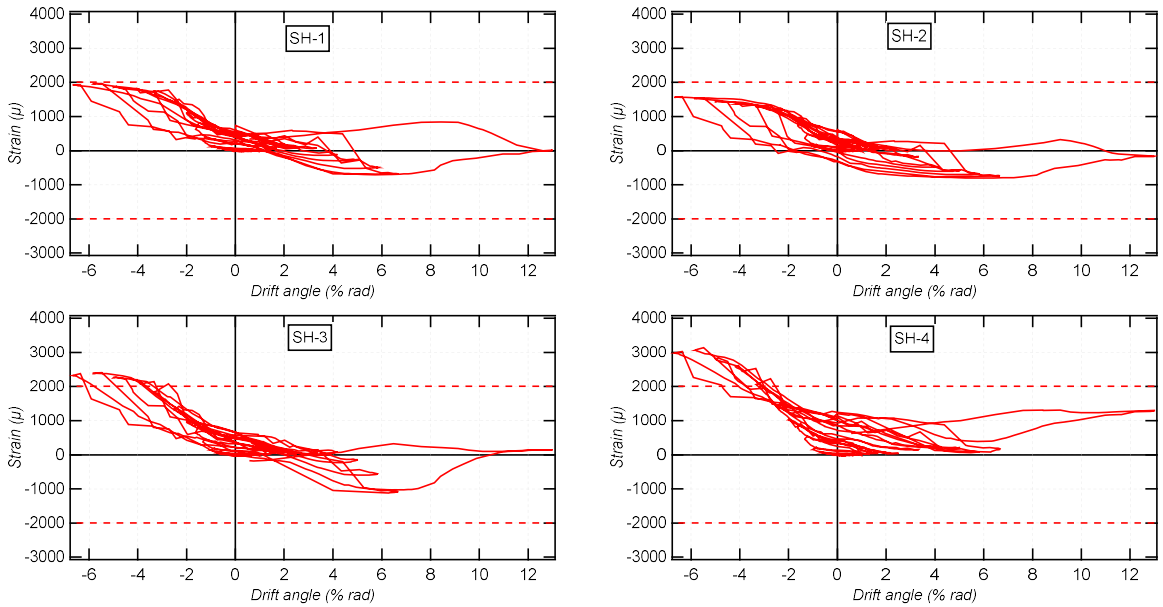

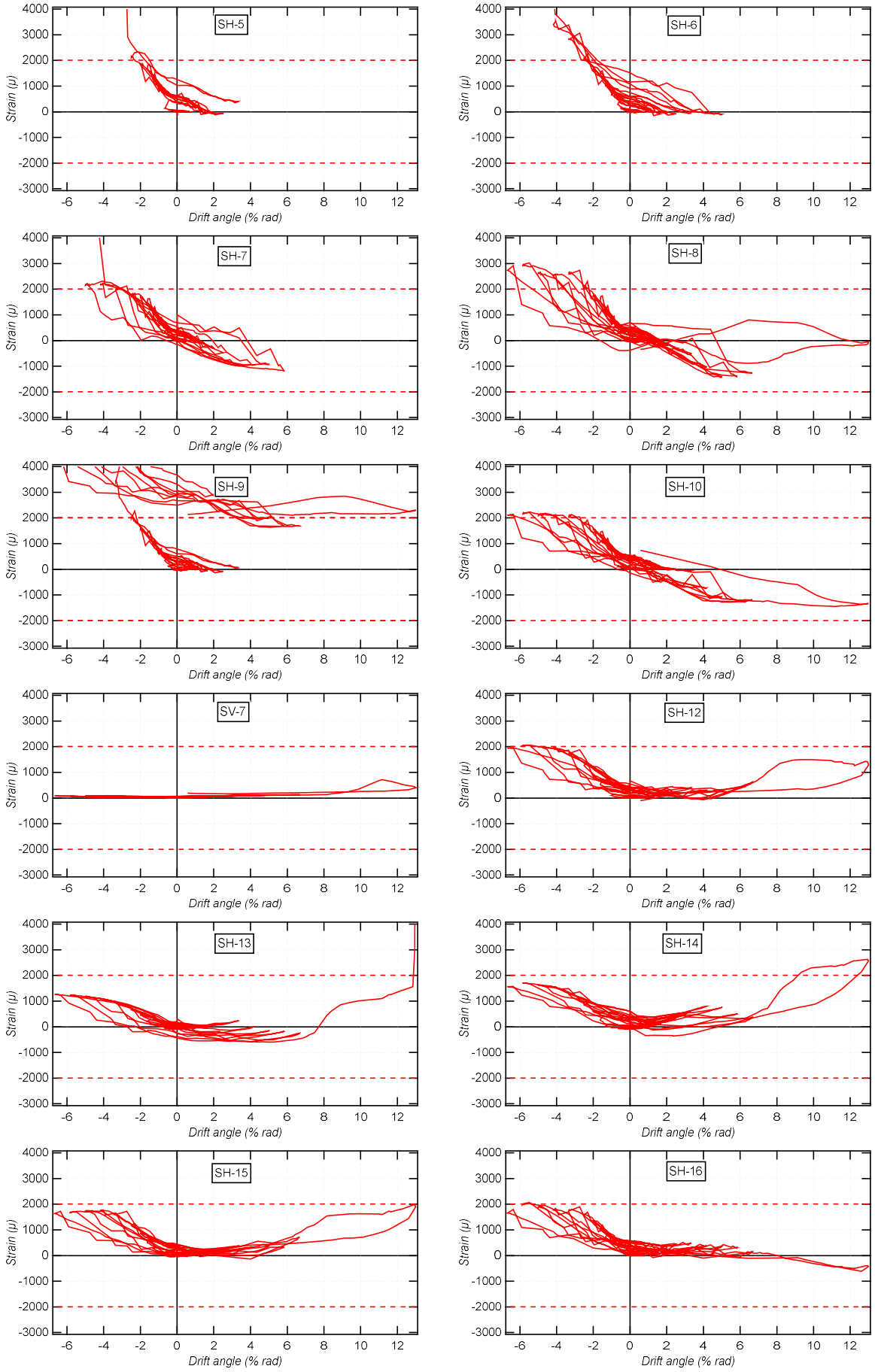
SH-5
SH-6
SH-7
SH-8
SH-9
SH-10
SV-7
SH-12
SH-13
SH-14
SH-15
SH-16
Strain (μ)
Drift angle (% rad)

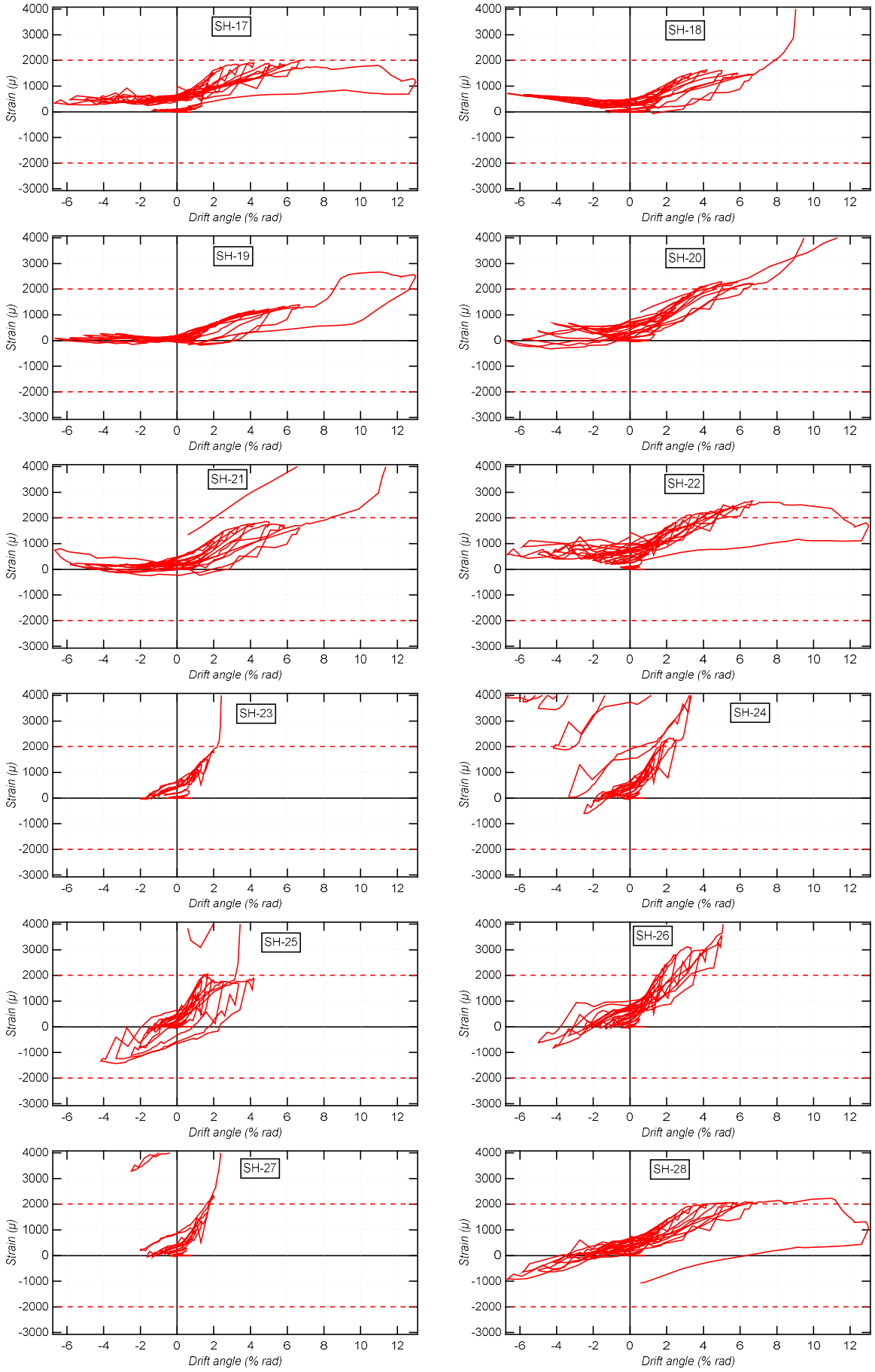
SH-17
SH-18
SH-19
SH-20
SH-21
SH-22
SH-23
SH-24
SH-25
SH-26
SH-27
SH-28
Strain (μ)
Drift angle (% rad)

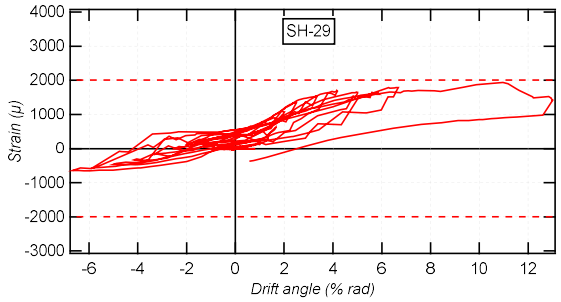
SH-29
Strain (μ)
Drift angle (% rad)

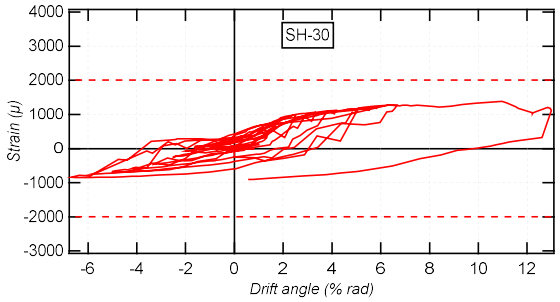
SH-30
Strain (μ)
Drift angle (% rad)

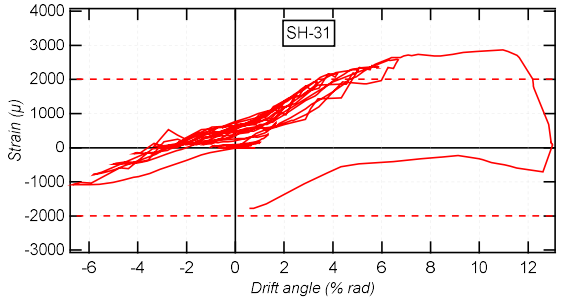
SH-31
Strain (μ)
Drift angle (% rad)

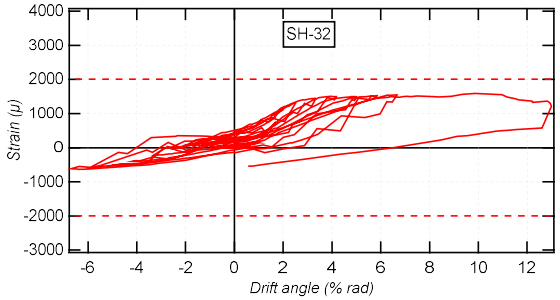
SH-32
Strain (μ)
Drift angle (% rad)

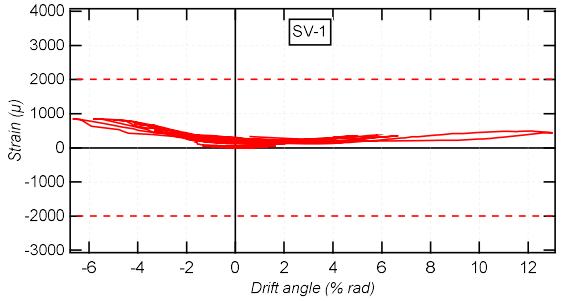
SV-1
Strain (μ)
Drift angle (% rad)

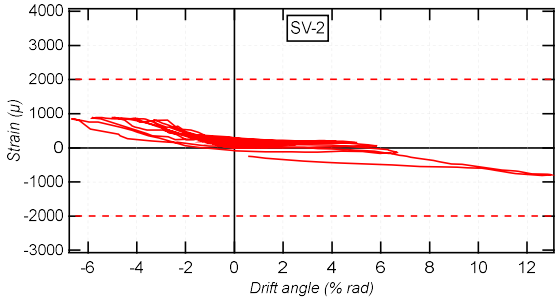
SV-2
Strain (μ)
Drift angle (% rad)

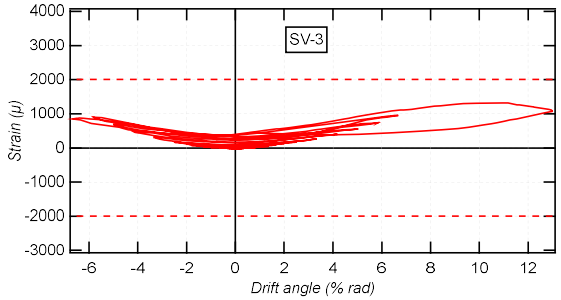
SV-3
Strain (μ)
Drift angle (% rad)

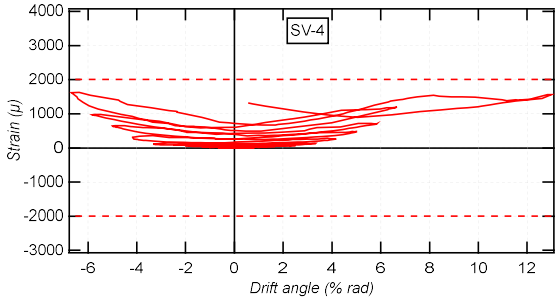
SV-4
Strain (μ)
Drift angle (% rad)

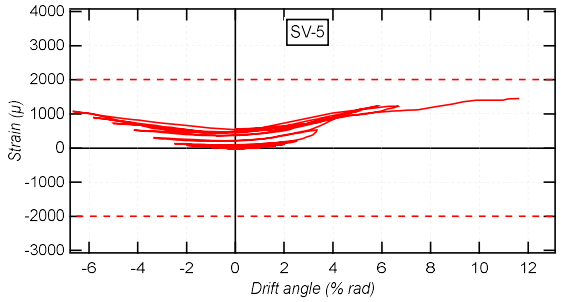
SV-5
Strain (μ)
Drift angle (% rad)

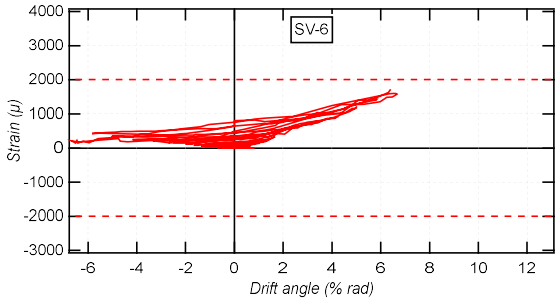
SV-6
Strain (μ)
Drift angle (% rad)

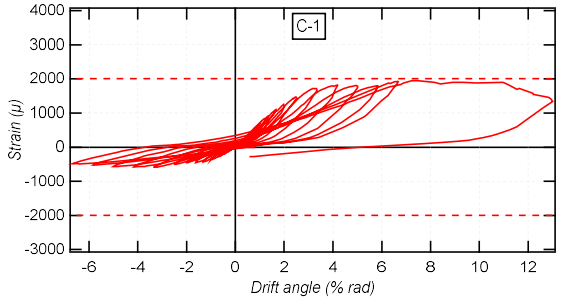
C-1
Strain (μ)
Drift angle (% rad)

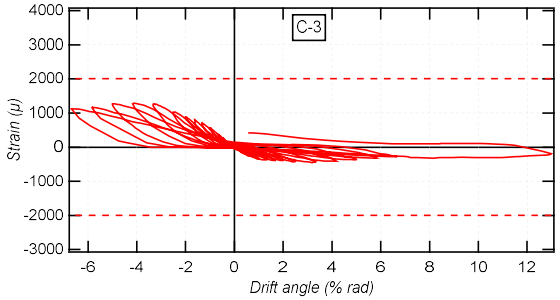
C-3
Strain (μ)
Drift angle (% rad)

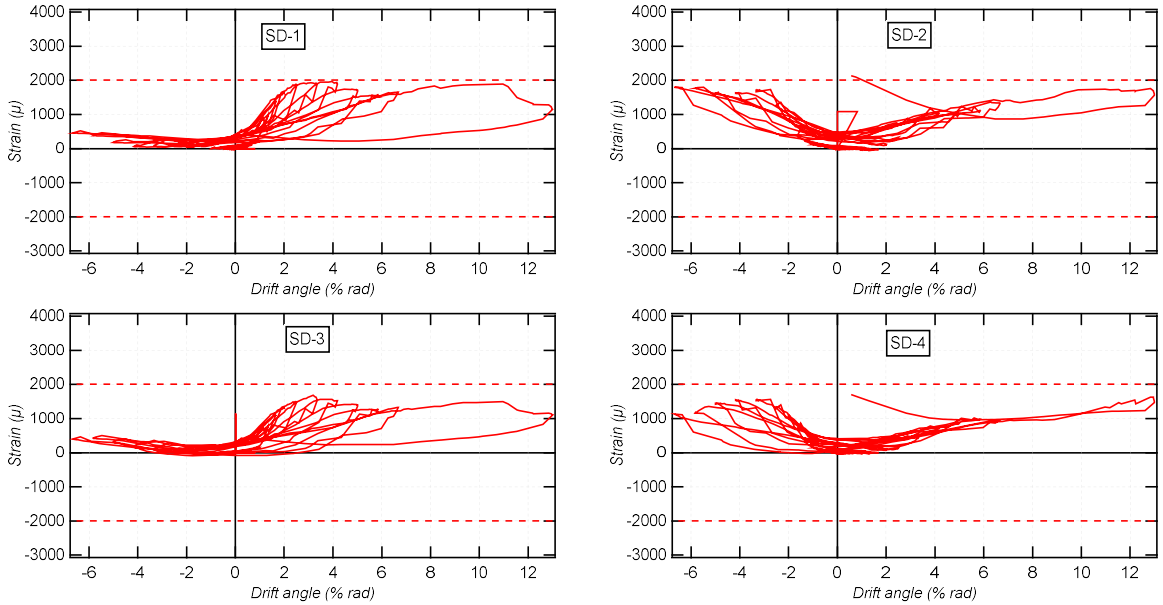

Figure A1.12 Strains of reinforcing bars for each strain gauge (specimen FP-D2)

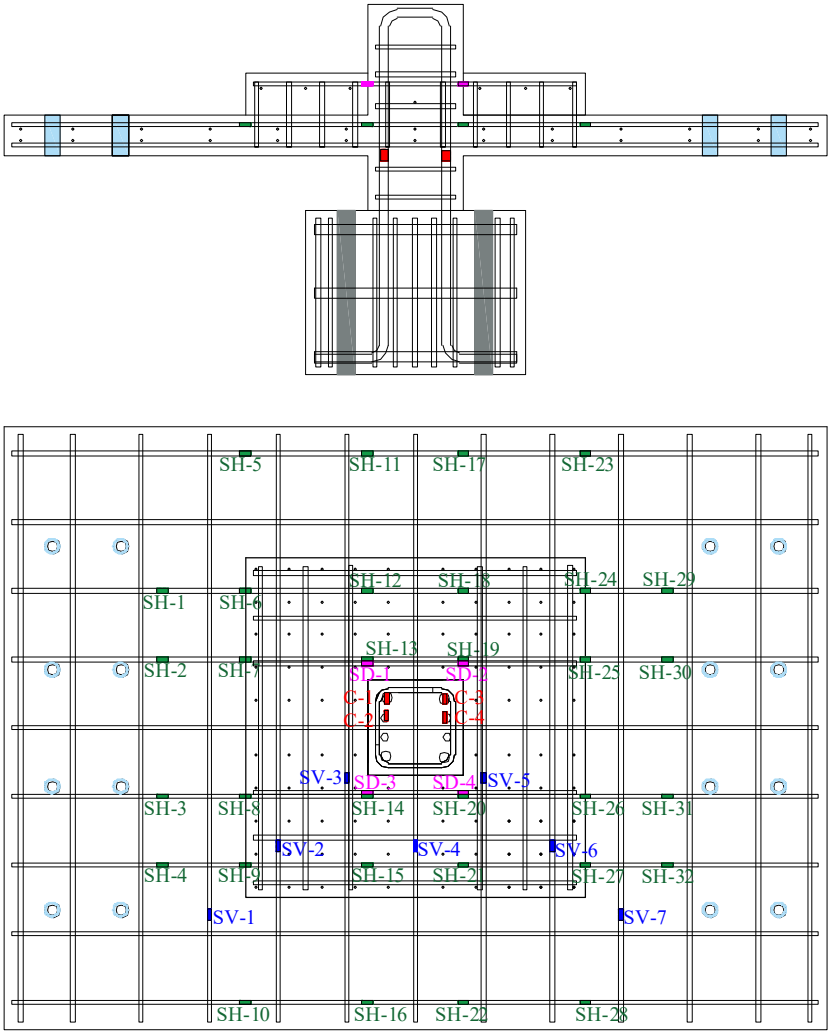

Figure A1.13 Position of strain gauges (specimen FP-D3)

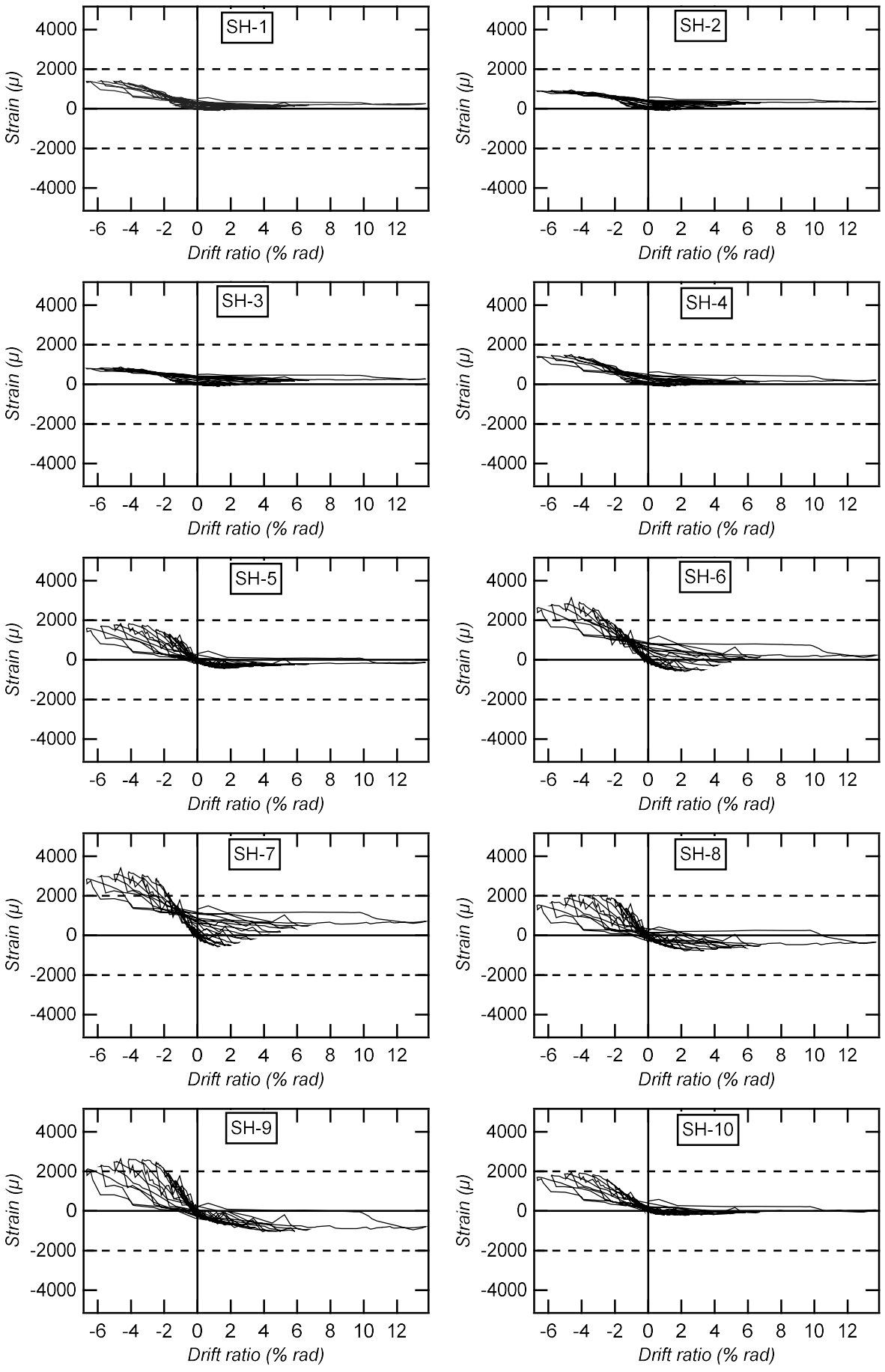
SH-1
SH-2
SH-3
SH-4
SH-5
SH-6
SH-7
SH-8
SH-9
SH-10
Strain (μ)
4000
2000
0
-2000
-4000
-6 -4 -2 0 2 4 6 8 10 12
Drift ratio (% rad)

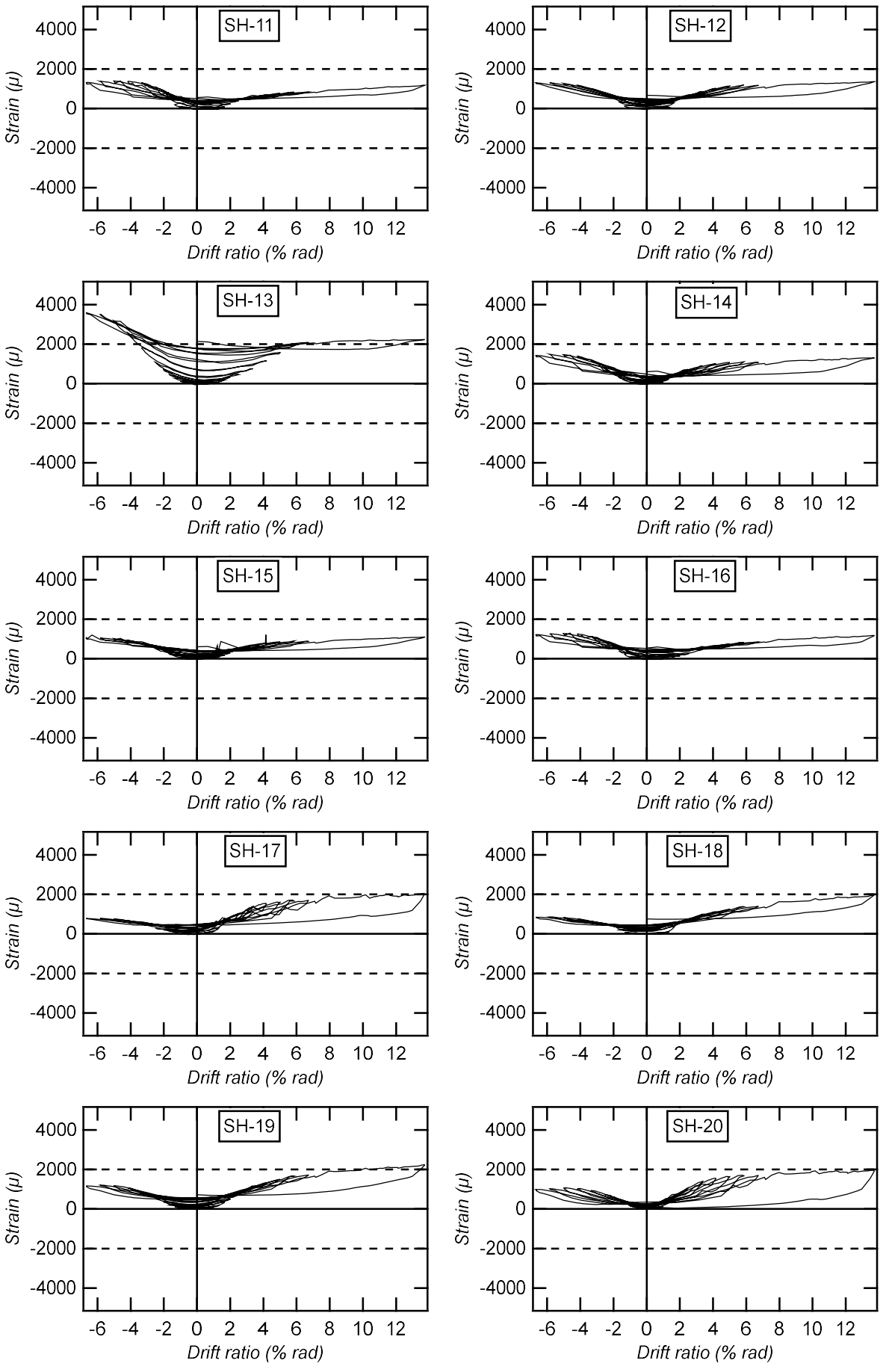
SH-11
SH-12
SH-13
SH-14
SH-15
SH-16
SH-17
SH-18
SH-19
SH-20
Strain (μ)
4000
2000
0
-2000
-4000
-6 -4 -2 0 2 4 6 8 10 12
Drift ratio (% rad)

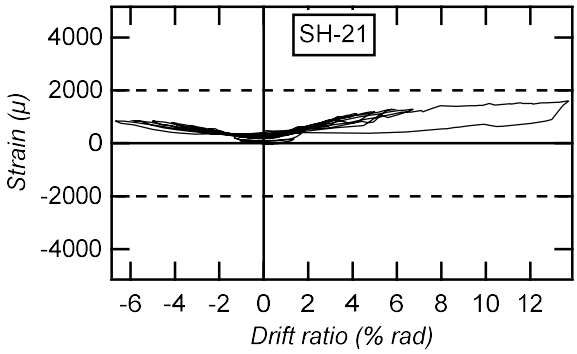
SH-21
Strain (μ)
4000
2000
0
-2000
-4000
-6 -4 -2 0 2 4 6 8 10 12
Drift ratio (% rad)

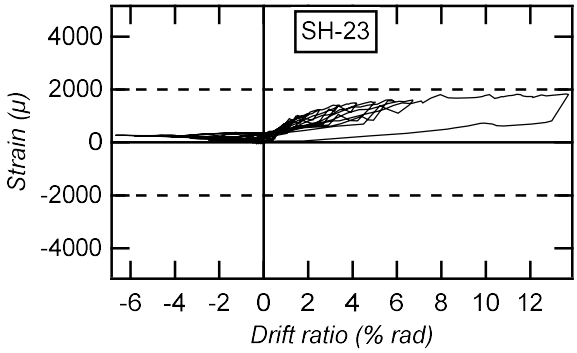
SH-23
Strain (μ)
4000
2000
0
-2000
-4000
-6 -4 -2 0 2 4 6 8 10 12
Drift ratio (% rad)

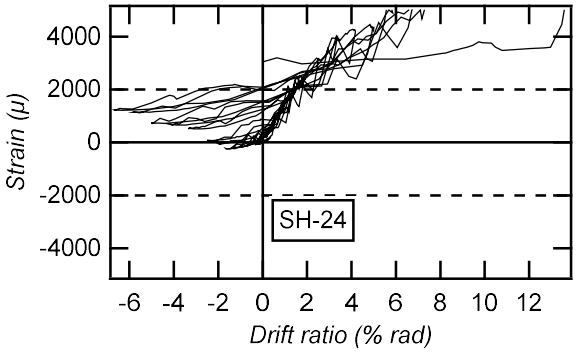
SH-24
Strain (μ)
4000
2000
0
-2000
-4000
-6 -4 -2 0 2 4 6 8 10 12
Drift ratio (% rad)

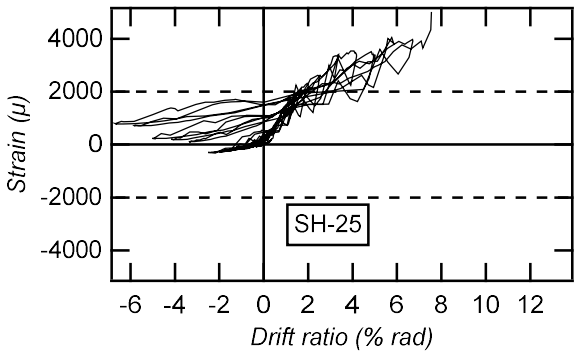
SH-25
Strain (μ)
4000
2000
0
-2000
-4000
-6 -4 -2 0 2 4 6 8 10 12
Drift ratio (% rad)

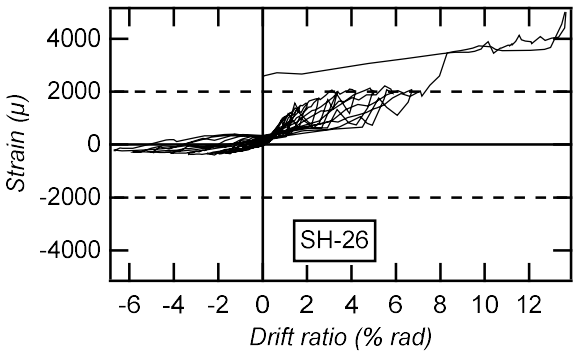
SH-26
Strain (μ)
4000
2000
0
-2000
-4000
-6 -4 -2 0 2 4 6 8 10 12
Drift ratio (% rad)

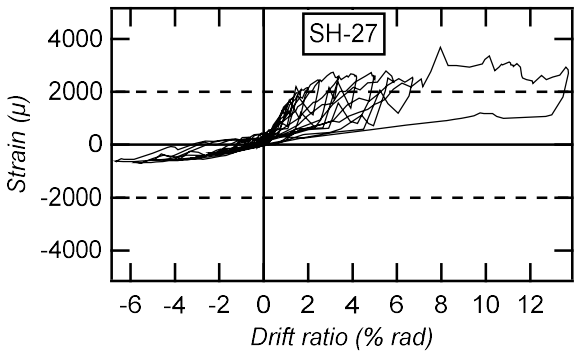
SH-27
Strain (μ)
4000
2000
0
-2000
-4000
-6 -4 -2 0 2 4 6 8 10 12
Drift ratio (% rad)

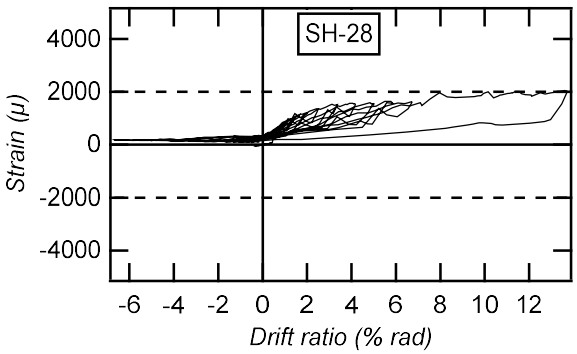
SH-28
Strain (μ)
4000
2000
0
-2000
-4000
-6 -4 -2 0 2 4 6 8 10 12
Drift ratio (% rad)

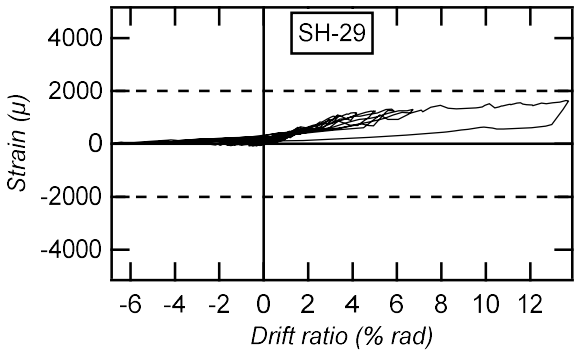
SH-29
Strain (μ)
4000
2000
0
-2000
-4000
-6 -4 -2 0 2 4 6 8 10 12
Drift ratio (% rad)

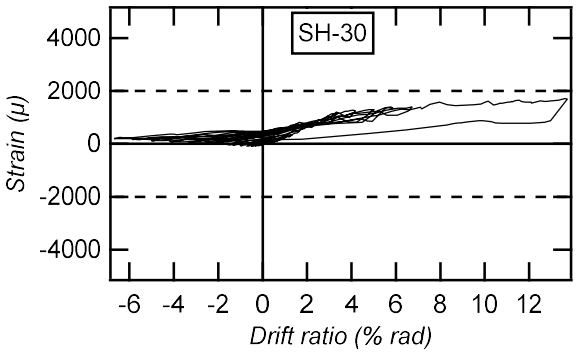
SH-30
Strain (μ)
4000
2000
0
-2000
-4000
-6 -4 -2 0 2 4 6 8 10 12
Drift ratio (% rad)

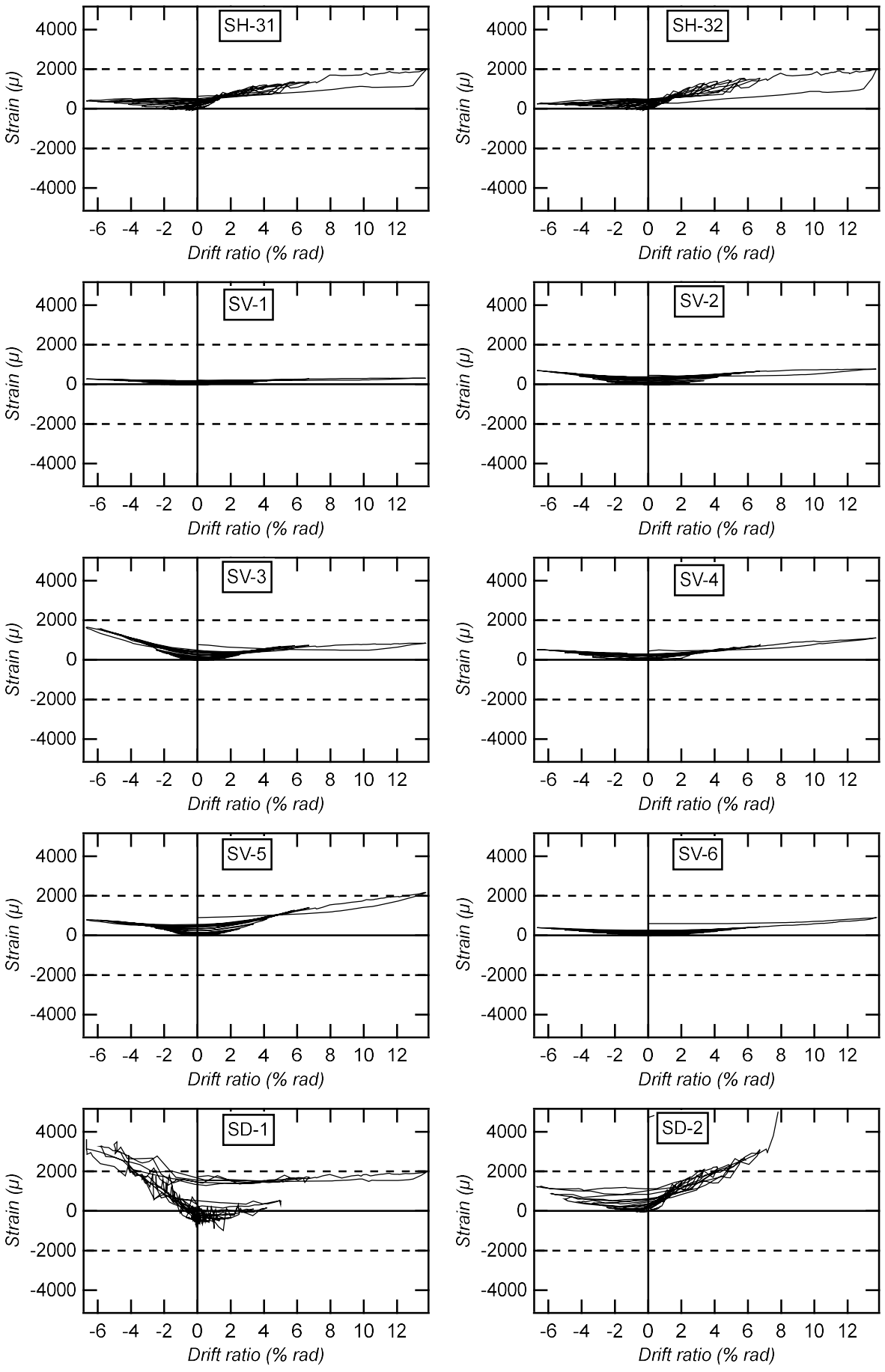
SH-31
SH-32
SV-1
SV-2
SV-3
SV-4
SV-5
SV-6
SD-1
SD-2
Strain (μ)
4000
2000
0
-2000
-4000
-6 -4 -2 0 2 4 6 8 10 12
Drift ratio (% rad)

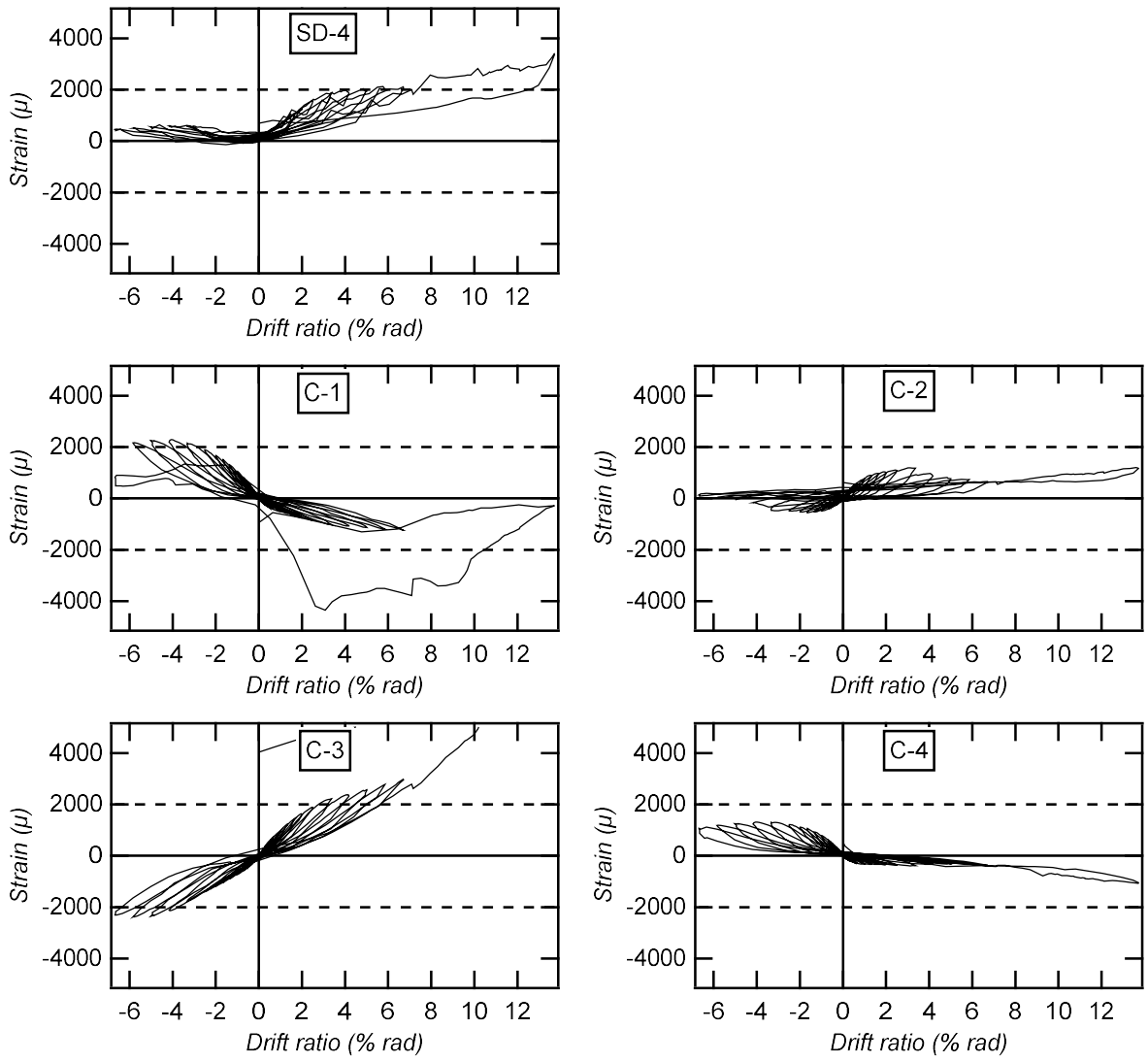

Figure A1.14 Strains of reinforcing bars for each strain gauge (specimen FP-D3)

Appendix A2

Position of displacement transducers and deflection of slab for each specimen

The appendix provides an explanation of the experimental results for the various items that are covered in Chapters 2, 3, and 4. This section contains a description of the findings of displacement of the slab.

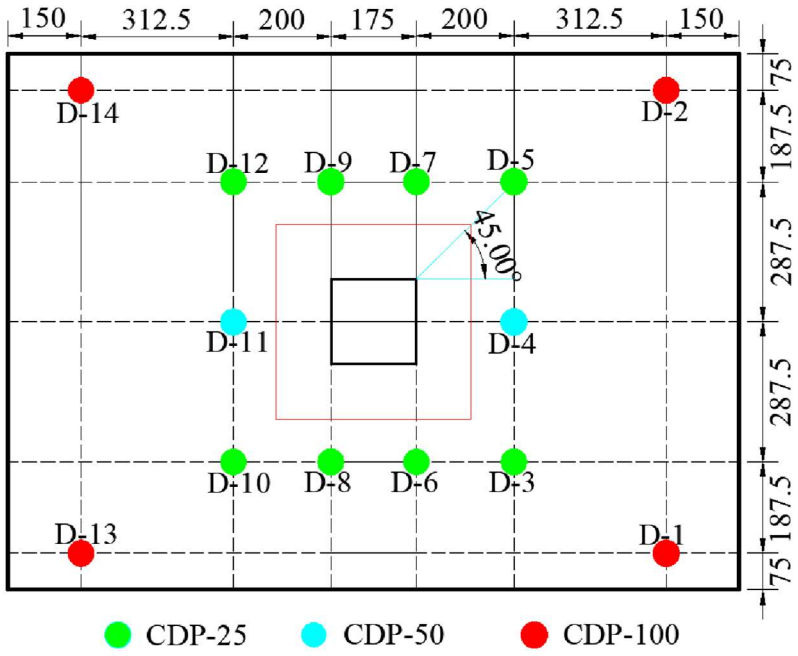

Figure A2.1 Position of displacement transducers (specimen FP-1)

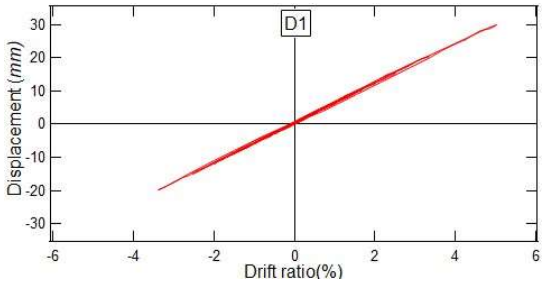

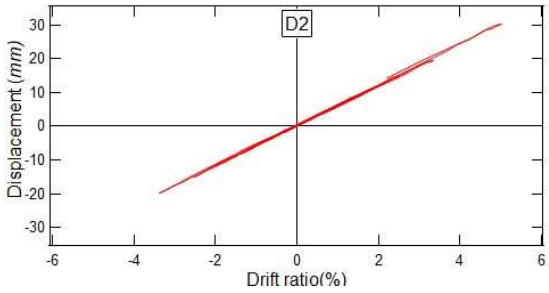

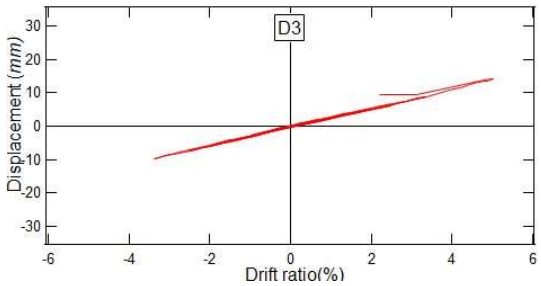
D3
Displacement (mm)
Drift ratio(%)

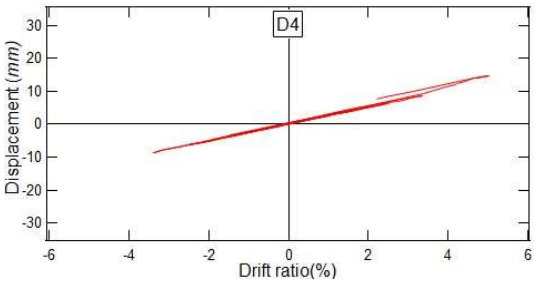
D4
Displacement (mm)
Drift ratio(%)

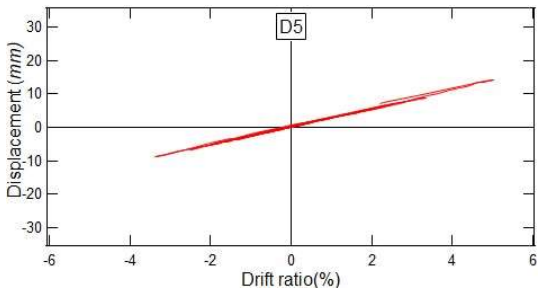
D5
Displacement (mm)
Drift ratio(%)

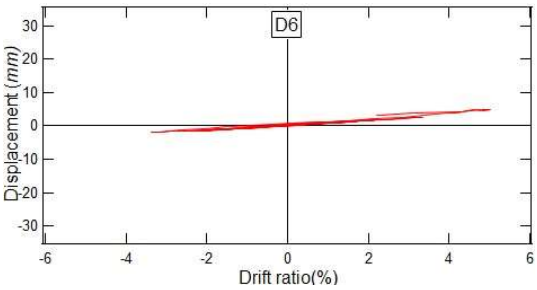
D6
Displacement (mm)
Drift ratio(%)

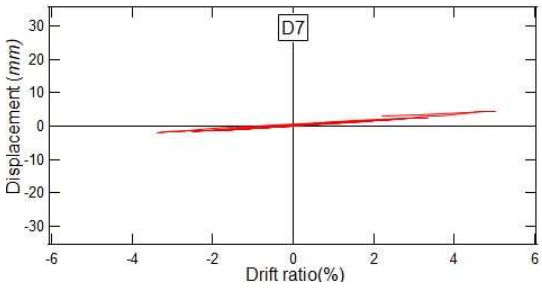
D7
Displacement (mm)
Drift ratio(%)

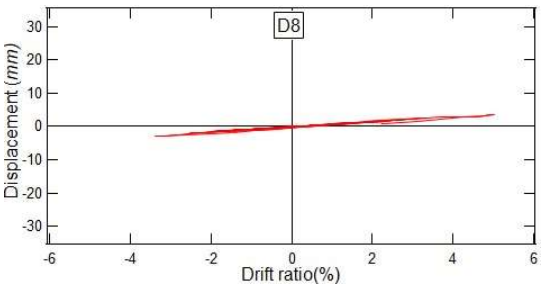
D8
Displacement (mm)
Drift ratio(%)

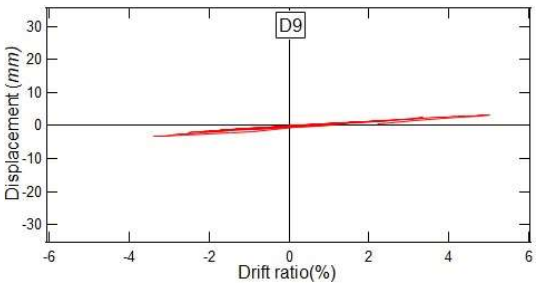
D9
Displacement (mm)
Drift ratio(%)

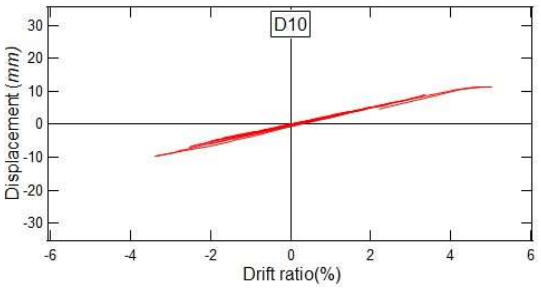
D10
Displacement (mm)
Drift ratio(%)

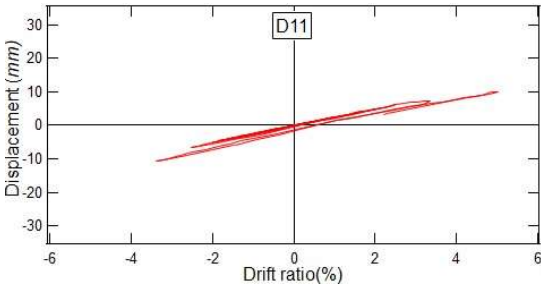
D11
Displacement (mm)
Drift ratio(%)

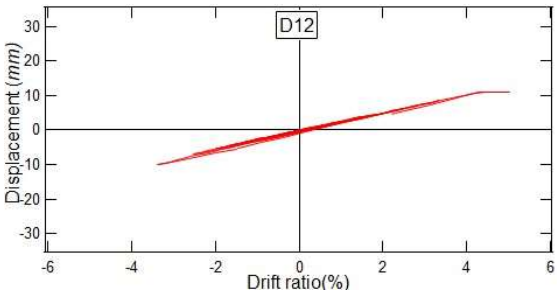
D12
Displacement (mm)
Drift ratio(%)

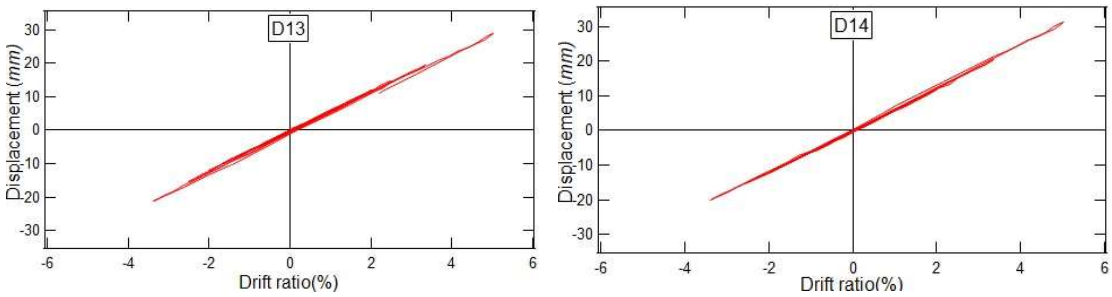

Figure A2.2 Displacement of transducers LVDT (specimen FP-1)

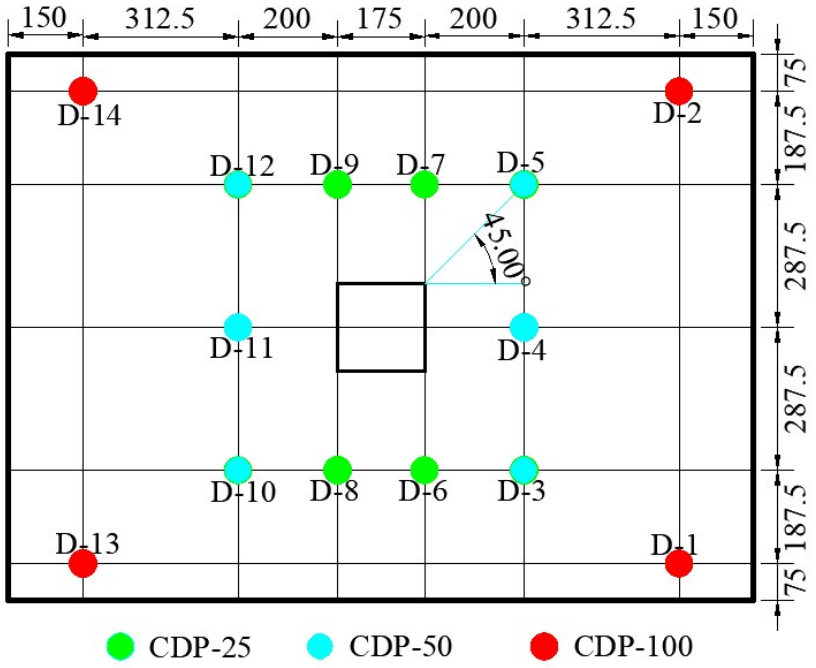

Figure A2.3 Position of displacement transducers (specimen FP-2)

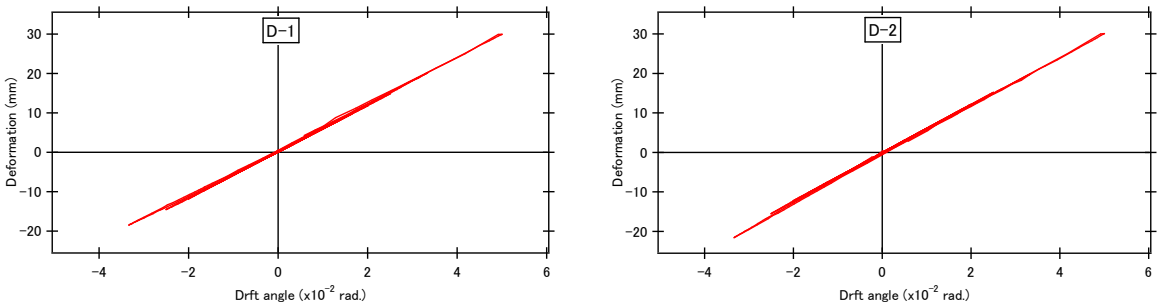

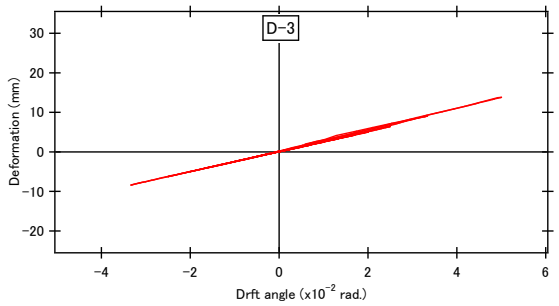
D-3
Deformation (mm)
Drft angle (x10^{-2} rad.)

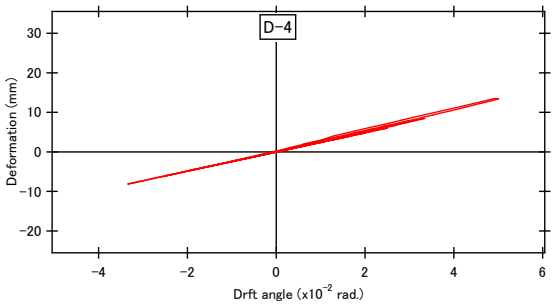
D-4
Deformation (mm)
Drft angle (x10^{-2} rad.)

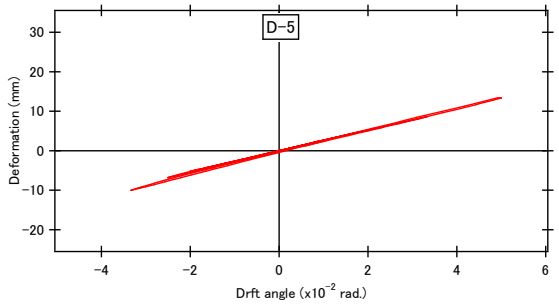
D-5
Deformation (mm)
Drft angle (x10^{-2} rad.)

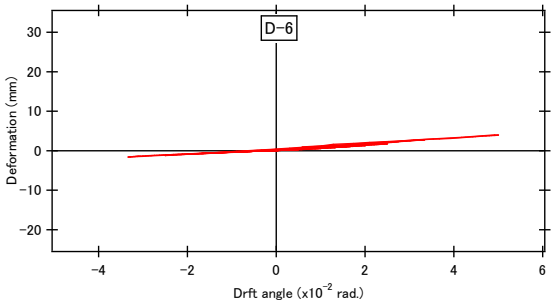
D-6
Deformation (mm)
Drft angle (x10^{-2} rad.)

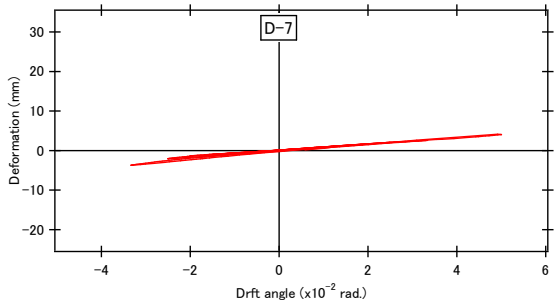
D-7
Deformation (mm)
Drft angle (x10^{-2} rad.)

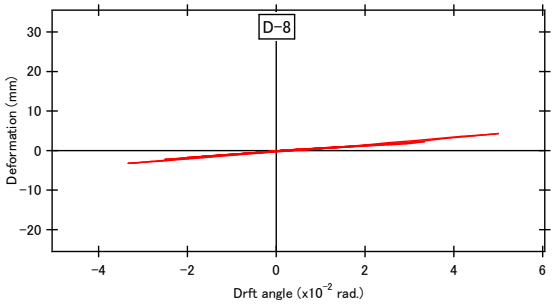
D-8
Deformation (mm)
Drft angle (x10^{-2} rad.)

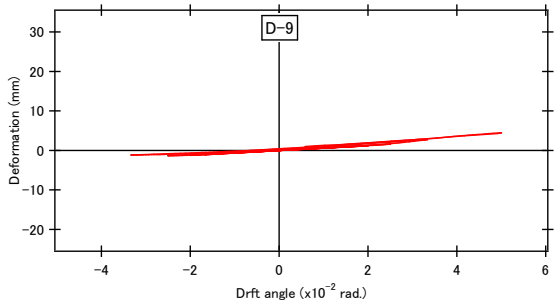
D-9
Deformation (mm)
Drft angle (x10^{-2} rad.)

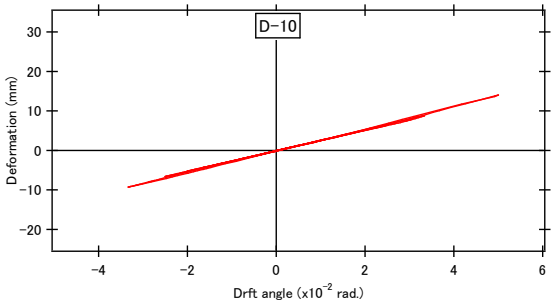
D-10
Deformation (mm)
Drft angle (x10^{-2} rad.)

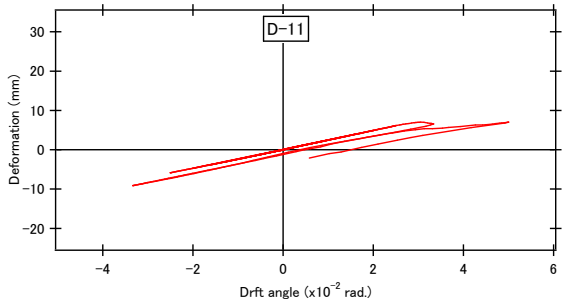
D-11
Deformation (mm)
Drft angle (x10^{-2} rad.)

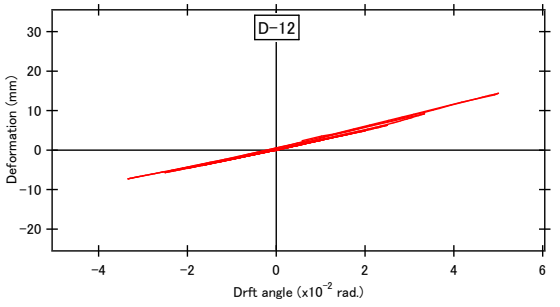
D-12
Deformation (mm)
Drft angle (x10^{-2} rad.)

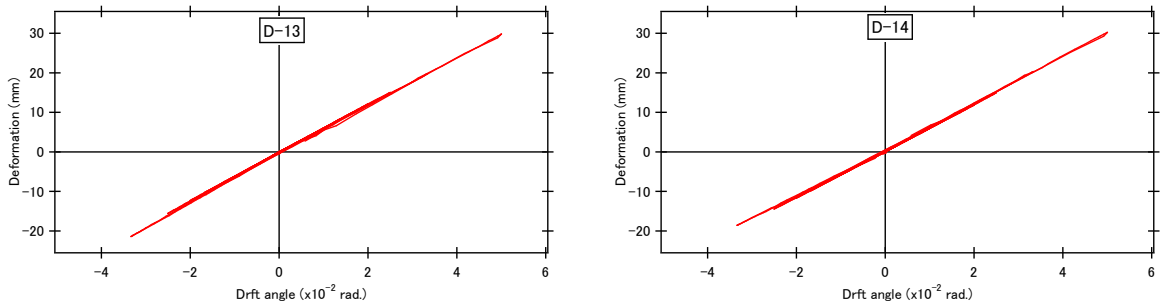

Figure A2.2 Displacement of transducers LVDT (specimen FP-2)

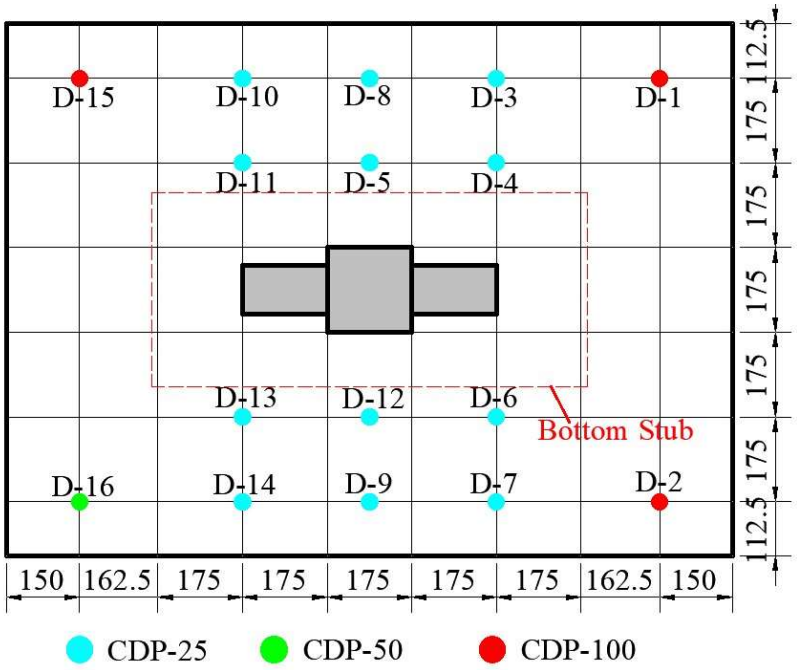

Figure A2.5 Position of displacement transducers (specimen FP-W1)

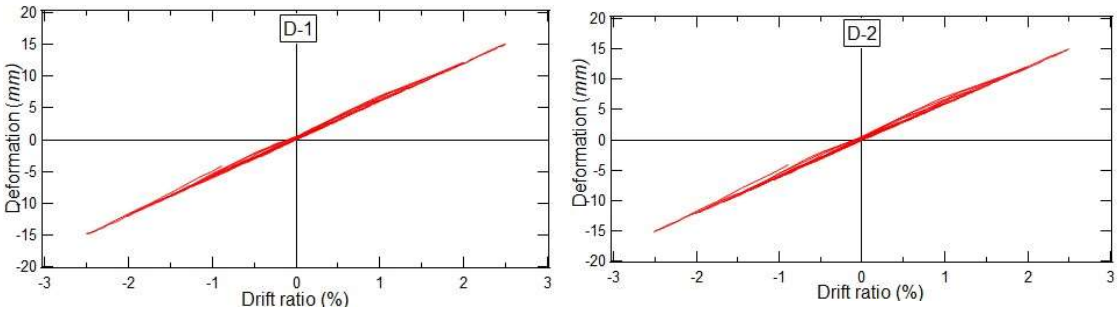

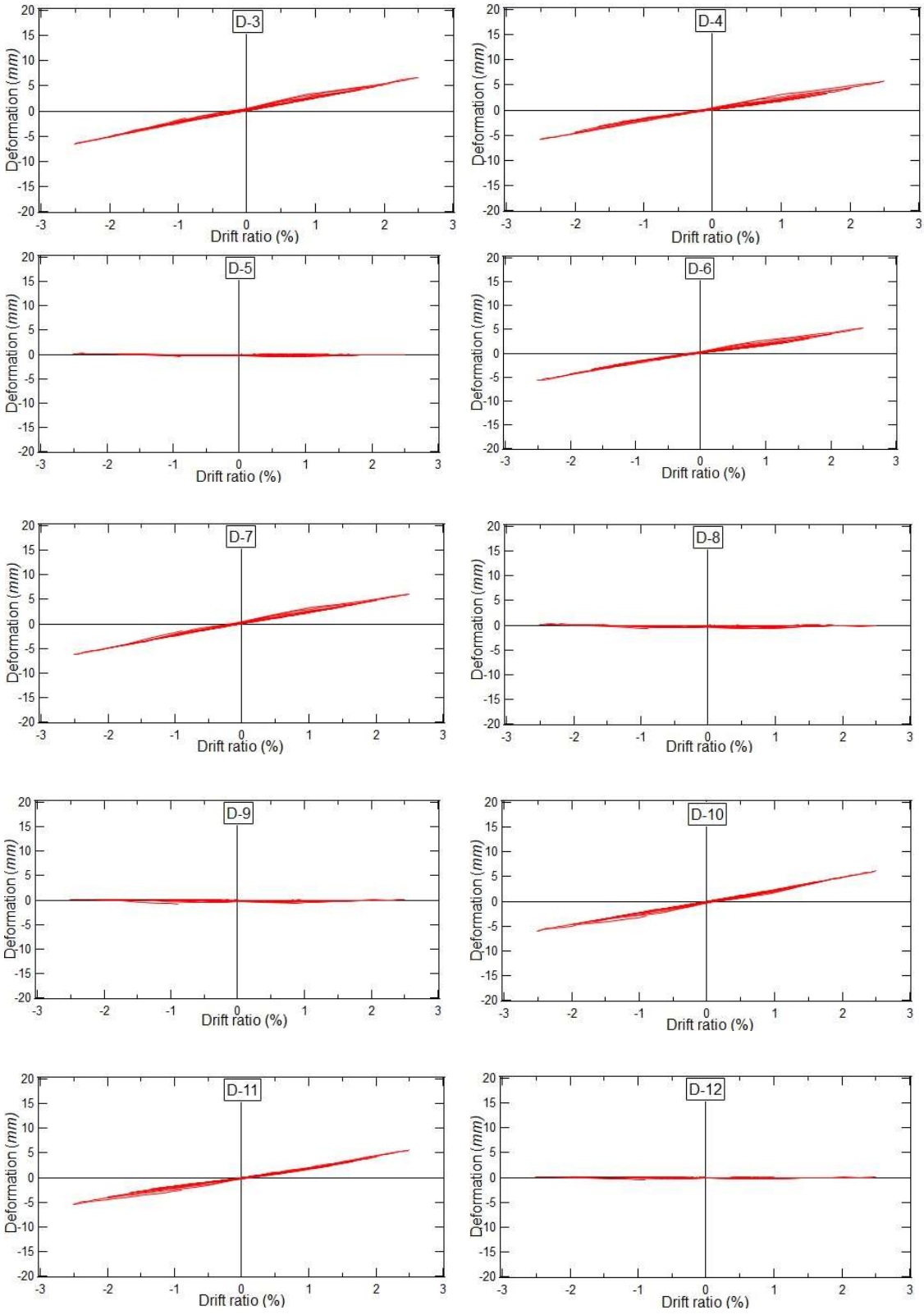
D-3
D-4
D-5
D-6
D-7
D-8
D-9
D-10
D-11
D-12
Deformation (mm)
Drift ratio (%)

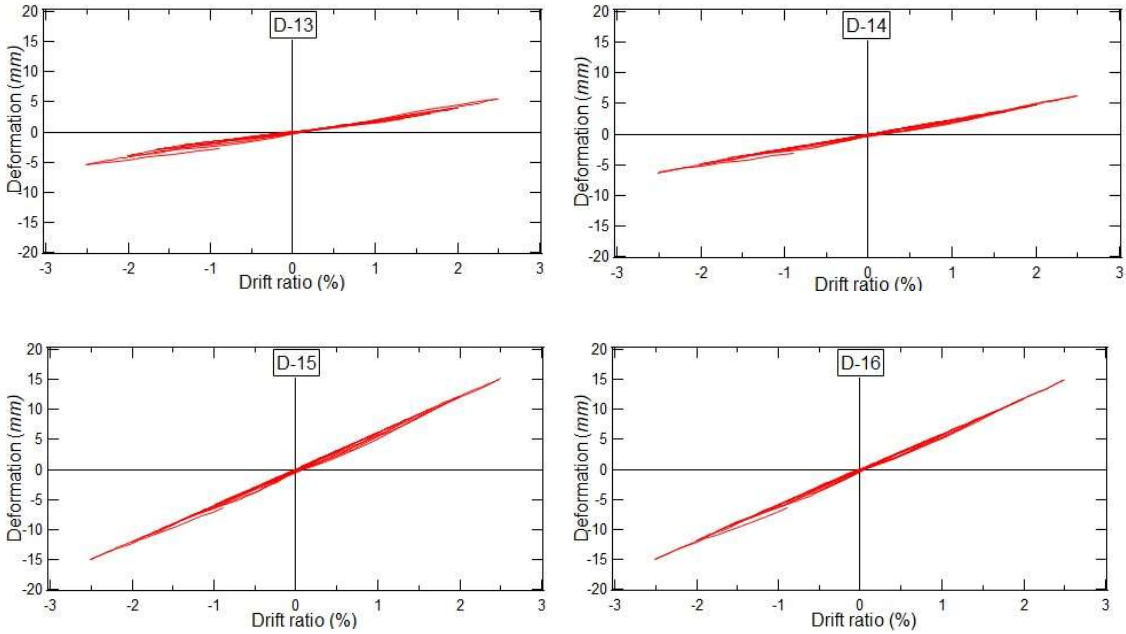

Figure A2.6 Displacement of transducers LVDT (specimen FP-W1)

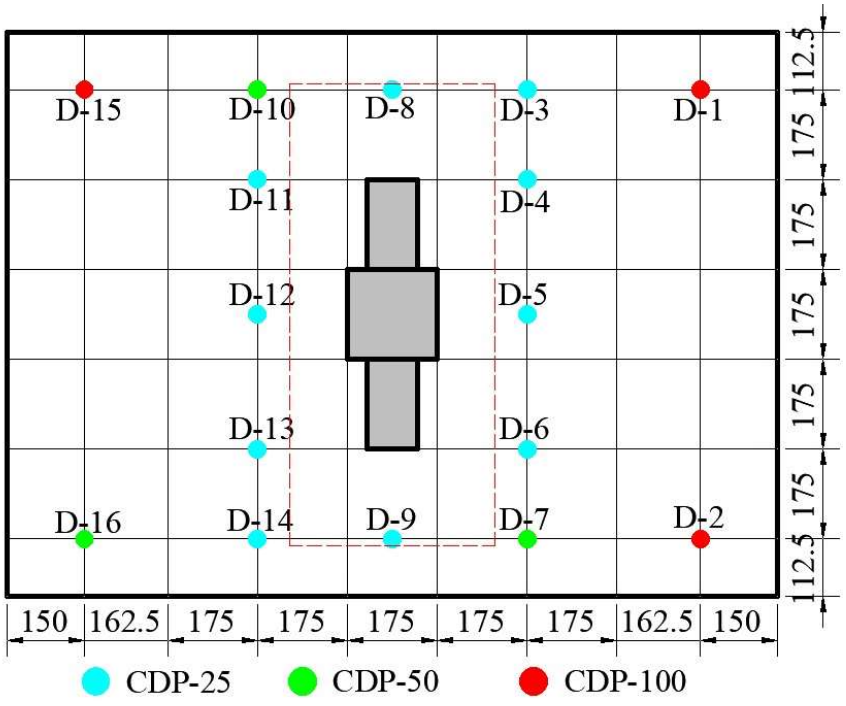

Figure A2.7 Position of displacement transducers (specimen FP-W2)

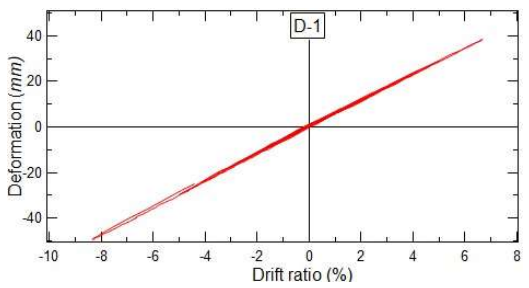
D-1
Deformation (mm)
Drift ratio (%)

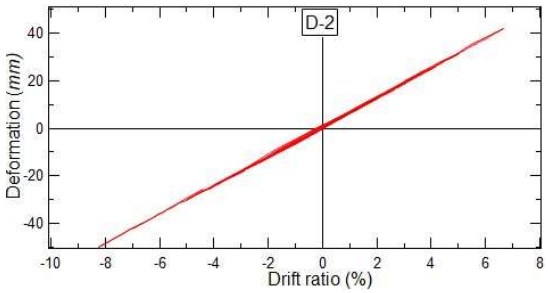
D-2
Deformation (mm)
Drift ratio (%)

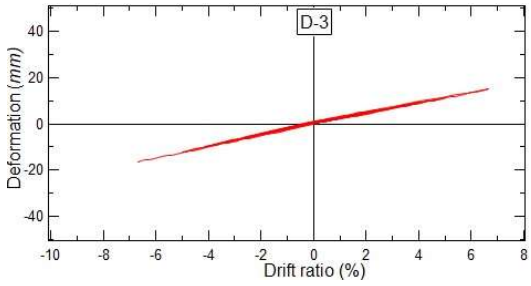
D-3
Deformation (mm)
Drift ratio (%)

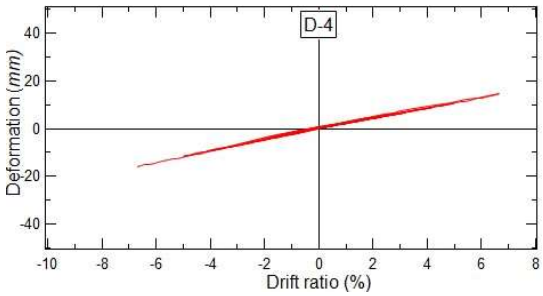
D-4
Deformation (mm)
Drift ratio (%)

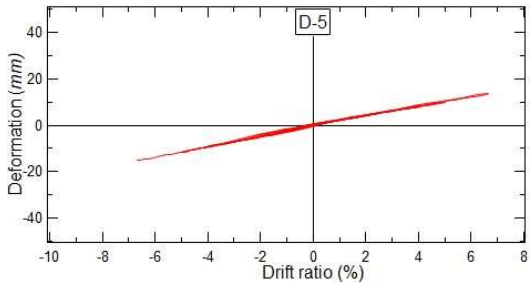
D-5
Deformation (mm)
Drift ratio (%)

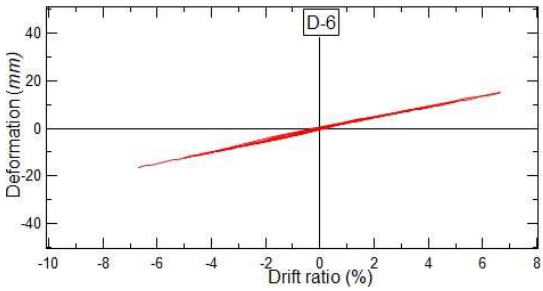
D-6
Deformation (mm)
Drift ratio (%)

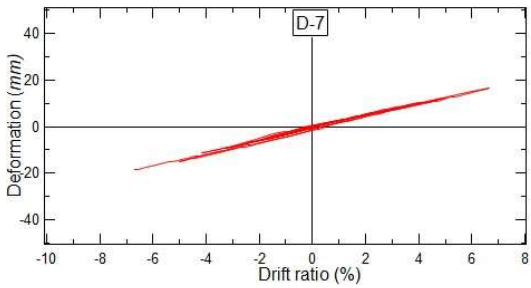
D-7
Deformation (mm)
Drift ratio (%)

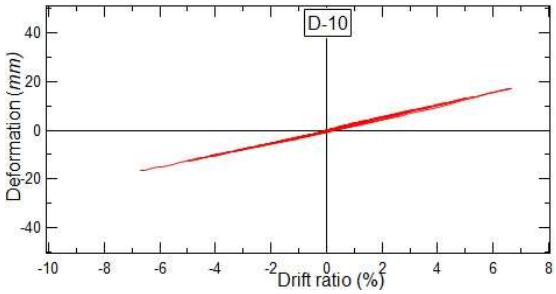
D-10
Deformation (mm)
Drift ratio (%)

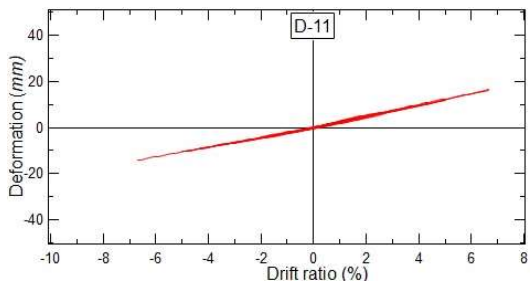
D-11
Deformation (mm)
Drift ratio (%)

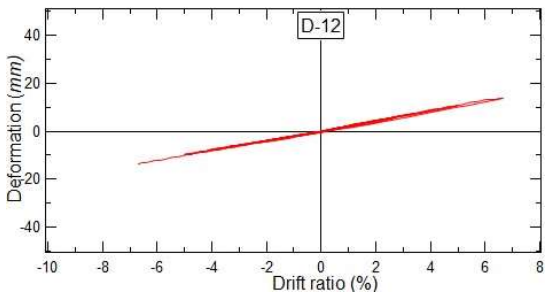
D-12
Deformation (mm)
Drift ratio (%)

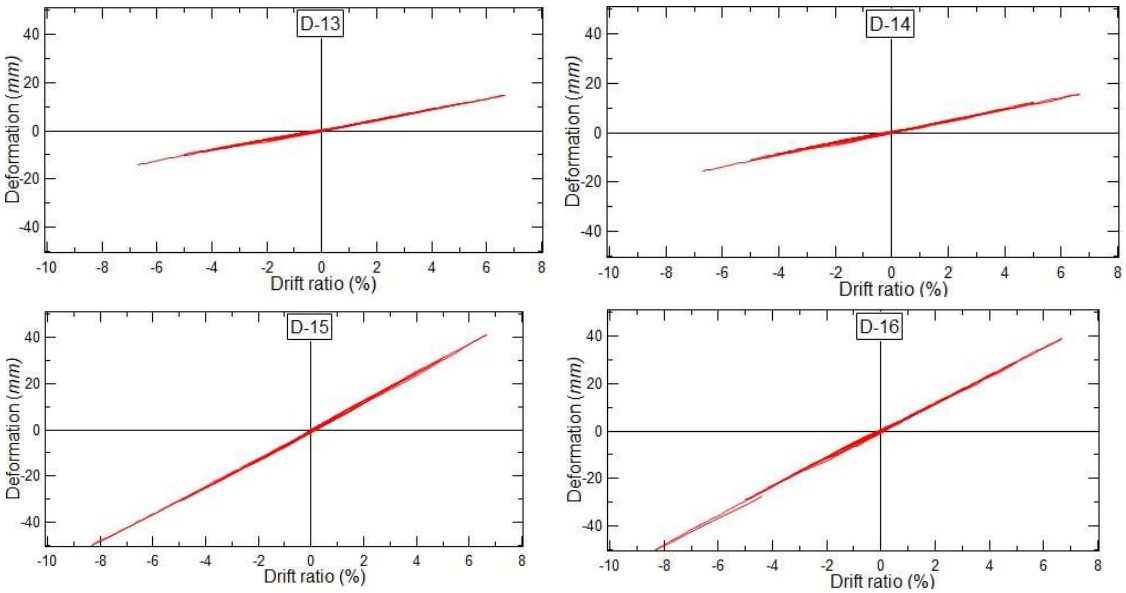

Figure A2.8 Displacement of transducers LVDT (specimen FP-W2)

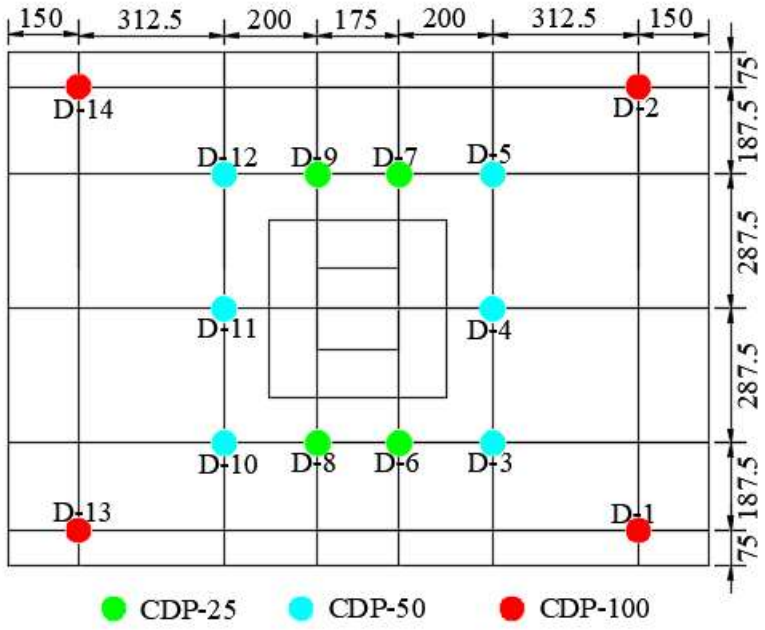

Figure A2.9 Position of displacement transducers (specimen FP-D1, FP-D2, FP-D3)

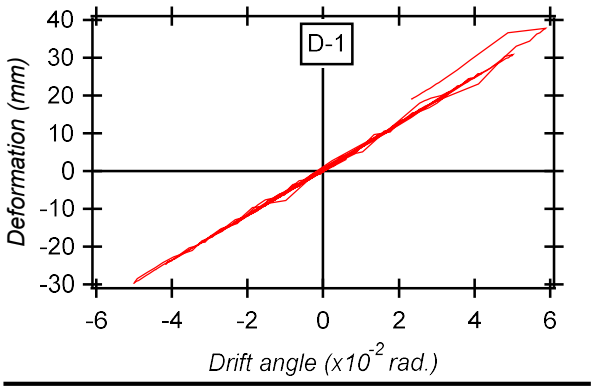
D-1
Deformation (mm)
Drift angle (x10-2 rad.)

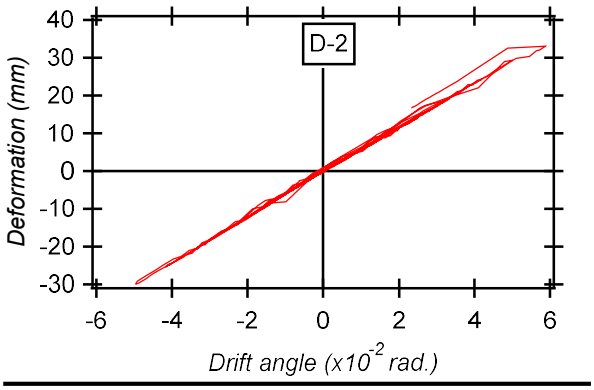
D-2
Deformation (mm)
Drift angle (x10-2 rad.)

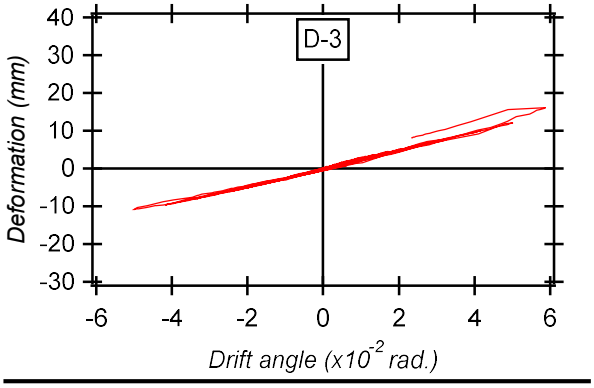
D-3
Deformation (mm)
Drift angle (x10-2 rad.)

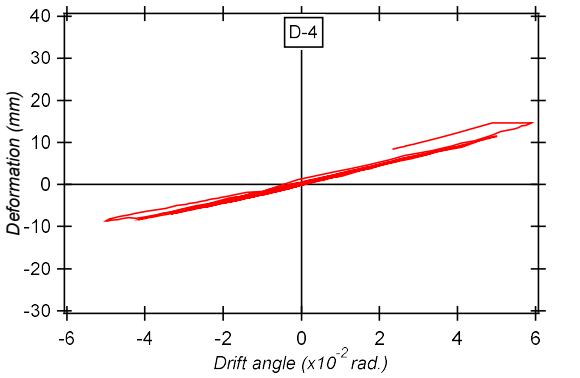
D-4
Deformation (mm)
Drift angle (x10-2 rad.)

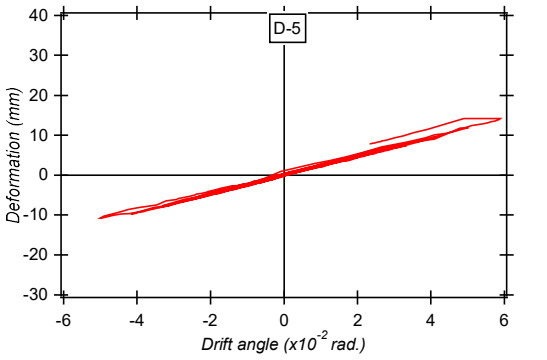
D-5
Deformation (mm)
Drift angle (x10-2 rad.)

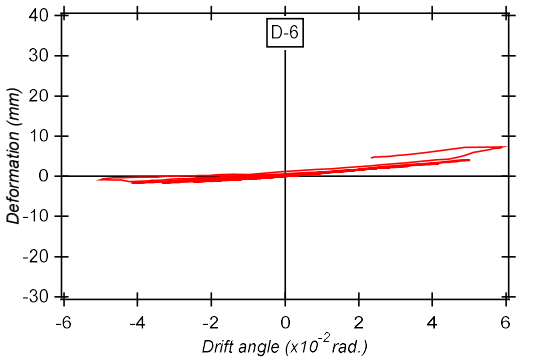
D-6
Deformation (mm)
Drift angle (x10-2 rad.)

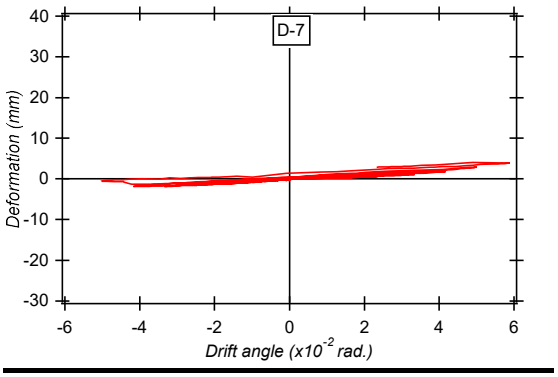
D-7
Deformation (mm)
Drift angle (x10-2 rad.)

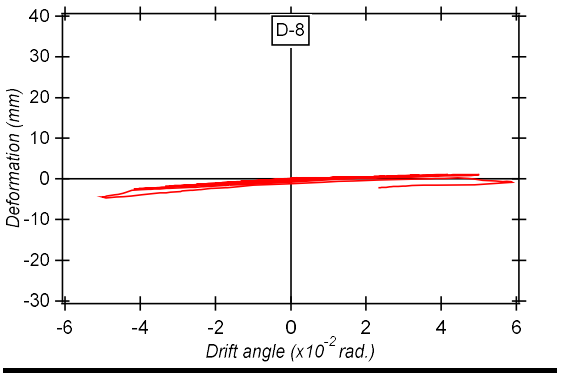
D-8
Deformation (mm)
Drift angle (x10-2 rad.)

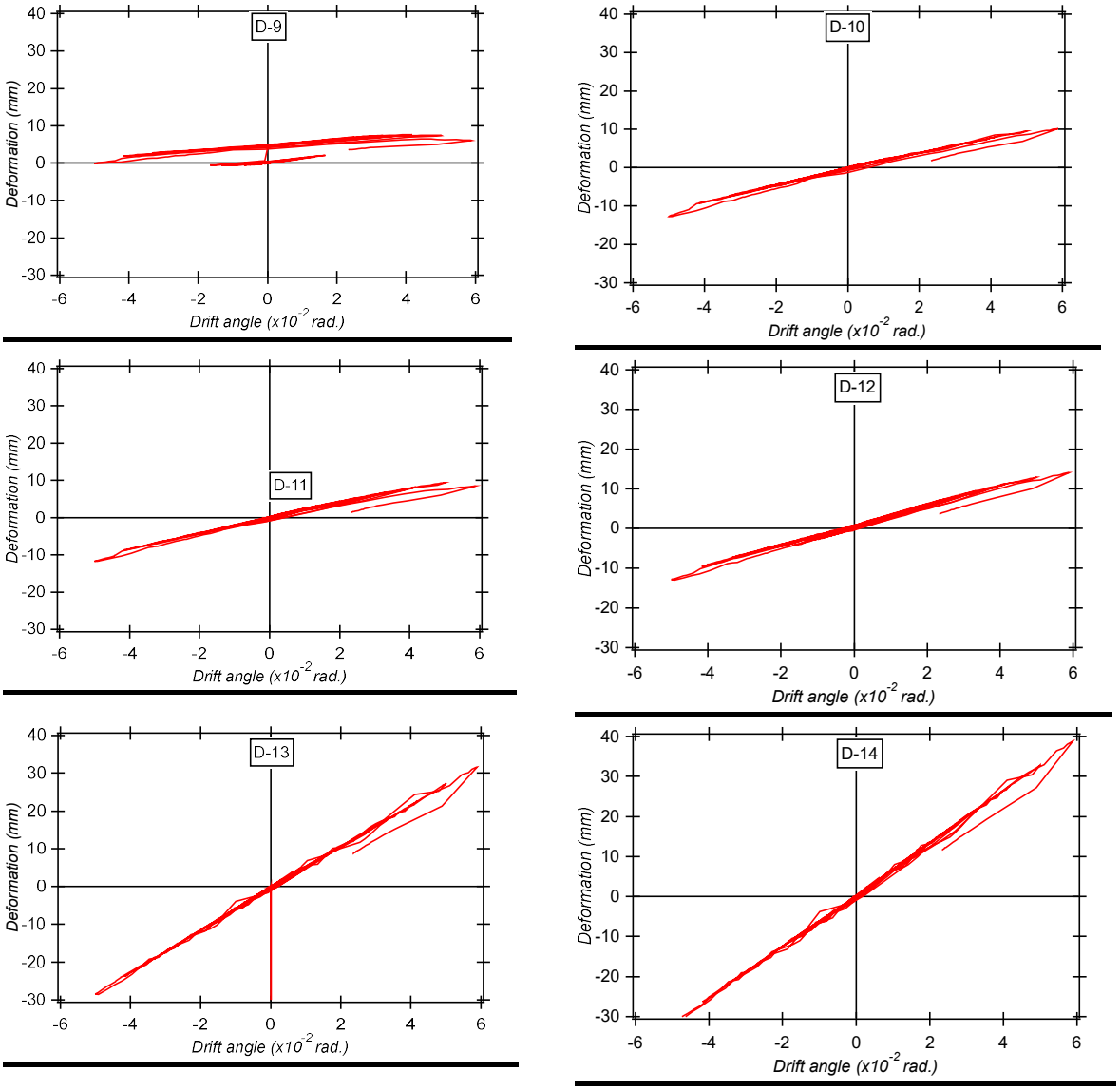

Figure A2.10 Displacement of transducers LVDT (specimen FP-D1)

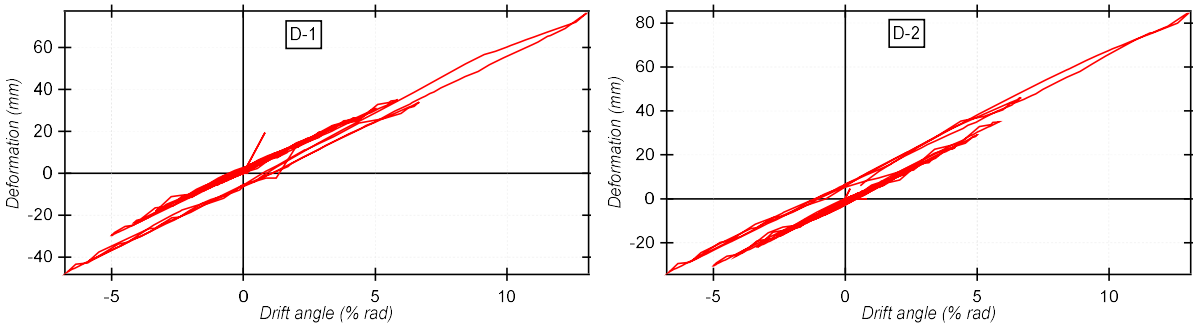

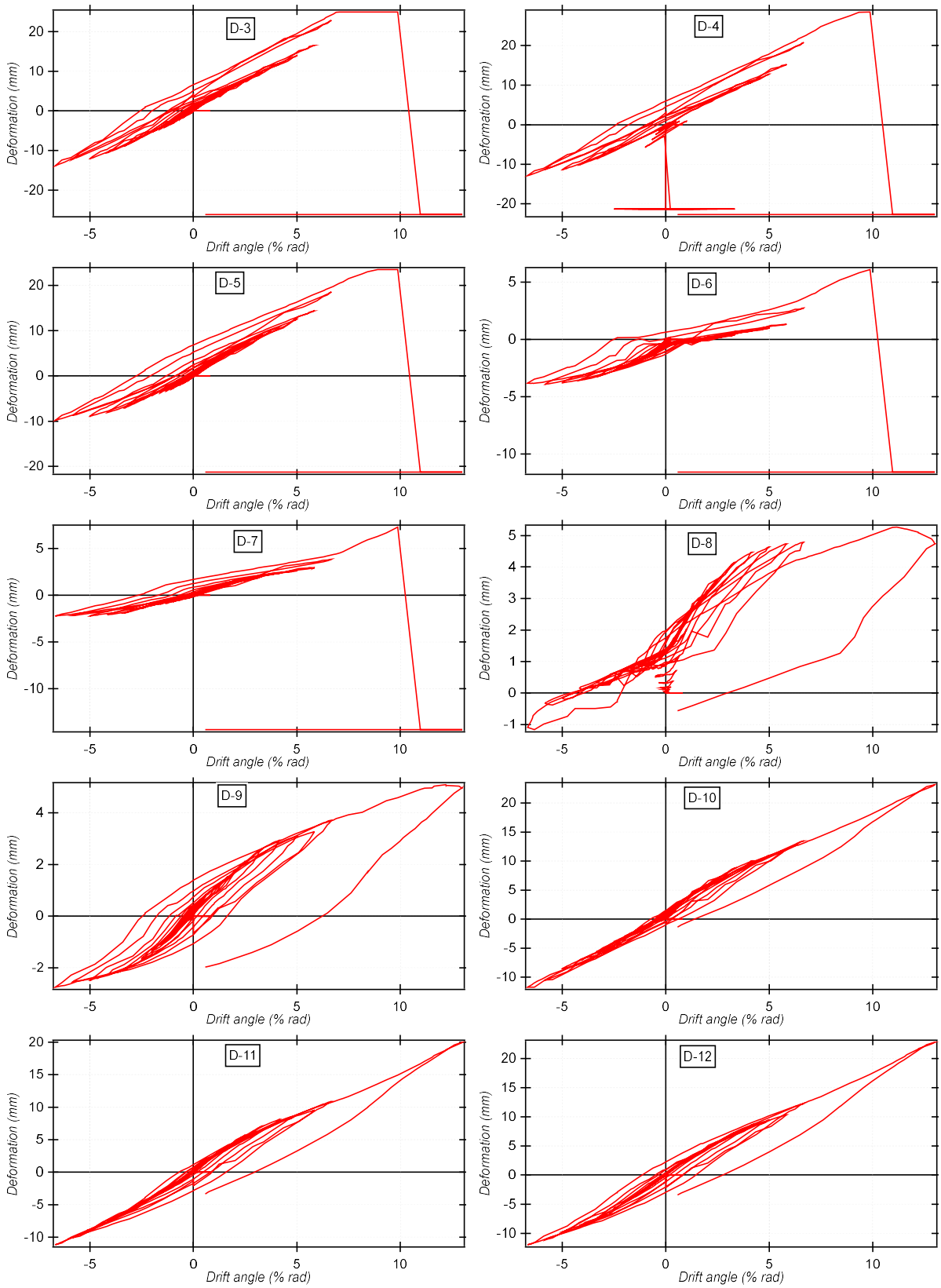
D-3
D-4
D-5
D-6
D-7
D-8
D-9
D-10
D-11
D-12
Deformation (mm)
Drift angle (% rad)

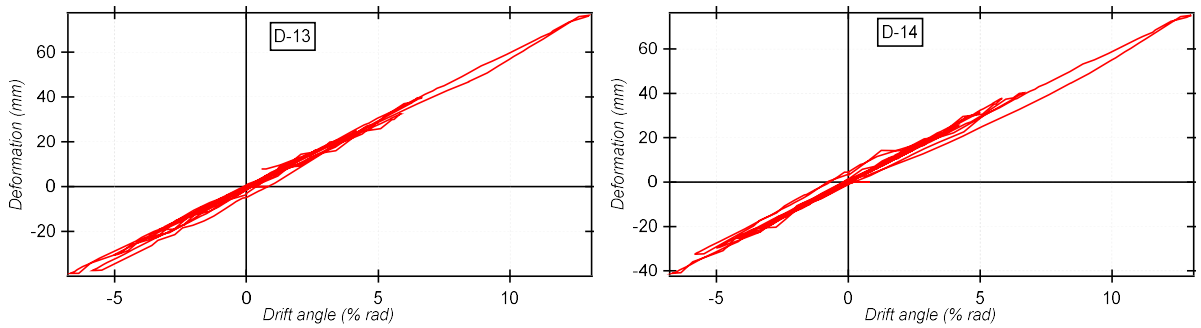

Figure A2.11 Displacement of transducers LVDT (specimen FP-D2)

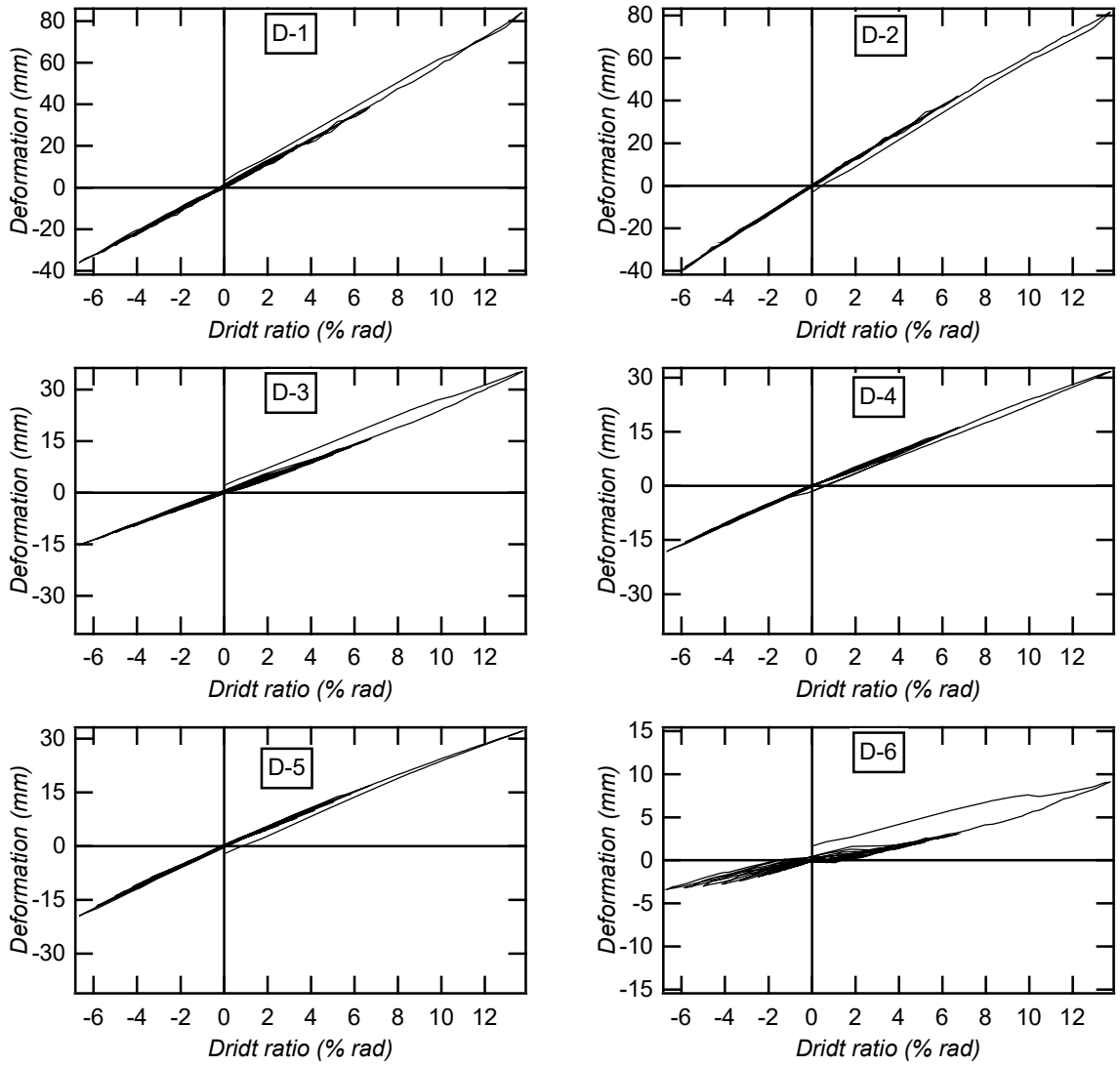

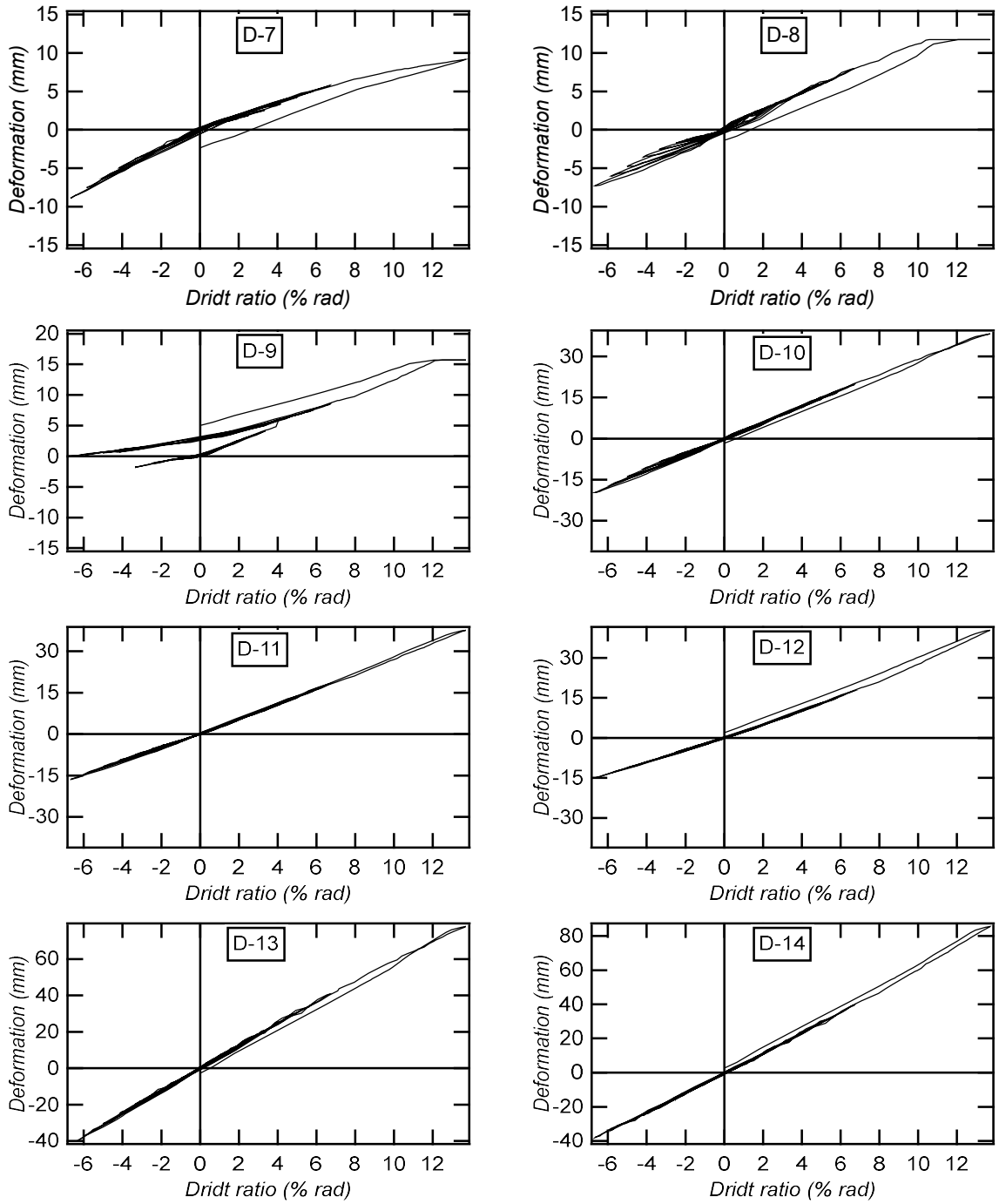

Figure A2.12 Displacement of transducers LVDT (specimen FP-D3)

Appendix A3

Detailed procedure of the sample calculation of the example building

Seismic Evaluation

Preliminary Calculation

The assumed typical floor weight is 12.0 kN/m^2.

Table A3.1 Summary of Floor weight of the structure

Storey	Floor Area (m^2)	Floor Weight W_i (kN)	Total weight (kN)
6	145.5	1746	1746
5	145.5	1746	3492
4	145.5	1746	5238
3	145.5	1746	6984
2	145.5	1746	8730
1	145.5	1746	10476

Storey shear modification factors for calculating E_0 are listed as follows. However, the calculation procedures are shown for 1st storey only; thus, the factor value will be 1.

Table A3.2 Storey modification factor

Storey	Modification factor
6	0.583
5	0.636
4	0.700
3	0.778
2	0.875
1	1.000

Table A3.3 Summary of Sustaining Force of Columns

Column ID	Story	Tributary area (m^2)	Weight W_i (kN)	Sustaining force (kN)
C1	1	11.9	143	856
C2	1	14.8	177	1063
C3	1	13.1	157	945
C4	1	10.0	120	720
C5	1	12.4	149	894
C6	1	11.0	133	795
C7	1	10.0	120	720
C8	1	12.4	149	894
C9	1	11.0	133	795
C10	1	11.6	139	835

C11	1	14.4	173	1063
C12	1	12.8	154	922

For the interior column, four types of failure modes were considered. The strength of each failure mechanism was calculated as the following. Based on the calculated strengths, the failure mode was determined by taking that showing the minimum value.

The general procedure for the judgment of the failure mode of the interior column C5 is shown as below:

$$_iQ_u = \min\ (Q_{mu}, Q_{su}, Q_{slab}, Q_{punch})$$

[Column]

$b \times D$: 550 mm×300 mm (22" × 12")

a_t: 6-D16 (6×201=1206 mm^2)

σ_y: 400 (N/mm^2) (Grade 60)

f_c': 24 (N/mm^2)

Axial Force: 894240 (N)

h_0: 3.6 (m) (1st floor)

H_0: 3.6-0.575 =3.025 (m) (1st floor)

Tie bar: D10@100

σ_y: 400 (N/mm^2)

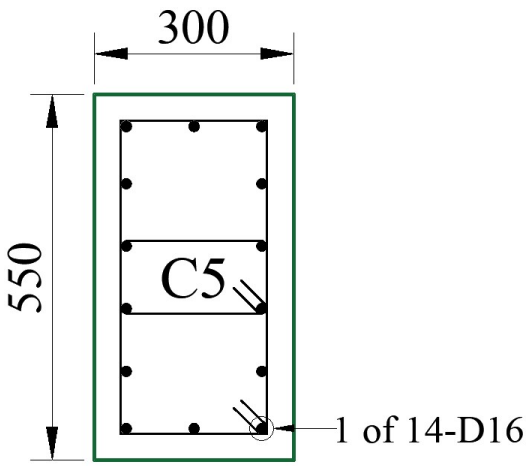

Interior column C5

[Slab]

Thickness: 200 (mm)

Span: (4400+2500)/2 =3.45 (m)

Reinforcement: D12@200 (extra top 1-D12)

σ_y: 275 (N/mm^2)

f_c': 20 (N/mm^2)

(a) Q_{mu}: Column shear resistance based on the flexural yielding at the top and bottom of column

In the case of this example, axial load N satisfies the following relation.

$0.4bD f_c' = 0.4 \times 550 \times 300 \times 24 = 1584{,}000$ (N)

$0.4bD f_c' > N > 0$

Storey height: 3.6 (m)

Clear height of column, h_0 =3.6-0.575 =0.3025 (m)

Therefore,

$$M_u = 0.8 a_t \sigma_y D + 0.5ND\left(1 - \frac{N}{bDf_c'}\right)$$

$$= 0.8 \times 1206 \times 400 \times 300 + 0.5 \times 894240 \times 300 \times \left(1 - \frac{894240}{550 \times 300 \times 24}\right)$$

$$= 219621652 \text{ (N} \cdot \text{mm)}$$

$$= 219.6 \text{ (kN} \cdot \text{m)}$$

$$Q_{mu} = M_u/(h_0/2) = 2 \times 219.6/3.025 = 145.2 \text{ (kN)}$$

(b) ***Q**su*: Column shear resistance based on the shear failure of column

$$p_t = \frac{1206}{550 \times 300} = 0.00731 = 0.731\%$$

$$d = 300 - 40 - 10 - \frac{16}{2} = 242 \text{ (mm)}$$

$$\frac{M}{Q.d} = \frac{h0}{2.d} = \frac{3.025 \times 1000}{2 \times 242} = 6.25 > 3; use\ 3$$

$$p_w \sigma_{wy} = \frac{2 \times 78.5}{550 \times 100} \times 400 = 1.14;$$

$$0.1\sigma_0 = 0.1 \times \frac{N}{b.j} = 0.1 \times \frac{894240}{550 \times 0.8 \times 300} = 0.677$$

Therefore, $Q_{su} = \left\{\frac{0.053 {p_t}^{0.23} (f_c^{'} + 18)}{M/(Qd) + 0.12} + 0.85\sqrt{p_w \sigma_{wy}} + 0.1\sigma_0\right\}. b. j$

$$= \left\{\frac{0.053 \times 0.731^{0.23} \times (24 + 18)}{3 + 0.12} + 0.85\sqrt{1.14} + 0.677\right\} 550 \times 240$$

$$= 296789 \text{ (N)}$$

$$= 296.8 \text{ (kN)}$$

(c) ***Q**slab*:Column shear resistance based on the flexural yielding of slab

Reinforcement: D12@200 alt. with extra top 1-D12@200

Number of reinforcement =transverse span length / spacing of rebar =6100/2*100 =31+1 =32 rebar for top slab and 18 rebar for bottom slab.

$$Q_{slab} = \frac{M_{slab}}{h_0}$$

where, M_{slab}: flexural yielding capacity of slab perspective with the nodal moment

h_0: clear height of column =3.025 (m)

The flexural yielding capacity of slab, M_{slab}:

$${}_lM_{slab} = 0.9 a_t \sigma_y d = 0.9 \times 32 \times 113.1 \times 275 \times 182$$

$$= 163026864 \text{ (N} \cdot \text{mm)} = 163.0 \text{ (kN} \cdot \text{m)}$$

$${}_rM_{slab} = 0.9 a_t \sigma_y d = 0.9 \times 16 \times 113.1 \times 275 \times 182$$

$$= 81513432 \text{ (N} \cdot \text{mm)} = 81.5 \text{ (kN} \cdot \text{m)}$$

$$M_{slab} = \frac{\frac{4025}{2} + \frac{300}{2}}{\frac{4025}{2}} \times 163 + \frac{\frac{2200}{2} + \frac{300}{2}}{\frac{2200}{2}} \times 81.5 \text{ (right)} = 267.7 \text{ (kN.m)}$$

$$Q_{slab} = M_{slab}/h_0$$
$$= 267.7\ /3.025$$
$$= 88.5\ (\text{kN})$$

To calculate Q_{slab}, the bending moment diagram (Grid Y2) was assumed as shown in **Figure A3.1** in the seismic evaluation guidelines. Different amounts of the slab top and bottom reinforcement lead to different moment resistances for the left and right slabs.

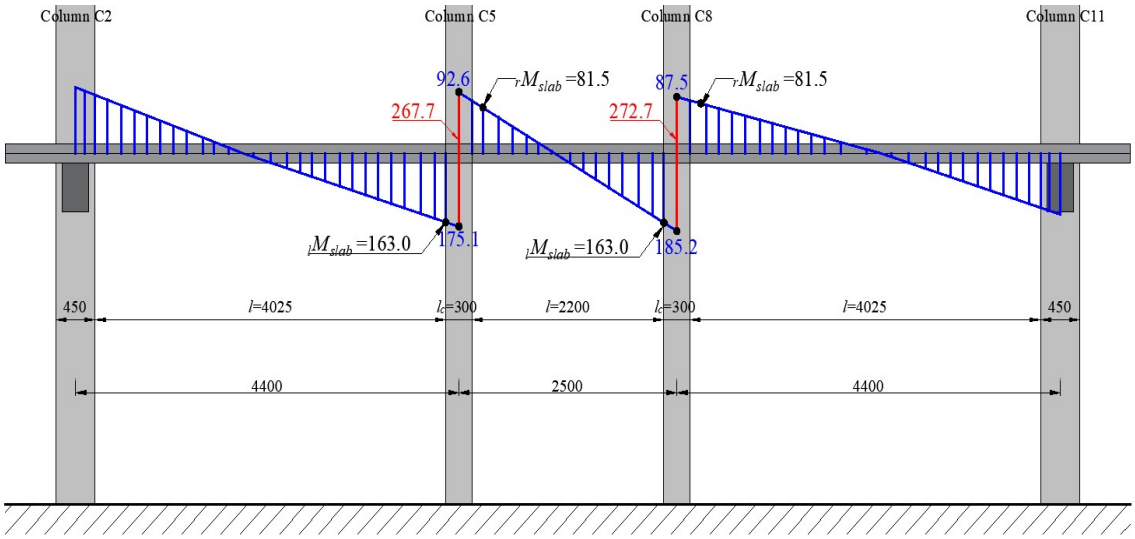

Figure A3.1 Assumed moment diagram at slab yielding (Grid Y2)

(d) Q_{punch}: Column shear resistance based on the punching shear failure

Thickness: 200 (mm)Reinforcement: D12@200 alt. with extra top 1-D12@200

c_1 = column depth = 300 (mm)

c_2 = column width =550 (mm)

σ_y : 275 (MPa) for slab (400 MPa for column)

F_c : 20 (MPa) for slab (24 MPa for column)

Axial load (one storey) V_u =149.0 (kN)

d : effective depth =200-18 =182 (mm)

$$M_f = 0.9a_{0t}.\sigma_y.d.\frac{c_2+d}{x_t} + 0.9a_{0b}.\sigma_y.d.\frac{c_2+d}{x_b}$$
$$= 0.9 \times 113.1 \times 275 \times 182 \times \frac{550+182}{100} + 0.9 \times 113.1 \times 275 \times 182 \times \frac{550+182}{200}$$
$$= 55938593\ (\text{N} \cdot \text{mm})$$
$$=55.9\ (\text{kN} \cdot \text{m})$$

$$M_s = \tau_u.(c_2+d).d.(c_1+d)$$
$$= 0.335 \times \sqrt{20} \times (550+182) \times 182 \times (300+182)$$
$$= 96203154\ (\text{N} \cdot \text{mm})$$

$=96.2\ (\text{kN}\cdot\text{m})$

$$M_t = \tau_{tu}\frac{d^2}{2}\left\{(c_1+d)-\frac{d}{3}\right\}\cdot 2$$

$$= 6\times 0.335\times\sqrt{20}\times\frac{182^2}{2}\left\{(300+182)-\frac{182}{3}\right\}\cdot 2$$

$$= 125452600\ (\text{N}\cdot\text{mm})$$

$$= 125.5\ (\text{kN}\cdot\text{m})$$

$$M_0 = M_f + M_s + M_t = 55.9 + 96.2 + 125.4 = 277.6\ (\text{kN}\cdot\text{m})$$

$$V_0 = \tau_u A_c = 0.335\sqrt{20}\times\{(300+182)\times 2+(550+182)\times 2\}\times 182$$

$$= 662033362\ (\text{N})$$

$$= 662.0\ (\text{kN})$$

$$\frac{V_u}{V_0}+\frac{M_u}{M_0}=\frac{149.0}{662.03}+\frac{M_u}{277.6}=1$$

$$M_u = 215.1\ (\text{kN}\cdot\text{m})$$

$$\therefore\ Q_{punch}=\frac{M_u}{h_0}=\frac{M_{u\,(top)}+M_{u\,(bottom)}}{h_0}=\frac{M_{u\,(top)}}{h_0/2}=\frac{215.1}{3.025}=71.1\ \ (\text{kN})$$

Therefore, ${}_iQ_u = 71.1$ (kN); **punching failure mode**

To calculate Q_{punch}, the bending moment diagram was assumed, as shown in **Figure A3.2** in the seismic evaluation guidelines.

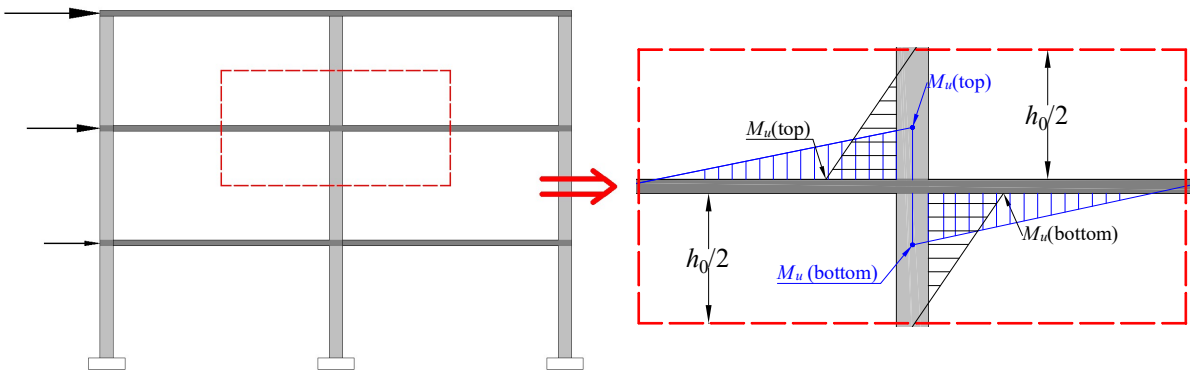

Figure A3.2 Assumed moment diagram for slab punching

The failure mode of the interior column was punching shear failure. Therefore, the *F*-index of the exterior columns (with beam) of this building should consider the upper limit of the drift angle of an exterior column ${}_cR_{max}$ of 1/50, which will be described later in this section.

The exterior column shear resistance ${}_eQ_u$ was calculated by the following equation according to the Chapter 5. Based on the calculated strengths, the failure mode can be determined by taking that showing the minimum value.

$$ {}_eQ_u = \min\ (Q_{mu}, Q_{su}) $$

where Q_{mu} is column shear force at the flexural yielding

Q_{su} is column shear strength at the shear failure

Typical Floor dimensions: 15×9.7 = 145.5 (m^2)

Total weight of the building =15×9.7×12×6=10476 (kN)

(a) Q_{mu}

In the case of this example, axial load N satisfies the following relation.

Axial load, N= 4.1×2.9×6×12 =856080 (N)

$b \times D$ = 300 (mm) × 500 (mm)

$0.4bD f_c'$ =0.4×300×500×24 =1440,000 (N)

$0.4bD f_c' > N > 0$

Therefore,

$$ M_u = 0.8a_t\sigma_y D + 0.5ND\left(1 - \frac{N}{bDf_c'}\right) $$

$$ = 0.8 \times 603 \times 400 \times 500 + 0.5 \times 856080 \times 500 \times \left(1 - \frac{856080}{500 \times 300 \times 24}\right) $$

$$ = 259.6\ (\text{kN} \cdot \text{m}) $$

$$ Q_{mu} = \frac{M_u}{\frac{h_0}{2}} = \frac{259.6}{3.025} * 2 = 171.7\ (\text{kN}) $$

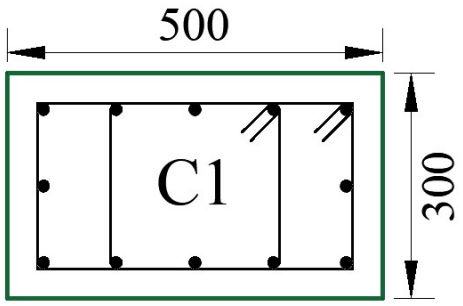

Exterior column C1

(b) Q_{su}

$$ p_t = \frac{603}{500\times300} = 0.004 = 0.4\% $$

$$ d = 500 - 40 - 10 - \frac{16}{2} = 442\ (\text{mm}) $$

$$ \frac{M}{Q.d} = \frac{h0}{2.d} = \frac{3.025\times1000}{2\times442} = 3.42 > 3; use\ 3 $$

$$ p_w\sigma_{wy} = \frac{2\times78.5}{300\times100} \times 400 = 2.09; $$

$$ 0.1\sigma_0 = 0.1 \times \frac{N}{b.D} = 0.1 \times \frac{856080}{300\times500} = 0.57 $$

j= 0.8×500 =400 (mm)

Therefore, $Q_{su} = \left\{\frac{0.053{p_t}^{0.23}({f_c}'+18)}{M/(Qd)+0.12} + 0.85\sqrt{p_w\sigma_{wy}} + 0.1\sigma_0\right\}.b.j$

$$= \left\{ \frac{0.053 \times 0.4^{0.23} \times (24+18)}{3+0.12} + 0.85\sqrt{2.09} + 0.57 \right\} 300 \times 400$$

=285.2 (kN) >171.7(kN); **Flexural column**

The ultimate shear strength of each exterior column was calculated in the same procedure. The calculated strength of each member is listed below.

Table A3.4 Summary of the column lateral resistances

Column ID	Floor	M_u (kN.m)	Q_{mu} (kN)	Q_{su} (kN)	Q_{slab} (kN)	Q_{punch} (kN)	Q_u (kN)	Failure mode	Remarks
C1	1	259.6	171.7	285.2	-	-	171.7	Flexure	Ext. column with beam
C2	1	Ignoring shear resistance							Ext. column without beam
C3	1	270.7	179.0	292.6	-	-	179.0	Flexure	Ext. column with beam
C4	1	204.2	135.0	265.2	-	-	135.0	Flexure	Ext. column with beam
C5	1	219.6	145.2	296.8	88.5	71.1	74.3	Punching	Int. column
C6	1	177.5	117.4	229.9	-	-	117.4	Flexure	Ext. column with beam
C7	1	204.2	135.0	265.2	-	-	135.0	Flexure	Ext. column with beam
C8	1	219.6	145.2	279.1	90.1	71.1	74.3	Punching	Int. column
C9	1	177.5	117.4	229.9	-	-	117.4	Flexure	Ext. column with beam
C10	1	256.9	169.8	283.8	-	-	169.8	Flexure	Ext. column with beam
C11	1	Ignoring shear resistance							Ext. column without beam
C12	1	267.9	177.1	290.7	-	-	177.1	Flexure	Ext. column with beam

Calculation of *C* index of the column C1

The strength index *C* was calculated as follows:

$$C = \frac{min(Q_{mu}, Q_{su})}{\sum W}$$

$\sum W$ =total weight of the building

Thus, C index of C_1 column = 171.7/10476 =0.0164

Calculation of *F* index of the column C1

The ductility index calculation of the vertical members with the perimeter beams shall follow the CNCRP manual. In principle, the upper limit of the drift angle of flexural column shall be calculated with the following equations. The CNCRP/BSPP Manuals provided detailed calculations; thus, the typical calculations are omitted in this extensive procedure.

$$_cR_{max} = \min\{\ _cR_{\max(n)},\ _cR_{\max(s)},\ _cR_{\max(t)},\ _cR_{\max(b)},\ _cR_{\max(h)}\}$$

$$\therefore\ \ _cR_{max} = \min\left\{\frac{1}{33},\frac{1}{30},\frac{1}{30},\frac{1}{30},\frac{1}{30}\right\} = 1/33$$

$_cR_{\max}$, the upper limit of the deflection angle of an exterior flexural column shall be determined by the failure mode of an interior column according to the Chapter 5. Therefore, $_cR_{\max(punc\ )}$ shall be considered when the failure mode of an interior column is punching.

So, $_cR_{\max(punc\ )} = \frac{1}{50}$

Here, $_cR_{\max} = \frac{1}{33} >\ _cR_{\text{punch}}\ \ \frac{1}{50}$; (Since the failure mode of an interior column is punching, the upper limit of the drift angle of members shall be $_cR_{max}$ = 1/50 = 0.02.)

Therefore, $_cR_{\max} = \frac{1}{50}$

$And,\ _cR_{\text{my}} = \frac{1}{150}, R_{mu} = \frac{1}{50}$

The ductility index:

Since $R_{mu} \geq R_y$

Therefore, $F = \frac{\sqrt{2R_{mu}/R_y - 1}}{0.75\left(1+0.05R_{mu}/R_y\right)} \leq 3.2\ \ for\ R_{mu} \geq R_y$

$$F = \frac{\sqrt{2\times\frac{1}{50}/\frac{1}{150} - 1}}{0.75\left(1+0.05\times\frac{1}{50}/\frac{1}{150}\right)} = 2.6$$

The strength index C and ductility index F of each exterior column can be calculated in the same procedure. The calculated index of each member is listed below.

Table A3.5 Ductility index *F* and strength index *C*

Column ID	Storey	Weight of the building	Q_u (kN)	*C*	Q_{su} /Q_{mu}	*F*	Remarks
C1	1	10476	171.7	0.0164	1.66	2.6	Ext. column with beam
C2	1		Ignoring shear resistance				Ext. column without beam
C3	1		179.0	0.0171	1.63	2.6	Ext. column with beam
C4	1		135.0	0.0129	1.96	2.6	Ext. column with beam
C5	1		-	-	-	-	Int. col. (punching)
C6	1		117.4	0.0113	1.96	2.6	Ext. column with beam
C7	1		135.0	0.0129	1.96	2.6	Ext. column with beam
C8	1		-	-	-	-	Int. col. (punching)
C9	1		117.4	0.0113	1.96	2.6	Ext. column with beam
C10	1		169.8	0.0162	1.67	2.6	Ext. column with beam
C11	1		Ignoring shear resistance				Ext. column without beam
C12	1		177.1	0.0169	1.64	2.6	Ext. column with beam

[**Note:** The columns without being connected to beams are flexible in their respective directions; thus, only the contributions of perimeter columns with beams can be considered to evaluate the seismic capacity of the structure. [For example: in this sample building, C2 and C11 columns are not connected with beams in the X-direction; thus, their contributions shall be ignored along with the interior columns of C5 and C8]

Therefore, the summation of *C* from all contributed columns is 0.117.

The seismic capacity of the building structure is expressed by the structural seismic index I_s calculated form:

$$I_s = E_0 \times S_d \times T$$

Here, the basic seismic index, $E_0 = C^*F = 0.1168^*2.59 = 0.303$, as shown in **Figure A3.3** (since, there is one group only)

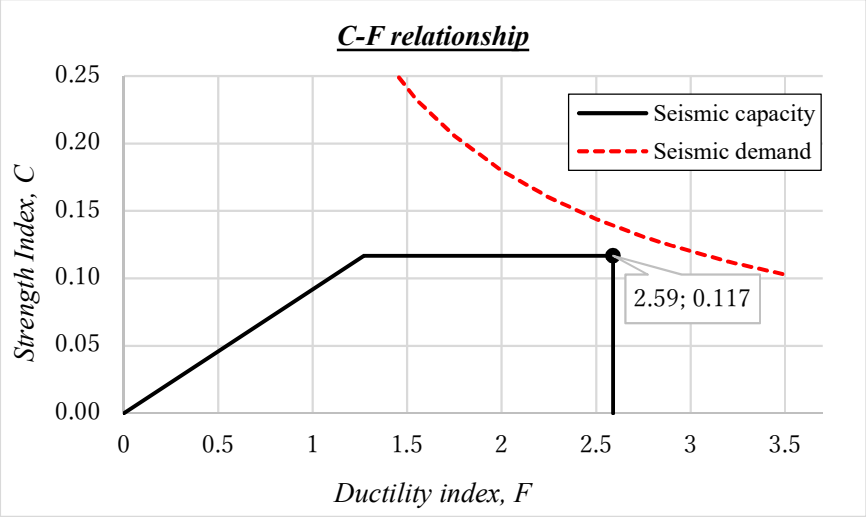

Figure A3.3 Relationship between strength index *C* and ductility index *F*

Therefore, the seismic index, $I_s = E_0 \times S_d \times T = 0.303 \times 1 \times 1 = 0.303$ (story modification factor = 1)

Where, E_0 = Basic seismic index, S_d = 1.0 (Irregularity index), T = 1.0 (time index)

Seismic demand index

Seismic demand index I_{s0} is determined as per the requirement of BNBC 2020.

$$I_{S0} = \frac{0.8 * 2}{3} . Z . I . C_s$$

Where:

Z =0.2, I = 1.0, Soil type-soft (SD) =1.5, h_n=18.6 (m)

T = C_t $(h_n)^m$ =0.0446 $(h_n)^{0.9}$ =0.619s (according to Section 2.5.7.2; Tables 6.2.16, 6.2.20 of BNBC 2020

C_s=2.5 $S\mu$ =2.5*1.35*1 =3.375; Table 6.2.13 (assuming soil type SD)

I_{s0} =0.8×2/3× 0.2 × 1.0 × 3.375 =**0.36** (low-rise residential building on soil type SD**)**

Therefore, seismic index of this building, I_s= 0.303 < I_{s0} = 0.36 (**Not safe**) (X-direction). Hence, more strengthening should be carried out, either installing by wing walls or drop panel, or shear wall as much as needed and possible.

Finally, seismic evaluation is done for each major direction and floor of the building (shown in **Figure A3.4**). The proposed I_{s0} is 0.36 for buildings located in Dhaka based on soil type SD of BNBC 2020. However, it was evaluated that the building was not safe in any direction. Therefore, it is desirable to establish some retrofit plans that will ensure that I_s>0.36 is achieved at each floor level and in each direction.

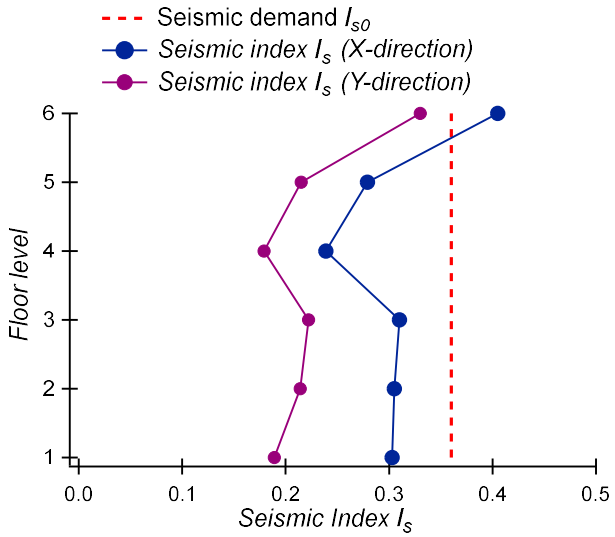

Figure A3.4 Comparison between seismic demand and capacity

Seismic Retrofit

The procedure of the seismic evaluation of a retrofitted flat plate structure is shown in this example calculation. The main purpose of the example is to show how to strengthen the existing flat plate structure based on the proposed evaluation method. The same building was retrofitted that presented in Chapter 5 for seismic evaluation of existing flat plate structure, as shown in **Figure 6.2.1**. The building was not appropriately designed against earthquake load. Seismic performance was low as per result of the seismic evaluation, as shown in **Figure A3.4**.

Seismic retrofit using drop panel

In the example building, the failure mode of an interior column was identified as punching shear failure, which is a brittle failure mode that is undesirable to this structural system. Therefore, the post-installed drop panel shall be installed to change the failure mode from brittle punching to ductile flexural failure, possibly leading to the improvement of the seismic capacity. The seismic retrofit flow chart using drop panel is shown in **Figure A3.5**.

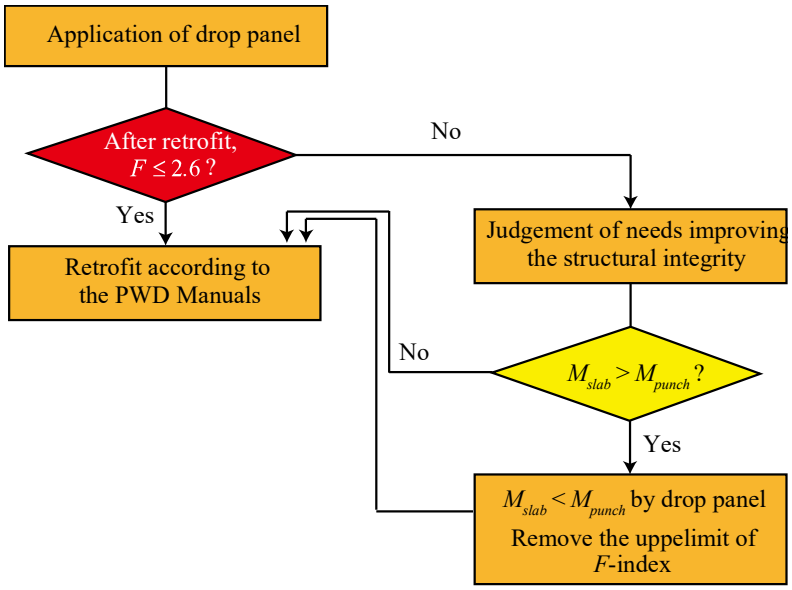

Figure A3.5 Flow Diagram of Seismic Retrofit using drop panel

Calculation procedure according to Chapter 6

The interior columns of C5 and C8 required to be strengthened using drop panel to prevent the punching shear failure. Here, the calculation procedure of seismic evaluation after installing the drop panel is shown step by step as follows:

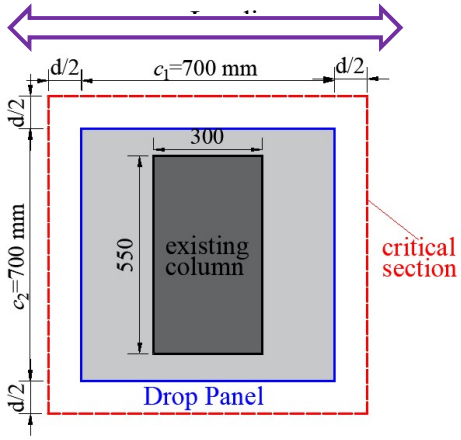

Figure A3.6 Assumed critical section of the column with drop panel

Reinforcement of slab: D12@200

Total length of slab span =4400/2+2500/2=3450 (mm).

The minimum size of drop panel is =1/5th of span length =1/5×3450 = 690 (mm), considering BNBC (2020) requirement.

Here, the assumed drop panel size is 700 mm × 700 mm. The thickness of drop panel is 200 mm (considering same as slab thickness). The assumed critical section of the column with drop panel is shown in **Figure A3.6**.

Here, $Q_{mu} = 137.3$ (kN), and $Q_{su} = 282.7$ (kN) [same calculation as exterior columns]

***Q_{slab}*:**

Q_{slab} : column shear resistance based on the flexural yielding of slab

$$Q_{slab} = \frac{M_{slab}}{h_0}$$

where, M_{slab}: flexural yielding capacity of slab perspective with the nodal moment

h_0: clear height of column

The flexural capacity of slab (M_{slab}) is calculated by assuming the moment diagram shown in **Figure A3.7** and using the following equation based on **Section 6.5**.

$$M_{slab} = \frac{{}_lM_{slab}}{l/2} \times \left(\frac{l}{2} + \frac{l_d}{2}\right) + \frac{{}_rM_{slab}}{l/2} \times \left(\frac{l}{2} + \frac{l_d}{2}\right)$$

where, ${}_lM_{slab}$ / ${}_rM_{slab}$: flexural yielding capacity of the slab in the corresponding side

l: clear span of the length in the corresponding side

l_d: length of the drop panel

Flexural yielding capacity of slab, M_{slab}:

$$_{l}M_{slab} = 0.9a_t\sigma_y d = 0.9 \times 32 \times 113.1 \times 275 \times 182 = 163.0\ (\text{kN} \cdot \text{m})$$

$$_{r}M_{slab} = 0.9a_t\sigma_y d = 0.9 \times 16 \times 113.1 \times 275 \times 182 = 81.5(\text{kN} \cdot \text{m})$$

Therefore,

$$M_{slab} = \frac{163}{3825/2} \times \left(\frac{3825}{2} + \frac{700}{2}\right) + \frac{81.5}{1800/2} \times \left(\frac{1800}{2} + \frac{700}{2}\right) = 306\ (\text{kN.m})$$

$$\therefore\ Q_{slab} = M_{slab}/h_0 = 306\ /3.025\ = 101.1\ (\text{kN})$$

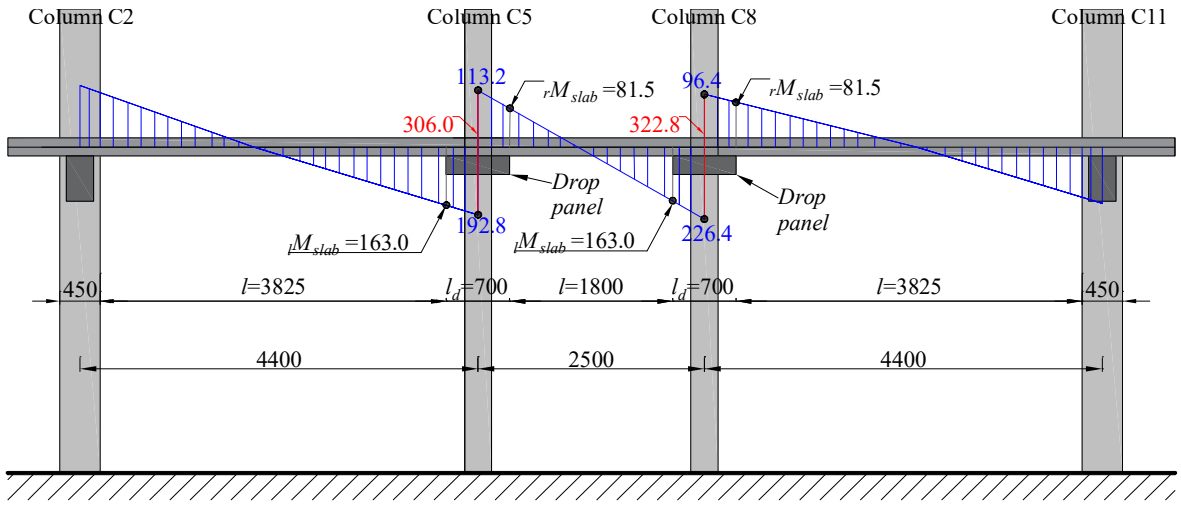

Figure A3.7 Nodal moment of slab (Grid Y2)

***Q**punch*:**

The thickness of drop panel is 200mm

c_1 = drop panel depth = 700 (mm)

c_2 = drop panel width =700 (mm)

σ_y : 275 (N/mm^2) for slab (400 N/mm^2) for column

F_c : 20 (N/mm^2) for slab

d : effective depth =200-18 =182 (mm)

$$M_f = 0.9a_{0t}.\sigma_y.d.\frac{c_2+d}{x_t} + 0.9a_{0b}.\sigma_y.d.\frac{c_2+d}{x_b}$$

$$= 0.9 \times 113.1 \times 275 \times 182 \times \frac{700+182}{100} + 0.9 \times 113.1 \times 275 \times 182 \times \frac{700+182}{200}$$

$$= 67.4\ (\text{kN} \cdot \text{m})$$

$$M_s = \tau_u.(c_2 + d).d.(c_1 + d)$$

$$= 0.335 \times \sqrt{20} \times (700 + 182) \times 182 \times (700 + 182)$$

$$= 212.1\ (\text{kN} \cdot \text{m})$$

$$M_t = \tau_{tu}\frac{d^2}{2}\left\{(c_1 + d) - \frac{d}{3}\right\} \cdot 2$$

$$= 6 \times 0.335 \times \sqrt{20} \times \frac{182^2}{2}\left\{(700 + 182) - \frac{182}{3}\right\} \cdot 2$$

$$= 244.5 \text{ (kN} \cdot \text{m)}$$

$$M_0 = M_f + M_s + M_t = 67.4 + 212.1 + 244.5 = 524.1 \text{ (kN} \cdot \text{m)}$$

$$V_0 = \tau_u A_c = 0.335\sqrt{20} \times \{(700 + 182) \times 2 + (700 + 182) \times 2\} \times 182$$

$$= 962 \text{ (kN)}$$

$$\frac{V_u}{V_0} + \frac{M_u}{M_0} = \frac{149}{962} + \frac{M_u}{524.1} = 1$$

$$M_u = 442.9 \text{ (kN} \cdot \text{m)}$$

$$\therefore\ Q_{punch} = \frac{442.9}{3.025} = 146.4 \text{ (kN)} > 101.1 \text{(kN)}$$

Therefore, the failure mode of the interior column was changed to slab flexure. The calculation procedure of ductility index *F* shall be the same as the normal moment-resisting structure.

From the previous calculation:

$$_cR_{max} = \min\left\{\frac{1}{33}, \frac{1}{30}, \frac{1}{30}, \frac{1}{30}, \frac{1}{30}\right\} = 1/33$$

Since the failure mode of interior column was not punching, the value of $_cR_{max}$ will not be bound for 1/50.

Therefore, $_cR_{max} = 1/33$

The ductility index:

Since $R_{mu} \geq R_y$

Therefore, $F = \frac{\sqrt{2R_{mu}/R_y - 1}}{0.75\left(1+0.05R_{mu}/R_y\right)} \leq 3.2 \quad for\ R_{mu} \geq R_y$

$$F = \frac{\sqrt{2 \times \frac{1}{33}/\frac{1}{150} - 1}}{0.75\left(1+0.05 \times \frac{1}{33}/\frac{1}{150}\right)} = 3.1 \leq 3.2$$

[**Note:** The columns without being connected to beams are flexible in their respective directions; thus, only the contributions of perimeter columns with beams can be considered to evaluate the seismic capacity of the structure. For example: in this sample building, C2 and C11 columns are not connected with beams in the X-direction; thus, their contributions shall be ignored along with the interior columns of C5, and C8]

The strength index *C* and ductility index *F* of each exterior column can be calculated in the same procedure. The calculated index of each member in X-direction is listed in **Table A3.6** as below.

Table A3.6 Ductility index F and strength index C

Column ID	Storey	Weight of the building	Q_u (kN)	C	Q_{su} /Q_{mu}	F	Remarks
C1	1	10476	171.7	0.0164	1.66	3.1	Ext. column with beam
C2	1		Ignoring shear resistance				Ext. column without beam
C3	1		179.0	0.0171	1.63	3.1	Ext. column with beam
C4	1		135.0	0.0129	1.96	3.1	Ext. column with beam
C5	1		-	-	-	-	Int. column
C6	1		117.4	0.0113	1.96	3.1	Ext. column with beam
C7	1		135.0	0.0129	1.96	3.1	Ext. column with beam
C8	1		-	-	-	-	Int. column
C9	1		117.4	0.0113	1.96	3.1	Ext. column with beam
C10	1		169.8	0.0162	1.67	3.1	Ext. column with beam
C11	1		Ignoring shear resistance				Ext. column without beam
C12	1		177.1	0.0169	1.64	3.1	Ext. column with beam

Therefore, the summation of C from all contributed columns is 0.1168.

Here, $E_0 = C*F$ = 0.1168*3.1 =0.361, as shown in **Figure A3.8**.

Therefore, the seismic index, $I_s = E_0 \times S_d \times T$ =0.361×1×1 = 0.361

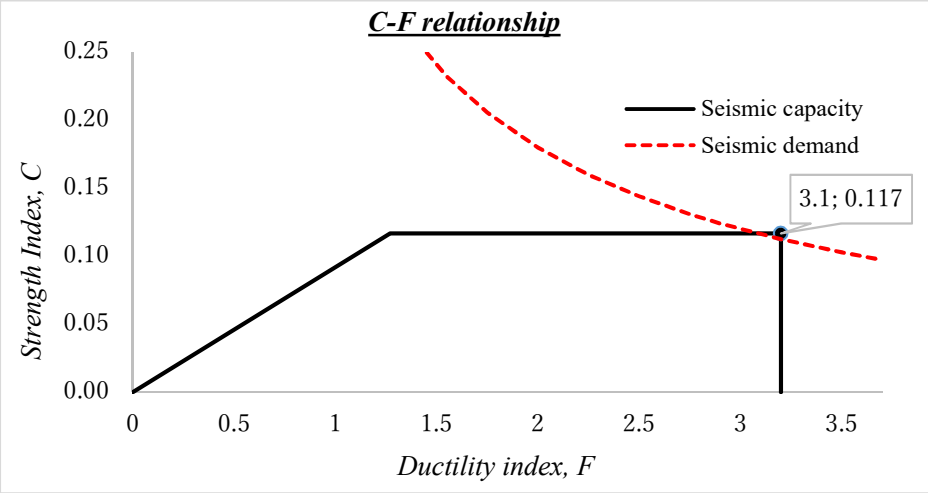

Figure A3.8 Relationship between strength index C and ductility index F

Therefore, the seismic index of this building in X-direction of the 1st-floor level was I_s= 0.361> I_{s0} = 0.36 (**Safe**). Though the building satisfied the seismic demand (minimum requirement), the large drift was expected to exhibit the seismic capacity with F of 3.1. In general, a drift of the structure is recommended to be kept as small as possible to prevent damage to the structure under large deformation.

For such purpose, another option is recommended by applying post-installed wing walls to increase/decrease the *C/F* index at the maximum performance in the following section.

Furthermore, it was evaluated that the building was not safe on the 1st to 5th floors in the Y-direction and on the 4th and 5th floors in the X-direction by using drop panels (as shown in **Figure A3.9**). Drop panels typically improve the ductility of the structure by preventing the punching shear failure of the interior slab, but they do not increase the lateral resistance of the column. Therefore, further strengthening is necessary to improve the seismic performance of the building in consideration of both directions. As a result, strength-oriented retrofit schemes are recommended (for example, wing walls, shear walls, etc.).

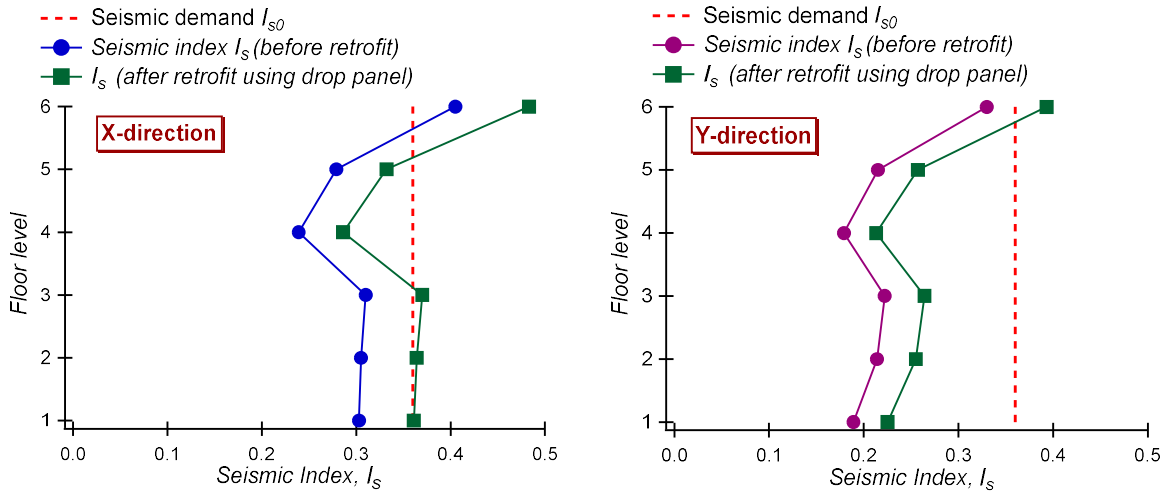

Figure A3.9 Comparison between seismic demand and capacity using drop panel

[**Note:** The building was considered to be safe in both directions on the 6th-floor level only after being retrofitted using post-installed drop panels. As a result, wing walls were planned to be installed from the 1st to 5th-floor level in the following section, considering the continuous installation of wing walls from the bottom of the building and lower values of I_s compared to those in the 6th floor].

Seismic retrofit using wing walls

The seismic retrofit flow chart using wing wall is shown in **Figure A3.10**. The wing walls were planned to be installed to increase/decrease the *C/F* index showing a strength-type retrofit design. The layout and dimensions of wing walls are shown in **Figure 6.6.1**. The wing walls were intended to be installed from the 1st to 5th-floor level of the building because the drop panel is sufficient to increase the seismic index in both X & Y-direction on the 6th floor. The detailed calculation of wing wills with beams is available JBDPA standard. Therefore, the calculation of wing walls without beam (interior column) is explained in this section.

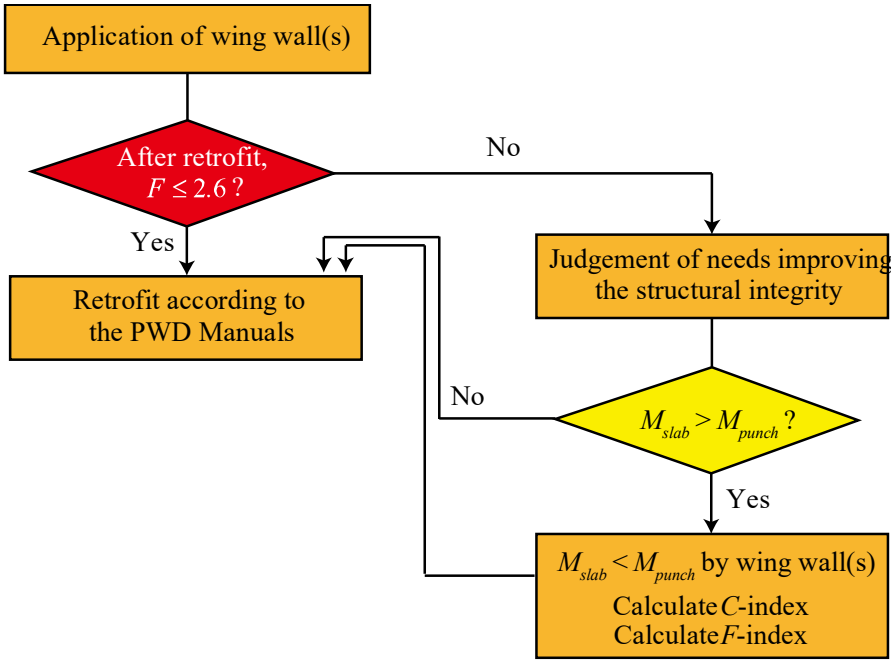

Figure A3.10 Flow Diagram of Seismic Retrofit using wing wall

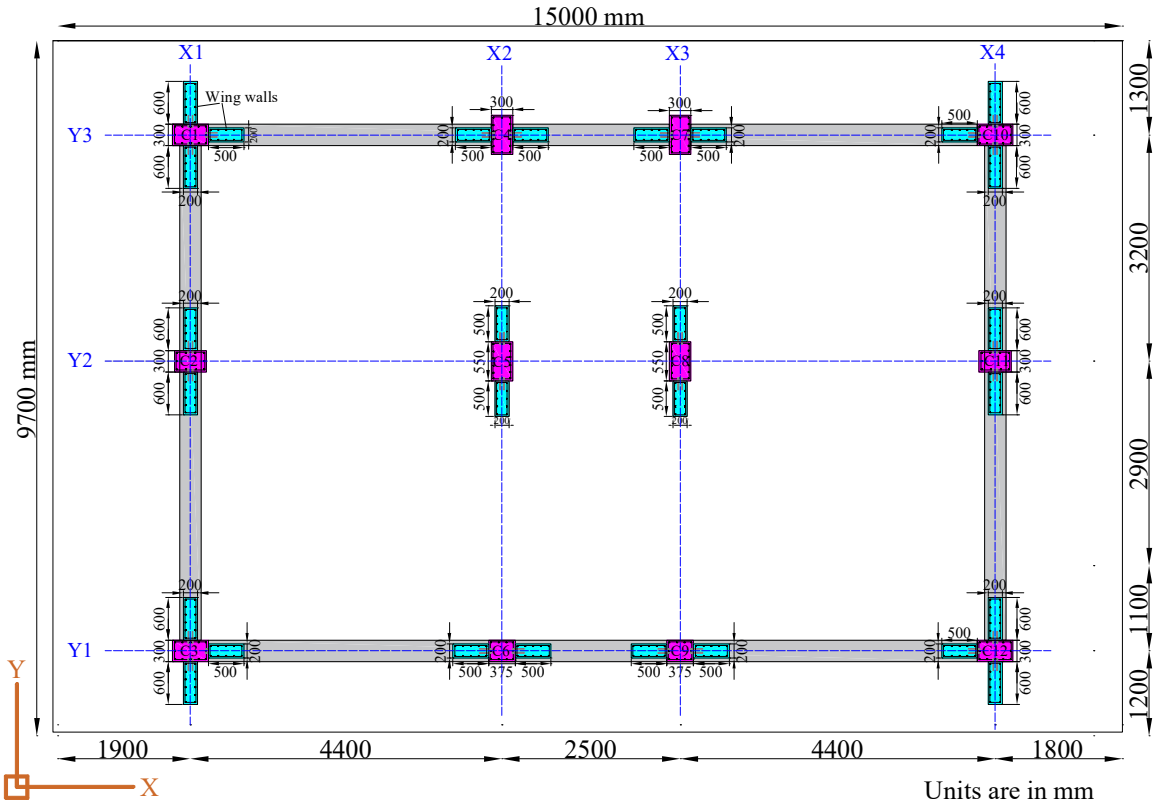

Figure 6.6.1 Layout of the wing wall after installation

Detailed calculation procedure of column with wing walls (C_5) in Y-direction (1st floor):

Original column:

Size = 300 (mm) × 550 (mm)

Tie bar = D10@200c/c

$F_c = 20$ (N/mm^2)

$\sigma_y = 400$ (N/mm^2)

Specification of wing walls:

Wing wall (thickness × length) = 200 (mm) × 500 (mm)

Additional vertical rebar = 10-D13

Hoop spacing = D10@100 c/c

$F_{c1} = 30$ (N/mm^2)

$\sigma_y = 500$ (N/mm^2)

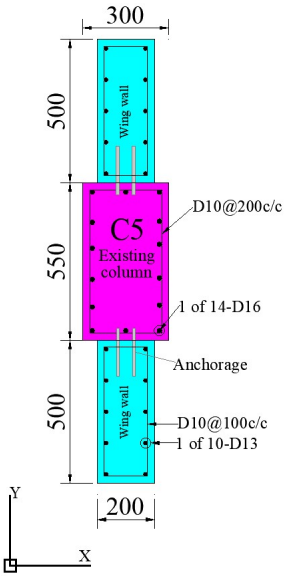

Figure A3.11 Plan of Column with wing walls

Figure A3.11 shows the detailed plan of the C5 column retrofitted with wing walls. The lateral load-carrying capacity of a column without beam retrofitted using wing wall installed parallel to the seismic force direction can be considered under the condition of $M_{slab} < M_{punch}$. According to Section 3.2 in the current guideline, it shall be evaluated by the following equation.

$$Q_u = \frac{{}_cM_w}{h} = \frac{{}_cM_w + N \cdot M_{slab}}{H} \leq \frac{2\ {}_cM_w}{H}$$

where, ${}_cM_w$: the flexural capacity of a column without beam retrofitted by with wing wall(s),

h: inflection height from the bottom of wing wall(s),

N: the number of stories installed wing wall(s),

H: the total height of wing wall(s).

The nodal moments at the flexural capacity of slab (M_{slab}) and the punching shear capacity (M_{punch}) are compared to prevent punching shear failure.

Calculation of M_{slab}:

The flexural capacity of slab (M_{slab}) is calculated by assuming the moment diagram shown in **Figure A3.12** and using the following equation based on Section 6.4.

$$M_{slab} = \frac{{}_lM_{slab}}{l/2} \times \left(\frac{l}{2} + l_w + \frac{D_c}{2}\right) + \frac{{}_rM_{slab}}{l/2} \times \left(\frac{l}{2} + l_w + \frac{D_c}{2}\right)$$

where, ${}_lM_{slab}$ / ${}_rM_{slab}$: flexural yielding capacity of the slab in the corresponding side

l: clear span of the length in the corresponding side

l_w: length of the wing wall

D_c: depth of the column

Reinforcement: D12@200 alt. with extra top 1-D12@200

Number of reinforcement =transverse span length / spacing of rebar =6900/2*100 =35+1 =36 rebar for top slab and 18 rebar for bottom slab.

The flexural yielding capacity of slab, M_{slab}:

$$_lM_{slab}\ (left) = 0.9a_t\sigma_y d = 0.9 \times 36 \times 113 \times 275 \times 182$$
$$= 183243060\ (\mathrm{N \cdot mm}) = 183.2\ (\mathrm{kN \cdot m})$$

$$_rM_{slab}\ (right) = 0.9a_t\sigma_y d = 0.9 \times 18 \times 113 \times 275 \times 182$$
$$= 91621530\ (\mathrm{N \cdot mm}) = 91.6\ (\mathrm{kN \cdot m})$$

Therefore, $M_{slab} = \frac{_lM_{slab}}{\frac{l}{2}} \times \left(\frac{l}{2} + l_w + \frac{D_c}{2}\right) + \frac{_rM_{slab}}{\frac{l}{2}} \times \left(\frac{l}{2} + l_w + \frac{D_c}{2}\right)$

$$= \frac{183.2}{1537.5} \times \left(\frac{3075}{2} + 500 + \frac{550}{2}\right) + \frac{91.6}{1075} \times \left(\frac{2150}{2} + 500 + \frac{550}{2}\right)$$
$$= 433.2\ \text{(kN.m)}$$

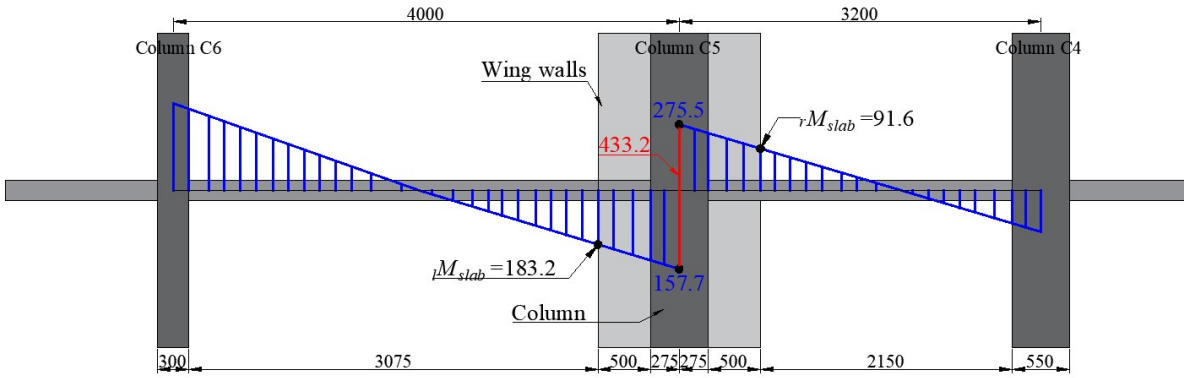

Figure A3.12 Assumed moment diagram after retrofitting by wing walls (X2 Grid)

Calculation of M_{punch}:

c_1 = column depth with wing walls =1550 (mm)

c_2 = column width with wing walls =300 (mm)

σ_y : 275 (N/mm^2) for slab, 400 (N/mm^2) for column

F_c : 20 (N/mm^2) for slab

Axial load (one storey) V_u=149.0 (kN)

d : effective depth =200-18 =182 (mm)

$$M_f = 0.9a_{0t}.\sigma_y.d.\frac{c_2+d}{x_t} + 0.9a_{0b}.\sigma_y.d.\frac{c_2+d}{x_b}$$
$$= 0.9 \times 113.1 \times 275 \times 182 \times \frac{300+182}{100} + 0.9 \times 113.1 \times 275 \times 182 \times \frac{300+182}{200}$$

$= 36.8\ (\text{kN} \cdot \text{m})$

$M_s = \tau_u.(c_2 + d).d.(c_1 + d)$

$= 0.335 \times \sqrt{20} \times (300 + 182) \times 182 \times (1550 + 182)$

$= 227.6\ (\text{kN} \cdot \text{m})$

$M_t = \tau_{tu} \frac{d^2}{2} \left\{(c_1 + d) - \frac{d}{3}\right\} \cdot 2$

$= 6 \times 0.335 \times \sqrt{20} \times \frac{182^2}{2} \left\{(1550 + 182) - \frac{182}{3}\right\} \cdot 2 = 497.6\ (\text{kN} \cdot \text{m})$

$M_0 = M_f + M_s + M_t = 36.83 + 227.6 + 497.6 = 762.1\ (\text{kN} \cdot \text{m})$

$V_0 = \tau_u A_c = 0.335\sqrt{20} \times \{(300 + 182) \times 2 + (1550 + 182) \times 2\} \times 182$

$= 1207.4\ (\text{kN})$

$\frac{V_u}{V_0} + \frac{M_u}{M_0} = \frac{149}{1207.4} + \frac{M_u}{762.1} = 1$

$M_u = M_{punch} = 668.0\ (\text{kN} \cdot \text{m}) > 433.2\ (\text{kN.m})$, slab flexural failure mode

Therefore, $M_{slab} < M_{punch}$. The assumed dimension of the wing wall is enough to prevent punching shear failure.

The flexural capacity ($_cM_w$) of the column with wing wall cast-in-place shall be calculated as follows. If only one wing wall is attached to the column, the contribution of the wing wall in the tension side shall be ignored. For details of wing wall Sec-3.2 of Japanese Guidelines is referred.

So, $_cM_w = (0.9 + \beta)a_t.\sigma_y.D + 0.5N.D\left\{1 + 2\beta - \frac{N}{\alpha_e.b.D.F_{c1}}\left(\frac{a_t.\sigma_y}{N} + 1\right)\right\}$

where,

a_t= gross sectional area of longitudinal reinforcing bars of column in tension side (mm^2) = 3×201 (mm^2)

σ_y=yield stress of the longitudinal reinforcing of column (N/mm^2) =400 (N/mm^2)

b= width of column = 300 (mm)

D= depth of column = 550 (mm)

t= wall thickness of installed wing wall (mm) =200 (mm)

$\alpha = t/b = 0.67$

β= wing wall length in compressive side divided by D $= L_w/D$= 500/550 =0.909

Now, $\alpha_e = \frac{1+2.\alpha.\beta}{1+2.\beta} = \frac{1+2\times0.67\times0.909}{1+2\times0.909} = 0.785$

N=axial force of C5 column = (3.45×3.6×6×12) = 894.2 (kN)

F_{c1}= specified design strength of concrete for wing wall (N/mm^2) = 30 (N/mm^2)

Therefore,

$$_cM_w = (0.9+\beta)a_t.\sigma_y.D + 0.5N.D\left\{1+2\beta-\frac{N}{\alpha_e.b.D.F_{c1}}\left(\frac{a_t.\sigma_y}{N}+1\right)\right\}$$

$$_cM_w = (0.9+0.909)\times 3\times 201\times 400\times 550 + 0.5\times 894.2\times 1000\times 550 \times\left\{1+2\times 0.909-\frac{894.2\times 1000}{0.785\times 300\times 550\times 30}.\left(\frac{3\times 201\times 400}{894.2\times 1000}+1\right)\right\}$$

= 861.1 (kN.m)

Therefore, $Q_u = \frac{_cM_w}{h} = \frac{_cM_w+N\cdot M_{slab}}{H} \le \frac{2\ _cM_W}{H}$

$= \frac{861.1+5\times 433.2}{15.6} \le \frac{2\times 861.1}{15.6} = 110.4$ (kN)

Total weight of the building =15*9.7*12*6 =10476 (kN)

The column's load-carrying capacity with wing wall = 99.2 kN and the flexural yielding precedes the shear failure.

Calculation of column with wing wall ductility index *F*:

C-Index, *C* =99.2/10476 =0.0947

The ductility Index, *F* of C_5 column with wing walls in Y-direction is 2.0; (since Q_{su}/Q_{mu}= 564.9/99.2 =5.69 ≥ 1.3)

The strength index *C* and ductility index *F* of each exterior column with wing walls can be calculated in the same procedure. The calculated index of each member is listed below.

Table A3.7 Ductility index *F* and strength index *C*

Column ID	Storey	Weight of the building	Q_u (kN)	*C*	Q_{su}/Q_{mu}	*F*	Remarks
C1	1	10476	265.2	0.0253	1.95	2.0	Installed wing walls in Y-direction (both side)
C2	1		284.8	0.0272	2.16	2.0	Installed wing walls in Y-direction (both side)
C3	1		340.1	0.0324	1.53	2.0	Installed wing walls in Y-direction (both side)
C4	1		Ignoring shear resistance				Exterior column without beam
C5	1		110.4	0.0105	5.69	2.0	Int. column installed wing walls in Y-direction (both side)

C6	1		Ignoring shear resistance				Exterior column without beam
C7	1		Ignoring shear resistance				Exterior column without beam
C8	1		110.4	0.0105	5.69	2.0	Int. column installed wing walls in Y-direction (both side)
C9	1		Ignoring shear resistance				Exterior column without beam
C10	1		261.5	0.0250	1.97	2.0	Installed wing walls in Y-direction (both side)
C11	1		284.8	0.0272	2.16	2.0	Installed wing walls in Y-direction (both side)
C12	1		309.4	0.0295	1.64	2.0	Installed wing walls in Y-direction (both side)

Therefore, the summation of C from all contributed columns is 0.1877.

Here, $E_0 = C*F = 0.1877*2 = 0.375$, as shown in **Figure A3.13**.

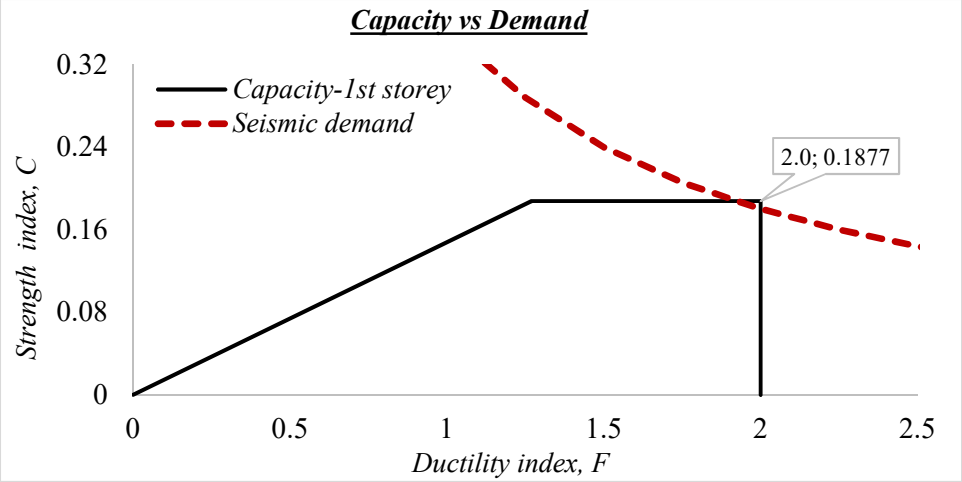

Figure A3.13 Relationship between strength index C and ductility index F

Here, the seismic index, $I_s = E_0 \times S_d \times T = 0.375 \times 1 \times 1 = 0.375$, as shown in **Figure A3.13**. Therefore, the seismic index of this building after the application of the wing wall retrofit scheme was 0.375 ($I_s = 0.375 > I_{s0} = 0.36$ (**Safe**)).

Finally, seismic evaluation is done for each major direction and each floor of the building (shown in **Figure A3.14**. In this case, the seismic capacity on the 5th floor level has been over-strengthened in the Y-direction; however, it is possible to reduce the capacity but a simple retrofitting strategy is the main objective for ease of understanding. The building is considered satisfactory after retrofitting wing walls up to the 5th-floor level and using drop panels on the 6th floor.

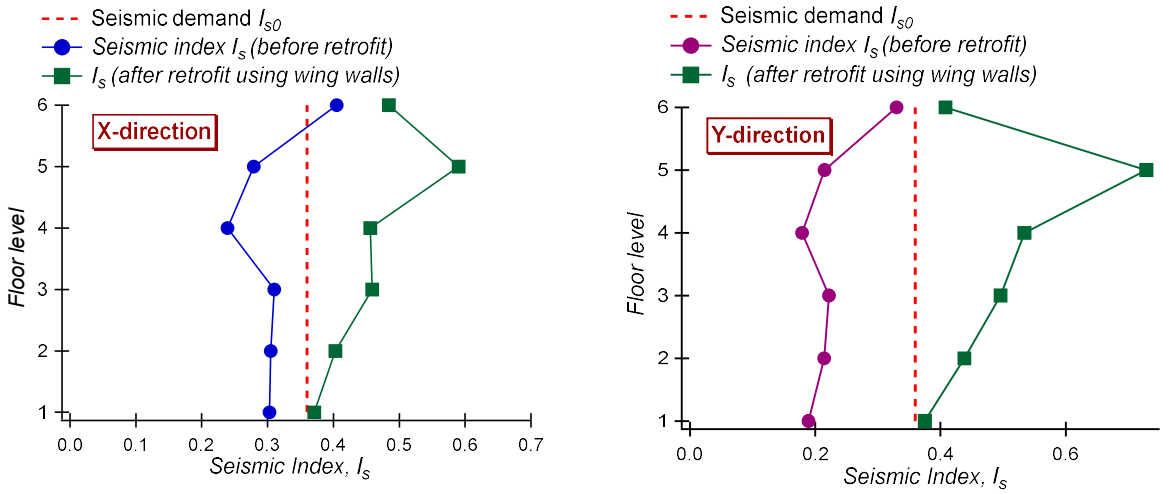

Figure A3.14 Comparison between seismic demand and capacity